MIOMD-XIII

The 13th International Conference on Mid-IR Optoelectronics: Materials and Devices

September 18th-22th, 2016
Beijing, China

PROGRAM & ABSTRACTS

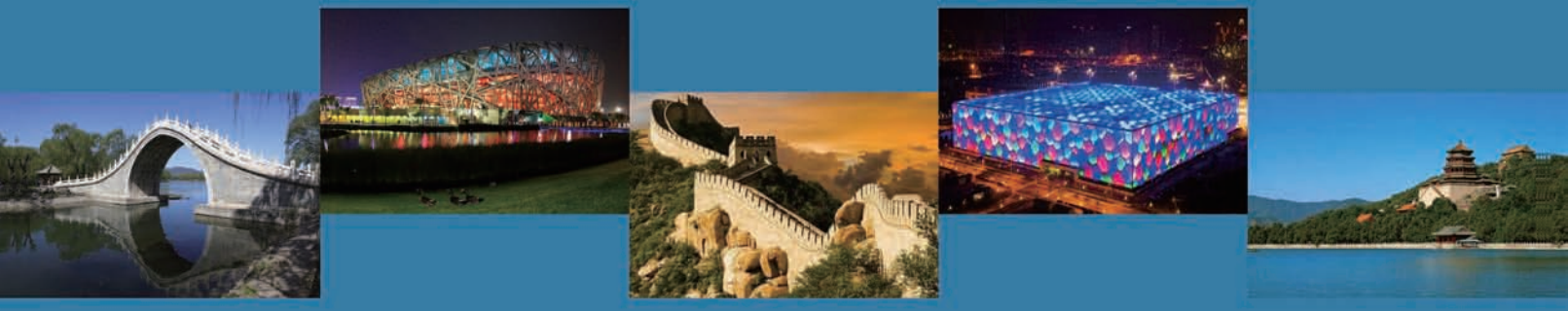

Conference Chair: Li He

Shanghai Institute of Technical Physics, Chinese Academy of Sciences

Sponsors

We would like to thank the following organizations and companies for their generous sponsorship and financial supports to the success of the MIOMD-XIII 2016:

Chinese Academy of Sciences
http://english.cas.cn

Shanghai Institute of Technical Physics,
Chinese Academy of Sciences
http://www.sitp.ac.cn

Key Laboratory of Infrared Imaging
Materials and Detectors,
Chinese Academy of Sciences

The 13th International Conference on **Mid-Infrared Optoelectronics: Materials and Devices (MIOMD-XIII)**

September 18-22, 2016

Beijing, China

Program and Abstracts

Organized by:

Shanghai Institute of Technical Physics

Chinese Academy of Sciences

Key Laboratory of Infrared Imaging Materials and Detectors, China

www.sitp.ac.cn

Impressum

Published by:

Shanghai Institute of Technical Physics

Chinese Academy of Sciences

500 Yutian Road,

Shanghai 200083, China

www.sitp.ac.cn

September, 2016

The 13th International Conference on Mid-Infrared Optoelectronics: Materials and Devices (MIOMD-XIII)

September 18-22, 2016
Beijing, China

Conference Chair

Li He (*Shanghai Institute of Technical Physics, CAS, China*)

Program Committee

Jianxin Chen (*SITP of CAS, China*) - Chair
Chun Lin (*SITP of CAS, China*) –Co-Chair
Lu Chen (*SITP of CAS, China*)- Co-Chair
Gangyi Xu (*SITP of CAS, China*)- Co-Chair

Scientific Committee

Alf Adams *(University of Surrey, UK)*
Markus-C. Amann *(Technical University of Munich, Germany)*
Alexei Baranov *(University Montpellier 2, France)*
Mathieu Carras *(3-5 Lab, France)*
Stephanie Haywood *(University of Hull, UK)*
Li He *(SITP of CAS, Shanghai, China)*
Eduard Hulicius *(Czech Academy of Sciences)*
Ron Kaspi *(Air Force Research Laboratory, USA)*
Abraham Katzir *(Tel Aviv University, Israel)*
Anthony Krier *(Lancaster University, UK)*
Aizhen Li *(SIMIT Shanghai, P.R.China)*
Hao-Hsiung Lin *(National Taiwan University)*
Tariq Manzur *(NAVAIR, USA)*
Jerry Meyer *(Naval Research Laboratory, USA)*
Maya Mikhailova *(Ioffe Institute, Russia)*
Manabu Mitsuhara *(NTT, Japan)*
Konstantin Moiseev *(Ioffe Institute, Russia)*

Manijeh Razeghi *(Northwestern University, USA)*
Stephen Sweeney *(University of Surrey, UK)*
Carlo Sirtori *(University Paris Diderot, France)*
Gunther Springholz *(University of Linz, Austria)*
Robert Suris *(Ioffe Institute, Russia)*
Frank Tittel *(Rice University, USA)*
Eric Tournié *(University Montpellier 2, France)*
Joachim Wagner *(Fraunhofer-Institut für Angewandte Festkörperphysik, Germany)*
Yury P. Yakovlev *(Ioffe Institute, Russia)*
Yong-Gang Zhang *(SIMIT of CAS, Shanghai, China)*

Organizing Committee

Ruijun Ding (*SITP of CAS, China*) – Chair
Xiangtuan Xia (*SITP of CAS, China*)
Yong Xu (*SITP of CAS, China*)
Jianrong Yang (*SITP of CAS, China*)
Jianguo Wu (*SITP of CAS, China*)
Jianzhen Pan (*SITP of CAS, China*)

Conference Coordinator

Jianzhen Pan (*SITP of CAS, China*)
Shiwen Sun (*SITP of CAS, China*)

FOREWORD

The international conference series on Mid-Infrared Optoelectronics: Materials and Devices (MIOMD) has passed twenty years since its inauguration in 1996 with the first conference organized in Lancaster. MIOMD is now held on a bi-annual basis and rotates between Europe, Asia and American. The last three conferences were held in Shanghai, China (2010), Chicago, USA (2012) and Montpellier, France (2014). The next conference will be held at Arizona State University, USA.

MIOMD-XIII brings together scientists and engineers from all over the world working in the area of mid-infrared and THz optoelectronics from materials, devices to applications. It covers topics of novel infrared and THz materials, materials growth and characterization, infrared and THz emitters and detectors, and applications of infrared optoelectronics. To celebrate the latest breakthroughs in this period, the MIOMD-XIII scientific committee strives to cover the lasts achievements and future trends in the fields with comprehensive reviews in its program. The conference consists of 5 plenary talks, 15 invited talks, 30 contributed oral papers and 41 posters. It provides an opportunity for researches to share their lasts achievements, exchange ideas, foster collaborative relationship and explore future directions.

We would like in particular to thank the Chinese Academy of Sciences and the National Natural Foundation of China, Beijing Municipal Government for their supports as well as our sponsors and exhibitors.

On behalf of the scientific committee and local organizing committee, I warmly welcome you to MIOMD-XIII. I hope you will enjoy the conference with its stimulating scientific program and the city of Beijing.

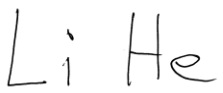

Conference Chair
Shanghai Institute of Technical Physics, Chinese Academy of Sciences

Program of MIOMD-XIII, 2016

The MIOMD-XIII meeting will be held at the Juying Ballroom which is located on the 2nd floor of Friendship Palace of Beijing Friendship Hotel.

<table>
<tr><th>Sunday,
18 September</th><th>Monday,
19 September</th><th>Tuesday,
20 September</th><th>Wednesday,
21 September</th><th>Thursday,
22 September</th></tr>
<tr><td rowspan="4"></td><td>Opening
08:30-08:45</td><td rowspan="2">Session 5: Plenary and invited
8:30-10:15</td><td rowspan="2">Session 8: Infrared detectors
8:30-10:15
1 invited
5 contribution</td><td rowspan="10">Social

Program</td></tr>
<tr><td>Session 1: Plenary
08:45-10:15</td></tr>
<tr><td>Coffee break
10:15-10:40</td><td>Coffee break
10:15-10:40</td><td>Coffee break
10:15-10:35</td></tr>
<tr><td>Session 2: Plenary
10:40-12:10</td><td>Session 6: Material growth
10:40-11:55
1 invited
3 contribution</td><td>Session 9: THz materials
10:35-12:05
2 invited
2 contribution</td></tr>
<tr><td></td><td>Lunch
12:10-13:30</td><td>Lunch
11:55-13:30</td><td>Lunch
12:05-13:30</td></tr>
<tr><td rowspan="4">Registration
15:00-19:00</td><td>Session 3: Materials for infrared optoelectronics
13:30-15:30
2 invited
4 contribution</td><td>Session 7: Infrared emitters
13:30-15:30
2 invited
4 contribution</td><td>Session 10: THz
13:30-15:30
1 invited
6 contribution</td></tr>
<tr><td>Coffee break
15:30-15:50</td><td>Coffee break
15:30-15:50</td><td>Coffee break
15:30-15:50</td></tr>
<tr><td rowspan="2">Session 4: Infrared detectors
15:50-17:50
2 invited
4 contribution</td><td rowspan="2">Poster session
15:50-17:50</td><td>Session 11: Application
15:50-17:20
2 Invited
2 contribution</td></tr>
<tr><td>Closing
17:20-17:30</td></tr>
<tr><td>Reception
18:30-20:30</td><td>/</td><td>Banquet
18:30-20:30</td><td>/</td></tr>
</table>

Program of MIOMD-XIII

Sunday September 18st

15:00-19:00 Registration
18:30-20:30 Reception

Monday Morning, September 19st

08:30-08:45	**Opening – Introduction and Welcome**
	He Li
08:45-10:15	**Session 1: Plenary 1**
8:45-9:30	**Materials and Device Concepts for MIR VCSELs** **25** M.-C. Amann* Walter Schottky Institut, Technische Universität München Am Coulombwall 4, D-85748 Garching, Germany
9:30-10:15	**IR Technology Based on MBE HgCdTe: Current Status and Future Directions** **26** Sivalingam Sivananthan*[1], S. Velicu[2] [1] University of Illinois at Chicago, Chicago, IL [2] EPIR Inc., Bolingbrook , IL
10:15-10:40	***Coffee break and group photo***
10:40-12:10	**Session 2: Plenary 2**
10:40-11:25	**Tunable infrared response of nanostructures** **27** Alessandro Tredicucci[1,2]* [1]Dipartimento di Fisica "E. Fermi", Università di Pisa, and NEST, Istituto Nanoscienze-CNR Largo Pontecorvo 3, I-56127 Pisa (Italy) [2] Fondazione Bruno Kessler, Via Sommarive 18, I-38123 Povo, (Italy)
11:25-12:10	**Localized-field enhanced two dimensional material infrared photodetectors** **28** Wenjin Luo, Peng Wang, Hehai Fang, Man Luo, Jianlu Wang, Weida Hu, Xiaoshuang Chen and Wei Lu* National Laboratory for Infrared Physics, Shanghai Institute of Technical Physics, Chinese Academy of Sciences, 500 Yutian Road, Shanghai 200083, China
12:10-13:30	**Lunch**

Monday Afternoon, September 19st

13:30-15:30	**Session 3: Materials for Infrared Optoelectronics**
13:30-14:00	**New materials approaches for interband mid-infrared photonic devices (Invited)** **29** Stephen J. Sweeney[1]*, Igor P. Marko[1]

	[1] Advanced Technology Institute and Department of Physics, University of Surrey, Guildford GU2 7XH, United Kingdom
14:00-14:30	**Antimonide based mid-infrared photonic detectors and focal plane arrays (Invited)** **30** Sanjay Krishna Director, Center for High Technology Materials Professor and Regents' Lecturer, Department of Electrical and Computer Engineering, University of New Mexico, Albuquerque NM
14:30-14:45	**Highly doped InAsSb nanoribbon on GaSb for plasmonics applications** **31** M.J. Milla[1,2], F. Barho[1,2], M. Bomers[1,2], F. González-Posada[1,2], L. Cerutti[1,2,*], E. Tournié and T. Taliercio[1,2,*] [1] Univ. Montpellier, IES, UMR 5214, F-34000, Montpellier, France [2] CNRS, IES, UMR 5214, F-34000, Montpellier, France
14:45-15:00	**GeSn Alloys for Mid-Infrared Optoelectronics** **33** Timothy Eales[1], Igor P. Marko[1], Seyed A. Ghetmiri[2], Wei Du[2], Yiyin Zhou[2], Shui-Qing Yu[2], Joe Margetis[3], John Tolle[3], Stefan Schulz[4], Edmond O'Halloran[4], Eoin P. O'Reilly[4] and Stephen J. Sweeney[1]* [1] Advanced Technology Institute and Department of Physics, University of Surrey, Guildford, GU2 7XH, United Kingdom [2] Department of Electrical Engineering, University of Arkansas, Fayetteville, AR, USA, 72701 [3] ASM, 3440 East University Drive, Phoenix, Arizona 85034, USA [4] Tyndall National Institute, Lee Maltings, Cork, Ireland
15:00-15:15	**Heterogeneous integration of InP-based type-II active devices on silicon for 2 μm wavelength range on-chip spectroscopy** **35** Ruijun Wang[1,2]*, Stephan Sprengel[3], Muhammad Muneeb[1,2], Gerhard Boehm[3], Aditya Malik[1,2], Roel Baets[1,2], Markus-Christian Amann[3], Gunther Roelkens[3] [1] Photonics Research Group, Ghent University-imec, Technologiepark-Zwijnaarde 15 iGent, 9052 Ghent, Belgium [2] Center for Nano- and Biophotonics (NB-Photonics), Ghent University, Ghent, Belgium [3] Walter Schottky Institut, Technische Universität München, Am Coulombwall 4, 85748 Garching, Germany.
15:15-15:30	**Mid-infrared InP-based Quantum Wells with Bismuth Surfactant or Incorporation** **37** Yi Gu, Y.G. Zhang, X.Y. Chen, S.P. Xi, B. Du, Y.J. Ma, W.Y. Ji, Y.H. Shi, A.Z. Li Shanghai Institute of Microsystem and Information Technology, Chinese Academy of Sciences,China
15:30-15:50	***Coffee break***
15:50-17:50	**Session 4: Infrared Detectors**
15:50-16:20	**InAs/InAsSb type-II superlattices: material properties and device applications (Invited)** **39** Yong-Hang Zhang School of Electrical, Computer and Energy Engineering，Arizona State University，

	Tempe, Arizona 85287
16:20-16:50	**Recent Progress in Mid-wavelength Infrared Type-II Superlattices （Invited）** **40** E. H. Steenbergen[1]*, G. Ariyawansa[2], C. J. Reyner[2], H. Bourassa[3], J. M. Duran[2], J. D. Reding[2], and J. E. Scheihing[2] [1]Air Force Research Laboratory, Space Vehicles Directorate, Kirtland AFB, NM 87117 [2]Air Force Research Laboratory, Sensors Directorate, Wright-Patterson AFB, OH 45433 [3]Air Force Research Laboratory, Materials & Manufacturing Directorate, Wright-Patterson AFB, OH 45433
16:50-17:05	**Recent progress on HgCdTe/ZnCdTe by MBE** **43** Lu Chen, Xiangliang Fu, Yushun Chen, Weiqiang Wang, Chuan Shen, Gao Wang, Shundong Bu, Bin Zhang, Feng Yang, Yin Wang, Li He Key lab of advanced materials and devices, Shanghai institute of Technical Physics, CAS, 500# Rd. Yutian, Shanghai, China, 200083
17:05-17:20	**High quantum efficiency in InAs/GaSb superlattice for very long wavelength detection with cutoff of 21 μm** **45** Guowei Wang[1,2]*, Dongwei Jiang[1,2], Wei Xiang[1,2], Hongyue Hao[1,2], Xi Han[1,2], Yingqiang Xu[1,2], Zhichuan Niu[1,2] [1]State Key Laboratory for Superlattices and Microstructures, Institute of Semiconductors, Chinese Academy of Sciences, Beijing 100083, China. [2]Synergetic Innovation Center of Quantum Information and Quantum Physics, University of Science and Technology of China, Hefei, Anhui 23026, China
17:20-17:35	**InP-based metamorphic avalanche photodiodes towards detecting of MWIR wavelengths** **47** Yingjie Ma, Yonggang Zhang, Yi Gu, Xingyou Chen, Yanhui Shi, Wangyan Ji, Suping Xi, Ben Du, Hengjing Tang, Yongfu Li, Jiaxiong Fang Shanghai Institute of Microsystem and Information Technology, Chinese Academy of Sciences,China
17:35-17:50	**Mid-IR detectors testing for space missions** **49** D. Sporea[1]*, L. Mihai[1], A. Sporea[1], I. Vaa[2], M. Straticiuc[2], I. Burducea [1] National Institute for Laser, Plasma and Radiation Physics, 409 Atomistilor St., Magurele, RO-077125, Romania [2] "Horia Hulubei" National Institute of Physics and Nuclear Engineering, 30 Reactorului St., Magurele, RO-077125, Romania
17:50-18:30	**Dinner**

Tuesday Morning, September 20th

08:30-10:15	**Session 5: Plenary and Invited**
08:30-09:15	**Interband cascade lasers and related devices (Plenary)** **51** Rui Q. Yang* School of Electrical and Computer Engineering, University of Oklahoma, Norman,

	OK
9:15-9:45	**Antimonide-based infrared detectors- a new perspective (Invited)** **52** Antoni Rogalski Institute of Applied Physics, Military University of Technology, 2 Kaliskiego Str., 00-908 Warsaw, Poland
9:45-10:15	**2-3μm band antimony free detectors and lasers: Material, device and applications (Invited)** **53** Zhang Yong-gang[1]*, Gu Yi[1], Li Xue[2], Shao Xiu-mei[2], Chen Xin-you[1], Ma Ying-jie[1], Li Ai-zhen[1], Tang Heng-jing[2], Li Tao[2], Xi Su-ping[1], Du Ben[1], Ji Wan-yan[1],Shi Yan-hui[1],Gong Hai-mei[2], Fang Jia-xiong[2] [1] State Key Laboratory of Functional Materials for Informatics, Shanghai Institute of Microsystem and Information Technology, Chinese Academy of Sciences. 865 Chang Ning Rd., Shanghai 200050, China. [2] Key Laboratory of Infrared Imaging Materials and Devices, Shanghai Institute of Technical Physics, Chinese Academy of Sciences.500Yu Tian Rd., Shanghai 200083, China.
10:15-10:40	***Coffee break***
10:40-11:55	**Session 6: Material Growth and Characterization**
10:40-11:10	**Growth and Characterisation of Site-controlled InAsSb Nanowires on Silicon for Photonic Devices (Invited)** **54** A. Krier[1]*, A. Alhodaib[1], A.R. Marshall[1], A.P. Craig[1], M.J. Thompson[1], J. Svensson[2], L.E. Wernersson[2], A.M. Sanchez[3] [1] Physics Department, Lancaster University, Lancaster, LA1 4YB, UK [2] Electrical and Information Technology, Lund University, Box 118, SE-221 00 Lund, Sweden [3] Department of Physics, University of Warwick, Coventry, CV4 7AL, UK
11:10-11:25	**Molecular Beam Epitaxy and characterization of high Bi content GaSbBi alloys** **56** O. Delorme[1,2], L. Cerutti[1,2 *], E. Tournié[1,2] and J.-B. Rodriguez[1,2 *] [1] Univ. Montpellier, IES, UMR 5214, F- 34000, Montpellier, France [2] CNRS, IES, UMR 5214, F- 34000, Montpellier, France
11:25-11:40	**Anisotropic Polarizability Matrix due to Electromagnetic Coupling of SPPs to Dirac-Electron Excitations in Graphene** **58** Danhong Huang[1]*, Oleksiy Roslyak[2], Godfrey Gumbs[3], Wei Pan[4], A. A. Maradudin[5] [1] Air Force Research Laboratory, Space Vehicles Directorate (AFRL/RVSW), 3725 Aberdeen Avenue SE, Kirtland AFB, NM 87117, United States of America [2] Department of Physics and Engineering Physics, Fordham University, 441 East Fordham Road, Bronx, NY 10458, United States of America [3] Department of Physics and Astronomy, Hunter College of the City University of New York, 695 Park Avenue New York, NY 10065, United States of America [4] Sandia National Laboratories, Albuquerque, New Mexico 87185, USA [5] Department of Physics and Astronomy and Institute for Surface and Interface Science, University of California at Irvine, Irvine, CA 92697, United States of America

11:40-11:55	**MBE Growth of InAs Nanowires on Graphene** **60** Chieh Chou[1], Che-Wei Yang[2], and Hao-Hsiung Lin[1,2]* [1]Graduate institute of electronics engineering, National Taiwan University, Taipei, [2]Department of eletrical engineering, national Taiwan University, Taipei
11:55-13:30	**Lunch**

Tuesday Afternoon, September 20th

13:30-15:30	**Session 7: Infrared Emitters**
13:30-14:00	**Quantum Cascade devices: from discrete to integrated systems (Invited)** **62** A. Harrer[1], B. Schwarz[1], R. Szedlak[1], D. Ristanic[2], H. Detz[1], A.M. Andrews[1], T. Zederbauer[2], D. MacFarland[2], W. Schrenk[2], G. Strasser[1,2]* [1] Institute of Solid State Electronics, TU Wien, Floragasse 7, 1040 Wien, Austria [2] Center for Micro- and Nanostructures, TU Wien, Floragasse 7, 1040 Wien, Austria
14:00-14:30	**Quantum Cascade Lasers for Industrial Applications (Invited)** **63** M. Troccoli* AdTech Optics Inc., City of Industry, CA 91748, USA
14:30-14:45	**Long-wavelength stimulated emission from HgCdTe quantum well heterostructures** **64** V.V.Rumyantsev[1,2*], S.V.Morozov[1,2], A.M. Kadykov[1], K.E.Kudryavtsev[1], A.A.Dubinov[1,2] [1]Institute for Physics of Microstructures of RAS, 603950, GSP-105, Nizhny Novgorod, Russia [2]Lobachevsky State University of Nizhny Novgorod, 603950, av. Gagarina 23, Nizhny Novgorod, Russia [3]A.V.Rzhanov Institute of Semiconductor Physics, Siberian Branch of Russian Academy of Sciences, 630090, pr. Lavrentieva 13, Novosibirsk, Russia [4]Institute of Ion Beam Physics and Materials Research, Helmholtz-zentrum Dresden−Rossendorf, Dresden, D−01328, Bautzner Landstraße
14:45-15:00	**Recombination Processes in Type I GaInAsSb Lasers** **66** T. Eales[1], I. Marko[1], B. Ikyo[1], A. R. Adams[1], S. Arafin[2], S. Sprengel[2], M.-C. Amann[2], S. J. Sweeney[1]* [1] Advanced Technology Institute and Department of Physics, University of Surrey, Guildford, GU2 7XH, United Kingdom [2] Walter Schottky Institut, Technische Universität München, Am Coulombwall 3, 85748 Garching, Germany
15:00-15:15	**Electroluminescence study of InAs/InAs(Sb)/InAsSbP LED heterostructures at 4.2–300 K** **68** Kh. Salikhov *[1], K.D. Mynbaev [2,3], N.L. Bazhenov [2], A.A. Semakova [3], M.P. Mikhailova [2], N.D. Stoyanov [4], S.S. Kizhaev [4], S.S. Molchanov [4], A.P. Astakhova [4], A.V. Chernyaev [4] [1] The Institute for Advanced Study, Academy of Sciences of Tatarstan, Russia [2] Ioffe Institute, 194021 Saint–Petersburg, Russia [3] ITMO University, 197101 Saint–Petersburg, Russia

	[4] Microsensor Technology, 194223 Saint–Petersburg, Russi
15:15-15:30	**A design of interband cascade laser's active region towards mode-locked operation 70** M. Dyksik[1], K. Ryczko[1], M. Motyka[1], J. Misiewicz[1], M. Kamp[2], G. Sęk[1] [1]Laboratory for Optical Spectroscopy of Nanostructures, Department of Experimental Physics, Faculty of Fundamental Problems of Technology, Wrocław University of Science and Technology, Wybrzeże Wyspiańskiego 27, 50-370 Wrocław, Poland [2]Technische Physik, University of Würzburg & Wilhelm Conrad Röntgen Research Center for Complex Material Systems, Am Hubland, D−97074 Würzburg, Germany
15:30-15:50	***Coffee break***
15:50-17:50	**Poster Session**
18:30-20:30	**Banquet**

Wednesday Morning, September 21st

8:30-10:15	**Session 8: Infrared Detectors**
8:30-9:00	**Towards photon counting beyond 2μm using InAs e-APD (Invited) 71** [1]Benjamin.S. White, Xinxin Zhou, Jo Shien Ng and Chee Hing Tan*, [2] Peter Vines and Gerald Buller [1]Department of Electronic and Eletrical Enginerring, Mappin Building, Mappin Street, Sheffield, S13JD, The University of Sheffield, UK [2] Institute of Photonics and Quantum Sciences, Heriot-Watt University, Edinburgh, EH14 4As, UK
9:00-9:15	**8×8 photodiode array based on P-InAsSbP/n-InAs single heterostructure 73** B.A. Matveev[1, 2].*, P.N. Brunkov[1], N.D. Il'inskaya[1], S.A. Karandashev[1], A.A.Lavrov[2], M.A. Remennyi[1, 2], N.M. Stus'[1, 2] and A.A. Usikova[1] [1] Ioffe Institute, 26 Politekhnicheskaya, St. Petersburg 194021, Russian Federation [2] IoffeLED, Ltd., 26 Politekhnicheskaya, St. Petersburg 194021, Russian Federation
9:15-9:30	**High Performance SWIR HgCdTe FPA on Si for Hyperspectral Detection 75** Xiaoning Hu*, Qingjun Liao, Aibo Huang, Lu Chen, Xin Chen, Hua Fan, Ruijun Ding, Li He Key Laboratory of Infrared Imaging Materials and Detectors, Shanghai Institute of Technical Physics, Chinese Academy of Sciences, Shanghai 200083, China
9:30-9:45	**Nanoantenna Integrated Infrared Pixels 76** Fei Yi[1]*, Ertugrul Cubukcu[2] [1] School of Optics and Electronic Information, Huazhong Univeristy of Science and Technology, Wuhan 430074, China [2] Department of Electrical and Computer Engineering, University of California, San Diego, 9500 Gilman Dr., La Jolla, CA 92093, USA
9:45-10:00	**640×512 InGaAs/InP focal plane array with response extended to visible wavelength band 78** YANG Bo[1,2,3], SHAO Xiu-Mei[1,2], TANG Heng-Jing[1,2], LI Xue[1,2], GU Yi[3], GONG Hai-Mei[1,2]* [1] State Key Laboratories of Transducer Technology, Shanghai Institute of Technical

	Physics, Chinese Acadamy of Sciences, 500 Yutian Road,Shanghai 200083, China [2] Key Laboratory of Infrared Imaging Materials and Detectors, Shanghai Institute of Technical Physics, Chinese Acadamy of Sciences, 500 Yutian Road, Shanghai 200083, China [3] State Key Laboratory of Functional Materials for Informatics, Shanghai Institute of Microsystem and Information Technology,Chinese Academy of Sciences,865 Changning Road, Shanghai 200050 ,China
10:00--10:15	**Tailor the functionalities of metasurfaces: From perfect absorption to phase modulation** **79** Jiaming Hao[1], Che Qu[2], Shaojie Ma[2], Meng Qiu[2], Xin Li[2], Shiyi Xiao[2], Ziqi Miao[2] Qiong He[2], Shulin Sun[2], Ning Dai[1] and Lei Zhou[2] [1] National Laboratory for Infrared Physics, Shanghai Institute of Technical Physics, Chinese Academy of Science, Shanghai 200083, China [2] State Key Laboratory of Surface Physics, Key Laboratory of Micro and Nano Photonic Structures (Ministry of Education) and Physics Department, Fudan University, Shanghai 200433, China
10:15-10:35	***Coffee break***
10:35-12:05	**Session 9: THz materials and Devices**
10:35-11:05	**Quantum cascade lasers: From mid infrared to THz (Invited)** **80** F.-Q. Liu, Y.H. Liu, Y.Y Li, J.C. Zhang, J.Q. Liu, and Z.G. Wang Key Laboratory of Semiconductor Materials Science, Institute of Semiconductors, Chinese Academy of Sciences, and Beijing Key Laboratory of Low Dimensional Semiconductor Materials and Devices,P.O. Box 912, Beijing 100083, China
11:05-11:35	**Extraordinary optical transmission through subwavelegnth hoe array on superconducting MgB2 thin films (Invited)** **81** X. Fang and X.G. Qiu* Institute of Physics, Chinese Academy of Sciences, Beijing, 100190, China
11:35-11:50	**Microwave radiation absorption and Shubnikov-de Haas oscillations of InAs/GaSb/AlSb quantum wells** **82** M.P. Mikhailova[1], A.I. Veinger[1], I.V. Kochman[1], P.V. Semenikhin[1], K.V. Kalinina[1], R.V. Parfeniev[1], V.A. Berezovets[1], A. Hospodkova[2], J. Pangrac[2], E. Hulicius[2*] [1] Ioffe Physical-Technical Institute, 194021, Saint-Petersburg, Russia [2] Institute of Physics CAS, v.v.i., 162 00, Prague, Czech Republic
11:50-12:05	**Homogeneously spectral spanning of terahertz quantum cascade lasers with radio frequency modulation** **84** W. J. Wan, H. Li*, J. C. Cao* Key Laboratory of Terahertz Solid State Technology, Shanghai Institute of Microsystem and Information Technology, Chinese Academy of Sciences, 865 Changning road, Shanghai 200050, China
12:05-13:30	**Lunch**

Wednesday Afternoon, September 21st

13:30-15:30	**Session 10: Infrared Emitters**

13:30-14:00	**New life of InAs-based quantum cascade lasers (Invited)** **85** Alexei Baranov*, M. Bahriz, R.Teissier Institute of Electronics and Systems, UMR 5214 CNRS-Universite Montpellier, 34095, Montpellier, France
14:00-14:15	**Terahertz master-oscillator power-amplifier quantum cascade laser with stable single-mode emission** **86** H. Zhu[1], F. F. Wang[1], L. H. Li[2], Q. Yan[1], C. R. Yu[1], J. X. Chen[1], L. Chen[2], E. H. Linfield[2], A. G. Davies[2], R. Colombelli[3], G. Xu[1]*, L. He[1] [1] Key Laboratory of Infrared Imaging Materials and Detectors, Shanghai Institute of Technical Physics, Chinese Academy of Sciences, Shanghai 200083, China. [2] School of Electronic and Electrical Engineering, University of Leeds, Leeds LS2 9JT, UK [3] Institut d'Electronique Fondamentale, Univ. Paris Sud, CNRS UMR8622, 91405 Orsay, France
14:15-14:30	**High-power terahertz quantum cascade lasers** **88** Y.Y. Li, J.Q. Liu*, J.C. Zhang, F.Q. Liu, Z.G. Wang Key Laboratory of Semiconductor Materials Science, Institute of Semiconductors, Chinese Academy of Sciences, P.O. Box 912, Beijing 100083, China
14:30-14:45	**Inducing changes in lateral mode selection in broad area quantum cascade lasers** **90** Ron Kaspi*, Chi Yang, Chunte Lu, Sanh Luong,Timothy C. Newell Air Force research Laboratory, Directed Energy Directorate AFRL/RDLTD Albuquerque, New Mexico, USA 87117
14:45-15:00	**Extending the wavelength of superluminescent LEDs to mid-infrared wavelengths** **92** S. Suomalainen*, J. Viheriälä, N. Zia, R. Koskinen, M. Koskinen,M. Guina Optoelectronics Research Centre, Tampere University of Technology, P.O.Box 692, 33101 Tampere, Finland
15:00-15:15	**New Structures for Single Lobe Operation Quantum Cascade Lasers Array** **94** S. Ferré[1,2]*, A. Peinado[3], E.Garcia-Caurel[3], Mathieu Carras[1] [1] mirSense, 86 rue de Paris, Bat. Erable, 91400 Orsay, France. [2]Thales Research & Technology, Route Départementale 128, 91767 Palaiseau, France [3]LPICM, CNRS, Ecole Polytechnique, Université Paris-Saclay, 91128 Palaiseau, France
15:15-15:30	**Heat dissipation schemes in QCLs monitored by CCD thermoreflectance 96** D. Pierścińska[1], K. Pierściński[1]*, M. Morawiec[1], P. Gutowski[1], P. Karbownik[1], O.Serebrennikova[1], M. Badura[2], D. Radziewicz[2], B. Ściana[2], M. Tłaczała[2], M. Bugajski[1] [1] Institute of Electron Technology, Al. Lotników 32/46, 02-668 Warszawa, Poland [2] Faculty of Microsystem Electronics and Photonics, Wrocław University of Technology,Janiszewskiego 11/17, 50-372 Wrocław, Poland
15:30:15:50	**Coffee break**
15:50-:17:30	**Session 11: Applications of Infrared Optoelectronic Devices**

15:50-16:20	**Mid-infrared laser based gas sensors for atmospheric applications (Invited)** **98** Dong Chen[1,2], Fengjiao Shen[1], Hongming Yi[1], Tao Wu[3], Gaoxuan Wang[1], Rabih Maamary[1], Dorothée Dewaele[1], Fabrice Cazier[1], Patrick Augustin[1], Marc Fourmentin[1], Cécile Coeur-Tourneur[1], Eric Fertein[1], Weidong Chen[1]* [1] LPCA, University of the Littoral Opal Coast, 59140 Dunkirk, France [2] Hefei University of Technology, Anhui 230009, China [3] Nanchang Hangkong University, Nanchang 330063, China
16:20-16:50	**MOEMS external cavity quantum cascade laser for time resolved MIR fingerprint spectroscopy (Invited)** **99** R. Ostendorf[1]*, L. Butschek[1], A. Merten[2], A. Dreyhaupt[2], J. Grahmann[2], M. Rattunde[1], J. Jarvis[1], M Härtelt[1], S. Hugger[1], F. Fuchs[1], J. Wagner* [1] Fraunhofer Institute for Applied Solid State Physics, Tullastr. 72, 79108 Freiburg, Germany [2] Fraunhofer Institute for Photonic Microsystems, Maria-Reiche-Str. 2, 01109 Dresden, Germany
16:50-17:05	**InAs and GaInAsSb based Thermophotovoltaic Devices for waste heat recovery applications below 1000 °C** **101** Qi Lu, Manoj Kesaria, Andrew Marshall, Susan Krier, S. McDougall, W. Meredith, J. Inskip, A. Scholes, Tony Krier Physics Department, Lancaster University, United Kingdom
17:05-17:20	**Photoelectrical Hydrogen Sensor Based on Pd-Oxide-InP Structure** **103** Yu.P.Yakovlev*, E.A. Grebenshchikova, A. N. Imenkov, V.A.Shutaev, A.M.Ospennikov Ioffe Physical-Technical Institute RAS,194021, St.Petersburg, Russia
17:20-17:30	**Closing**

Thursday, September 22nd

09:00-	**Social Program**

Post Session, Tuesday, September 20th

The Key Laboratory of Semiconductor Materials Science, Institute of Semiconductors, Chinese Academy of Sciences, Qinghua East Road A 35, Beijing 100083, China

Key Laboratory of Infrared Imaging Material and Detectors, Shanghai Institute of Technical Physics, Chinese Academy of Sciences, Shanghai, China

P22 Study of the characteristics of LPE p^+-on-n heterojunction LWIR photovoltaic detectors in Variable-area Diode Test Structures **146**

Wang Xi[1,2], Lin Chun[2], Wei Yanfeng[2], Zhu Mingxing[2]

[1]University of Chinese Academy of Sciences, Beijing 100039, China

[2]Key Laboratory of Infrared Imaging Materials and Detectors，Shanghai Institute of Technical Physics, Chinese Academy of Sciences, Shanghai 20083, China

P23 InGaAs/GaAsSb superlattice photodiodes with P-type compensation-doped absorption regions **149**

Chuan Jin[1,2], Qingqing Xu[1], Chengzhang Yu[1], Jianxin Chen[1]

[1]Infrared Imaging Materials and Detector, Shanghai Institute of Technical Physics, Chinese Academy of Sciences, Shanghai, 200083, China

[2]University of Chinese Academy of Sciences, Beijing 100049, China

P24 Molecular Beam Epitaxial (MBE) Growth of 3μm Laser using InGaAsSb/AlInAsSb Quantum Well Structure **151**

Chunte Lu, Ron Kaspi, Tim Newell, Chi Yang, Sun Luong, and Don Gianardi

Air Force Research Laboratory, Directed Energy Directorate Albuquerque, New Mexico, 87117 USA

P25 Surface morphology study of ZnTe crystals grown from Te solution **153**

Rui Yang[1,2], Yasir Zaman[2], Chensheng Wang[1], Zhijie Zhang[1], Wanqi Jie[2]

[1]Huazhong Institute of Electro-Optics－Wuhan National Laboratory for Optoelectronics, Wuhan 430223, China

[2]State Key Laboratory of Solidification Processing, Northwestern Polytechnical University, Xi'an 710072, China

P26 Grading strategyof the buffers for high indium InGaAs photodetectors **154**

B. Du, Y. Gu, Y. G. Zhang, X. Y. Chen, S. P. Xi, Y. J. Ma, W. Y. Ji, Y. H. Shi

State Key Laboratory of Functional Materials for Informatics, Shanghai Institute of Microsystem and Information Technology, Chinese Academy of Sciences, Shanghai, China

P27 Influences of Chemical Etching on Nanosized Patterns on the Surface of HgCdTe Epilayers **156**

Changzhi Shi, Chun Lin, Yanfeng Wei

[1]Shanghai Institute of Technical Physics, 500 Yutian Road, Shanghai, China

P28 The junction profile of LW HgCdTe conversed through ion beam milling **158**

Zhou Songmin, Weng Bin, Lin Chun, Li Hao, Wang Xi, Wei Yanfeng, Ye Zhenhua, Ding Ruijun and He Li.

Key laboratory of Infrared Imaging Material and Detectors, Shanghai Institute of Technical Physics, Chinese Academy of Sciences, Shanghai 200083, P. R. China

Abstracts

Oral Sessions

Materials and Device Concepts for MIR VCSELs

M.-C. Amann*

Walter Schottky Institut, Technische Universität München
Am Coulombwall 4, D-85748 Garching, Germany

Laser applications requiring single-mode, wavelength-tunable and/or low-power laser sources greatly benefit from using vertical-cavity surface-emitting lasers (VCSELs) instead of the more common edge-emitting semiconductor lasers. This particularly holds for tunable diode laser absorption spectroscopy (TDLAS), which is an import application field for near- and mid-infrared laser diodes [1]. Emitting in a single longitudinal mode with threshold currents of the order 1mA and high power-efficiency, near-infrared (up to ~1.3µm) VCSELs based on GaAs have conquered wide application areas ranging from high-bitrate datacom links to mass products such as laser mice [2, 3]. With successive improvements and advanced active region designs, their InP-based counterparts meanwhile cover the entire wavelength range from 1.3µm to about 2.6µm [4, 5]. These devices operate in a single transverse and longitudinal mode and can continuously be tuned without mode jumps over ~ 10 nm and ~ 100 nm by electrothermal and micromechanical tuning, respectively [6, 7]. Further extension into the mid-infrared has been achieved with GaSb-based VCSELs that today offer single-mode and tunable laser operation in the 2.3-3.0µm wavelength range [8, 9]. Experimental demonstrations of successful TDLAS applications have clearly proven the suitability of VCSELs, particularly in low-power and mobile systems [10].

We present advanced material concepts and quantum well designs to improve the long-wavelength performance of InP- and GaSb-based lasers and VCSELs. We describe in detail the device concept of the buried-tunnel-junction (BTJ-) VCSEL that revealed most successful for InP- and GaSb-based devices enabling high-performance continuous-wave lasing at room-temperature. Typically, the BTJ-VCSELs show polarization-stable single-mode lasing with threshold currents in the milliamp range and electrothermal tuning ranges of several nm. Finally, practical applications in TDLAS systems are demonstrated.

References

1. P. Werle. Spectrochimica Acta, Part A, Vol. 54, pp. 197–236, 1998.
2. W. H. Hofmann, P. Moser, D. Bimberg, IEEE Photonics Journal, vol. 4, pp. 652-656, 2012.
3. R. Michalzik (ed.). VCSELs, Springer, Heidelberg, Germany, pp. 521-538, 2013.
4. M. Ortsiefer et al. 20. IEEE Intl. Semicond. Laser Conf., Waikola, pp. 113-114, 2006.
5. S. Sprengel et al. Appl. Phys. Lett., vol. 106, pp 151102, 2015.
6. M. Ortsiefer et al. SPIE Photonics West, San Francisco, 2011.
7. T. Gründl et al. IEEE Phot. Technol. Lett., vol. 25, pp. 841-843, 2013
8. S. Arafin et al. 22. IEEE Intl. Semicond. Laser Conf., Kyoto, Japan, pp. 58-59, 2010.
9. A. Andrejew, S. Sprengel, M.-C. Amann. Opt. Lett., vol. 41, pp. 2799-2802, 2016.
10. J. Chen et al., Appl. Phys. B, vol. 102, pp. 381-389, 2011.

*corresponding author: mcamann@wsi.tum.de

*IR Technology Based on MBE HgCdTe: Current Status and Future Directions

S. Sivananthan *[1], S. Velicu [2]

[1] *University of Illinois at Chicago, Chicago, IL*

[2] *EPIR Inc., Bolingbrook , IL*

The molecular beam epitaxy (MBE) growth of HgCdTe enables the fabrication of multilayer structures for a large choice of infrared focal plane array (IRFPA) sensor designs. HgCdTe has two major advantages that explain its dominance in infrared photon detection. Its thermal generation rate per unit volume is lower, and its quantum efficiency for photon absorption in the infrared is higher, than in any competing material. We will discuss the material growth, fabrication and demonstration of low noise equivalent temperature difference (NETD), high operability IRFPAs fabricated from MBE-grown HgCdTe on Si-based and CdZnTe substrates. We will also discuss our R&D, focusing primarily on improving IRFPA operating conditions and adding new functionalities to the arrays.

We are implementing innovative multilayer structures to increase IRFPA operating temperatures. They are enabled by the MBE growth technique, and are capable of noise suppression and producing high signal-to-noise ratios. Noise suppression allows IRFPA integration in lighter and more compact sensor systems, and the transition of high-end sensor systems to the military and commercial markets. We have demonstrated the noise suppression concept with mid-, long- and very long-wavelength infrared (MWIR, LWIR and VLWIR) single element devices and are currently transitioning the technology to IRFPAs.

We will also present our work on developing a miniaturized infrared imaging spectrometer by coupling a HgCdTe-based IRFPA with a microelectromechanical systems (MEMS)-based Fabry-Perot filter. The filter's membranes are fabricated from silicon-on-insulator wafers using bulk micromachining technology. The fixed membrane is a standard silicon one, fabricated using a back etching processes. The movable membrane is implemented as an X-beam structure to improve mechanical stability.

Employing detectors with internal gain, such as avalanche photodiodes (APDs), is critical for low flux infrared detection. HgCdTe has fundamental properties that make it ideal for devices with internal gain. The small ratio of electron to hole effective masses and differences in carrier impact ionization threshold energies lead to a large difference in the impact ionization coefficients for electron and holes, enabling low excess noise, high gain bandwidth product APDs. We will present our work on short wavelength infrared (SWIR), MWIR and LWIR APDs with low excess noise and exponential gain increase.

*[1] siva@uic.edu

Tunable infrared response of nanostructures

Alessandro Tredicucci[1,2]*

[1] *Dipartimento di Fisica "E. Fermi", Università di Pisa, and NEST, Istituto Nanoscienze-CNR Largo Pontecorvo 3, I-56127 Pisa (Italy)*

[2] *Fondazione Bruno Kessler, Via Sommarive 18, I-38123 Povo, (Italy)*

Nanoplasmonics exploits light-matter interaction in nanostructures as a tool to tailor the optical response well below the diffraction limit. This possibility - combined with the continuing progress of miniaturization - is strongly contributing to the emergent field of nano-optoelectronics. Plasmonic systems are typically based on metals and devices such as resonators, antennas, emitters have been predicted and demonstrated using metallic systems. A major effort is dedicated today in expanding its scope to semiconducting materials, which add the exciting possibility of achieving electrically tunable and/or active devices. A remarkable example is provided by the recent progresses shown in graphene, where the high electron mobility allows a gate-tuning of the propagation of surface plasmons. Another idea is the excitation of localized plasmon resonances (LPRs), analogous to those of metallic nanoparticles, which could however be manipulated and transported in a sort of device circuit. Here I will examine a few such systems and device concepts which yield promise of developing new functionalities and enhanced operation performances.

*corresponding author: alessandro.tredicucci@unipi.it

Localized-field enhanced two-dimensional material infrared photodetectors

Wenjin Luo, Peng Wang, Hehai Fang, Man Luo, Jianlu Wang, Weida Hu, Xiaoshuang Chen and Wei Lu*

National Laboratory for Infrared Physics, Shanghai Institute of Technical Physics, Chinese Academy of Sciences, 500 Yutian Road, Shanghai 200083, China

* Corresponding author: luwei@mail.sitp.ac.cn

Two dimensional (2D) materials, especially graphene, transition metal dichalcogenides, and their heterostructures, have attracted intense attention owing to their bandgap tunability and potential optoelectrical applications. Diverse prototype 2D materials photodetectors based on different response mechanisms, such as the photovoltaic effect, photo-thermoelectric effect, photogating effect and bolometric effect, have been investigated to develop high-performance graphene detectors. Here, we report the controllable fabrication of localized-field enhanced 2D material structure used for infrared photodetector. With a hybrid-structure induced localized-field, the 2D material (graphene, MoS_2/PVDF, WS_2/graphene/MoS_2, GaSe/GaSb, etc.) has presented a good performance on the photo-electrical conversion process in the wavelength range from visible to near-infrared. Our study may open a new avenue for 2D material based infrared detector.

New Materials Approaches for Interband Mid-Infrared Photonic Devices

Stephen J. Sweeney[1*], Igor P. Marko[1]

[1] *Advanced Technology Institute and Department of Physics, University of Surrey, Guildford GU2 7XH, United Kingdom*

The incorporation of Bismuth into III-V semiconductors creates a range of possibilities for multiple applications in semiconductor lasers, photovoltaics, spintronics, and thermoelectrics. Adding Bi strongly reduces the bandgap, E_g, by ~80 meV/Bi% and ~56 meV/Bi% in GaAsBi and InGaAsBi, respectively. This also opens up the possibility to grow (In)GaAsBi material where the spin-orbit-splitting energy (Δ_{SO}) is greater than E_g and to push the corresponding emission wavelengths for GaAsBi/GaAs and InGaBiAs/InP alloys from the near-IR up to 6 μm while maintaining zero or low strain levels on standard InP substrates. Achieving the condition that $\Delta_{SO} > E_g$ is highly significant as it promises to suppress the dominant efficiency-limiting loss processes in infrared lasers, namely Auger recombination, involving the generation of "hot" holes in the spin-orbit split-off band (the so-called "CHSH" process), and inter-valence band absorption (IVBA), where emitted photons are re-absorbed in the active region, thereby increasing the internal optical losses and negatively impacting upon characteristics of laser and light emitting diodes [1]. We show that further flexibility can be achieved by adding nitrogen to the GaAsBi alloys on GaAs substrate [2], whereby lattice matched narrow band gap semiconductor heterostructures may be produced with the possibility of wide control of the conduction and valence offsets. Related opportunities also exist for type II GaAsN/GaAsBi zero net strain systems. In this study we combine both experiment (optical absorption, photo-luminescence and photo-modulated reflectance) and theory to study the key band-structure aspects of InGaBiAs/InP alloys as functions of composition and temperature. The band parameters, including E_g, band offsets, Δ_{SO} and strain of InGaAsBi alloys on InP [3] and GaAsBiN on GaAs [2] are considered in the context of photonic device applications with flexible control of the band offsets and spin-orbit splitting for the design of Auger-, IVBA-, and carrier leakage-free devices in mid-IR.

References

1. S. J. Sweeney et al., Bismuth-based semiconductors for mid-infrared photonic devices, 2015 IEEE Photonics Society Summer Topical Meeting Series (SUM), p 181-2 (2015)
2. S. J. Sweeney, S. R. Jin, Bismide-nitride alloys: Promising for efficient light emitting devices in the near- and mid-infrared, Journal of Applied Physics, Vol.113, 043110 (2013).
3. S. Jin, S. J. Sweeney, InGaAsBi alloys on InP for efficient near- and mid-infrared light emitting devices, Journal of Applied Physics, Vol.114, 213103 (2013).

*corresponding author: s.sweeney@surrey.ac.uk

Antimonide based Mid-Infrared Photonic Detectors and Focal Plane Arrays

Sanjay Krishna
Director, Center for High Technology Materials
Professor and Regents' Lecturer,
Department of Electrical and Computer Engineering,
University of New Mexico, Albuquerque NM

Infrared imaging (3-25 m) has been an important technological tool for the past sixty years since the first report of infrared detectors in 1950s. There has been a dramatic progress in the development of infrared antimonide based detectors and low power electronic devices in the past decade with new materials like InAsSb, InAs/GaSb superlattices and InAs/InAsSb superlattices demonstrating very good performance. One of the unique aspects of the 6.1A family of semiconductors (InAs, GaSb and AlSb) is the ability to engineer the bandstructure to obtain designer band-offsets. Our group (www.krishnairlab.com) has been exploring the vision of the 4th generation of infrared detectors.

In this talk, we will invesitigate some of the material science and device physics of the antimonide systems. I will describe some of the challenges in these systems including the identification of defects that limit the performance of the detector. The use of "unipolar barrier engineering" to realize high performance infrared detectors and focal plane arrays will be discussed. I will also explore the possibility of realizing the 4th Gen infrared imaging systems. Using the concept of a bio-inspired infrared retina, I will make a case for an enhanced functionality in the pixel. The key idea is to engineer the pixel such that it not only has the *ability* to sense multimodal data such as color, polarization, dynamic range and phase but also the *intelligence* to transmit a reduced data set to the central processing unit. The design and demonstration of meta-infrared detectors will be discussed.

Biography of the Speaker:

Sanjay Krishna is the Director of the Center for High Technology Materials and Professor and Regents Lecturer in the Department of Electrical and Computer Engineering at the University of New Mexico. Sanjay received his M.S. from IIT, Madras, MS in Electrical Engineering in 1999 and PhD in Applied Physics in 2001 from the University of Michigan. He joined UNM as a tenure track faculty member in 2001. He currently heads a group of 15 researchers involved with the development of next generation infrared imagers. Sanjay received the Gold Medal from IIT, Madras, Ralph Powe Junior Faculty Award, IEEE Outstanding Engineering Award, ECE Department Outstanding Researcher Award, School of Engineering Jr Faculty Teaching Excellence Award, NCMR-DIA Chief Scientist Award for Excellence, the NAMBE Young Investigator Award, IEEE-NTC, SPIE Early Career Achievement Award and the ISCS Young Scientist Award. He was also awarded the UNM Teacher of the Year and the UNM Regents Lecturer award. Sanjay has more than 200 peer-reviewed journal articles (h-index=42), two book chapters and seven issued patents. He is the co-founder and CTO of Skinfrared, a UNM start-up involved with the use of IR imaging for dual use applications including early detection of skin cancer. He is a Fellow of IEEE, OSA and SPIE.

Highly doped InAsSb nanoribbon on GaSb for plasmonics applications

M.J. Milla[1,2], F. Barho[1,2], M. Bomers[1,2], F. González-Posada[1,2], L. Cerutti[1,2,*], E. Tournié and T. Taliercio[1,2,*]

[1] *Univ. Montpellier, IES, UMR 5214, F-34000, Montpellier, France*
[2] *CNRS, IES, UMR 5214, F-34000, Montpellier, France*

During the last decade, plasmonic structures have been extensively investigated for the development of many applications fields including biosensing[1], nano-bio-photonics[2], and nanophotonics integrated circuits[3] among others. The traditionally used noble metals, such as gold and silver, are limited in the mid-IR range where molecules are distinguishable by their vibrational absorptions. Highly doped semiconductor (HDSC) show less losses in the mid-IR range and present a further degree of freedom thanks to the tuning of the plasma frequency by adjusting the doping level.

This work will demonstrate the potential of highly doped InAsSb grating on GaSb substrate for sensing applications. Because it is needed to control accurately the frequency of the localized surface plasmon resonance (LSPR), we have first developed a technique to determine precisely the plasma frequency and thus the doping level from the InAsSb layer based on the measure of the Brewster mode[4]. Thus, the figure 1 presents the tuning of the plasma frequency for 100 nm of InAsSb in dependence of the temperature of the Si doping cell. Then, the structure is processed by standard lithography and wet etching to form nanoribbons with a pattern of 2 μm pitch and adjustable width. Figure 2 shows the variation of the maximum reflection peak of the plasmonic structure, for different doping level as a function of the ribbon width. These results demonstrate the possibility of tuning the LSPR frequency, by either changing the doping level or designing the appropriate ribbon width.

To demonstrate the potential for sensing of the highly doped InAsSb nanoribbons, we have coated a sample with PDMS. As it showed in figure 3, it is possible to detect both shift of the LSPR related to change of the index surrounded the nanorribons and absorption due to surface enhanced infrared absorption (SEIRA) from the PDMS.

To conclude we have demonstrated a simple procedure to control accurately the LSPR of InAsSb nanoribbons with a high potential for mid-IR bio-sensing plasmonic applications.

This work was partially funded by the French "Investment for the Future" program (EquipEx EXTRA, ANR 11-EQPX-0016), by the French ANR (SUPREME-B, ANR-14-CE26-0015), by the "Languedoc-Roussillon-Midi-Pyrénées region", and European Union H2020 Program (PROMIS ITN European network grant agreement No. 641899).

References

[1] K.M. Mayer, J.H. Hafner, and A.À. Antigen, Chem. Rev. **111**, 3828 (2011).

[2] A. V. Zayats, I.I. Smolyaninov, and A.A. Maradudin, Phys. Rep. **408**, 131 (2005).

[3] A. V. Kabashin, P. Evans, S. Pastkovsky, W. Hendren, G.A. Wurtz, R. Atkinson, R. Pollard, V.A. Podolskiy, and A. V. Zayats, Nat. Mater. **8**, 867 (2009).

[4] T. Taliercio, V.N. Guilengui, L. Cerutti, E. Tournié, J.J. Greffet, Opt. Express **22**, 24294 (2014).

*corresponding author: Laurent.cerutti@umontpellier.fr , Thierry.taliercio@umontpellier.fr

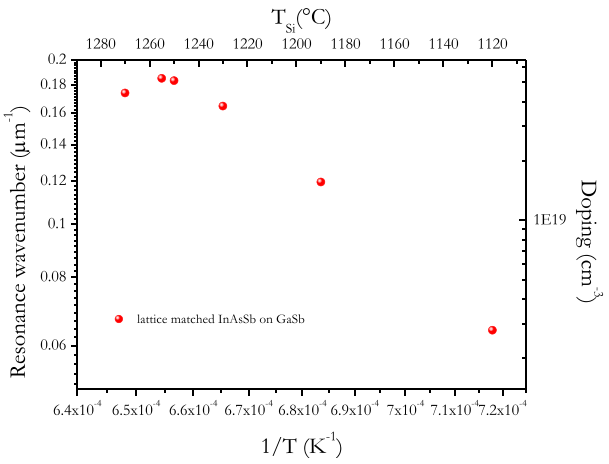

Fig.1. Variation of the plasma frequency and doping concentration function of the temperature of the Si dopant cell for a 100 nm of $InAs_{0.92}Sb_{0.08}$ grown by MBE.

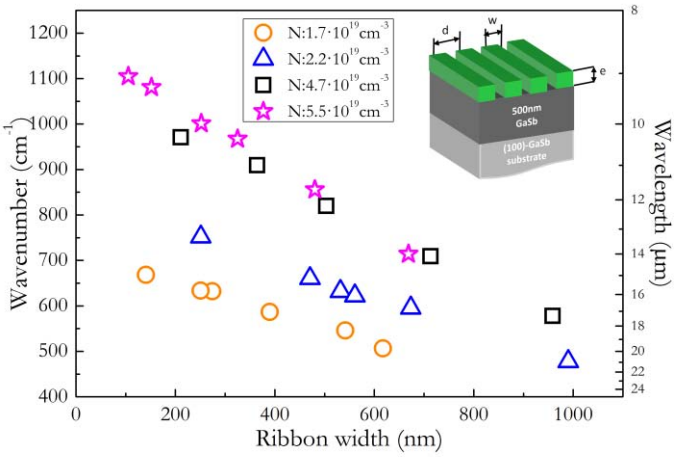

Fig.2. Evolution of the LSPR plasmon resonance (maximum peak) for different doped structures as a function of the ribbon width (w)

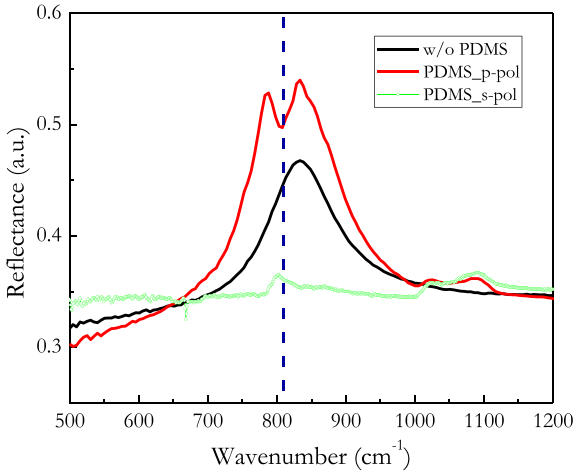

Fig. 3. Evolution of the reflectance spectra coated with and without PDMS, showing both spectral shift due to the change in optical index of the environment and enhanced absorption at 800 cm^{-1} related to the absorption of the C-Si-C stretching.

GeSn Alloys for Mid-Infrared Optoelectronics

T. Eales[1], I. Marko[1], S. A. Ghetmiri[2], W. Du[2], Y. Zhou[2], S. Yu[2], J. Margetis[3], J. Tolle[3], S. Schulz[4], E. O'Halloran[4], E. P. O'Reilly[4] and Stephen J. Sweeney[1]*

[1] *Advanced Technology Institute and Department of Physics, University of Surrey, Guildford, GU2 7XH, United Kingdom*

[2] *Department of Electrical Engineering, University of Arkansas, Fayetteville, AR, USA, 72701*

[3] *ASM, 3440 East University Drive, Phoenix, Arizona 85034, USA*

[4] *Tyndall National Institute, Lee Maltings, Cork, Ireland*

The mid-infrared spectral region contains a number of significant spectral features, offering applications in free space communications and lab-on-chip trace gas detection. Mid-infrared light sources compatible with current silicon CMOS technology is one of the most important milestones in achieving fully integrated optoelectronics.[1] Due to the small energy difference between the L and Γ conduction band minima in Ge, the optical properties are readily augmentable through band engineering. Introducing tin (Sn) into the Ge lattice reduces the energy of the Γ valley relative to the L valley. However, significant discrepancies exist in the literature for the Sn concentration at which GeSn becomes direct and the extent to which a GeSn alloy may provide a direct band gap across the mid-infrared. An improved understanding of the bandgap character in GeSn is necessary to address these ambiguities in the literature. To identify the character of the band edge in GeSn, we use photocurrent spectroscopy under high hydrostatic pressure to determine its movement under pressure. This approach reversibly manipulates the band structure by shifting the conduction band Γ- and L-minima upwards in energy at different rates as a function of pressure. For Ge, dE_Γ/dP = 12.9meV/kbar and dE_L/dP = 4.3meV/kbar. Using this method, the pressure dependence of the bandgap for the three GeSn samples was measured. Further details of the samples can be found in Ref. [2]. The change in the band edge with pressure for the three Sn concentrations is displayed in figure 1. In these measurements we do not observe a sharp transition from an indirect to direct bandgap behavior. Instead, the character of the band edge dependence on pressure changes smoothly with Sn concentration. This is investigated theoretically through DFT-HSE calculations of the band structure of ordered GeSn supercells. The theoretical variation of the band gap for a $Ge_{0.94}Sn_{0.06}$ supercell is plotted in figure 2, showing good agreement with the experimental data; the implications of which will be discussed further at the conference.

References

1. Z. Zhou, B. Yin, J. Michel, On-chip light sources for silicon photonics, Light: Science and Applications, Vol.4, N.11, pp. e358, 2015.
2. Wei Du, et al, Room-temperature electroluminescence from Ge/Ge1-xSnx/Ge diodes on Si substrates, Applied Physics Letters, Vol.104, pp. 241110, 2014.

*corresponding author: s.sweeney@surrey.ac.uk

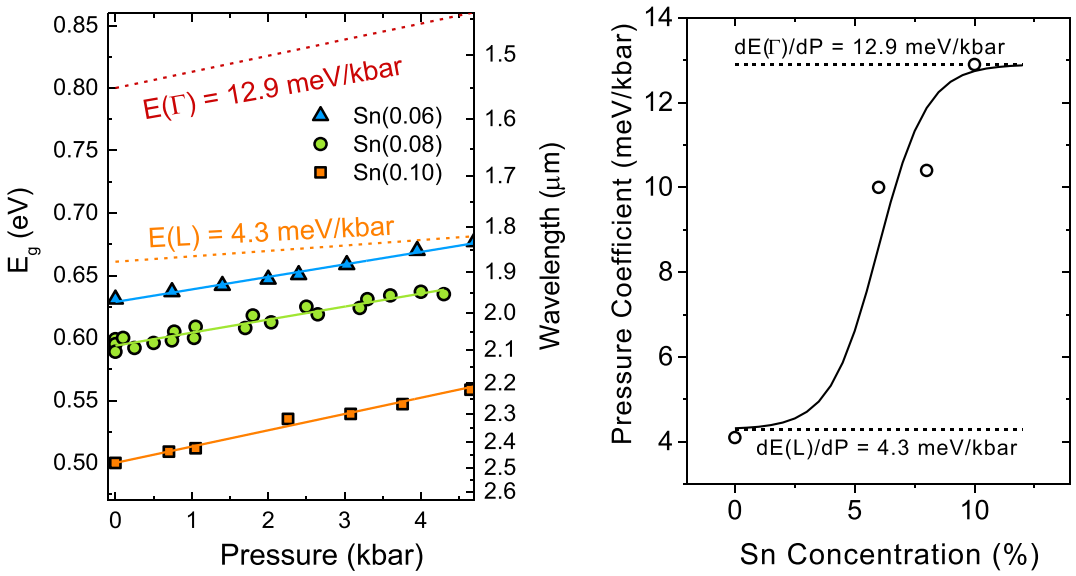

Fig.1. a) The movement of the absorption edge under pressure in GeSn with different Sn concentrations. The dashed lines correspond to the pressure dependence of the Γ and L minima band gaps in Ge. b) The pressure coefficient as a function of Sn concentration, the sigmoidal fit shows the expected functional dependence.

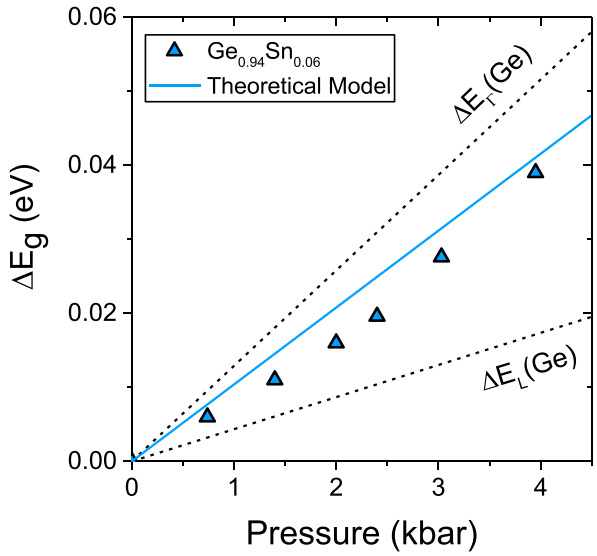

Fig.2. Comparison between the experimental and theoretical movement of the band edge for the $Ge_{0.94}Sn_{0.06}$ sample. The theoretical results were obtained through DFT-HSE calculations of the band structure of a $Ge_{15}Sn_1$ supercell as a function of applied hydrostatic pressure, using VASP.

Heterogeneous integration of InP-based type-II active devices on silicon for 2 μm wavelength range on-chip spectroscopy

Ruijun Wang[1,2]*, Stephan Sprengel[3], Muhammad Muneeb[1,2], Gerhard Boehm[3], Aditya Malik[1,2], Roel Baets[1,2], Markus-Christian Amann[3], Gunther Roelkens[3]

[1] *Photonics Research Group, Ghent University-imec, Technologiepark-Zwijnaarde 15 iGent, 9052 Ghent, Belgium*

[2] *Center for Nano- and Biophotonics (NB-Photonics), Ghent University, Ghent, Belgium*

[3] *Walter Schottky Institut, Technische Universität München, Am Coulombwall 4, 85748 Garching, Germany.*

Silicon photonics has emerged as one of the most prominent integrated photonics platforms as it takes advantage of mature CMOS processes, allowing the fabrication of large scale photonic circuits with low cost. Since many important industrial gases have strong absorption lines in the 2 μm wavelength range, the development of silicon photonic ICs in this wavelength range enables many applications.

Here we present the heterogeneous integration of InP-based type-II active devices on silicon-on-insulator (SOI) waveguide circuits for on-chip spectroscopy. Adhesive bonding technology using a 100 nm thick benzocyclobutene layer as bonding agent is used to integrate III-V devices on SOI. The active region of the heterogeneously integrated III-V devices consists of a "W"-shaped InGaAs/GaAsSb quantum well structure, which was used to realize InP-based type-II lasers for wavelengths up to 2.7 μm. Figure 1(a) shows a microscope image of an InP-based type-II superluminescent light emitting diode (SLED) integrated with an SOI arrayed waveguide grating (AWG). The light is efficiently coupled from the III-V active region to the silicon waveguide using a spot size converter by tapering both the III-V waveguide and silicon waveguide. Broadband light between 2.2 μm and 2.45 μm with peak position around 2.35 μm is coupled to the AWG as shown in Fig. 1(b). The broadband light is filtered by the AWG and coupled to different channels with a channel spacing of 5 nm and free spectral range of 50 nm. The AWG insertion loss and crosstalk is estimated to be 3 dB and -22 dB, respectively. Besides light sources, photodetectors are also one of the key components that should be developed for a functional integrated spectroscopic system. An array of adiabatically-coupled photodetectors is integrated with an SOI AWG spectrometer as shown in Fig. 2(a). The light is coupled from silicon waveguide to photodetector absorbing active region using a similar taper structure as above. The photodetectors show a responsivity of 1.6 A/W at 2.35 μm wavelength and dark current of 10 nA at −0.5 V. With integrated photodetectors, the AWG exhibits an insertion loss of 3dB and crosstalk level of -27dB. The type-II structure used for integrated photodetectors is same to what is used for the SLED, which enables the realization of a fully integrated spectroscopic sensing system.

*corresponding author: ruijun.wang@intec.ugent.be

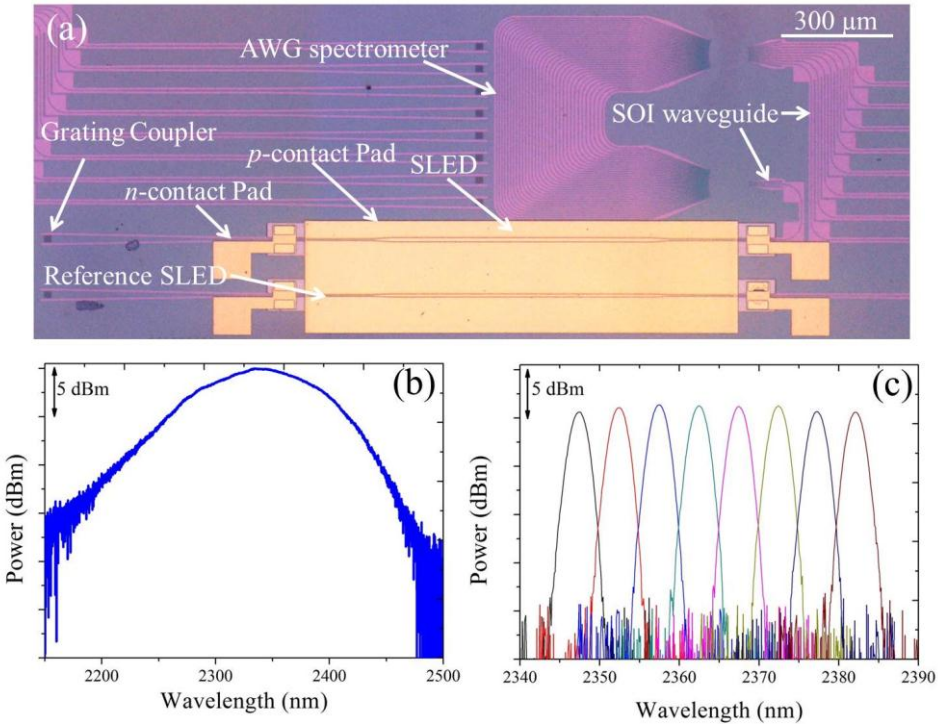

Fig.1. (a) Microscope image of an AWG integrated with an InP-based type-II SLED, (b) fiber-coupled emission spectrum of the heterogeneously integrated SLED, (c) filtered spectrum of the light coupled from SLED to the different channels of the AWG.

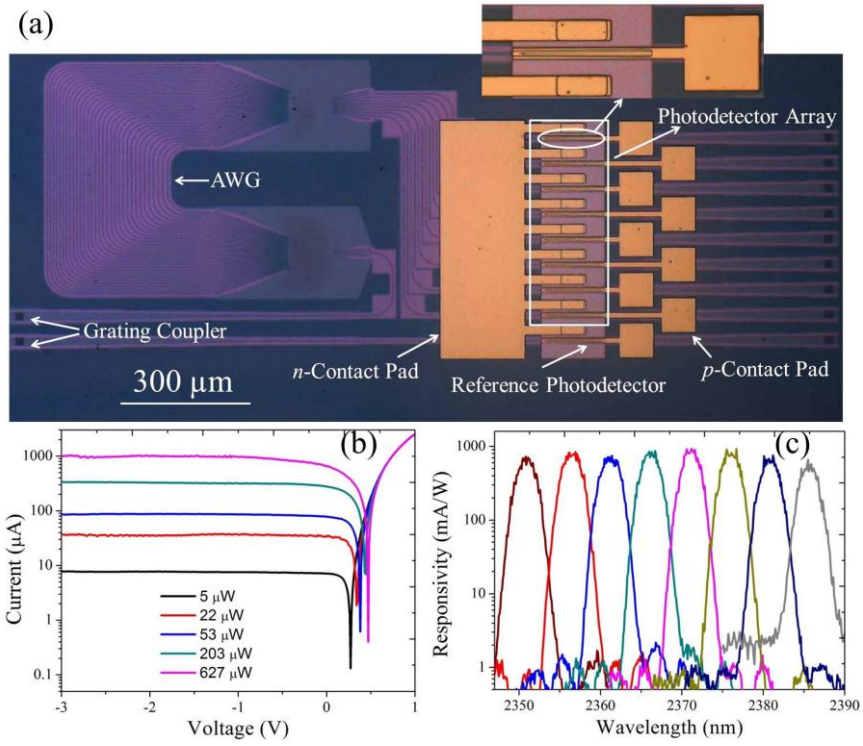

Fig.2. (a) Microscope image of an AWG integrated with InP-based type-II photodetectors, (b) photoresponse of the heterogeneously integrated photodetector under different input power, (c) response of the AWG spectrometer integrated with type-II photodetectors.

Mid-infrared InP-based Quantum Wells with Bismuth Surfactant or Incorporation

Y. Gu, Y. G. Zhang, X. Y. Chen, S. P. Xi, B. Du, Y. J. Ma, W. Y. Ji, Y. H. Shi, A. Z. Li

State Key Laboratory of Functional Materials for Informatics, Shanghai Institute of Microsystem and Information Technology, Chinese Academy of Sciences, Shanghai, China

InP-based pseudomorphic and metamorphic In(Ga)As quantum wells (QWs) with indium content higher than 0.53 are very attractive to demonstrate mid-infrared lasers beyond 2 μm. Recently, pseudomorphic InAs/InGaAs triangular QW (TQW) lasers at 2.4 μm and metamorphic InAs QW lasers at 2.9 μm have been demonstrated on InP [1,2]. However, further extending of lasing wavelength is limited by the lattice-mismatch and reduced carrier confinement in the QW. The incorporation of bismuth (Bi) into traditional III-V material can dramatically narrow the bandgap and increase the valence band offset between QW and barrier layers, where the material needs to be grown at a relatively low temperature. Meanwhile, Bi acts as a surfactant when the material is grown at normal growth temperature. In this presentation, we will introduce our recent work on applying Bi in 2-3 μm InP-based QWs.

To investigate the effects of Bi surfactant, a series of pseudomorphic InAs/InGaAs TQW samples were grown on InP at normal growth temperatures and the schematic structure is shown in the inset of Fig. 1. The nominal 10 nm TQW structure was grown using the digital alloy technology and constructed by 10 pairs of ultra-thin InAs/$In_{0.53}Ga_{0.47}As$ layers. For the samples grown under moderate Bi flux, the surface morphology is smoother, and X-ray diffraction curve shows more distinct satellite peaks. As shown in Fig. 1, photoluminescence (PL) signals at around 2.2 μm were observed at room temperature (RT). The PL intensity was significantly enhanced for the samples with Bi surfactant, which is very promising to improve the optoelectronic performances of those strained QWs.

To extend the emission wavelength longer, an $In_{0.83}Al_{0.17}As$ metamorphic layer was grown on an $In_xAl_{1-x}As$ graded buffer, where x was from 0.52 to 0.83. InAsBi/$In_{0.83}Al_{0.17}As$ single QW samples were then grown on the metamorphic structure and an InAs QW was also grown for reference. The nominal thickness of the QW was about 15 nm. The buffer and cap layers were grown at normal growth temperatures, and the substrate temperature was reduced for the QW growth. As shown in Fig. 2, PL signal beyond 3.1 μm was observed at 300 K, which was longer than the reference InAs QW sample. The PL intensity of InAsBi QW was decreased to about half of the reference sample. The samples will be characterized transmission electron microscope and the results will be shown in the presentation.

References

1. Y. Gu, Y. G. Zhang, Y. Y. Cao, et al., Appl. Phys. Express 7, 032701 (2014).
2. Y. Gu, Y. G. Zhang, Y. J. Ma, et al., Appl. Phys. Lett. 106, 121102 (2015).

*corresponding author: ygzhang@mail.sim.ac.cn

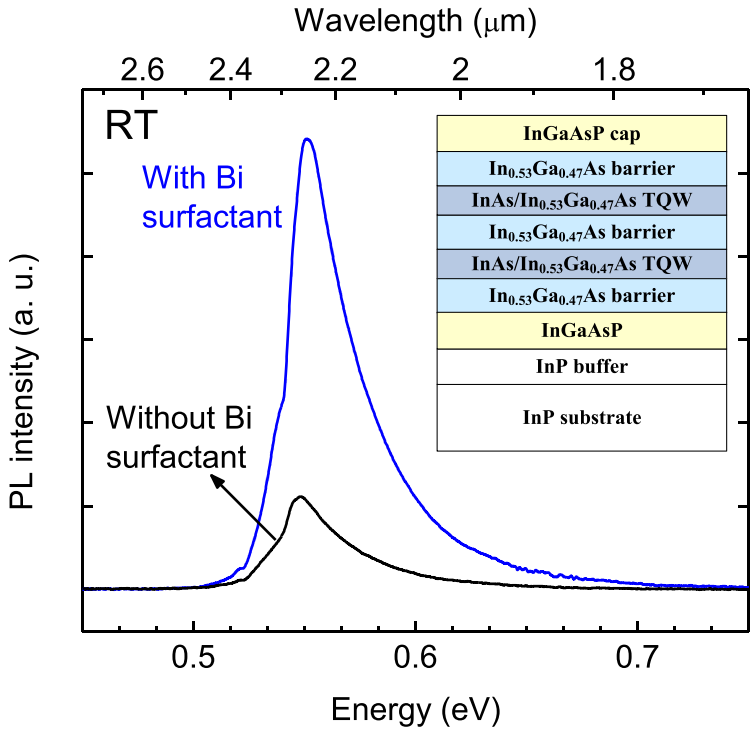

Fig.1. PL spectra of the InP-based InAs/InGaAs TQW samples grown with and without Bi surfactant. The inset shows the schematic structure.

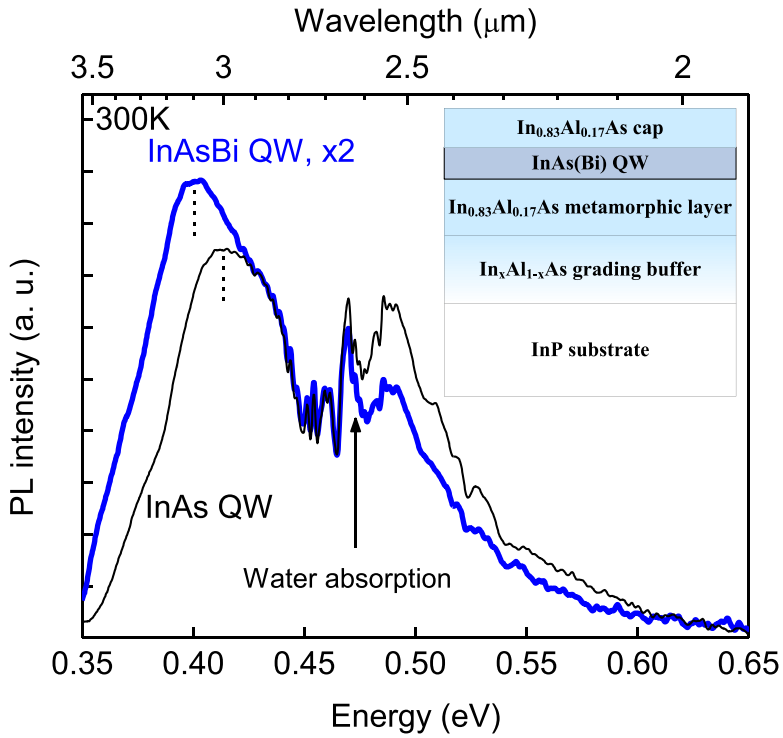

Fig.2. PL spectra of InP-based InAsBi and InAs QW samples on $In_{0.83}Al_{0.17}As$ metamorphic layers. The inset shows the schematic structure.

InAs/InAsSb type-II superlattices: material properties and device applications

Yong-Hang Zhang
School of Electrical, Computer and Energy Engineering
Arizona State University
Tempe, Arizona 85287
Email:yhzhang@asu.edu

Abstract:

This talk will review the research on Ga-free InAs/InAsSb type-II superlattices (T2SL), especially their growth, structural and electronic properties, and applications to IR lasers and photodetectors with the following highlights: 1) Review of the previous study of InAs/InAsSb T2SL and its application to IR lasers and photodetectors in the 90's. 2) Long minority carrier lifetime up to 12.8 μs in mid-wavelength infrared (MWIR) InAs/InAsSb T2SL was observed at 15 K, and 412 ns for long-wavelength infrared (LWIR) InAs/InAsSb T2SL were measured using time-resolved photoluminescence. The record long carrier lifetime in the MWIR range is due to carrier localization, which is confirmed by a 3 meV blue shift of the photoluminescence peak energy with increasing temperature from 15 K to 50 K, along with a photoluminescence linewidth broadening up to 40 K. In contrast, no carrier localization is observed in the LWIR T2SL. Modeling results show that carrier localization is stronger in shorter period (9.9 nm) MWIR T2SL as compared to longer period (24.2 nm) LWIR T2SL, indicating that the carrier localization originates mainly from InAs/InAsSb interface disorder. Although carrier localization enhances carrier lifetimes, it also adversely affects carrier transport. 3) Pressure-dependent photoluminescence (PL) experiments under hydrostatic pressures up to 2.16 GPa were conducted on a MWIR InAs/InAsSb T2SL structure at different pump laser excitation powers and sample temperatures. The results show a pressure coefficient of the T2SL transition was found to be 93 ± 2 meV·GPa^{-1}; a clear change in the dominant photo-generated carrier recombination mechanism from radiative to defect related, providing evidence for a defect level situated at 0.18 ± 0.01 eV above the conduction band edge of InAs at ambient pressure. 4) LWIR InAs/InAsSb T2SL nBn photodetectors on GaSb substrates were demonstrated. The typical device consisted of a 2.2 micron thick absorber layer and has a 50% cutoff wavelength of 13.2 μm, a measured dark current density of 5e-4 A/cm^2 at 77 K under a bias of -0.3 V, a peak responsivity of 0.24 A/W at 12 μm and a maximum RA product of 300 ohm-cm^2 at 77 K. The calculated generation-recombination noise limited specific detectivity (D*) and experimentally measured D* at 12 μm and 77 K are 1e10 (cm-Hz$^{1/2}$)/W and 1e8 (cm-Hz$^{1/2}$)/W, respectively.

Recent Progress in Mid-wavelength Infrared Type-II Superlattices

E. H. Steenbergen,[1]* G. Ariyawansa,[2] C. J. Reyner,[2] H. Bourassa,[3]
J. M. Duran,[2] J. D. Reding,[2] and J. E. Scheihing[2]

[1]*Air Force Research Laboratory, Space Vehicles Directorate, Kirtland AFB, NM 87117*
[2]*Air Force Research Laboratory, Sensors Directorate, Wright-Patterson AFB, OH 45433*
[3]*Air Force Research Laboratory, Materials & Manufacturing Directorate, Wright-Patterson AFB, OH 45433*

The last two decades have seen tremendous progress in the design and performance of mid-wavelength infrared (MWIR) type-II superlattices (T2SL) for detectors. The materials of focus have evolved from the initial InAs/(In)GaSb T2SL to include InAs/InAsSb T2SLs and most recently InGaAs/InAsSb SLs, with each materials system offering particular advantages and disadvantages. However, all the SLs have the advantages of tunable infrared bandgaps, higher electron effective masses to reduce tunneling currents, and, in theory, the ability to suppress Auger recombination by design and thereby achieve longer minority carrier lifetimes than bulk materials. At this point in time, the T2SLs have not yet achieved the theoretically-predicted Auger-limited performance due to Shockley-Read-Hall recombination and high background carrier concentrations in the superlattice.

As the material quality of the InAs/(In)GaSb superlattices increased to the point of being viable for devices, the problem of short minority carrier lifetimes was exposed [1]. Then InAs/InAsSb superlattices were found to have longer minority carrier lifetimes [2] at the cost of lower absorption coefficients due to smaller band offsets than those of the InAs/(In)GaSb superlattices. Part of the reason for the longer minority carrier lifetime in InAs/InAsSb superlattices has been found to be due to carrier localization [3] from the group-V As/Sb interface intermixing. Figure 1 shows the temperature-dependent photoluminescence (PL) peak position and peak full-width-half-maximum (FWHM) of a MWIR InAs/InAsSb T2SL with the signatures of carrier localization: peak position blue shift and non-monotonic FWHM below the delocalization temperature (40 K). For devices operating above the delocalization temperature, it is expected that the effects of carrier localization will be minimal. However, if the operating temperature is within the localization regime, the collection of photogenerated carriers may be impeded by localization and may result in a lower detector quantum efficiency (QE). To address the lower absorption coefficient of InAs/InAsSb superlattices, the InGaAs/InAsSb superlattices have been designed to be lattice matched to GaSb with equal layer thicknesses, and a 30-35% increase in the absorption coefficient as compared to the reference InAs/InAsSb superlattice design has been demonstrated for an InGaAs/InAsSb superlattice with 20% Ga [4]. Figure 2 also reveals evidence of carrier localization in the InGaAs/InAsSb superlattices but with higher delocalization temperatures (60 – 80 K), indicating greater composition variation. Despite the localization at low temperatures, the nBn device with 20% Ga in the absorber has higher QE from 80 – 150 K than the device with 0% Ga, possibly indicating greater vertical hole mobility. Further comparisons between the different superlattice photoluminescence spectra and device characteristics will be presented.

References

1. D. Donetsky, S. P. Svensson, L. E. Vorobjev, G. Belenky, Carrier lifetime measurements in short-period InAs/GaSb strained-layer superlattice structures, Appl. Phys. Lett. 95, 212104 (2009).
2. E.H. Steenbergen, B.C. Connelly, G.D. Metcalfe, H. Shen, M. Wraback, D. Lubyshev, Y. Qiu, J.M. Fastenau, A.W.K. Liu, S. Elhamri, O.O. Cellek, Y.-H. Zhang, Significantly improved minority carrier lifetime observed in a long-wavelength infrared III-V type-II superlattice comprised of InAs/InAsSb, Appl. Phys. Lett 99, 251110 (2011).
3. Z.-Y. Lin, S. Liu, E. H. Steenbergen, and Y.-H. Zhang, Influence of carrier localization on minority carrier lifetime in InAs/InAsSb type-II superlattices, Appl. Phys. Lett 107, 201107 (2015).

*Corresponding Author: Elizabeth.Steenbergen.1@us.af.mil

4. G. Ariyawansa, C J. Reyner, E. H. Steenbergen, J. M. Duran, J. D. Reding, J. E. Scheihing, H. R. Bourassa, B. L. Liang, D. L. Huffaker, InGaAs/InAsSb strained layer superlattices for mid-wave infrared detectors, Appl. Phys. Lett. 108(2), 022106 (2016).

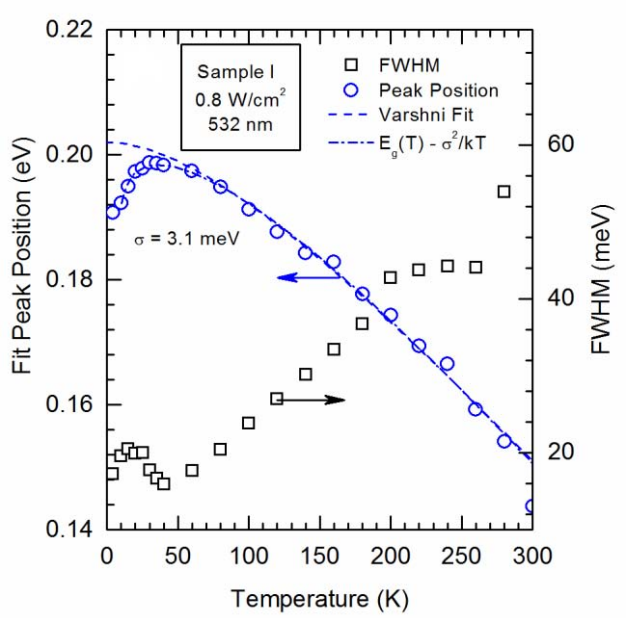

Figure 1. PL peak position (left axis) and FWHM (right axis) vs. temperature for a MWIR InAs/InAsSb T2SL. The PL peak blue shift and non-monotonic FWHM at low temperatures indicate carrier localization.

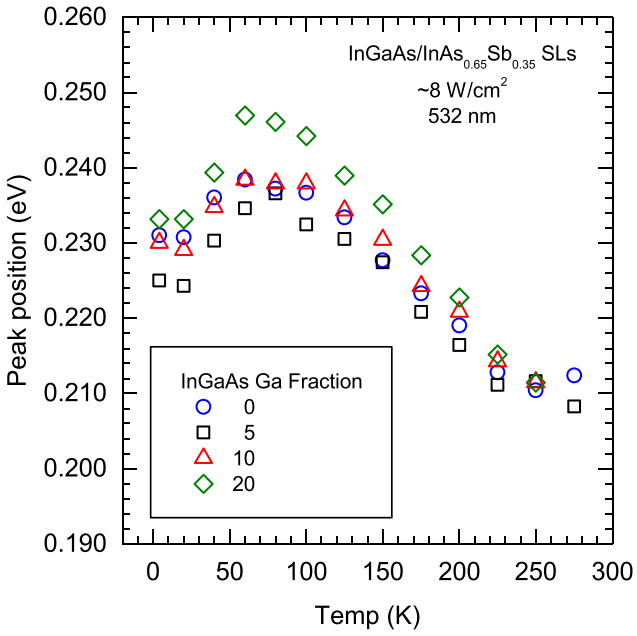

Figure 2. PL peak position vs. temperature for a set of MWIR InGaAs/$InAs_{0.65}Sb_{0.35}$ superlattices, also indicating low temperature carrier localization.

*Corresponding Author: Elizabeth.Steenbergen.1@us.af.mil

Recent progress on HgCdTe/ZnCdTe by MBE

Lu Chen*, Xiangliang Fu, Yushun Chen, Weiqiang Wang, ChuanShen, Gao Wang, Shundong Bu, Bin Zhang, Feng Yang, Yin Wang, Li He

Key lab of advanced materials and devices, Shanghai institute of Technical Physics, CAS, China
500# Rd. Yutian, Shanghai, China, 200083

Abstract:
High performance LW HgCdTe IRFPAs on ZnCdTe were demonstrated by many published papers. Compared with the results on alternative substrates, the crystal quality advantages of HgCdTe on ZnCdTe have been indicated in LW device fabrications. Recent progress on HgCdTe/ZnCdTe by MBE was reported. The improvement of crystal quality and surface morphology on Hg1-xCdxTe/ZnCdTe(x=0.21-0.23) were studied, which were evaluated by FWHM of XRD DCRC and SEM. The relations between HgCdTeFWHM and lattice mismatch, substrates quality, growth conditions as well, were clarified. It was found that lattice mismatch between HgCdTe and ZnCdTe substrate(a_{mct}-a_{zct}/a_{zct}) greatly effects on the performance of epilayers, while it was inappreciable with growth temperature. To obtain good layer with FWHM less than 30arcsec, the optimal lattice mismatch should be in the range of 0-0.05%. The average EPD on 10μm HgCdTe was less than 1 ×10^{-5} cm^{-2}, with the best result of 3 × 10^{4} cm^{-2}. The average FWHM valve across whole wafer was less than 25arcsec.It was also demonstrated by reproducible experiments that theneedle defects and diamond shaped defects were significantly related with substrate chemical polishing treatment. Macro defect density was less than 200cm^{-2} by improved polishing process.

Keywords:
HgCdTe, ZnCdTe, IRFPAs, MBE

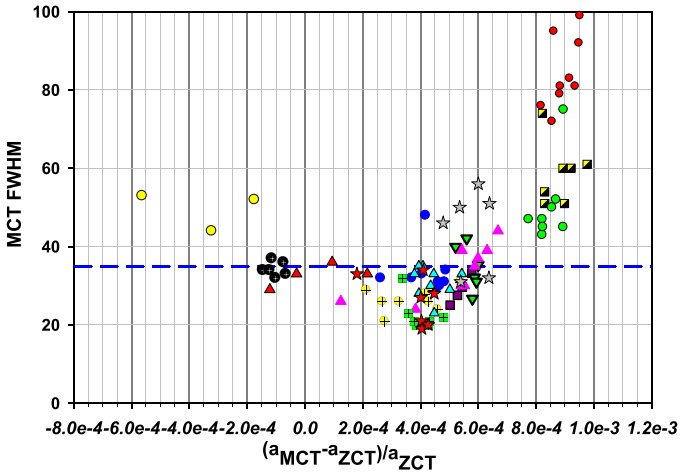

Fig1. FWHM of HgCdTe vs lattice mismatch

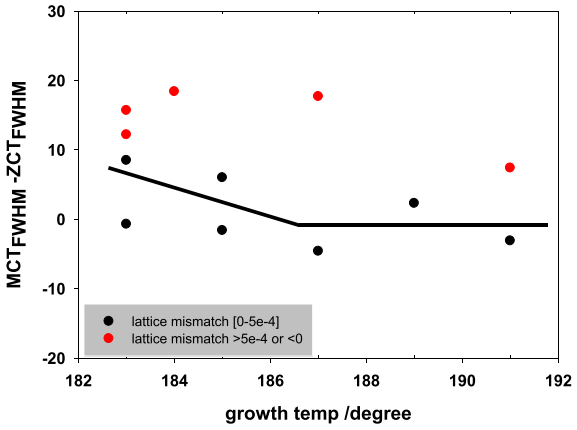

Fig2. The effects of growth temperature and lattice is mismatch on crystal quality

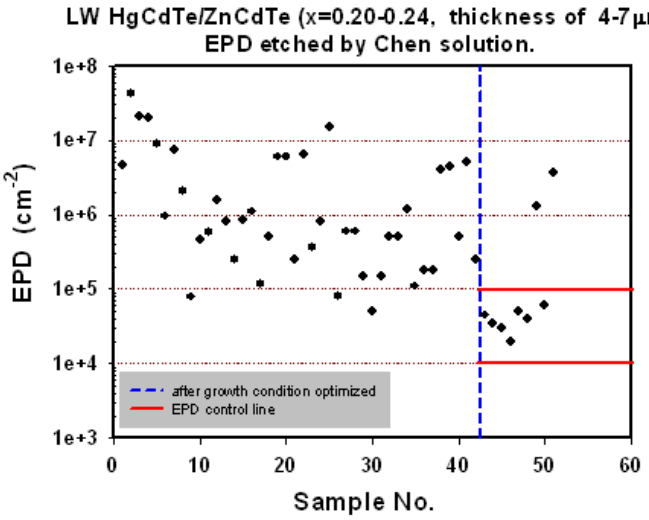

Fig3. EPD results by run-to-run

High quantum efficiency in InAs/GaSb superlattice for very long wavelength detection with cutoff of 21 μm

Guowei Wang[1,2*], Dongwei Jiang[1,2], Wei Xiang[1,2], Hongyue Hao[1,2], Xi Han[1,2], Yingqiang Xu[1,2], Zhichuan Niu[1,2]

[1] *State Key Laboratory for Superlattices and Microstructures, Institute of Semiconductors, Chinese Academy of Sciences, Beijing 100083, China.*

[2] *Synergetic Innovation Center of Quantum Information and Quantum Physics, University of Science and Technology of China, Hefei, Anhui 23026, China.*

In the past three decades, since Esaki and Tsu [1] introduced the type-II InAs/GaSb superlattices (T2SL), it emerges as a good candidate for infrared detector especially for long and very long wavelength detection. Two parameters to measure the performance of the detectors are the differential resistance area product at zero bias (R_0A) and the quantum efficiency (QE). Improving R_0A and QE is the ultimate goal for any device to increase its specific detectivity $D^* \propto QE\sqrt{R_0A}$. Usually, the performances trends of the QE and the R_0A trend in opposite directions [2] so that one often has to sacrifice one quantity in order to improve the other. In long wavelength detectors, especially in very long wavelength detectors, QE is always not the main optimization parameter due to the limitation of material quality or the special needs of high R_0A to match the readout integrated circuits in FPAs. However, it seems the QE contributes more efficiently to the increase of D^* than R_0A.

In this paper, we report the dependence of the quantum efficiency on beryllium concentration in the active region of type-II InAs/GaSb superlattice infrared detector with a cutoff wavelength around 21 μm. It is found that the quantum efficiency and responsivity show a clear delineation in comparison to the doping concentration, as shown in Fig.1. The quantum efficiency is further improved by gradually doping in the absorbing region. At 77K, the 50% cutoff wavelength of the VLWIR detector is 18 μm, and the R_0A is kept at a stable value of 6 Ωcm^2. Different beryllium concentration leads to an increase of an average quantum efficiency in the 8-15 μm window from 35% to 55% with a π-region thickness of 3.0 μm, for Ubias = -0.3 V, and no anti-reflection coating. As for a further result, the quantum efficiency reaches at a maximum value of 66% by gradually doping in the absorbing region with the Johnson Detectivity of 3.09×10^{11} cm $Hz^{1/2}$/W at 15 μm.

References

1. L. Esaki and R. Tsu, IBM J. Res. Dev. ,Vol.14, pp.61-65, 1970
2. M. Walther, J. Schmitz, R. Rehm, S. Kopta, F. Fuchs, J. Fleißner, W. Cabanski, and J. Ziegler, J. Cryst. Growth , Vol.278, pp.156–161. 2005

***corresponding author**: wangguowei@semi.ac.cn*

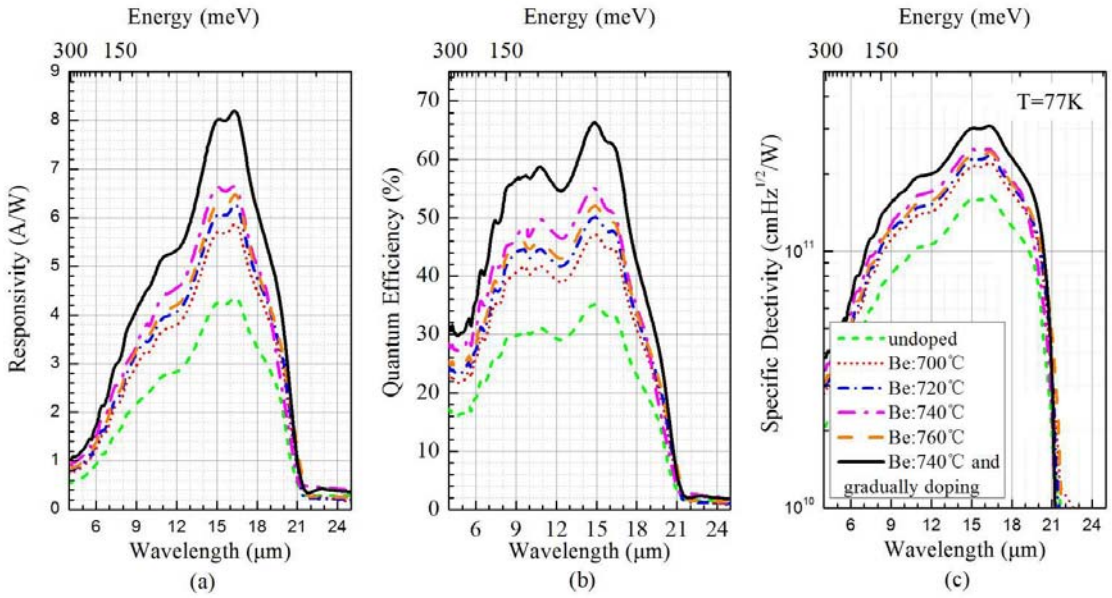

Fig. 1. Spectral response measured at 77K of devices with π-region Be doped ranging from undoped to 760℃. (a) shows the absolute responsivity, (b) shows the quantum efficiency, and (c) shows the specific detectivity.

InP-based metamorphic avalanche photodiodes towards detecting of MWIR wavelengths

Y. J. Ma[1], Y. G. Zhang[1,*], Y. Gu[1], X. Y. Chen[1], Y. H. Shi[1], W. Y. Ji[1], S. P. Xi[1], B. Du[1], H. J. Tang[2], Y. F. Li[3], and J. X. Fang[2,3]

[1] *State Key Laboratory of Functional Materials for Informatics, Shanghai Institute of Microsystem and Information Technology, Chinese Academy of Sciences, Shanghai, China*

[2] *Key Laboratory of Infrared Imaging Materials and Devices, Shanghai Institute of Technical Physics, Chinese Academy of Sciences, Shanghai, China*

[3] *Advanced Research Center for Optics, Shandong University, Jinan, China*

Avalanche photodiodes (APDs) operating at long IR wavelengths are attractive for various applications, including new generation optical communication networks, LIDAR system to profile gas distribution, defense and imaging; particularly where weak signals are of concern. Existing commercially available APDs based on Si and $In_{0.53}Ga_{0.47}As$/InP have only been able to cover the optical spectrum at $\lambda<1.6$ μm satisfactorily. An increasing amount of research is now focusing on the development of high performance wavelength extended APDs. HgCdTe [1] and InAs [2] p-i-n homojunction APDs, as well as InGaAsSb/AlGaAsSb [3] and $In_{0.53}Ga_{0.47}As$-$GaAs_{0.51}Sb_{0.49}$ type-II SL/InP [4] separated absorption, charge and multiplication (SACM) APDs have been demonstrated in the lattice-matched regime, exhibiting responsivity gains in 2-4.3 μm albeit at the expense of relatively high dark currents or low operating temperatures. By contrast, metamorphic growth in the lattice-mismatched regime can greatly expand the freedom in designing of APDs with longer wavelengths by taking advantage of advanced heteroepitaxy techniques.

We demonstrate a metamorphic $In_{0.75}Ga_{0.25}As/In_{0.52}Al_{0.48}As$ SACM APD with cutoff wavelength up to 2.25 μm on InP substrate. Photons are absorbed in a metamorphic $In_{0.75}Ga_{0.25}As$ layer while the photo-generated electrons are injected into a lattice-matched $In_{0.52}Al_{0.48}As$ multiplier on InP. A responsivity gain of 4 is attained at 250 K and increases to 22 at 77 K. A primary dark current of 2.2×10^{-3} A/cm^2 at -15 V is measured at 77 K, which is dominated by dislocation defect-assisted tunneling with activation energies between 0.1 to 0.2 eV. This demonstration opens up the possibility towards high performance wavelength extended or MWIR APDs with great freedom in tailoring the cutoff wavelengths.

References

1. S. Bailey, W. McKeag, J. Wang, M. Jack, and F. Amzajerdian, Proc. SPIE 7660, 76603I (2010).
2. S. J. Maddox, W. Sun, Z. Lu, H. P. Nair, J. C. Campbell, and S. R. Bank, Appl. Phys. Lett. 101, 151124 (2012).
3. E. K. Duerr, M. J. Manfra, M. A. Diagne, R. J. Bailey, J. P. Donnelly, M. K. Connors, and G. W. Turner, Appl. Phys. Lett. 91, 231115 (2007).
4. R. Sidhu, L. Zhang, N. Tan, J. C. Campbell, A. L. Holmes, C. F. Hsu, and M. A. Itzler, Electron Lett. 42, 181 (2006).

*corresponding author: ygzhang@mail.sim.ac.cn

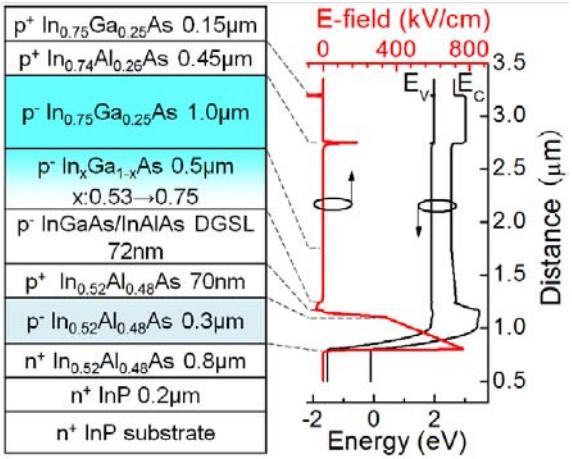

Fig.1. Schematic of the metamorphic APD structure and the calculated -2 V biased energy band line-up as well as the -16.5 V biased E-field profile.

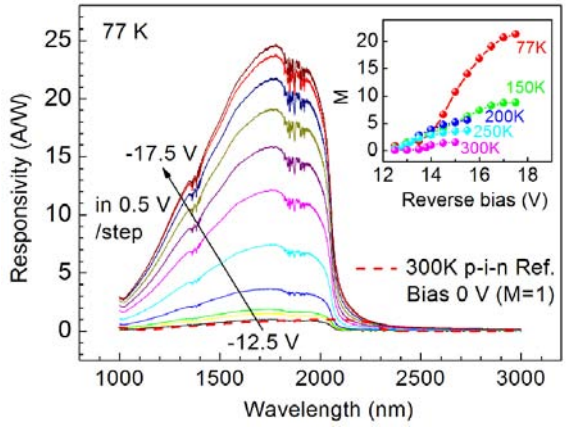

Fig.2. Bias-dependent spectral responsivity of a 200 μm diameter APD at 77 K. The unity gain reference spectrum is also shown (red dash-line). Inset: the extracted bias-dependent M at 77-300 K

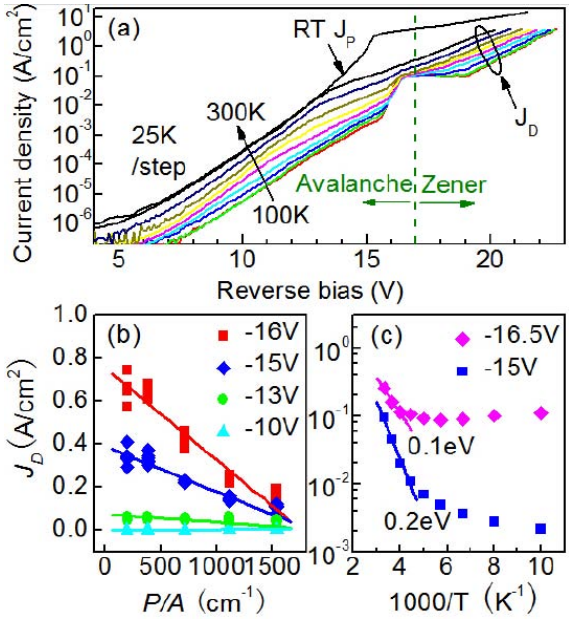

Fig. 3. (a) RT photocurrent (J_P) and the temperature-dependent dark current (J_D) versus reverse bias of the APD. Bias-dependent (b) RT J_D as a function of P/A and (c) Arrhenius plot of J_D.

Mid-IR detectors testing for space missions

D. Sporea[1]*, L. Mihai[1], A. Sporea[1], I. Vaţă[2], M. Straticiuc[2], I. Burducea[2]

[1]*National Institute for Laser, Plasma and Radiation Physics, 409 Atomistilor St., Magurele, RO-077125, Romania*

[2]*"Horia Hulubei" National Institute of Physics and Nuclear Engineering, 30 Reactorului St., Magurele, RO-077125, Romania*

In the last decade quantum cascade lasers were considered by experts for applications related to astronomy, astrophysics, astrochemistry, space missions [1-4]. They were seen as a viable alternative to FTIR type investigations: heterodyne instruments to address atmospheric, astrophysical and cometary research; FIR to provide information on gas and dust located into deep space; atmospheric chemistry for the detection of specific molecule in the 3 μm to 12 μm spectral range; for planetary atmosphere gas tracing and identification. In this context, we started to investigate ionizing radiations effects on mid-IR passive (optical windows) and active components to estimate their reliability for applications in space missions [5,6].

This paper reports the results of our investigations of photovoltaic and photoconductive commercial detectors subjected to alpha particles and proton irradiations, performed in three subsequent steps. Alpha particles irradiations were carried out at the Cyclotron facility with charges from 2.26 to 2.86 mC, while the proton irradiations were performed at the 3MV Tandetron accelerator using energy of 3MeV, a beam current of 5nA, and 10^{16} p/cm^2 fluence. Before any irradiation and between the irradiation steps the spectral responsivity and dark current of each detector was measured with the Gooch and Housego OL Series 750 Automated Spectroradiometer (Fig. 1), over the spectral ranges of 0.8-5 μm (PbSe), and 1-4.2 μm (InAs). The degradation of the detectors windows was checked for optical spectral transmittance and diffused spectral reflectance (Fig. 2). THz spectroscopy and imaging were used for the evaluation of radiation induced changes in these windows (Fig. 3).

References

1. H.-W. Hiibers et al., High resolution spectroscopy with a quantum cascade laser at 2.5 THz, in *Proc. 17th International Symposium on Space Terahertz Technology*, Paris, pp. 343-346 (2006).
2. H.-W. Hübers, R. Eichholz, S. G. Pavlov and H. Richter, High resolution terahertz spectroscopy with quantum cascade lasers, *J. Infrared Milli. Terahz Waves*, Vol. 34, pp. 325–341 (2013).
3. J. Demaison, K. Sarka, E. A. Cohen (Eds.), *Spectroscopy from Space*, Kluwer, pp. 317-339 (2001).
4. S. Forouharet al., *Mid-IR semiconductor lasers for space*, Conference Mid-IR Optoelectronics, MIOMD 2014, 5-9 October 2014, Montpellier, France.
5. L. Mihai, D. Sporea, A. Sporea, I. Vâta, "Testing of ZnSe , CaF2, BaF2, and sapphire windows under alpha particles irradiation," The 3rd International Conference on Lasers, Optics & Photonices 2015, Valencia, September 1-3, 2015
6. D. Sporea, L. Mihai, A. Sporea, G. Craciun, E. Manaila, "Electron beam irradiation of materials and components to be used in mid-IR spectroscopy," Proc. SPIE 9899, 98990O (2016).

*corresponding author: dan.sporea@inflpr.ro

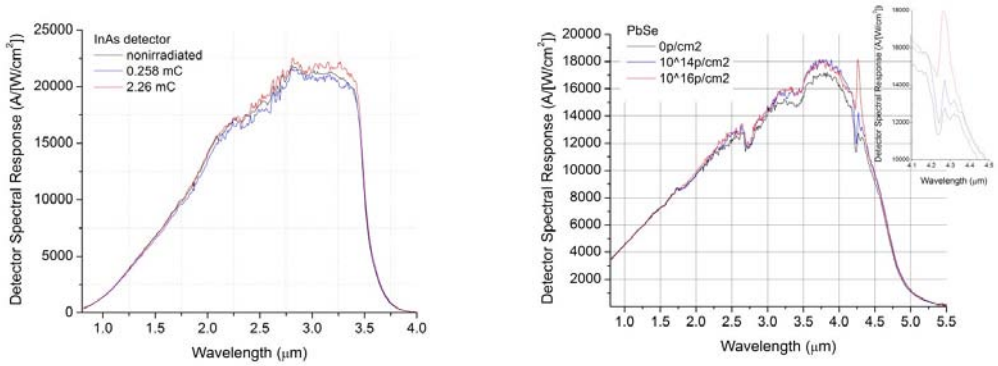

a b

Fig.1. Radiation induced change in the spectral responsivity for: the InAs detector under alpha particles irradiation (a); the PbSe detector under proton irradiation (b).

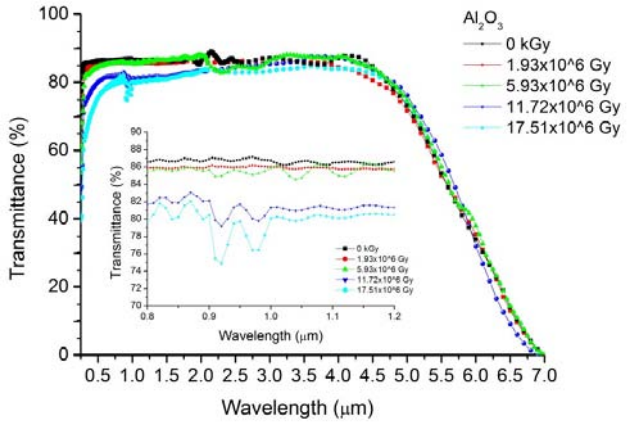

Fig.2. Variation of sapphire window spectral transmittance under alpha particles irradiation.

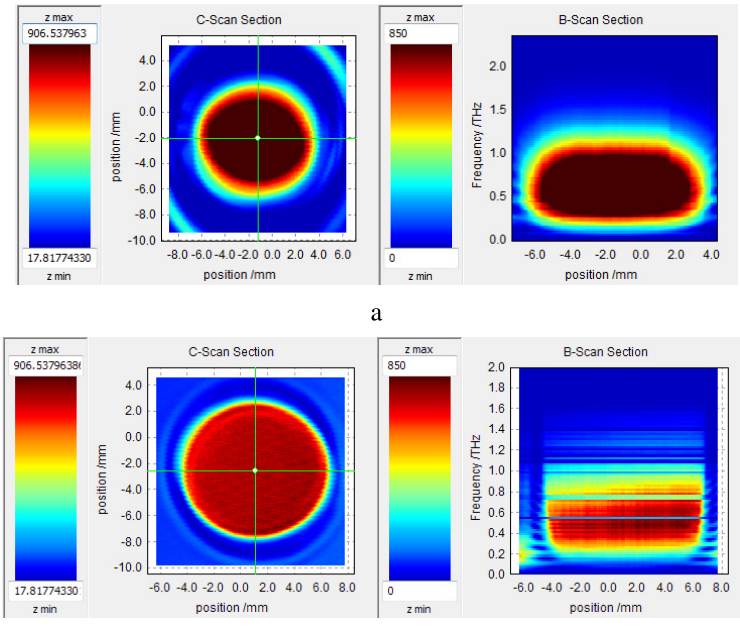

a

b

Fig.3. 2D image of a sapphire window a before (a) and after alpha (b) irradiation at the dose of 5.93×10^6 Gy.

Interband Cascade Lasers and Related Devices

Rui Q. Yang*

School of Electrical and Computer Engineering, University of Oklahoma, Norman, OK

Interband cascade (IC) lasers take advantage of the broken band-gap alignment in type-II InAs/Ga(In)Sb quantum wells to reuse injected electrons in cascade stages for photon generation with high quantum efficiency [1]. IC lasers use interband (conduction to valence bands) transitions for photon emission without involving fast phonon scattering, making it possible to significantly lower the threshold current density. Significant progress has been achieved in the development of high-performance IC lasers with low power consumption [2-3], which includes successful operation of an IC lasers in Curiosity Rover on Mars for detection of CH_4 and commercial availability. Also, the IC architecture has been explored for other optoelectronic devices such as infrared photodetectors and photovoltaic cells [4-7]. Combination of interband transition and fast carrier transport in IC structures provides more flexibilities and advantages to achieve high device performance for photodetectors and photovoltaic cells. The unique features and prospects of IC lasers and relevant optoelectronic devices will be reviewed and discussed with recent experimental results.

References

1. R. Q. Yang, at *7th Inter. Conf. on Superlattices, Microstructures and Microdevices*, Banff, Canada, August, 1994; *Superlattices and Microstructures* **17**, 77 (1995); "Novel concepts and structures for infrared lasers", chapter 2 in *Long Wavelength Infrared Emitters Based on Quantum Wells and Superlattices*, M. Helm, editor, Gordon and Breach, Singapore, 2000.
2. I. Vurgaftman, R. Weih, M. Kamp, J R Meyer, C. L. Canedy, C. S. Kim, M. Kim, W. W. Bewley, C. D. Merritt, J. Abell and S. Höfling, "Interband cascade lasers", J. Phys. D: Appl. Phys. **48** 123001 (2015).
3. L. Li, Y. Jiang, H. Ye, R. Q. Yang, T. D. Mishima, M.B. Santos, and M. B. Johnson, "Low-threshold InAs-based interband cascade lasers operating at high temperatures," Appl. Phys. Lett, **106**, 251102 (2015); and references therein.
4. R. Q. Yang, Z. Tian, Z. Cai, J. F. Klem, M. B. Johnson, and H. C. Liu, "Interband cascade infrared photodetectors with superlattice absorbers", J. Appl. Phys. **107**, 054514 (2010).
5. H. Lotfi, R. T. Hinkey, L. Li, R. Q. Yang, J. F. Klem, M. B. Johnson, "Narrow-bandgap photovoltaic devices operating at room temperature and above with high open-circuit voltage", Appl. Phys. Lett, **102**, 211103 (2013).
6. R. T. Hinkey and R. Q. Yang, "Theory of multiple-stage interband photovoltaic devices and ultimate performance limit comparison of multiple-stage and single-stage interband infrared detectors", J. Appl. Phys. **114**, 104506 (2013).
7. N. Gautam, S. Myers, A. V. Barve, B. Klein, E. P. Smith, D. R. Rhiger, L. R. Dawson, and S. Krishna, "High operating temperature interband cascade midwave infrared detector based on type-II InAs/GaSb strained layer superlattice," Applied Physics Letters **101**, 021106 (2012).

*corresponding author: Rui.q.Yang@ou.edu

Antimonide-based infrared detectors – A new perspective

Antoni Rogalski
Institute of Applied Physics, Military University of Technology, 2 Kaliskiego Str., 00-908 Warsaw, Poland

Abstract

Discovery of variable band gap $Hg_{1-x}Cd_xTe$ (HgCdTe) ternary alloy in 1959 by Lawson and co-workers, triggered an unprecedented degree of freedom in infrared detector design. Over the five decades, this material system has successfully fought off major challenges from different material systems, but despite that it has more competitors today than ever before. It is interesting however, that none of these competitors can compete in terms of fundamental properties. They may promise to be more manufacturable, but never to provide higher performance or, with the exception of thermal detectors, to operate at higher temperature.

Recently, there has been considerable progress towards the materials development and device design innovations. In particular, significant advances have been made during the last two decades in the band-gap engineering of various $A^{III}B^{V}$ compound semiconductors that has led to new detector architectures. Among the materials used in their fabrication, 6.1 Å III–V family plays decisive role offering high performance connected with high design flexibility, direct energy gaps and strong optical absorption. The most exotic band alignment is that of InAs/GaSb heterojunctions, which is identified as the broken gap alignment. A new emerging detector strategies include low-dimensional solids (especially antimonide-based type-II superlattices), barrier structures such as nBn detector with lower generation-recombination leakage mechanisms, photon trapping detectors and multi-stage/cascade infrared devices.

This paper describes the present status of new concepts antimonide-based infrared detectors. It is especially addressed to the InAsSb ternary alloys system and type-II superlattice materials. It seems to be clear that certain of these solutions have merged as a real competitions of HgCdTe photodetectors.

From economical point of view and future technology perspective, an important aspect concerns industry organization. The HgCdTe array industry is vertically integrated; there are no commercial wafer suppliers because there are no diverse commercial applications of HgCdTe focal plane arrays to be profitable. The wafers are grown within each FPA fabrication facility (or its exclusive partner). One important disadvantage of this integrity is the high cost. In the case of III-V semiconductors, horizontal integration is more profitable. This solution is especially effective for avoiding the heavy investment in capital equipment and subsequent upgrading and maintenance, as well as the cost of highly skilled engineers and technicians.

2-3 μm band antimony free detectors and lasers: material, device and applications

Zhang Yong-gang[1]*, Gu Yi[1], Li Xue[2], Shao Xiu-mei[2], Chen Xin-you[1], Ma Ying-jie[1], Li Ai-zhen[1], Tang Heng-jing[2], Li Tao[2], Xi Su-ping[1], Du Ben[1], Ji Wan-yan[1], Shi Yan-hui[1], Gong Hai-mei[2], Fang Jia-xiong[2]

[1]*State Key Laboratory of Functional Materials for Informatics, Shanghai Institute of Microsystem and Information Technology, Chinese Academy of Sciences. 865 Chang Ning Rd., Shanghai 200050, China.*

[2]*Key Laboratory of Infrared Imaging Materials and Devices, Shanghai Institute of Technical Physics, Chinese Academy of Sciences. 500 Yu Tian Rd., Shanghai 200083, China.*

Detectors and lasers in 2-3 μm band are important, especially for satellite remote sensing. Although Sb-containing materials on GaSb/InAs substrates or HgCdTe materials could cover this band well, their also arouses many problems. Development of antimony free materials on InP substrate become a favorable choice. Our detector work was concentrated on high indium content InGaAs [1], the research involves buffer schemes, grading of hetero-interfaces, suppression of dark current by using supperlattice electron barriers. Considering the particular features of gas source MBE, a series of explore has been taken, including homo or hetero-structure, p-on-n or n-on-p configuration, front or back illumination, etc. With optimized structure, focal plane array chips, devices and modules have been developed for space applications, such as meteorology and ocean, resource and circumstance, lunar exploration and manned spaceflight. For lasers in this band, two schemes of pseudomorphic triangle quantum wells and metamorphic virtual substrate strain compensated quantum wells have been explored [2]. Using pseudomorphic scheme the CW operation of the InP-based Sb-free lasers above room temperature have been reached in 2.0-2.43 μm range, and above 10 mW CW output power could be obtained from narrow ridge device at RT. Based on those devices battery-driven miniaturized laser modules have been developed, which have been used for the characterization of the photodetector materials and devices favorably, as well as some other utilities. Using metamorphic scheme the laser reached 2.7 μm CW lasing at 110K, and 2.9 μm pulse lasing at 230K, but with lower power, and RT-CW operation of the laser have not been reached yet. The performance degradation of the longer wavelength virtual substrate lasers is mainly because of the quite week confinement of the carriers, which is an inherent effect for this narrower band gap material system. In this talk our continuous efforts on detectors and lasers of this band will be introduced.

References

1. Yong-gang Zhang, Yi Gu, Gas source MBE grown wavelength extending InGaAs photodetectors. In: Advances in photodiodes. Chapter 19, InTech. pp. 349-376, (2011)
2. Yi Gu, Yong-gang Zhang, InP-based antimony-free MQW lasers in 2-3 μm band. In: Optoelectronics- Materials and Devices. Chapter 4, InTech. pp. 83-107, (2015)

*corresponding author: ygzhang@mail.sim.ac.cn

Growth and Characterisation of Site-controlled InAsSb Nanowires on Silicon for Photonic Devices

A. Krier[1]*, A. Alhodaib[1], A.R. Marshall[1], A.P. Craig[1], M.J. Thompson[1], J. Svensson[2], L.E. Wernersson[2], A.M. Sanchez[3]

[1] *Physics Department, Lancaster University, Lancaster, LA1 4YB, UK*

[2] *Electrical and Information Technology, Lund University, Box 118, SE-221 00 Lund, Sweden*

[3] *Department of Physics, University of Warwick, Coventry, CV4 7AL, UK*

The growth of III-V semiconductor nanowires on Si is considered to be an attractive technology to realise heteroepitaxial materials of high optical quality for next generation photonic devices[1]. In particular, InAs-based nanowires have great potential for use in emitters and photodetectors operating in the technologically important mid-infrared spectral range. Adding Sb to InAs leads to a reduction in the band gap and offers an interesting route towards tailoring the emission or detection wavelength and developing high performance devices. Compared with traditional thin film technology, the nanowire growth mechanism provides a natural way of relaxing the strain at the interface resulting in "defect free" material of high crystalline quality. In our research, catalyst-free growth has been used to produce site-controlled InAsSb nanowires using molecular beam epitaxy on Si (111) substrates, patterned by electron beam lithography, to position the nanowires in a two dimensional array. Uniform nanowires were obtained oriented along the growth direction with average diameters of 80 nm and more than 1μm in length such that electrons are free to travel along the wire, but quantum confined in the other two directions[2]. Scanning electron microscopy and x-ray diffraction measurements were used to determine the morphology, Sb composition and crystal quality of the samples (Fig.1). The nanowires exhibit strong photoluminescence emission at 4 K. Deconvolution of the emission spectrum reveals emission at 0.435 eV characteristic of the InAs seed near the Si interface, as well as more intense emission from the InAsSb at 0.370 eV. The NWs exhibited phase pure- zinc blende crystal structure. Photodetectors fabricated from axially doped p-i-n nanowires have shown a dark current density around 2 mA/cm^2 and a 20% cutoff of 2.3 μm at 300 K (Fig. 2). These high quality, well-aligned InAsSb nanowires are promising for novel infrared optoelectronic devices and their integration with silicon technology[3].

References

1. K. Tomioka, T. Tanaka, S. Hara, K. Hiruma, and T. Fukui, IEEE Journal of Selected Topics in Quantum Electronics, **17**, 1112, (2011).
2. G. Koblmüller, K. Vizbaras, S. Hertenberger, et al, Appl. Phys. Lett. **101**, 053103, (2012)
3. M. Thompson, A. Alhodaib, A.R. Marshall et al, Nano Letters, **16**(1): 182-187, (2016)

*corresponding author: a.krier@lancaster.ac.uk

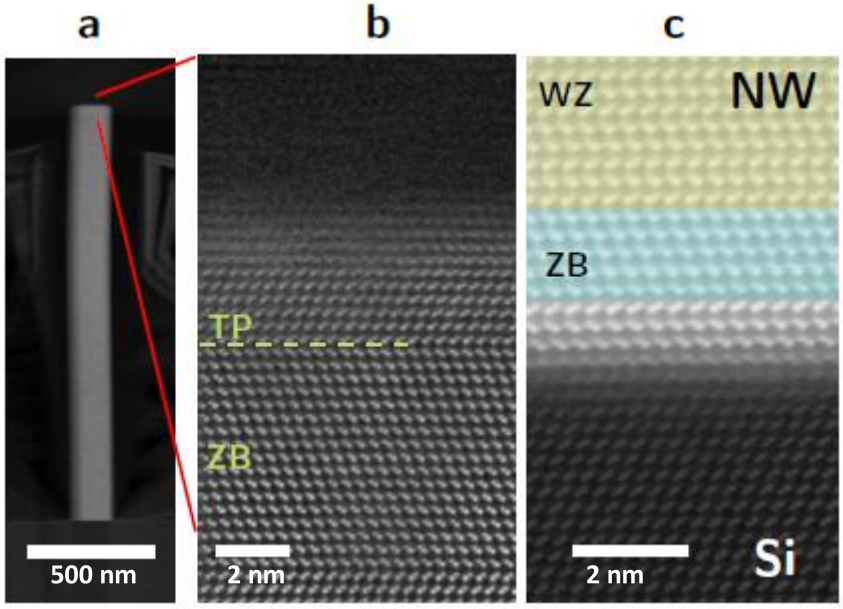

Fig. 1. Structural characterisation of InAsSb nanowires. (a) HRTEM image of InAsSb nanowire, (b) The top of the nanowire is flat and shows the multi-twinned ZB structure of the InAsSb, (c) HRTEM of the InAs nanowire/Si interface shows that the nanowires have grown directly onto the substrate, the InAs section shows a mix of WZ and ZB regions.

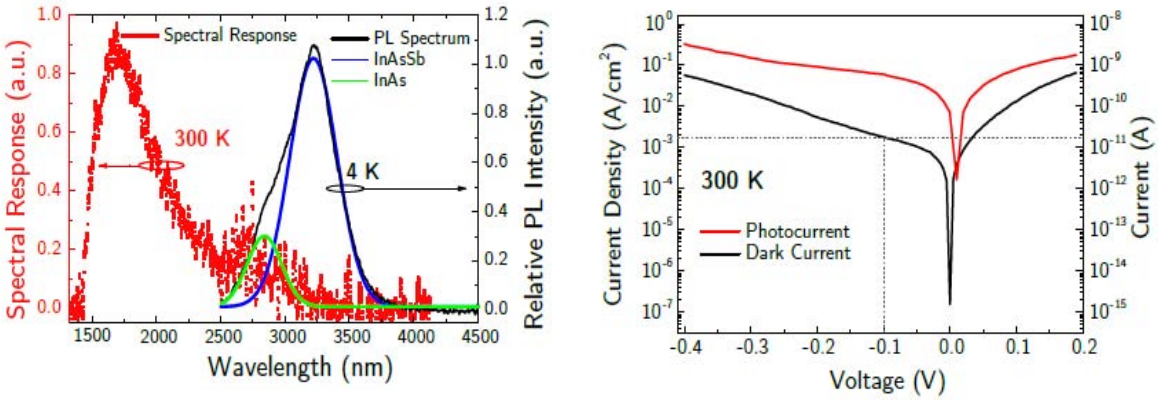

Fig. 2. (a) Spectral response at 300 K and -0.1 V bias (red) and 4 K PL (black) of $InAs_{0.93}Sb_{0.07}$ nanowires. The PL spectrum is de-convoluted using two Gaussian peaks to show the contributions of the InAs (green) and InAsSb (blue) sections of the wire; (b) Semi-log current-voltage characteristic of $InAs_{0.93}Sb_{0.07}$ p-i-n photodiode at 300 K with nanowire diameter of 80 nm and length 1.7 µm. The black and red plots show the dark and photocurrent density respectively for 200 contacted nanowires. At a typical operational bias of -0.1 V the dark current is 18 pA which corresponds to a dark current density ~2 mA/cm^2.

Acknowledgements: We are grateful for financial support provided from DSTL under CDE project CDE65947 and also to the Embassy of the Kingdom of Saudi Arabia for providing a studentship for A. Alhodaib.

Molecular Beam Epitaxy and characterization of high Bi content GaSbBi alloys

O. Delorme[1,2], L. Cerutti[1,2 *], E. Tournié[1,2] and J.-B. Rodriguez[1,2 *]

[1]*Univ. Montpellier, IES, UMR 5214, F- 34000, Montpellier, France*
[2]*CNRS, IES, UMR 5214, F- 34000, Montpellier, France*

In recent years, dilute bismuth (Bi) III-V compound semiconductors have attracted great attention, particularly due to their properties of band gap reduction. Such properties make GaSbBi suitable for optoelectronics device applications operating in the mid-infrared ranges (2 - 5 µm). This alloy however has been very little studied till now and the maximum reported incorporation is 9.6% [1].

$GaSb_{1-x}Bi_x$ ($0 < x \leqslant 17\%$) layers have been grown on GaSb (001) substrates in a Riber Compact 21 solid-source molecular beam epitaxy (MBE). Due to its large size, Bi does not readily incorporate into III-V alloys. Consequently, the growth of GaSbBi needs very low growth temperature compared to common values used for the growth of standard antimonides materials. Various sets of samples were grown at different V/III ratio and substrate temperatures.

A set of samples was grown below 300°C at a fixed Bi beam equivalent pressure (BEP) and a growth rate ~0.3 ML/s. The Bi fraction in the GaSbBi layers was then deduced from X-Ray diffraction and confirmed by Rutherford Backscattering (RBS), assuming a zinc blende GaBi lattice parameter of 6.272 Å. The Bi content was found to increase as the growth temperature decreases and reaches a plateau corresponding to x = 5.6% for growth temperatures below approximately 150°C (Fig.1).

Another set of samples was grown at 150°C, by varying the Sb:Bi ratio to reach a higher Bi content. The Bi BEP flux was increased, while the Sb BEP flux was decreased to keep the V/III ratio constant. Optical microscopy of two GaSbBi samples with 8.4% and 11.4% shows a smooth and droplet free surface on the entire samples. The Pendellösung fringes on the XRD measurements attest of the epitaxial quality of layers and interfaces (Fig. 2). The sample with 17% Bi incorporation is however covered by numerous Bi droplets.

Photoluminescence measurements at room temperature were carried out for different Bi incorporation and indicate a decrease of the band gap with the increase of the Bi content, as expected. The sample with the largest Bi content (17%) showed room temperature photoluminescence peak at 3.8 µm (Fig. 3).

To conclude, we have grown GaSbBi layers with droplet free surface up to 11.4%. The maximum Bi content reached was 17%. In spite of the presence of Bi droplets at the surface of this sample, a strong photoluminescence signal could be measured at room temperature with an emission at 3.8 µm. The next step is to grow quantum wells of GaSbBi within GaSb to make efficient optoelectronic devices in the 3-5 µm wavelength range.

This work was partially supported by the French "Investment for the Future" program (EquipEx EXTRA, ANR-11-EQPX-0016) and by the French ANR (BIOMAN NR-15-CE24-0001-01)

References

1. M. Rajpalke et al. “High Bi content GaSbBi alloys” J. of Appl. Phys., vol. 116 (4), pp. 043511, 2014

*corresponding author: laurent.cerutti@umontpellier.fr , rodriguez@ies.univ-montp2.fr

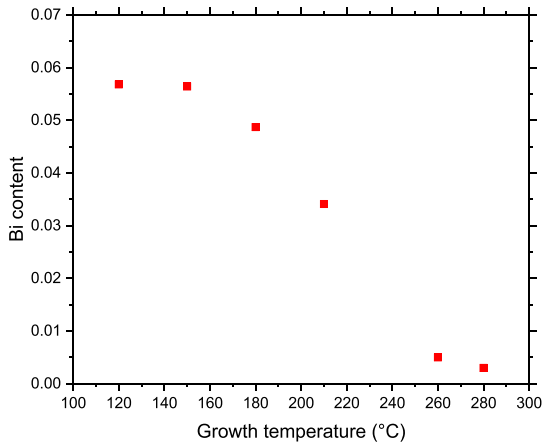

Fig. 1 : Evolution of Bi content with the variation of the growth temperature at fixed Bi BEP flux and growth rate

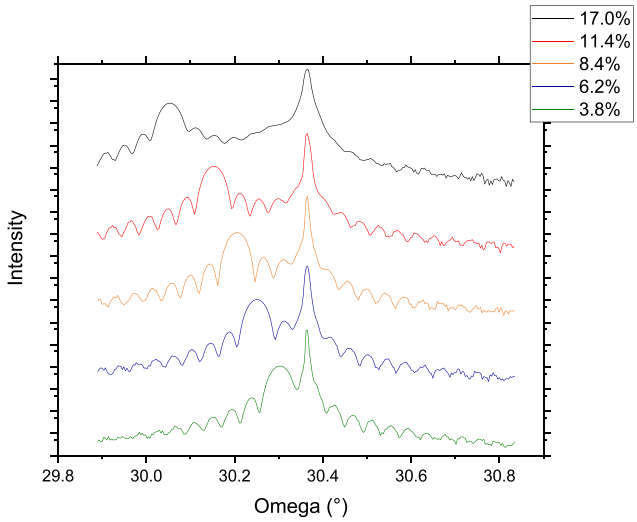

Fig. 2 : XRD scans of GaSbBi layers with different Bi content on GaSb substrates

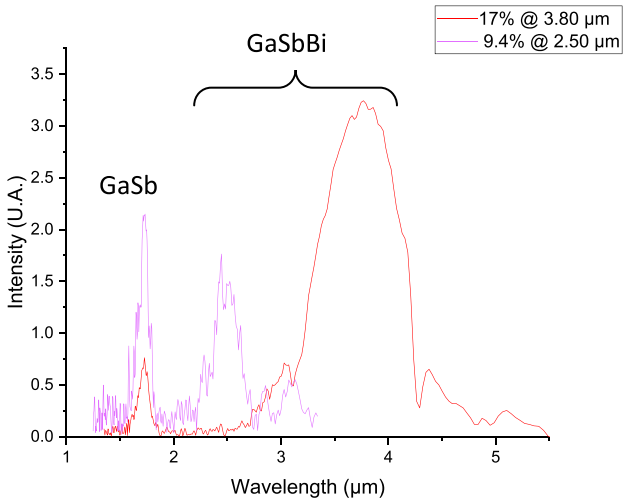

Fig. 3 : Photoluminescence measurements at RT of the GaSbBi with different Bi content

Anisotropic Polarizability Matrix due to Electromagnetic Coupling of SPPs to Dirac-Electron Excitations in Graphene

Danhong Huang[1]*, Oleksiy Roslyak[2], Godfrey Gumbs[3], Wei Pan[4], A. A. Maradudin[5]

[1] *Air Force Research Laboratory, Space Vehicles Directorate (AFRL/RVSW), 3725 Aberdeen Avenue SE, Kirtland AFB, NM 87117, United States of America*

[2] *Department of Physics and Engineering Physics, Fordham University, 441 East Fordham Road, Bronx, NY 10458, United States of America*

[3] *Department of Physics and Astronomy, Hunter College of the City University of New York, 695 Park Avenue New York, NY 10065, United States of America*

[4] *Sandia National Laboratories, Albuquerque, New Mexico 87185, USA*

[5] *Department of Physics and Astronomy and Institute for Surface and Interface Science, University of California at Irvine, Irvine, CA 92697, United States of America*

Electromagnetic coupling of surface-plasmon polaritons (SPPs), which are localized adjacent to the surface of a conductive substrate [1], to collective excitations of Dirac electrons in a graphene sheet [2] close to the surface is studied and the hybrid Dirac-SPPs are predicted. For a two-layer graphene structure, the competition between the interlayer Coulomb coupling and electromagnetic couplings of Dirac electrons to SPPs is investigated. The anisotropic polarizability matrix for such a combined system has been derived analytically. Moreover, such an anisotropic polarizability matrix is expected to be crucial for constructing an effective-medium theory for more complex systems, involving the exploration of optical properties for inserted nanorods either between two graphene sheets or between sheets and a conductive surface.

References

1. D. H. Huang, M. M. Easter, G. Gumbs, A. A. Maradudin, S.-Y. Lin, D. A. Cardimona, and X. Zhang. *Controlling quantum-dot light absorption and emission by a surface-plasmon field*, Optics Express, Vol. 22, No. 22, pp. 27576-27605, 2014.
2. G. Gumbs, A. Iurov, D. H. Huang, and W. Pan. *Tunable surface plasmon instability leading to emission of radiation*, Journal of Applied Physics, Vol. 118, No. 5, Article ID 054303(10), 2015.

*corresponding author: danhonghuang1647@msn.com

MBE Growth of InAs Nanowires on Graphene

Chieh Chou[1], Che-Wei Yang[2], and Hao-Hsiung Lin[1,2]*

[1] *Graduate Institute of Electronics Engineering, National Taiwan University, Taipei, 10617, China*

[2] *Department of Electrical Engineering, National Taiwan University, Taipei, 10617, China*

Epitaxial growth of III-V semiconductors on 2D materials has recently drawn a lot of attentions [1]. The success of this growth could combine the advantages of 2D materials and semiconductors for novel applications. The growth mechanism is also a very interesting research subject. So far, though the growth is via van der Waals interaction, models for the correlation between two lattices have been proposed [1, 2]. In this work, we have used molecular beam epitaxy to deposit InAs nanowires (NWs) on graphene coated on SiO_2/Si substrates with various growth temperature. The NWs were grown under a fixed V/III ratio of 400 and at a nominal growth rate of 0.0864 μm/hr for 1 hour. Substrate temperature varied from 440 to 500°C. Fig. 1 shows the SEM images of the grown NWs with a 45-degree tilt. Obviously, the NW density decreases with increasing temperature. An Arrhenius plot for the NW density is shown in Fig. 2 and gives an activation energy of 5.70 eV, which is close to the cohesive energy of InAs. It implies that the formation energy of NWs on graphene is very low and nearly independent of temperature. The easy NW formation makes the InAs dissociation dominate the NW density. From the images for samples grown at 440 and 460°C, we can see that the cluster densities are almost the same, suggesting that the InAs clusters could be grown from the imperfection area of the graphene layer. Improving in the graphene could eliminate the clusters. Raman scattering was measured to check the quality of graphene as well as the InAs NWs and the result is shown in. Fig. 3. The G and 2D modes for the graphene are clear observed. However, their intensity ratio suggests the graphene contains several layers. Even though, it does not hinder the growth of NWs. A strong InAs TO is observed at ~215 cm^{-1}. Since the intensity increases with the increasing NW density, we believe that the signal is from NWs. Because the TO frequency is in between those for zincblende and wurtzite InAs, the NWs are likely composed of the two structures. The LO or A mode could be too weak to be resolved. In conclusion, we have successfully grown InAs NWs graphene using MBE. Graphene is clearly a good template for the growth of InAs NWs.
This work is supported by Ministry of Science and Technology, ROC, Taiwan under contract number MOST 104-2622-8-002-003.

References

1. A. M. Munshi, D. L. Dheeraj, V. T. Fauske, D.-C. Kim, A. T. J. van Helvoort, B.-O. Fimland, H. Weman, Vertically aligned GaAs nanowires on graphite and few-layer graphene: generic model and epitaxial growth, Nano Lett. 12, 4570-4576, 2012.
2. A. Koma, A New Epitaxial Growth Method for a Highly Lattice-mismatched System, Thin Solid Films, 216, 72-76, 1992.
3. A. C. Ferrari, Raman spectroscopy of graphene and graphite: Disorder, electron–phonon coupling, doping and nonadiabatic effects, Solid State Commun.143, 47, 2007.

*corresponding author: hhlin@ntu.edu.tw

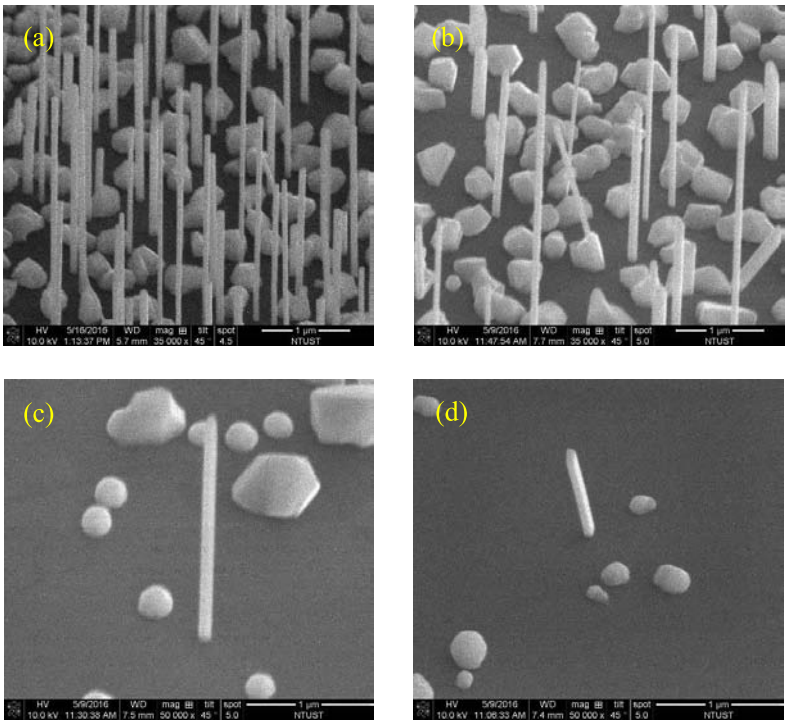

Fig. 1. NWs grown under V/III ratio of 400 for 1 hour at (a) 440°C, (b) 460°C, (c) 480°C and (d) 500°C.

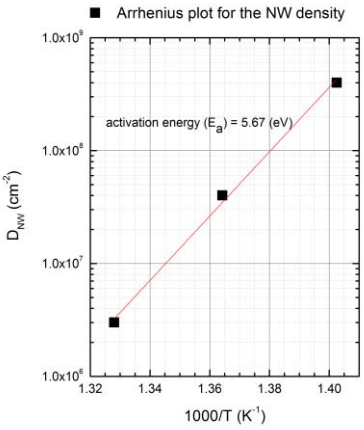

Fig. 2. Arrhenius plot for the NW density. NW density were calculated from three samples with growth temperature of 440°C, 460°C, 480°C, respectively.

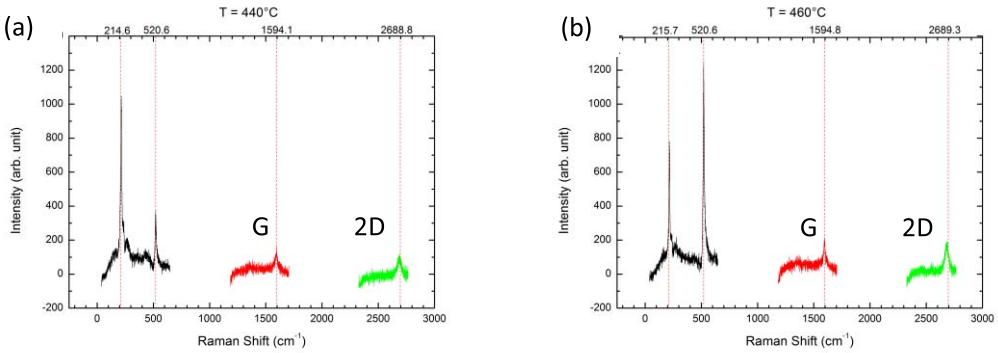

Fig. 3. Raman spectroscopy of samples with different growth temperature, (a) 440°C, and (b) 460°C .

Quantum Cascade devices: from discrete to integrated systems

A. Harrer[1], B. Schwarz[1], R. Szedlak[1], D. Ristanic[2], H. Detz[1], A.M. Andrews[1], T. Zederbauer[2], D. MacFarland[2], W. Schrenk[2], G. Strasser[1,2]*

[1] *Institute of Solid State Electronics, TU Wien, Floragasse 7, 1040 Wien, Austria*
[2] *Center for Micro- and Nanostructures, TU Wien, Floragasse 7, 1040 Wien, Austria*

Mid-infrared spectroscopy is a reliable tool for the identification of gaseous and liquid mixtures due to their unique and inherent absorption spectra. We used a specially designed intersubband material working as a laser for a given bias voltage and as a detector without any external bias. By the use of such a bi-functional quantum cascade structure material for light sources and detectors, operating at the same frequencies in the same material, the realization of mid infrared on-chip sensors is possible [1, 2]. A bi-functional QC structure will be presented [1,2], that can be operated as coherent light emitter as well as intersubband detector, depending on the bias applied to the structure [3].

This opens the way to on-chip sensing solutions with a high integration density [4]. Liquid sensing at room temperature with a monolithic integrated sensor was achieved by a QCL, a dielectric loaded Surface Plasmon Polariton (SPP) waveguide as interaction section of the infrared light with the liquid, and a QCD.

To demonstrate gas sensing with the same technology a surface emitting and detecting sensor was processed using the very same heterostructure material. A distributed feedback ring quantum cascade laser is integrated on-chip with a detector element. The surface emitted light is collimated, guided through a gas cell, back reflected by a flat mirror, focused, and detected by the sensor element on the very same device. The surface operation mode enables for comparable long interaction lengths as needed for gas absorption measurements [5].

References

1. Schwarz, B. et al., Monolithically integrated mid-infrared quantum cascade laser and detector, Sensors 13, 2196, 2013
2. Schwarz, B. et al., High performance bi-functional quantum cascade laser and detector, Appl. Phys. Lett. 107, 071104, 2015
3. Schwarz, B. et al., Monolithically integrated mid-infrared lab-on-a-chip using plasmonics and quantum cascade structures, Nat. Commun. 5, 4085, 2014
4. Ristanic, D. et al., Monolithically integrated mid-infrared sensor using narrow mode operation and temperature feedback, Appl. Phys. Lett. 106, 041101, 2015
5. Harrer, A. et al., Mid-infrared surface transmitting and detecting quantum cascade device for gas-sensing applications, Scientific Reports 6, 21795, 2016

*corresponding author: gottfried.strasser@tuwien.ac.at

Quantum Cascade Lasers for Industrial Applications

M. Troccoli*

AdTech Optics Inc., City of Industry, CA 91748, USA

In this presentation we will review our most recent results on development of Quantum Cascade Lasers (QCLs) for analytical and industrial applications. QCLs have demonstrated the capability to cover the entire range of Mid-IR, Far-IR, and THz wavelengths by skillful tuning of the material design and composition and by use of intrinsic material properties via a set of techniques collectively called "bandgap engineering". The use of MOCVD, pioneered on industrial scale by AdTech Optics, has further opened the deployment of QCL devices into diverse types of environments and applications. QCLs can be tailored to the specific application requirements due to their unprecedented flexibility in design and thanks to the leveraging of well-known III-V fabrication technologies inherited from the NIR domain. Nevertheless, several applications and new frontiers in R&D need the constant support of new developments in device features, capabilities, and performances.

We have developed a wide range of devices, from high power, high efficiency multi-mode sources, to narrow-band, single mode devices with low-power consumption, and from non-linear, multi-wavelength generating devices to broadband sources and multi-emitter arrays. All our devices are grown and processed using MOCVD technology and allow us to attain competitive performances across the whole mid-IR spectral range. This talk will present an overview of our current achievements.

References

1. M. Troccoli, "High power emission and single mode operation of quantum cascade lasers for industrial applications", *J. Sel. Topics in Quantum Electron.*, **21** (6), 1-7 (2015). *Invited Review*.
2. Seungyong Jung, Aiting Jiang, Yifan Jiang, Karun Vijayraghavan, Xiaojun Wang, Mariano Troccoli, and Mikhail A. Belkin, "Broadly Tunable Monolithic Terahertz Quantum Cascade Laser Sources", *Nature Comm.* ***5***, 4267 (2014)..
3. Mariano Troccoli, Arkadiy Lyakh, Jenyu Fan, Xiaojun Wang, Richard Maulini, Alexei G Tsekoun, Rowel Go, C Kumar N Patel, "Long-Wave IR Quantum Cascade Lasers for emission in the λ = 8-12μm spectral region", *Opt. Mat. Expr.*, **3** (9), 1546-1560 (2013).

*corresponding author: mariano.troccoli@atoptics.com

Long-wavelength stimulated emission from HgCdTe quantum well heterostructures

V.V.Rumyantsev[1,2]*, *S.V.Morozov*[1,2], *A.M. Kadykov*[1], *K.E.Kudryavtsev*[1], *A.A.Dubinov*[1,2], *A.A. Fadeev*[1,2], *N.N. Mikhailov*[3], *S.A. Dvoretcky*[3], *V.I.Gavrilenko*[1,2], *S. Winnerl*[4], *M. Helm*[4]

[1] *Institute for Physics of Microstructures of RAS, 603950, GSP-105, Nizhny Novgorod, Russia*

[2] *Lobachevsky State University of Nizhny Novgorod, 603950, av. Gagarina 23, Nizhny Novgorod, Russia*

[3] *A.V.Rzhanov Institute of Semiconductor Physics, Siberian Branch of Russian Academy of Sciences, 630090, pr. Lavrentieva 13, Novosibirsk, Russia*

[4] *Institute of Ion Beam Physics and Materials Research, Helmholtz-zentrum Dresden−Rossendorf, Dresden, D−01328, Bautzner Landstraße*

Infrared spectroscopy applications demand compact semiconductor lasers tunable in a wide spectral range. Quantum cascade lasers (QCLs) deliver radiation in 3 – 20 μm range at 300 K [1], but experience formidable problems in 20 – 60 μm wavelength range due to strong lattice absorption in A3B5 materials that are typically used for QCLs production. HgCdTe material provides variable bandgap in conjunction with optical phonon frequencies low enough for furthering the emission wavelength up to 50 μm. Spectra and kinetics studies of long-wavelength photoconductivity and photoluminescence have revealed the remarkable figures of merit of the HgCdTe epitaxial structures grown on GaAs (013) substrates [2 - 5].

Previously, lasing in HgCdTe was studied only at wavelengths up to 5.3 μm (at 45K) [6]. We report on stimulated emission (SE) at wavelengths up to 10.2 μm from waveguide HgCdTe structures with several QWs inside waveguide core (Fig. 1, 2). Threshold as low as 0.12 kW/cm^2 is demonstrated at 18K for SE wavelength ~ 10 μm [7]. The threshold current density that would be necessary to achieve SE if the same QWs were placed into a p-n junction is I_{th} ~ 11 A/cm^2 which is equal to the threshold current density of InAs-based interband QCL emitting near 10.4 μm at 80 K [8].

As well as some previous works, our studies indicate that Auger recombination can be suppressed in HgCdTe QWs [5]. Pump-probe studies of HgCdTe QWs with bandgap ~25 meV yield lifetime of 100 ps, which is enough to achieve gain in 20 – 50 μm wavelength range at pumping intensity of ~ 30 kW/cm^2. Thus, there is an appreciable reserve for furthering the SE wavelength above 20 μm, where HgCdTe based lasers can be competitive with the alternatives and the incumbent technologies, in particular, QCLs.

The work was supported by the Russian Foundation for Basic Research (grant #16-02-00685, #16-32-00609, #15-02-05154, #15-42-02249) and Ministry of Education and Science of the Russian Federation (MK-6923.2016.2).

References

1. M. S. Vitiello, G. Scalari, B. Williams, P. De Natale, Opt Express. **23**(4): p. 5167-82. (2015)
2. S. V. Morozov, V. V. Rumyantsev, A. V. Antonov, K. V. Maremyanin, K. E. Kudryavtsev, L. V. Krasilnikova, N. N. Mikhailov, S. A. Dvoretskii, V. I. Gavrilenko, Applied Physics Letters. **104**(7): p. 072102 (2014)

3. S. V. Morozov, V. V. Rumyantsev, A. A. Dubinov, A. V. Antonov, A. M. Kadykov, K. E. Kudryavtsev, D. I. Kuritsin, N. N. Mikhailov, S. A. Dvoretskii, V. I. Gavrilenko, Applied Physics Letters. **107**(4): p. 042105. (2015)
4. V. V. Rumyantsev, S. V. Morozov, A. V. Antonov, M. S. Zholudev, K. E. Kudryavtsev, V. I. Gavrilenko, S. A. Dvoretskii, N. N. Mikhailov, Semiconductor Science and Technology. **28**(12): p. 125007. (2013)
5. S. V. Morozov, V. V. Rumyantsev, A. V. Antonov, A. M. Kadykov, K. V. Maremyanin, K. E. Kudryavtsev, N. N. Mikhailov, S. A. Dvoretskii, V. I. Gavrilenko, Applied Physics Letters. **105**(2): p. 022102. (2014)
6. J. M. Arias, M. Zandian, R. Zucca, J. Singh, Semiconductor Science and Technology. **8**(1S): p. S255. (1993)
7. S. V. Morozov, V. V. Rumyantsev, A. M. Kadykov, A. A. Dubinov, K. E. Kudryavtsev, A. V. Antonov, N. N. Mikhailov, S. A. Dvoretskii, V. I. Gavrilenko, Applied Physics Letters. **108**(9): p. 092104. (2016)
8. Z. Tian, L. Li, H. Ye, R. Q. Yang, T. D. Mishima, M. B. Santos, M. B. Johnson, Electronics Letters. **48**(2): p. 113-114. (2012)

*corresponding author: rumyantsev@ipmras.ru

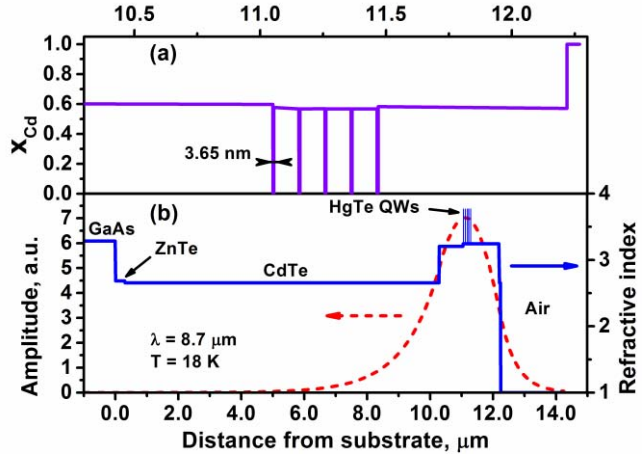

Fig. 1 (a) Cd distribution in the waveguide of structure under study; (b) the refractive index distribution throughout the structure and calculated mode localization for λ = 8.7 microns.

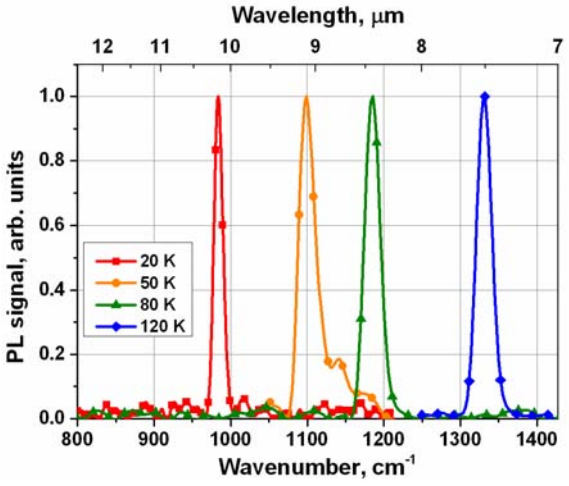

Fig.2. Spectra of stimulated emission from structure under study at different temperatures.

Recombination Processes in Type I GaInAsSb Lasers

T. Eales[1], I. Marko[1], B. Ikyo[1], A. R. Adams[1], S. Arafin[2], S. Sprengel[2], M.-C. Amann[2], S. J. Sweeney[1]*

[1] *Advanced Technology Institute and Department of Physics, University of Surrey, Guildford, GU2 7XH, United Kingdom*

[2] *Walter Schottky Institut, Technische Universität München, Am Coulombwall 3, 85748 Garching, Germany*

Mid-infrared optical devices between 2 and 3 μm are motivated by a diverse array of applications which include trace gas detection and communications [1]. Type-I quantum well (QW) laser structures, based on the GaInAsSb/GaSb material system are the standard approach for this wavelength range. However, loss processes such as Auger recombination, inter-valence band absorption and carrier leakage all effect the temperature stability of these devices. In this work we study the dominant recombination mechanisms affecting the operating characteristics of type-I GaInAsSb based lasers emitting at 2.3, 2.6 and 2.9 μm [2]. The characteristic temperature (T_0) is a measure of the temperature sensitivity of the threshold current density. The temperature dependence of T_0 for the three wavelength devices is presented in Fig. 1. The same qualitative behaviour is observed in each device with T_0 decreasing rapidly (decreasing stability), approaching, and then exceeding the predicted temperature sensitivity of a device dominated by Auger recombination ($T_0 \sim T/3$). These processes can be explored in more detail using hydrostatic pressure since the different loss processes have distinctive behaviour as a function of pressure. In a device dominated by the CHCC process the threshold current would be expected to decrease exponentially with increasing pressure (increasing bandgap) while a device dominated by the CHSH process is expected to increase exponentially as the bandgap increases and approaches resonance with the spin-orbit splitting energy (Δ_{SO}). This work can be supplemented with previous high hydrostatic pressure measurements on GaInAsSb lasers, extending the wavelength range to 1.83 μm [3]. To account for structural differences the non-radiative component of the threshold current density in each device was independently normalized, generating a smooth dependence with lasing energy. This is shown Fig. 2. Modelling the experimental data provides clear evidence of the dominance of the CHCC process at longer wavelengths and the importance of the spin orbit split off resonance in enhancing the CHSH process.

References

1. A. Joullié and P. Christol, GaSb-based mid-infrared 2-5 μm laser diodes, Comptes Rendus Phys, Vol. 4, N.6, pp. 621–637, 2003.
2. A. B. Ikyo et al., Temperature stable mid-infrared GaInAsSb/GaSb Vertical Cavity Surface Emitting Lasers (VCSELs), Sci. Rep., vol. 6, p. 19595, Jan. 2016.
3. K. O'Brien, et al., Carrier recombination mechanisms in mid-infrared GaInAsSb quantum well lasers, Phys. Status Solidi, Vol. 207, N.1, pp. 203–207, 2007.

*corresponding author: s.sweeney@surrey.ac.uk

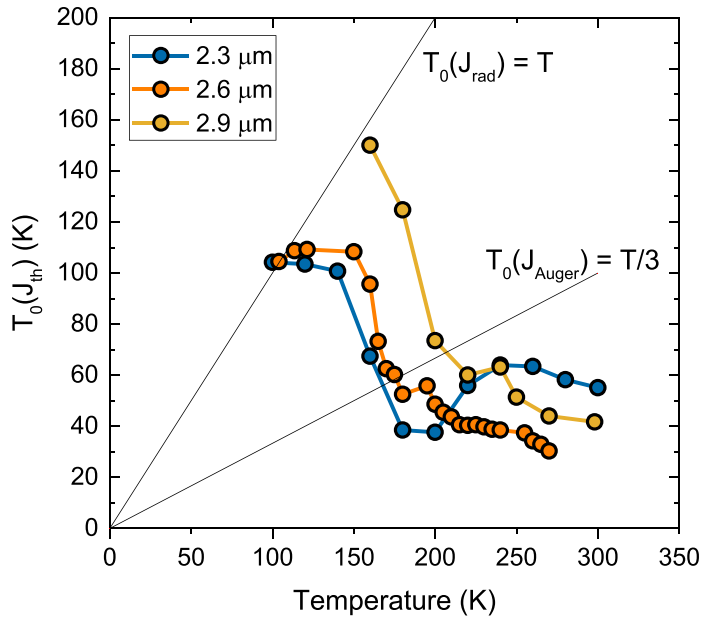

Fig.1. T_0 for the three devices as a function of temperature. The dotted lines indicate highest theoretical T_0 for a device dominated by radiative and Auger recombination.

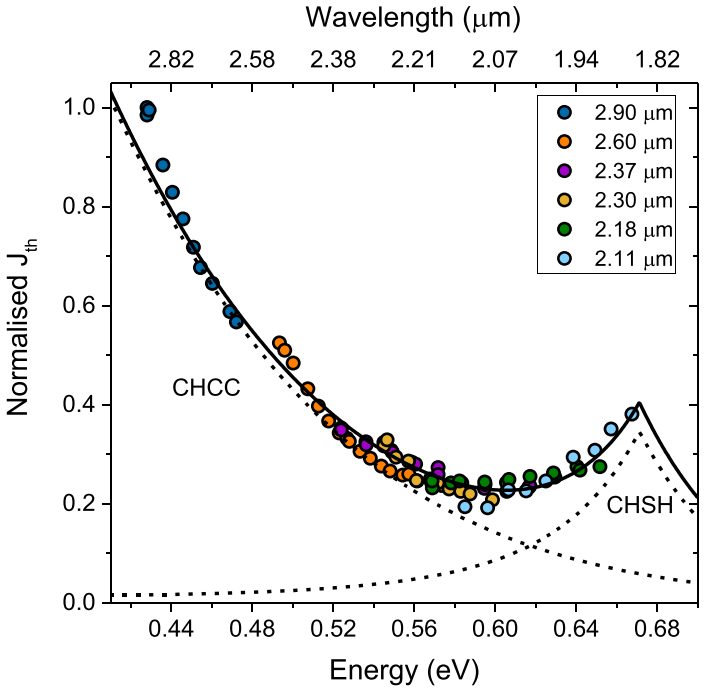

Fig.2. The normalized non-radiative component of the threshold current density as a function lasing photon energy. The dotted lines show the modelled contribution from the CHCC and CHSH processes.

Electroluminescence study of InAs/InAs(Sb)/InAsSbP LED heterostructures at 4.2–300 K

Kh. Salikhov [*1], K.D. Mynbaev [2,3], N.L. Bazhenov [2], A.A. Semakova [3], M.P. Mikhailova [2], N.D. Stoyanov [4], S.S. Kizhaev [4], S.S. Molchanov [4], A.P. Astakhova [4], A.V. Chernyaev [4]

[1] *The Institute for Advanced Study, Academy of Sciences of Tatarstan, Russia*
hafizms@mail.ru
[2] *Ioffe Institute, 194021 Saint–Petersburg, Russia*
[3] *ITMO University, 197101 Saint–Petersburg, Russia*
[2] *Microsensor Technology, 194223 Saint–Petersburg, Russia*

Electroluminescence of InAs/InAsSbP and $InAs_{0.93}Sb_{0.07}$/InAsSbP heterostructures grown on InAs substrates was studied in the temperature range T=4.2–300 K. A remarkable feature was observed: despite the fact that the heterostructures were fabricated to be used solely in light-emitting diodes (LEDs), at low temperatures (T=4.2–100 K) stimulated emission was observed at the short-wavelength shoulders of the spontaneous emission spectra. The wavelengths of stimulated emission peaks at T=4.2 K were 3.03 μm and 3.55 μm for InAs/InAsSbP and InAsSb/$InAs_{0.93}Sb_{0.07}$ heterostructures, respectively. Threshold current for stimulated emission for InAs/InAsSbP structures at T=4.2 K was j_{th}~140 A/cm^2. With temperature increasing, the emission became spontaneous at T>100 K due to the resonant "switch-on" of CHHS Auger recombination process, when the energy of recombining electron-hole pair was transferred to a hole with the latter transitioning to the spin-orbit-splitted band, and remained such up to the room temperature because of the influence of other Auger processes. Strong effect of non-radiative recombination was observed at low temperatures, too, as following the value of the threshold current from T=100 K down to T=30 K, we found that it was limited by an Auger process, most likely, of CHHC type, with participation of two electrons and a heavy hole with excitation of electron in more energetic state. The intensity of stimulated emission from the surface was much greater than that from the cleft edges of the chips (and the edges did not have mirror-like surface). Also, the resonator length determined according to inter-mode distance in the electroluminescence spectrum, appeared to be much closer to the total chip thickness rather than to the distance between the cleft edges. This indicated that the resonators were actually formed normal to the growth plane and thus, structures based on InAs(Sb)/InAsSbP are promising for fabrication of vertical-emitting mid-infrared lasers as even under the strong influence of Auger recombination it appears to be possible to get stimulation emission with minimum requirements for optical resonators.

*corresponding author: hafizms@mail.ru

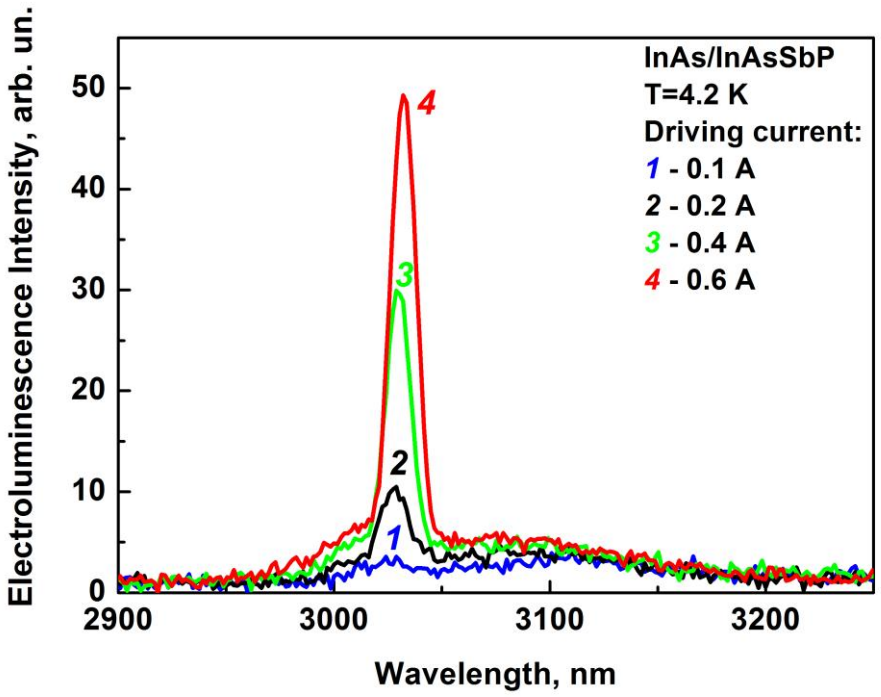

Fig. 1. Electroluminescence spectra of a typical InAs/InAsSbP LED heterostructure at T=4.2 K and various pumping currents: 0.1 (1), 0.2 (2), 0.4 (3) и 0.6 A (4)

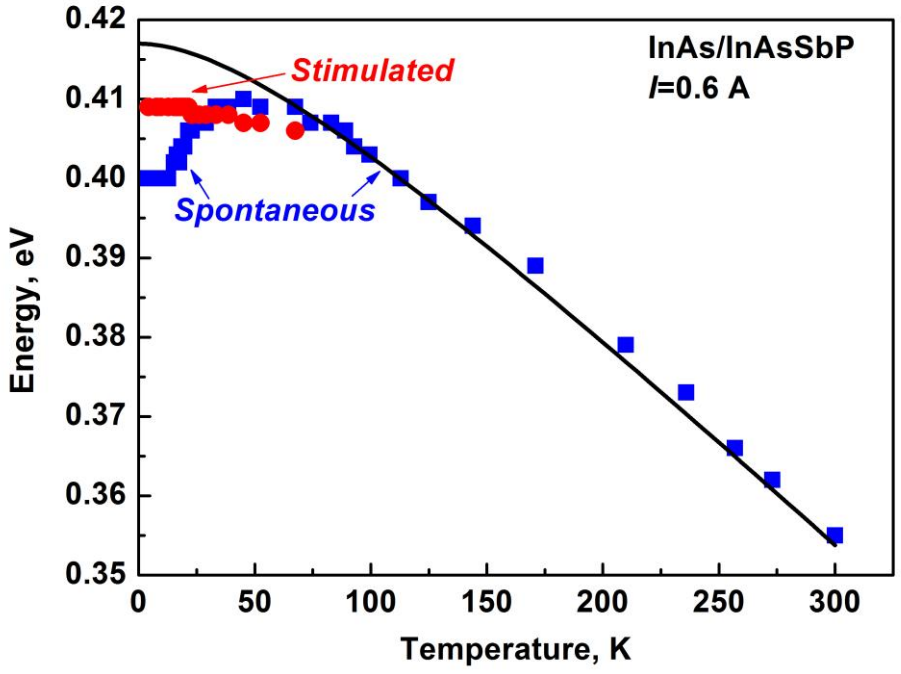

Fig. 2. The experimental dependence of the energy position of electroluminescence peaks on the temperature for an InAs/InAsSbP LED heterostructure (symbols, driving current 0.6 A) and calculated temperature dependence of the energy gap of the active layer made of InAs (straight curve)

A design of interband cascade laser's active region towards mode-locked operation

M. Dyksik[1], K. Ryczko[1], M. Motyka[1], J. Misiewicz[1], M. Kamp[2], G. Sęk[1]

[1]*Laboratory for Optical Spectroscopy of Nanostructures, Department of Experimental Physics, Faculty of Fundamental Problems of Technology, Wrocław University of Science and Technology, Wybrzeże Wyspiańskiego 27, 50-370 Wrocław, Poland*
[2]*Technische Physik, University of Würzburg & Wilhelm Conrad Röntgen Research Center for Complex Material Systems, Am Hubland, D−97074 Würzburg, Germany*

Interband cascade lasers (ICLs) have already been proven as a promising mid-infrared (MIR) source desirable for many applications. Their potential originates mostly from unique operational characteristics as, e.g., single mode, continuous-wave and high power operation at elevated temperatures in the range from below 3 to about 6 μm [1,2], broad spectral tunability [3], and low threshold currents and hence small electrical power consumption [4] when compared to the main competitor which are quantum cascade lasers.

A device that has not yet been realized is a mode-locked interband cascade laser. Such a source is of great interest for dual-comb spectroscopy, where two mode combs with a slightly different spacing are used to sample a wide spectral range [5]. While this is in principle possible with two Fabry-Perot lasers, the stable phase relation between the modes in a mode-locked device offers significant advantages for the practical implementation of dual comb spectroscopy. Passive mode-locking can be achieved by the insertion of a saturable absorber into the laser resonator. In semiconductor lasers, the saturable absorber can be realized by the application of reverse bias, which in case of ICL requires very careful band structure engineering since alignment of the levels in the minibands used to carrier transport depends on the polarity and the magnitude of the internal electric field. In addition to possible applications in mode-locked lasers, engineering of the active regions towards smaller oscillator strength is also beneficial for Q- or gain switched lasers.

In this work, we present results of theoretical modeling in the framework of eight-band k•p theory of the ICLs' band structure under external electric field performed in order to investigate the effect of the bias value and direction, i.e. from normal lasing conditions as in the gain section to the reversed bias of the absorber part. We present several solutions of the respectively modified type-II QWs of InAs/(In,Ga)(As,Sb)/AlSb materials' system which allow obtaining the demanded lifetime (oscillator strength) ratio in the two parts of the mode-locked laser.

References

1. J. Scheuermann et al., Appl. Phys. Lett. 106, 161103 (2015)
2. M. Dallner et al., Appl. Phys. Lett. 107, 181105 (2015)
3. Y. Jiang et al., J. Appl. Phys. 115, 113101 (2014)
4. I. Vurgaftman et al., Nat. Commun. 2, 585 (2011)
5. G. Villares et al., Nat. Commun. 5, 5192 (2014)

Towards photon counting beyond 2μm using InAs e-APDs

[1]Benjamin. S. White, Xinxin Zhou, Jo Shien Ng and Chee Hing Tan*, [2]Peter Vines and Gerald Buller

[1]*Department of Electronic and Electrical Engineering, Mappin Building, Mappin Street, Sheffield, S1 3JD, U.K*

[2]*Institute of Photonics and Quantum Sciences, Heriot-Watt University, Edinburgh, EH14 4AS, UK*

Single photon detection provides the ultimate sensitivity in photon-starved applications such as remote sensing, quantum communications and time resolved photoluminescence. When the impact ionization process can only be initiated by the electrons only, this single carrier ionization process dramatically reduces the statistical fluctuation in avalanche multiplication. In the absence of feedback ionization events by holes, this so-called electron-avalanche photodiode (e-APD) exhibits an excess noise factor below the classical value of 2 and unlimited gain-bandwidth product, independent of the magnitude of avalanche gain. When operated at very high gain the e-APD can be used to achieve single photon detection. Recent progress in APD development has shown that InAs and HgCdTe have the ionization characteristics of e-APDs. In this work we present recent progress in detection of low photon number, development of planar InAs e-APDs and picosencond laser ranging are presented.

Mesa InAs e-APD was evaluated for low photon detection applications. We demonstrated that when cooled to 130 K, the dark current of is significantly below the noise of a commercial low noise amplifier such that increasing the internal gain has the obvious benefit of increasing the signal without degrading the overall noise of the measurement system. We achieved detection of around 110 photons per pulse at the wavelength of 1550 nm as shown in Fig.1. This demonstrates the potential of InAs for photon counting applications. Time of flight measurements using a pulsed laser at 2.1μm were performed at Heriot-Watt University. A small timing jitter of 46 ps was obtained [1].

To reduce the influence of surface leakage current, we have developed planar InAs e-APD via implantation of Be. A post implant annealing at 550 ^{o}C was performed to produce bulk dominated dark current performance. Planar InAs e-APDs were fabricated. Gain as high as 330 was achieved at 200 K [2] as shown in Fig.2. These results demonstrated the potential of InAs e-APDs for photon counting applications at wavelengths of 2μm or higher.

References

1. Picosecond laser ranging at wavelengths up to 2.4 μm using an InAs avalanche photodiode, Electronics Letters, Vol. 52, No. 5, pp.385-386, 2016.
2. High Gain InAs Planar Avalanche Photodiodes, IEEE J. Lightwave Technology, Vol. 34, No.11, pp. 2639-2644, 2016.

*corresponding author: c.h.tan@sheffield.ac.uk

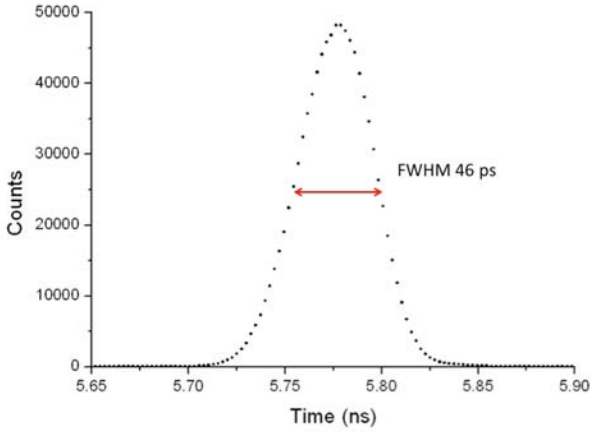

Fig.1. Example of a timing histogram from the APD when illuminated by the supercontinuum laser at 2.1 μm wavelength.

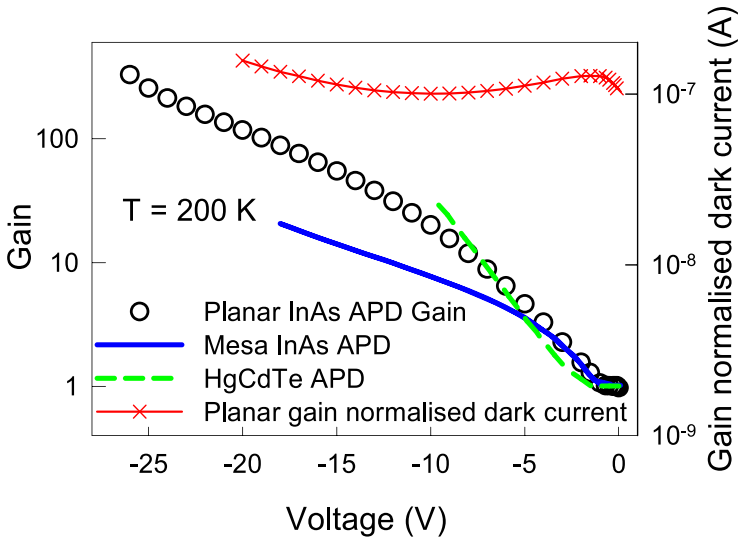

Fig. 2. The gain of a planar APD measured at 200 K using a 1550 nm laser in comparison to data from Mesa InAs APD and HgCdTe APD. The gain normalised dark current of a 200 μm diameter planar APD is also shown at 200 K.

8×8 photodiode array based on P-*InAsSbP*/n-*InAs* single heterostructure

B.A. Matveev[1, 2.*], P.N. Brunkov[1], N.D. Il'inskaya[1], S.A. Karandashev[1], A.A.Lavrov[2], M.A. Remennyi[1, 2], N.M. Stus'[1, 2] and A.A. Usikova[1]

[1] *Ioffe Institute, 26 Politekhnicheskaya, St. Petersburg 194021, Russian Federation*

[2] *IoffeLED, Ltd., 26 Politekhnicheskaya, St. Petersburg 194021, Russian Federation*

There have been considerable progress over the last decade in developing *InAs* homojunction photodiodes (PDs) including the p-i-n PD arrays for fast response sensing of IR radiation around 3 μm [1]. InAs based heterojunction photodiodes, e.g. *InAsSbP/InAs* based ones, potentially offer high R_oA product values but most of related investigations were devoted to PDs with abrupt impurity distribution near a p-n junction that is not optimal for high speed operation. To the best of our knowledge there has been only one paper describing operation of InAs heterostructure array near room temperature [2], however room temperature detectivity value was not high enough for some of the sensing applications.

The report presents characterization of P-*InAsSbP*/n-*InAs*/n+-*InAs*(100) single heterostructure PD array of 8×8 dimensions in the 77-385 K temperature range.

Wafers onto heavily doped n^+-*InAs* (*Sn*) (100) substrates with an electron concentration of $n^+ = (2\text{-}3)\cdot10^{18}$ cm^{-3} contained two epitaxial layers: 3-4 μm thick n-*InAs* active region and P- *InAsSbP* (*Zn*) ($E_g \approx 0.48$ eV, 77 K, $P=(2\text{-}5)\cdot10^{17}$ cm^{-3}) cap layer. Monolithic 8×8 matrix contained 64 individually addressable PD elements of ~190×190 μm size.

Capacitance measurements revealed no impact of the frequency on zero bias capacitance in the 0-2 MHz range and showed reverse cubic dependence on bias suggesting nearly linear impurity distribution near a p-n junction. I-V_{FB} curve ideality factor exhibited minima around 200 K (β =1.03) and reached β =1.2 value at low and elevated temperatures showing negligible influence of tunneling. The latter together with the independence of the (C^{-3})-V slope on temperature states negligible influence or lack of deep recombination centers in P-*InAsSbP*/n-*InAs* single heterostructures under study. As a result nearly unity internal quantum efficiency and nice PD operating parameters have been achieved at low temperatures including low capacitance (10^{-7} F·cm^{-2}, 77 K) and high detectivity values in the thermoelectric range of temperatures and BLIP operation at ~190 K.

The work performed at IoffeLED, Ltd. has been supported by RF state program under contract #14.576.21.0057 (ID: RFMEFI57614X0057).

References

1. W.Sun, Zh.Lu, X.Zheng, J.C.Campbell, Sc.J.Maddox, H.P.Nair, and S.R.Bank, IEEE Journal of Quantum Electronics, VOL. 49, NO. 2, p.154-161 (2013).
2. N.D.Il'inskaya, S.A.Karandashev, N.G.Karpukhina, A.A.Lavrov, B.A.Matveev, M.A.Remennyi, N.M.Stus', and A.A.Usikova, Applied Physics, issue 6, Pages 47-51(2014).

*corresponding author: ioffeled@mail.ru

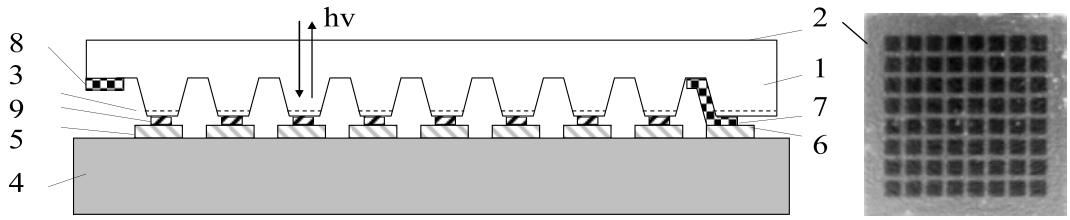

Fig.1. Schematic (left) and IR image (I_{RB}=-2 mA, right) of the BSI array. 1- P-*InAsSbP*/n-*InAs*/n^+-*InAs* single heterostructure, 2 –n^+- *InAs* surface, 3 – mesa walls/p-n junction, 4 – *Si* read-out plate, 5 – anode bonding pads, 6 – cathode bonding pad , 7 – contact to n^+-*InAs*, 8 –ring contact to n^+-*InAs*, 9 – contacts to individual anodes. Items 7 and 8 are electrically connected with each other.

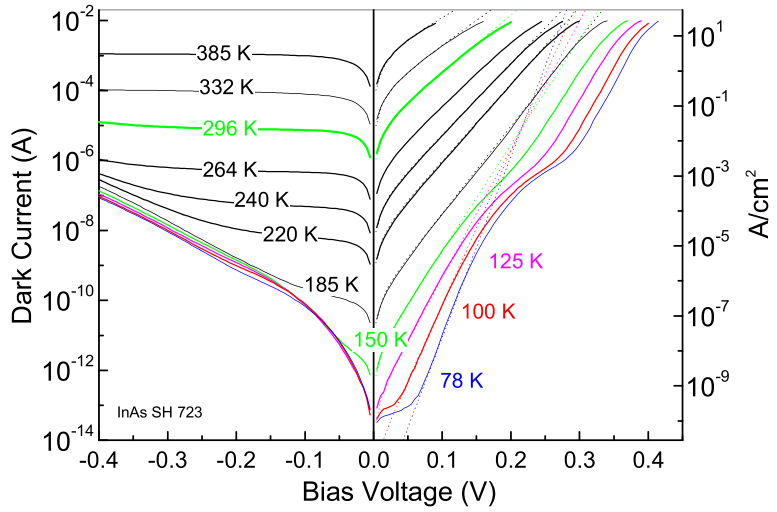

Fig.2. I-V characteristics of the single array element in the 73-385 K temperature range..

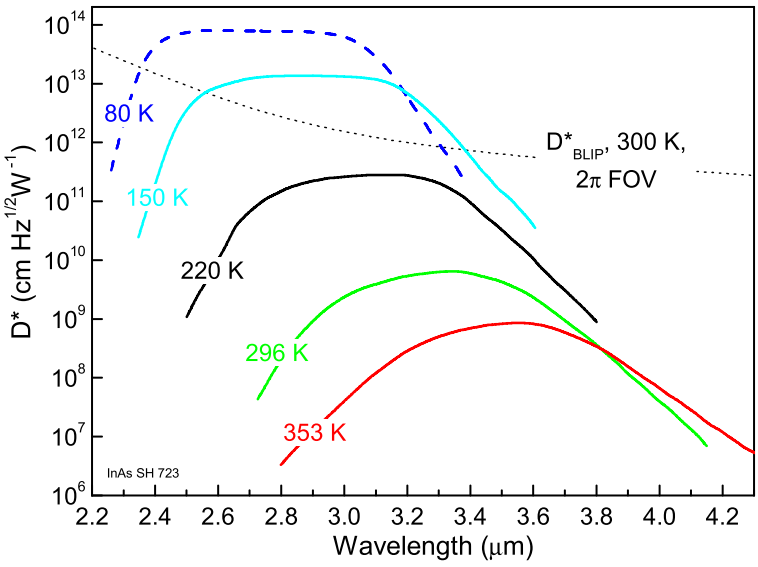

Fig.3. Detectivity spectra of a single array element at 80, 150, 220, 296 and 353 K.

High Performance SWIR HgCdTe FPA on Si for Hyperspectral Detection

Xiaoning Hu[1]*, Qingjun Liao[1], Aibo Huang[1], Lu Chen[1], Xin Chen[1], Hua Fan[1], Ruijun Ding[1], Li He[1]

[1]*Key Laboratory of Infrared Imaging Materials and Detectors, Shanghai Institute of Technical Physics, Chinese Academy of Sciences, Shanghai 200083, China*

This paper reports the development of high performance SWIR FPA from MBE-grown HgCdTe on Silicon substrate in SITP for space-borne hyperspectral detection. To meet the demands of very low flux detection in the short wave infrared range (SWIR), low dark current, high quantum efficiency and high SNR (Signal to Noice Ratio) of FPA are needed. Large thermal mismatch except lattice mismatch between HgCdTe and Si substrate would induce the detector performance deduction when the detector cooled down. In this paper, we design stress-release construction of HgCdTe chip on Si to resolve this issue, and we fabricate 512×512 pixel 30μm pitch SWIR HgCdTe diode array on Si by using this technique. To meet the hyperspectral low flux detection needs, low noise, variable conversion gain and large dynamic range read-out integrated circuit (ROIC) has been designed and hybridized on the HgCdTe diode array on Si substrate. This 512×512 HgCdTe on Si FPA characterizations have been carried out and reveal that the array dark current densities on an order of 10^{-9}A/cm^2, quantum efficiency exceeding 70%, and the operability of 99.5% at operating temperature of around 110K. The SNR of this FPA achieved 120 when illuminated under 5×10^4photons/pixel.

References

1. O. Gravrand, L. Mollard, O. Boulade, V. Moreau, E. Sanson, G. Destefanis, Proc. of SPIE Vol. 8353 (2012)
2. R. Bommena, J.D. Bergeson, R. Kodama, J. Zhao, S. Ketharanathan, H. Schaake, H. Shih, S. Velicu and F. Aqariden, P.S. Wijewarnasuriya, N.K. Dhar. Proc. of SPIE Vol. 9070 (2014)
3. A.R. Wichman, B. Pinkie, E. Bellotti. Dense Array Effects in SWIR HgCdTe Photodetecting Arrays. Journal of Elec. Materials, Vol. 44, p3134-3143（2015）
4. Jonathan Getty, Ellie Hadjiyska et al. VIS/SWIR Focal Plane and Detector Development at Raytheon Instruments Performance Data and Future Developments at Raytheon. Proc. of SPIE vol. 6660 (2007)

*corresponding author: xnhu@mail.sitp.ac.cn

Nanoantenna Integrated Infrared Pixels

A. Fei Yi[1*], B. Ertugrul Cubukcu

[1] *School of Optics and Electronic Information, Huazhong Univeristy of Science and Technology, Wuhan 430074, China*

[2] *Department of Electrical and Computer Engineering, University of California, San Diego, 9500 Gilman Dr., La Jolla, CA 92093, USA*

The concept of the antenna is widely used in the microwave regime to convert freely propagating electromagnetic waves into localized energy, and vice versa[1]. By simple scaling down of antennas, through "scale-invariance" of Maxwell's equations and ignoring kinetic inductance, one gets an antenna for light that has nanoscale dimensions commensurate with the much shorter optical wavelengths. Unlike conventional photonic devices (lenses, mirrors and diffractive elements) which redirect the wave front of optical radiation through the reflection and refraction of electromagnetic waves, resonantly excited optical antennas support localized surface plasmon resonances(LSPR), or the collective oscillation of electron plasma at the surface of nanostructured metals[2]. Since metals are usually not perfect conductors at optical frequencies, the oscillating electron plasma in the optical antenna can cause high losses to the electromagnetic energy and the high optical absorption has led to the demonstration of absorbers for radiation from THz frequencies to the visible region[3]. The electromagnetic energy dissipated in plasmonic absorber is eventually turned into heat and the thermal effects of plasmonic absorbers have enabled the investigation of such structures as nanoscale heat sources in many applications[4].

In this presentation I will talk about our recent works on nanoantenna integrated thermomechanical infrared pixels towards spectral selective mid-infrared detector free of discrete optics such as optical filters and polarizers[5,6]. I will also talk about our proposed thermal infrared pixel array integrated with narrowband nanoantenna absorbers towards on-chip infrared spectroscopy.

References

1. L. Novotny, and N. van Hulst, Antennas for light, Nature Photonics, vol. 5, no. 2, pp. 83-90, 2011.
2. K. B. Crozier, A. Sundaramurthy, G. S. Kino et al., Optical antennas: Resonators for local field enhancement, Journal of Applied Physics, vol. 94, no. 7, pp. 4632-4642, 2003
3. Nathan C Lindquist, Prashant Nagpa, Kevin M McPeak, David J Norris and Sang-Hyun Oh, Engineering metallic nanostructures for plasmonics and nanophotonics，Reports on Progress in Physics, vol. 75, no. 3, pp. 063501-063562, 2012.
4. J. Wang, Y. T. Chen, X. Chen et al., Photothermal reshaping of gold nanoparticles in a plasmonic absorber, Optics Express, vol. 19, no. 15, pp. 14726-14734, 2011.
5. F. Yi, H. Zhu, J. C. Reed et al., Plasmonically Enhanced Thermomechanical Detection of Infrared Radiation," Nano Letters, vol. 13, no. 4, pp. 1638-1643, 2013.
6. F. Yi, H. Zhu, J. C. Reed et al., Thermoplasmonic Membrane-Based Infrared Detector, IEEE Photonics Technology Letters, vol. 26, no. 2, pp. 202-205, 2014.

*corresponding author: feiyi@hust.edu.cn

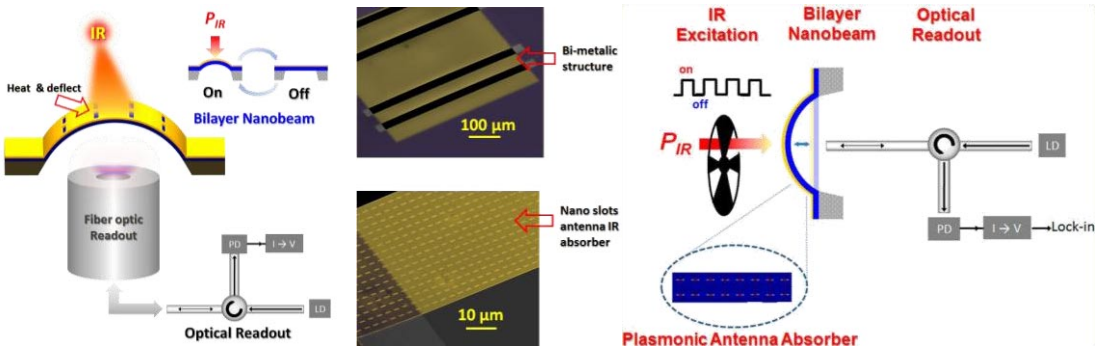

Fig. 1 Nanoantenna integrated thermomechanical infrared detector

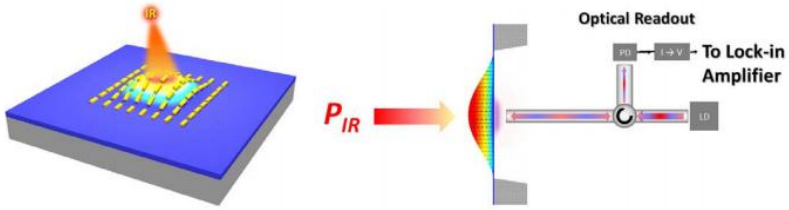

Fig. 2 Thermoplasmonic Membrane-Based Infrared Detector

640×512 InGaAs/InP focal plane array with response extended to visible wavelength band

YANG Bo[1,2,3], SHAO Xiu-Mei[1,2], TANG Heng-Jing[1,2], LI Xue[1,2], GU Yi[3],GONG Hai-Mei[1,2*]

[1] *State Key Laboratories of Transducer Technology, Shanghai Institute of Technical Physics, Chinese Acadamy of Sciences, 500 Yutian Road,Shanghai 200083, China*

[2] *Key Laboratory of Infrared Imaging Materials and Detectors, Shanghai Institute of Technical Physics, Chinese Acadamy of Sciences, 500 Yutian Road,Shanghai 200083, China*

[3] *State Key Laboratory of Functional Materials for Informatics, Shanghai Institute of Microsystem and Information Technology,Chinese Academy of Sciences,865 Changning Road, Shanghai 200050 ,China*

Abstract: In this paper we report our 640×512 InGaAs/InP focal plane array with response extended to visible wavelength band. We have fabricated a 640×512 pixel InGaAs/InP focal plane array, which consists of a backside-illuminated InGaAs/InP detector bump bonded to a silicon read out integrated circuit with a 25 μm pixel pitch. After removing the InP substrate, the response of the focal plane array has covered the wavelength band from 400nm to 1700nm. Quantum efficiency is approximately 16% at 500nm, 54% at 850nm, 91% at 1550nm. The influence of substrate removal process on the performance of the focal plane array has been analyzed. To reduce the reflection from the surface of the array, wide-band antireflection multilayer structures have been designed and simulated. With the deposition of the optimized antireflection coating, the response of the InGaAs/InP focal plane array has been improved for the visible light, as well as the short-wavelength infrared. This focal plane array is suitable for man-portable and night vision applications.

*corresponding author: hmgong@mail.sitp.ac.cn

Tailor the functionalities of metasurfaces: From perfect absorption to phase modulation

Jiaming Hao[1], Che Qu[2], Shaojie Ma[2], Meng Qiu[2], Xin Li[2], Shiyi Xiao[2], Ziqi Miao[2] Qiong He[2], Shulin Sun[2], Ning Dai[1] and Lei Zhou[2]

[1] *National Laboratory for Infrared Physics, Shanghai Institute of Technical Physics, Chinese Academy of Science, Shanghai 200083, China*

[2] *State Key Laboratory of Surface Physics, Key Laboratory of Micro and Nano Photonic Structures (Ministry of Education) and Physics Department, Fudan University, Shanghai 200433, China*

Metamaterials, artificial EM composites composed by subwavelength-engineered units, can possess arbitrary values of electric permittivity and magnetic permeability and thus exhibit amazing EM wave manipulation abilities. As a quintessential example in the big family of metamaterials, Metal-insulator-metal (MIM) resonant configuration consisting of a layer of periodic metallic arrays and a continuous metallic film separated by a dielectric spacer has captured a great deal of attention in recent years, since host of charming wave-manipulation effects were discovered based on the structure, such as, polarization control, reflection-phase modulation, perfect absorption, anomalous light reflection, focusing, and holograms . It is intriguing that MIM metasurfaces can behave distinctly under slight structural tuning and thus realize such diversified applications. But why and when such structures can realize what functionalities are not yet fully understood. Here we provide a general guidance for designing MIM metasurfaces with tailored functionalities. We establish a generic phase diagram in which the functionality of a MIM metasurface is governed by two simple parameters, which are in turn, linked with the system's structural/material details through two relationships that can be derived analytically under certain conditions. Such a phase diagram can greatly facilitate the design of appropriate metasurfaces with tailored functionalities, demonstrated by our experiments and simulations in the Terahertz regime.

References

1. N. Yu, F. Capasso, "Flat optics with designer metasurfaces, Nat. Mater. Vol. 13, pp. 139-150, 2014.
2. J. Hao, Y. Yuan, L. X. Ran, *et al*., "Manipulating Electromagnetic Wave Polarizations by Anisotropic Metamaterials," Phys. Rev. Lett., Vol. 99, pp.063908-4, 2007.
3. J. Hao, J. Wang, X. Liu, *et al*., "High performance optical absorber based on a plasmonic metamaterial," Appl. Phys. Lett., Vol. 96, pp.251104-3, 2010.
4. Qu, C., S. Ma, *et al.*, "Tailor the Functionalities of Metasurfaces Based on a Complete Phase Diagram," Phys. Rev. Lett., Vol. 115, pp.235503-6, 2015.
5. Ma, S., S. Xiao, and L. Zhou, "Resonant modes in metal-insulator-metal metamaterials: An analytical study on near-field couplings,"Phys. Rev. B, Vol. 93, pp.045305-11, 2016.

*corresponding author: jiaming.hao@mail.sitp.ac.cn

Quantum Cascade Lasers: From Mid-infrared to THz

F.-Q. Liu, Y.H. Liu, Y.Y Li, J.C. Zhang, J.Q. Liu, and Z.G. Wang

Key Laboratory of Semiconductor Materials Science, Institute of Semiconductors, Chinese Academy of Sciences, and Beijing Key Laboratory of Low Dimensional Semiconductor Materials and Devices,P.O. Box 912, Beijing 100083, China

Quantum cascade lasers are (QCLs) semiconductor laser sources based on intersubband transitions in multiple quantum well systems. Their unique operation principle and good performance have established themselves as the leading tunable coherent semiconductor source in the infrared and terahertz (THz) regimes. Despite eminent improvements obtained in the past years, the development of mid-infrared and THz QCLs with high power, high efficiency, high spectral performance and good beam quality is still a challenging task. Here, we report some results on design, growth, fabrication, and operation of mid-infrared and THz QCLs in the Institute of Semiconductors, Chinese Academy of Sciences. The following representative results are demonstrated. (1) Mid-infrared distributed feedback (DFB) QCLs with characteristics of low power consumption, high-power substrate-emitting, surface-emitting with a low threshold current density, collimated laser beam with a small divergence of 2.9°×0.12°, coupled-ridge waveguide laser array with a nearly diffraction limited beam pattern, and sample grating laser array with a broad tunability. (2) The first quantum dot cascade laser operated at room temperature in continuous-wave mode with wavelength of 7.15 μm. (3) THz QCLs with emitting powers of > 1.37 W and single mode power of 286 mW.

References

1. Y.H. Liu, J. C. Zhang, Z.W. Jia, D.Y. Yao, F. Q. Liu et al., Development of low power consumption DFB quantum cascade lasers, IEEE Photon.Technol.Lett. 27, 2335-2338 (2015).
2. D.Y. Yao, J. C. Zhang, F. Q. Liu et al., 1.8W room temperature pulsed operation of substrate-emitting quantum cascade lasers, IEEE Photon.Technol.Lett. 26, 323-325 (2014).
3. J. C. Zhang, D.Y. Yao, N. Zhuo, F.L.Yan, F. Q. Liu et al., Directional collimation of substrate emitting quantum cascade laser by nanopores arrays, Appl. Phys. Lett. 104, 052109 (2014).
4. Y.H. Liu, J. C. Zhang, F.L.Yan, F. Q. Liu et al., Coupled ridge waveguide distributed feedback quantum cascade laser arrays, Appl. Phys. Lett. 106, 142104 (2015).
5. F.L.Yan, J.C. Zhang, C.W. Liu, N. Zhuo, FQ. Liu et al., Sample Grating Distributed Feedback Quantum Cascade Laser Array, Nanoscale Research Letters 10,406 (2015).
6. N. Zhuo, F.-Q. Liu et al., quantum dot cascade laser, Nanoscale Research Letters 9, 144(2014).
7. Y.Y. Li, J.J. Liu, F. Q. Liu et al., High-performance operation of distributed feedback terahertz quantum cascade lasers, Electron. Lett., EL20160700.3d (2016).

*corresponding author: fqliu@semi.ac.cn

Extraordinary optical transmission through subwavelength hole array on superconducting MgB_2 thin films

X. Fang, X,G. Qiu*

Institute of Physics, Chinese Academy of Sciences, Beijing 100190, China

Light transmission through subwavelength holes on metallic films works beyond the traditional diffraction limit when light excites evanescent surface waves on the film (*1*). Although geometric factors, such as hole diameters, of the excitation have been extensively investigated (*2*), the influence of the intrinsic properties of the metal remains to be explored. Especially in the THz regime, metals are routinely treated as perfect electromagnetic conductors, completely overlooking their specific material properties. Here we show that THz transmission through subwavelength holes, on either MgB_2 or gold thin films, can be greatly enhanced with decreasing temperature, and become much more pronounced in the superconducting state of the MgB_2 film. This enhancement is attributed to the temperature-induced change of the complex conductivity of MgB_2 and gold.

*corresponding author: xgqiu@iphy.ac.cn

Microwave radiation absorption and Shubnikov-de Haas oscillations of InAs/GaSb/AlSb quantum wells

M.P. Mikhailova[1], A.I. Veinger[1], I.V. Kochman[1], P.V. Semenikhin[1], K.V. Kalinina[1], R.V. Parfeniev[1], V.A. Berezovets[1], A. Hospodkova[2], J. Pangrac[2], E. Hulicius[2*]

[1] *Ioffe Physical-Technical Institute, 194021, Saint-Petersburg, Russia*
[2] *Institute of Physics CAS, v.v.i., 162 00, Prague, Czech Republic*

Magnetotransport, optical, spin-dependent and topological properties of the composite InAs/GaSb/AlSb quantum wells (CQWs) based on the broken-gap heterojunctions (see Fig 1) are actively studied during two last decades as promising materials for new applications. We report on microwave radiation absorption and Shubnikov-de Haas (SdH) oscillation study in semimetal InAs/GaSb/AlSb CQWs at low temperatures of 2.7-20 K and in magnetic field H up to 14 kOe (see Fig 2). Mid-infrared superlinear electroluminescence was observed in deep AlSb/InAsSb QWs [1]. Recently low temperature transport measurement of the invert InAs/GaSb/AlSb CQWs was studied. Hybridization gap and Quantum Spin Hall effect were observed by applying of the electric and magnetic field [2].

CQWs were grown by MOVPE on n-GaSb (100) substrates with various widths of InAs QWs (15 nm or 12.5 nm) and GaSb (10 nm or 8 nm) surrounded by AlSb barriers (30 nm) and GaSb cap layer (3 nm).

Method of EPR spectroscopy was used and derivate microwave power (*dP/dH*) was measured (f=10 GHz). Intensive oscillations were observed at H > 7-14 kOe. Temperature and orientation dependence of SdH oscillation amplitudes were recorded. 2D-electron concentration ns ≈ 2×10^{12} cm^{-2} was obtained from the filling factor dependence on inverse magnetic field. Cyclotron frequency and non-parabolicity of effective mass were evaluated (m^*_e=0.028 m_0 and m^*=0.0408 m_0) for the samples with different QW widths. Unusual anisotropy of angular dependence of the oscillation amplitudes on orientation of CQW samples in magnetic field was observed in the angle range from 0° up to 180°. These results can be explained by an inversion asymmetry which is the feature of substances with lack of inversion center.

References

1. M.P. Mikhailova, E.V. Ivanov, L.V. Danilov, K.V. Kalinina, N.D. Stoyanov, G.G. Zegrya, Yu.P. Yakovlev, E. Hulicius, A. Hospodková, J. Pangrác, M. Zíková, J. Appl. Phys. 112 (2012) 023108.
2. L. Du, I. Knez, G. Sullivan, R.R. Du, Robust Helical Edge Transport in Gated InAs/GaSb Bilayers, Phys. Rev. Let. **114** (2015) 096802.

Acknowledgements

The authors acknowledge support from MPNS COST ACTION MP1204 - TERA-MIR Radiation: Materials, Generation, Detection and Applications and partly by RFFI grant project 15-02-03151, CSF project number 13-15286S, 16-11769S, 14-21285P and Infrastructural MSMT projects LM 2011 026 and NPU LO1603 - ASTRANIT.

* *corresponding author:* hulicius@fzu.cz

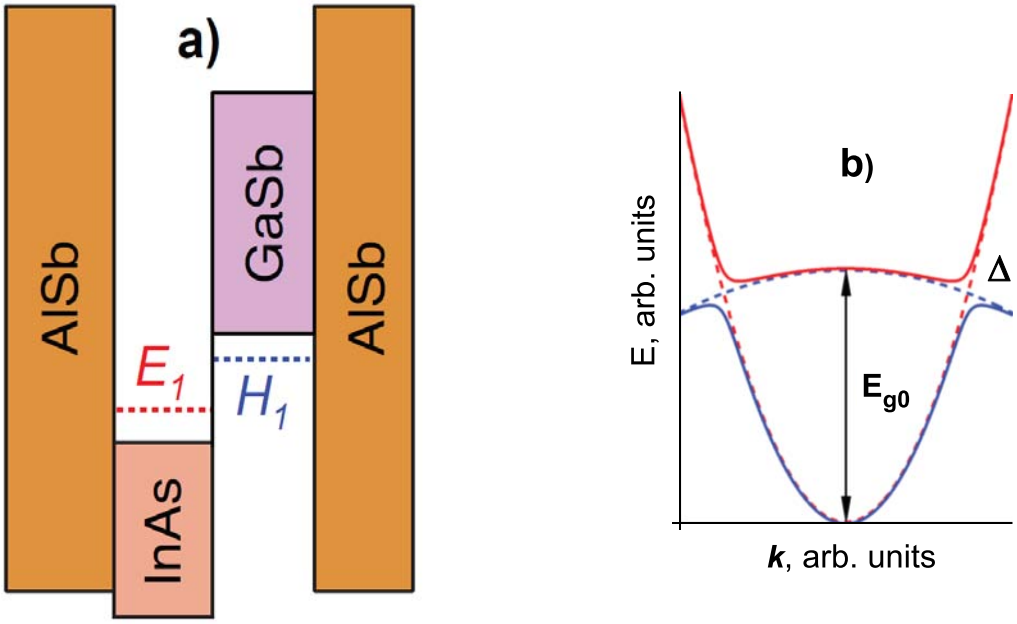

Fig.1. Inverted energy band diagram of the structure and scheme of InAs/GaSb/AlSb QW – sample **B** (InAs a_e = 12.5 nm, GaSb a_h = 8 nm). $E_1 = h^2/8 \bullet m_e \bullet a_e^2$ =100 meV, $E_H = E_{g0} - h^2/8 \bullet m_h \bullet a_h^2$ =136 meV, E_{g0}=150 meV.

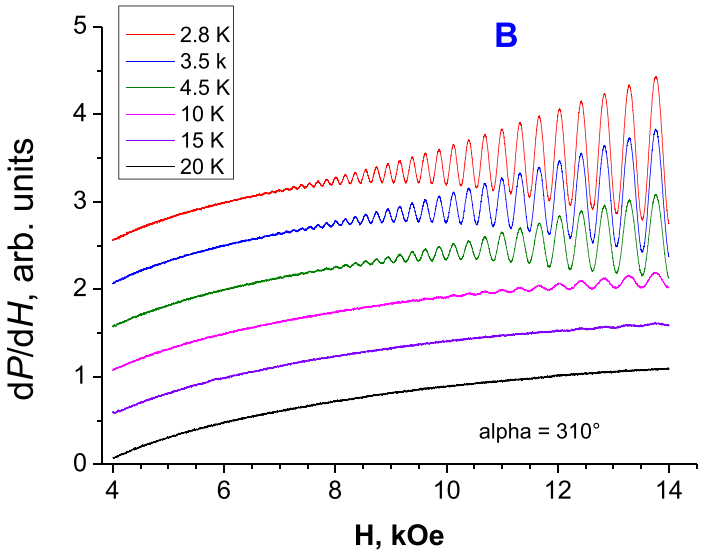

Fig.2. SdH oscillation amplitude dependence of sample **B** on magnetic field. Temperatures: 2.8 K; 3.5 K; 4.5 K; 10 K; 15 K; 20 K. Derivative of the microwave power dP/dH is on y-axes, magnetic field on x-axis.

Homogeneously spectral spanning of terahertz quantum cascade lasers with radio frequency modulation

W. J. Wan, H. Li*, J. C. Cao*

Key Laboratory of Terahertz Solid State Technology, Shanghai Institute of Microsystem and Information Technology, Chinese Academy of Sciences, 865 Changning road, Shanghai 200050, China

The terahertz quantum cascade laser (QCL) is the unipolar emitting device based on the electron intersubband transitions in the multiple-quantum-well active region. Among all the electrically pumped semiconductor lasers, the terahertz QCL shows the highest performance in the frequency range between 1 and 5 THz. Followed by the fast development of frequency combs in the visible and infrared wavelengths, the research on terahertz QCL-based broadband combs has attracted wide interest[1-4].

In this work, we employ an active region structure combining the bound-to-continuum and resonant-phonon designs. The molecular beam epitaxy-grown wafer is processed into single plasmon waveguide ridge lasers. At the low temperature of 10 K, the fabricated lasers show ultralow threshold current density around 50 A/cm^2 in the continuous wave (cw) mode. We systematically investigate the electrical inter-mode beat note of a 6-mm long cavity QCL and its eye diagram to show the stability of the laser longitudinal modes. Since the inter-mode beating frequency is the result of the mixing between the adjacent longitudinal modes and the frequency falls in the radio frequency (RF) range, the laser can be modulated with the external RF signal. With RF modulation, we finally observe a homogeneously spectral spanning of 320 GHz which continuously covers the spectral range from 4.01 to 4.33 THz. The modes are evenly spaced by the external RF frequency at 6.1 GHz. The homogenous emission spectra can be used for spectroscopic applications with a spectral resolution of few GHz. As examples, we use the long cavity QCL to measure the transmission of a GaAs etalon sample and the oscillation feature in the transmission can be clearly observed; we also show that the QCL can be used to measure the absorption lines of NH_3 gas around 4.2 THz and the measured results show good agreement with the HITRAN data.

References

1. G. Villares, A. Hugi, S. Blaser, and J. Faist. Dual-comb spectroscopy based on quantum-cascade-laser frequency combs, Nature Communications 5, 5192, 2014.
2. H. Li, L. Pierre, G. Djamal, A. Marc, et al., Dynamics of ultra-broadband terahertz quantum cascade lasers for comb operation, Opt. Express 23 (26), 33270, 2015.
3. M. Rosch, G. Scalari, M. Beck, and J. Faist. Octave-spanning semiconductor laser, Nature Photonics, 9 (1), 42, 2015.
4. Y. Yang, D. Burghoff, D. J. Hayton, J. R. Gao, J. L. Reno, and Q. Hu. Terahertz multiheterodyne spectroscopy using laser frequency combs, Optica 3 (5), 499, 2016.

*corresponding author: hua.li@mail.sim.ac.cn, jccao@mail.sim.ac.cn

New life of InAs-based quantum cascade lasers

A.N. Baranov*, M. Bahriz, R. Teissier

Institute of Electronics and Systems, UMR 5214 CNRS – University of Montpellier, 34095 Montpellier, France

Quantum cascade lasers (QCLs) have become nowadays light sources of choice for a large variety of applications including gas sensing, infrared imaging etc. The development of InAs-based quantum cascade lasers was initially inspired by the giant conduction band discontinuity of 2.1 eV between InAs and AlSb. This large band offset allows hosting high energy intersubband transitions, necessary to fabricate short wavelength QCLs [1]. The InAs/AlSb material family made possible fabrication of the first QCLs emitting below 3.5 μm. The shortest QCL emission wavelength of 2.6 μm has been obtained in the InAs-based devices [1].

The successful development of interband cascade lasers and type-I quantum well lasers during the last decade made the competition around 3 μm very strong and InAs-based QCLs have lost their exclusivity in this domain. New life has been breathed into this technology by extension of the spectral range of their operation beyond 15 μm. In the far-infrared devices it is possible to fully exploit another advantage of this material family, the small electron effective mass in InAs, providing a high QCL gain, because this benefit is higher when the lasing transition levels are close to the bottom of the conduction band and the effect of nonparabolicity is weak [1].

Even the very first InAs/AlSb QCLs operating above 15 μm exhibited lower thresholds and higher maximum operation temperatures compared with InP- and GaAs-based devices. Employing a double-metal surface plasmon waveguide we have demonstrated InAs-based QCLs emitting at 16-21 μm and operating up to room temperature (RT) in pulsed mode [1]. Further performance improvement and, notably, a decrease in the RT threshold current density below 1 kA/cm^2 has been obtained in the devices with a dielectric InAs-based waveguide and a design optimized to reduce the QCL transparency current. This progress allowed us to achieve the continuous wave (cw) regime at room temperature in lasers emitting at 15 μm, now the longest cw RT wavelength for any semiconductor laser [2]. Due to the smaller optical phonon energy compared with GaAs- and InP-based materials the InAs/AlSb QCLs are supposed to be able to enter farther into the reststrahlen band, providing emitters for the region near 30 μm not yet accessible for semiconductor lasers. The higher intersubband gain can also be exploited in THz QCLs.

References

1. A.N. Baranov and R. Teissier, *IEEE J. Select. Topics Quantum Electron.* **21**, 1200612 (2015).
2. A.N. Baranov, M. Bahriz and R. Teissier, to be published in *Optics Express* (2016).

*corresponding author: baranov@univ-montp2.fr

Terahertz master-oscillator power-amplifier quantum cascade laser with stable single-mode emission

H. Zhu[1], F. F. Wang[1], L. H. Li[2], Q. Yan[1], C. R. Yu[1], J. X. Chen[1], L. Chen[2], E. H. Linfield[2], A. G. Davies[2], R. Colombelli[3], G. Xu[1*], L. He[1]

1 Key Laboratory of Infrared Imaging Materials and Detectors, Shanghai Institute of Technical Physics, Chinese Academy of Sciences, Shanghai 200083, China.

2 School of Electronic and Electrical Engineering, University of Leeds, Leeds LS2 9JT, UK

3 Institut d'Electronique Fondamentale, Univ. Paris Sud, CNRS UMR8622, 91405 Orsay, France

Master-oscillator power-amplifier (MOPA) is an effective architecture to achieve single-mode lasing with high output power and directional beam pattern. MOPA semiconductor lasers have been realized in near- and mid-infrared frequency ranges [1, 2]. However, extending the MOPA concept to THz frequency is a challenge. Because of the very long wavelength, the anti-reflection layers used to suppress self-lasing in the amplifier are so thick that the deposition becomes extremely difficult.

In this paper, we report novel MOPA semiconductor lasers that feature stable single-mode lasing and power amplification in THz frequency range. The device uses a quantum cascade active region as the gain medium, and we call it as a THz-MOPA-QCL. Fig. 1 (a) shows the scheme of a THz-MOPA-QCL, where a double-metal waveguide is used. Both the master-oscillator (MA) and the power-amplifier (PA) share the same active region and can be separately pumped. The MO section is a first-order distributed feedback laser. A diffraction grating is formed in the top metallization of the PA section to extract THz radiation, while an absorbing boundary is set at the end of the PA to suppress facet reflection, and thus to eliminate self-lasing. Fig. 1(b) illustrates the calculated electromagnetic field in the whole structure, which clearly shows the mode oscillation in the MO, the THz wave injection and propagation in the PA, as well as the wave extraction from it.

Fig. 2 (a) and (b) present the experiment results of the THz-MOPA-QCLs. Fig. 2(a) shows the emission spectra of three devices, where the grating periodicity of the MO section varies. Single-mode emission is achieved and the wavelength scales linearly with the grating periodicity. We note that, once the MO driven current is above the threshold, the device exhibits single-mode emission and the wavelength keeps unchanged with all tested currents in the MO and PA sections. In addition, no emission was observed when only the PA was pumped, indicating that self-lasing is effectively suppressed in the PA. These results demonstrate that the device operates on the DFB mode, and the THz emission is stimulated in the MO. Fig. 2(b) shows the light-current-voltage (*L-I-V*) curves of a typical device measured at 20 K, where the output power was measured as a function of the MO current at various PA bias. When the PA is biased at the laser threshold (3.41 V), where it can be approximately regarded as transparent, the device peak output power is 34.7 mV (the readout of the photodetector). When the PA bias is 4.30 V, corresponding to the peak gain, the output power reaches 177.8 mV. We note the output power of a typical second-order DFB laser – fabricated from the same material and measured under the same conditions – peaks at 82.8 mV. Fig. 3 (a) and (b) show the measured and calculated far-filed emission pattern of a typical THz-MOPA-QCL, respectively. The divergence angle of the emission beam is ~15×45, in good agreement with the calculation.

In conclusion, our THz-MOPA-QCLs demonstrate stable generation and power amplification of single mode emission. The amplification factor is about 5, and the output power is approximately twice that of second-order DFB lasers. Our work provides a new solution for high power THz sources.

References

[1] M. Troccoli, C. Gmachl, F. Capasso, D. L. Sivco, A. Y. Cho, "Mid-infrared (λ≈7.4 μm) quantum cascade laser amplifier for high power single-mode emission and improved beam quality," Appl. Phys. Lett. **80,** 4103 (2002).

[2] C. Mauro, R. P. Green, A. Tredicucci, F. Beltram, H. E. Beere, D. A. Ritchie, "Amplification of terahertz radiation in quantum cascade structures", J. Appl. Phys. **102**, 063101 (2007).

* Corresponding author: gangyi.xu@mail.sitp.ac.cn

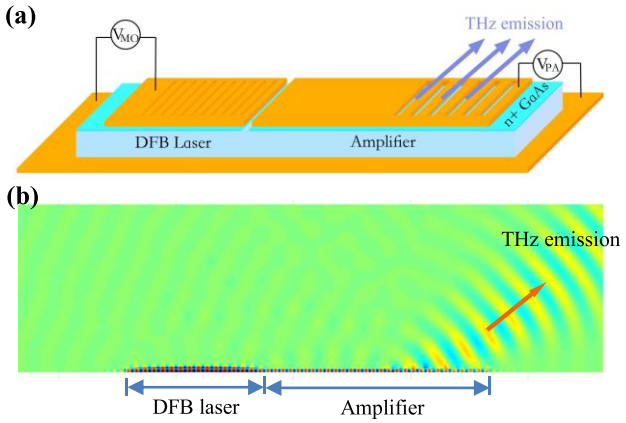

Fig. 1 (a) Schematic illustration of a THz-MOPA-QCL based on a metal-metal waveguide. The MO section is a first-order DFB laser. The PA section contains a diffraction grating to exact the THz radiation, and an n^+ GaAs absorbing boundary to suppress self-lasing. (b) Mode distribution (vertical component of the electric field) along the cross-section of the device.

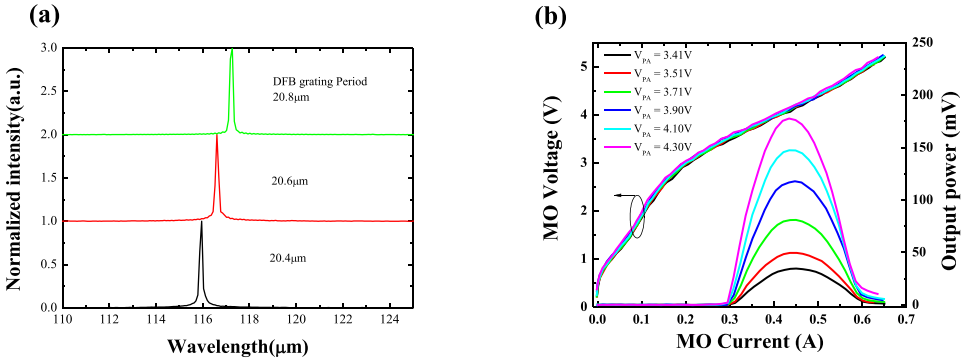

Fig. 2 (a) Emission spectra of 3 THz-MOPA-QCLs, where the grating periodicities of DFB laser (MO) varies from 20.4 to 20.8 μm. (b) *L-I-V* curves of a typical THz-MOPA-QCL measured at 20K, where the output power was measured as a function of the MO current at different PA bias (V_{PA}). V_{PA}=3.41 V corresponds to the threshold bias, while V_{PA}=4.30 V to the maximum output power.

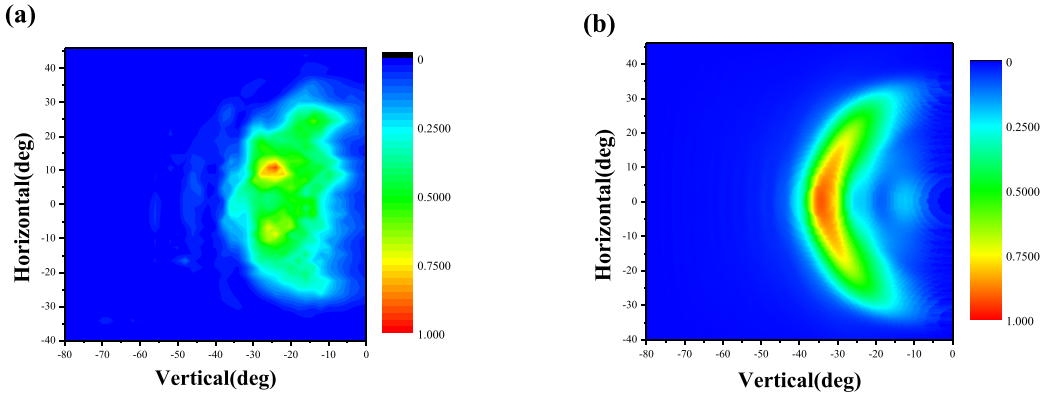

Fig. 3 (a) 2D far-field beam pattern of a THz-MOPA-QCL measured at 20K, where the MO and PA sections were all pumped. (b) Calculated beam pattern of the device by finite difference time domain (FDTD) simulation.

High-power terahertz quantum cascade lasers

Y.Y. Li, J.Q. Liu*, J.C. Zhang, F.Q. Liu, and Z.G. Wang

Key Laboratory of Semiconductor Materials Science, Institute of Semiconductors, Chinese Academy of Sciences, P.O. Box 912, Beijing 100083, China

We demonstrate high-power terahertz (THz) quantum cascade lasers (QCLs) with semi-insulating surface-plasma (SISP) waveguide. The active region is based on a bound-to-continuum transition, combined with a single-quantum-well phonon extraction/injection stage. Epitaxial-side down mounted lasers and distributed feedback (DFB) tapered lasers are both fabricated with high output power and good beam pattern.

THz QCLs with SISP waveguide can provide high output power and well-shaped beam pattern due to the small optical confinement factor in the active region. However, the performance is affected seriously by the poor heat removal ability in the active core. In order to enhance the heat extraction from the active region, we adopt an epitaxial-side down (Epi-down) mounting [1] scheme in coplanar waveguide for SISP THz QCLs. Figure 1 shows the pulsed light-current (*L-I*) curves from a wide ridge Epi-down mounted laser (500 μm × 4 mm). At 10 K, a threshold current density (J_{th}) of 110 A/cm^2 is obtained with a peak power of 685 mW from a single facet. Taking into account the radiation emitted from both facets, the device delivers 1.37 W of power with a slope efficiency of 574 mW/A which means each injected electron generates a differential quantum efficiency (DQE) of ~45 photons. The lasing is observed continue up to a temperature of ~110 K.

For various applications, THz QCLs with good emission characteristics of not only high-power, but also stable single-mode and well-shaped beam pattern are desirable. Based on the same active region structure, we designed surface metallic-stripe grating structure with tapered geometry. The straight ridge section is narrow enough to select the fundamental transverse mode TM_{00} for good beam pattern as well as the large tapered section is used to broaden the gain area for higher output power. The inset of Figure 2 depicts the top schematic diagram of the laser. The narrow straight ridge is 200 μm. The tapered ridge is 2.5-mm-long with a taper half-angle θ of 2.5°. The normalized spectra for tapered DFB lasers are displayed in Figure 2. These devices lase at 96.4, 97.1 and 98.8 μm, respectively. Stable single-mode of ＞20 dB is realized under all tested currents and temperatures. Figure 3a shows the pulsed operation characteristics of the tapered lasers. The maximum emission powers are 165 mW, 286 mW, and 188 mW at 10 K, respectively. Single-lobe beam patterns are obtained due to the fundamental transverse mode selection effect of the narrow straight section and the existence of high-loss boundary conditions shown as in Figure 3b.

References

1. F.L. Yan, J.C. Zhang, C.W. Liu, N. Zhuo, F.Q. Liu, S.Q. Zhai and Z.G. Wang, Nanoscale Res. Lett., Vol. 10, pp. 406-1–406-5, 2015.

*corresponding author: jqliu@semi.ac.cn

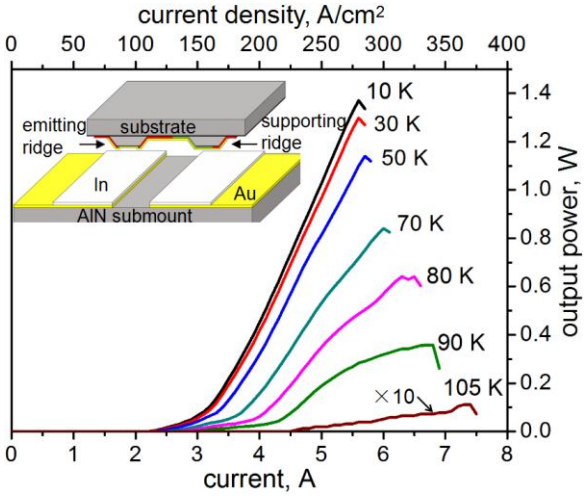

Fig.1. Light against current from a 500 μm-wide and 4 mm-long Epi-down mounted device in pulsed mode.

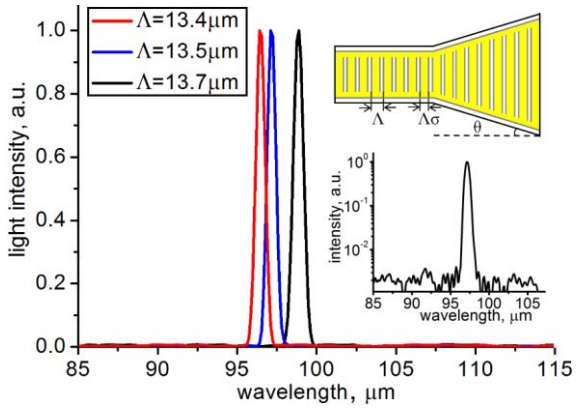

Fig.2. Lasing spectra of tapered DFB lasers with different grating periods.

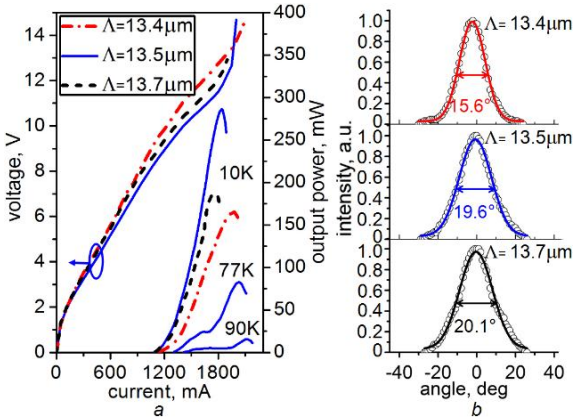

Fig.3. Light-voltage-current curves, and beam patterns for 2.5° tapered DFB lasers.

Inducing changes in lateral mode selection in broad area quantum cascade lasers

Ron Kaspi*, Chi Yang, Chunte Lu, Sanh Luong and Timothy C. Newell

Air Force research Laboratory, Directed Energy Directorate AFRL/RDLTD
Albuquerque, New Mexico, USA 87117

Power scaling in quantum cascade lasers is possible by fabricating broad area devices with a large cavity width. When the cavity width is larger than ~10μm, however, higher order cavity modes become operational. At cavity widths near ~100μm, the high order cavity mode will produce two beams that are largely divergent in the far-field [1], diminishing the usefulness of such devices, and limiting the brightness that can be achieved.

We will demonstrate how a simple plane wave model can be used to explain mode selection in a typical broad area rectangular box waveguide geometry.

A focused ion beam tool (FIB) can be used to carve and create unconventional geometries of the cavity after the fabrication is complete [2]. We have used this tool to change the geometry, as well as the index profile to deliberately reduce the viability of the high order modes while enhancing the operation of the fundamental mode.

Through incremental changes to the cavity, we will show how the mode behavior affected. For example, we find that FIB milling of unfilled narrow trenches that span only ~3% of the cavity length can induce sufficient coupling loss to the higher order modes at all power levels. A comparison of far field spectra measured from unaltered Fabry-Perot device and the same device after a 30% and 50% lateral constriction is shown in the figure, where most of the power is transferred to the fundamental mode.

The authors are grateful to the US Air Force Office of Scientific Research for funding this work.

References

1. Y. Bai, S. Slivken, S. R. Darvish, A. Haddadi, B. Gokden, and M. Razeghi, “High power broad area quantum cascade lasers,” Appl. Phys. Lett. **95**, 221104 (2009).
2. P.M. Bouzi, P.Q. Liu, N. Aung, X. Wang, J-Y. Fan, M. Troccoli, and C.F. Gmachl, “Transverse mode control in quantum cascade lasers via lossy lateral constrictions,” Proc. Of SPIE Vol. 8640, 864001V-1 (2013).

*corresponding author: rkaspi@comcast.net

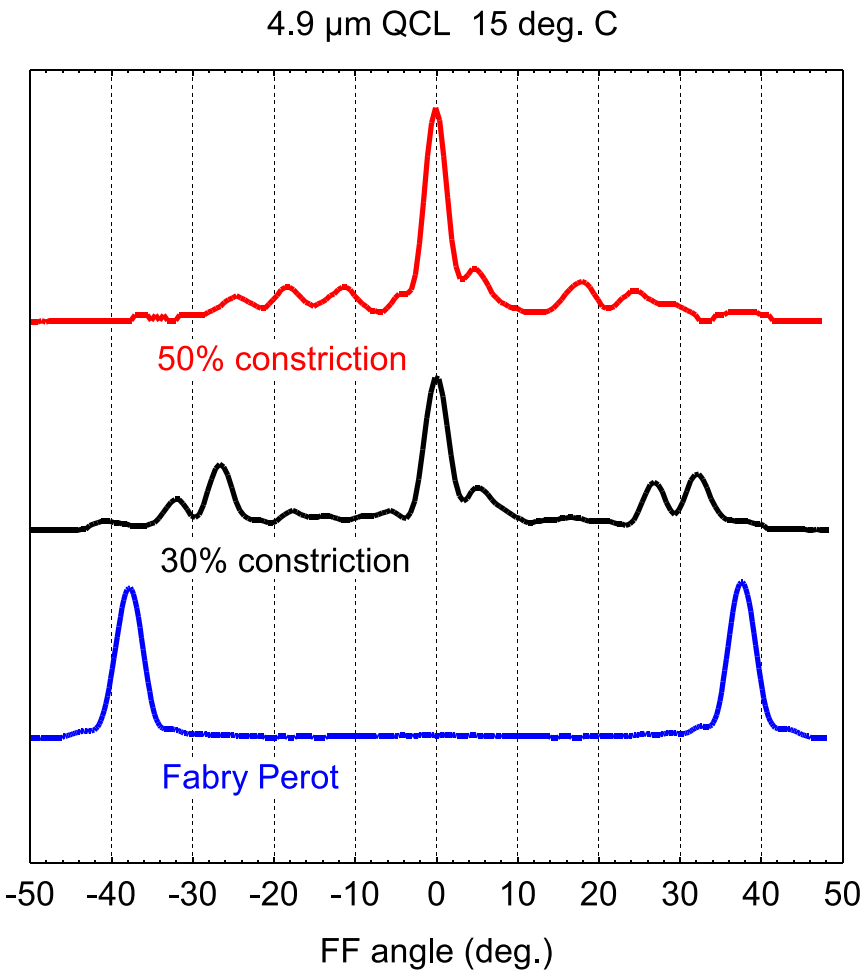

Fig. 1. Far field spectra collected from broad area QCL device showing changes in lateral mode selection.

Extending the wavelength of superluminescent LEDs to mid-infrared wavelengths

S. Suomalainen[1*], J. Viheriälä[1], N. Zia[1], R. Koskinen[1], M. Koskinen[1] and M. Guina[1]

[1] *Optoelectronics Research Centre, Tampere University of Technology, P.O.Box 692, 33101 Tampere, Finland*

Compact, wavelength tunable, single-mode light source with low-power consumption emitting at mid-infrared spectral region (2-4 μm) are on the demand list of many applications, such as gas sensing or medical spectroscopy. Superluminescent light emitting diodes (SLEDs) are light sources offering a unique combination of optical characteristics including high brightness, good beam directionality and the broad emission spectrum. Detection of multiple environmental gasses with single measurement would be enabled by integration of mid-infrared SLED with novel Si-filter [1].

The development of SLEDs emitting in the 2–3 μm spectral range has until recently received little attention due to several peculiar aspects of GaSb-technology, which is not widely available [2, 3]. We have recently demonstrated GaSb-SLEDs emitting at 2 μm with different waveguide designs [4]. By selecting the waveguide design, we were able to increase the output power from sub-mW level to several tens of mW.

In this work, we report SLEDs emitting at 2.65 μm emission. The structure consists of two GaInAsSb-quantum wells embedded in lattice-matched AlGaAsSb-waveguide- and cladding-layers on GaSb-substrate. The SLED exhibited nearly 0.5 mW output power and the spectrum was 300 nm wide, as shown in Fig 1. To the best of or knowledge these are the first SLED results at such long wavelength. The development path for wavelength extension towards 3 μm region will be also discussed.

References

1. *http://www.h2020-miregas.eu/H2020-MIREGAS/Home.html*

2. M. Wootten, J. Tan, Y. Chien, J. Olesberg, J. Prineas, "Broadband 2.4 μm superluminescent GaInAsSb/AlGaAsSb quantum well diodes for optical sensing of biomolecules, " Semicond. Sci. Technol. 29, 115014 (2014).

3. K. Vizbaras, E. Dvinelis, I. Simonyte, A. Trinkunas, M. Greibus, R. Songaila, T. Zukauskas, M. Kausylas, and A. Vizbaras, "High power continuous-wave GaSb-based superluminescent diodes as gain chips for widely tunable laser spectroscopy in the 1.95-2.45 μm wavelength range, " Appl. Phys. Lett. 107, 011103 (2015).

4. N. Zia, J. Viheriälä, R. Koskinen, M. Koskinen, S. Suomalainen, and M. Guina, "Fabrication and characterization of broadband superluminescent diodes for 2 μm wavelength," Photonics West 2016, 9768-24 (2016).

*corresponding author: soile.suomalainen@tut.fi

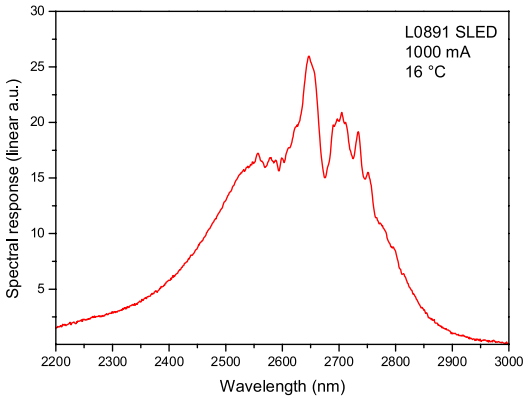

Fig. 1. Typical spectrum demonstrating the broadband emission capabilities.

New Structures for Single Lobe Operation Quantum Cascade Lasers Array

S. Ferré[1,2*], A. Peinado[3], E.Garcia-Caurel[3], Mathieu Carras[1]

[1] *mirSense, 86 rue de Paris, Bat. Erable, 91400 Orsay, France.*
[2] *Thales Research & Technology, Route Départementale 128, 91767 Palaiseau, France*
[3] *LPICM, CNRS, Ecole Polytechnique, Université Paris-Saclay, 91128 Palaiseau, France*

Latest record-breaking high power Quantum Cascade Lasers (QCL) have opened the way for applications in need of high performances [1], such as direct countermeasures, or high precision spectroscopy. To reach higher power, one can increase the QCL ridge width. Nevertheless the optical and thermal performances are quickly degraded in this way [2]. In fact, more transverse mode are allowed to lase, strongly affecting the beam spot quality. In addition, the thermal load becomes too large to be dissipated in continuous mode (CW) confining large devices to very short pulse operation. To address both optical issues, coupled QCLs arrays have been developped, either with evanescent or antiguided coupling. However bi-lobed farfield impinges upon evanescently coupled devices [3] whereas antiguided ones are suffering from a complex fabrication with two regrowth and lossy modal filtering [4].

We will propose new ways to reach single, or quasi-single, lobe emission. In particular, we will present advantages and limitations of non-uniform arrays and structures providing antiguiding by using an innovative material to fill the spacing in between the ridges, later called stripes, as shown in Fig. 1. We obtain by Mueller ellipsometry the refractive index of this material, to prove that it is higher than the active region (AR) index, typically 3.2 to 3.35, which is a necessary condition for antiguiding. Increasing the stripes spacing, we sequentially favor in-phase and out of phase modes as shown in Fig. 3. The first 4 modes are presented in Fig. 4a-4d. Optical and thermal simulations will be presented to explain how to design the geometry of such devices. First fabrication steps will be detailed and exhibited.

References

1. Y. Bai, N. Bandyopadhyay, S. Tsao, S. Slivken, M. Razeghi, “Room temperature quantum cascade lasers with 27% wall plug efficiency”, APL 98, 181102 (2011)
2. Y. Bai, S. Slivken, S. R. Darvish, A. Haddadi, B. Gokden, M. Razeghi, “High power broad area quantum cascade lasers”, APL 95, 221104 (2009)
3. S. Ferré., B. Simozrag, V. Trinité, M. Carras, “µ-Stripes Quantum Cascade Lasers Arrays at 4.6 µm”. In CLEO (p. CB_11_6) (2015)
4. J. D. Kirch, C. C. Chang, C. Boyle, L.J. Mawst, D. Lindberg III, T. Earles, D, Botez, “5.5 W near-diffraction-limited power from resonant leaky-wave coupled phase-locked arrays of quantum cascade lasers”, APL, 106(6), 061113 (2015)

*corresponding author: simon.ferre@mirsense.com

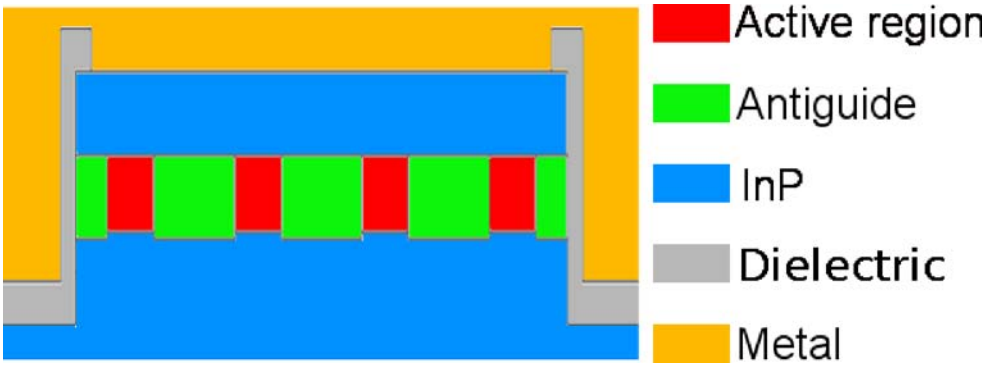

Fig.1. Typical structure for an antiguided QCL array. The AR stripes are surrounded laterally by a higher index material, sandwiched between two InP cladding layers

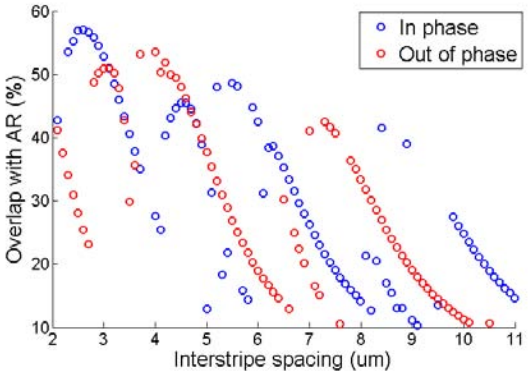

Fig 2. Overlap of the in-phase and out-of-phase modes with the AR vs the stripes spacing

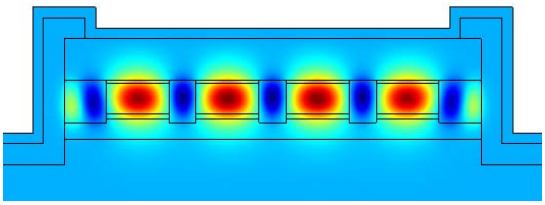

Fig 4a. Simulated antiguided mode 1

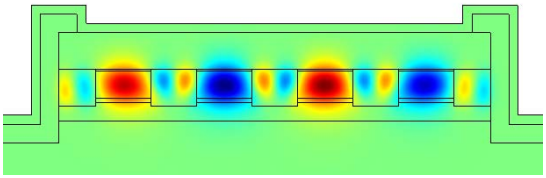

Fig 4b. Simulated antiguided mode 2

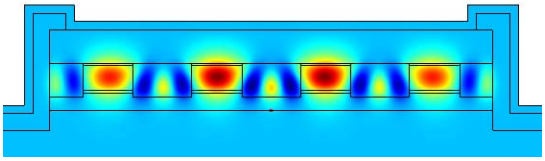

Fig 4c. Simulated antiguided mode 3

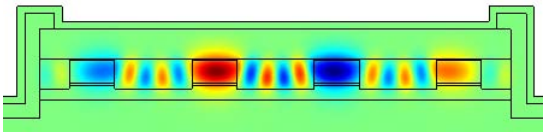

Fig 4d. Simulated antiguided mode 4

Heat dissipation schemes in QCLs monitored by CCD thermoreflectance

D. Pierścińska[1], K. Pierściński[1]*, M. Morawiec[1], P. Gutowski[1], P. Karbownik[1], O.Serebrennikova[1], M. Badura[2], D. Radziewicz[2], B. Ściana[2], M. Tłaczała[2], M. Bugajski[1]

[1] *Institute of Electron Technology, Al. Lotników 32/46, 02-668 Warszawa, Poland*
[2]*Faculty of Microsystem Electronics and Photonics, Wrocław University of Technology, Janiszewskiego 11/17, 50-372 Wrocław, Poland*

In this paper we present the development of the instrumentation for accurate evaluation of the thermal characteristics of quantum cascade lasers based on CCD thermoreflectance (CCD TR). This method allows for rapid thermal characterization of QCLs, as the registration of high-resolution map of the whole device lasts only several seconds. The capabilities of the CCD TR are compared with the standard thermoreflectance spectroscopy and with Raman spectroscopy.

We report on the investigation of thermal performance of QCLs developed at the Institute of Electron Technology, with a particular emphasis on the influence of different material system, processing technology and device designs. We investigate GaAs/AlGaAs QCLs as well as AlInAs/InGaAs/InP QCLs (lattice matched and strain compensated). Different architectures of devices have been compared, i.e., double trench and buried heterostructure (BH).

Experimental results are in very good agreement with numerical predictions of heat dissipation in various device constructions, validating the numerical model

Figure 1 and 2 present exemplary QCL CCD-TR maps and maximum temperature increases versus current density.

We observed improvement of thermal properties of devices based on InP materials, especially for buried heterostructure type. The use of buried heterostructure enhanced the lateral heat dissipation from the active region of QCLs. The BH structure and epilayer-down bonding help dissipate the heat generated from active core of the QCL.

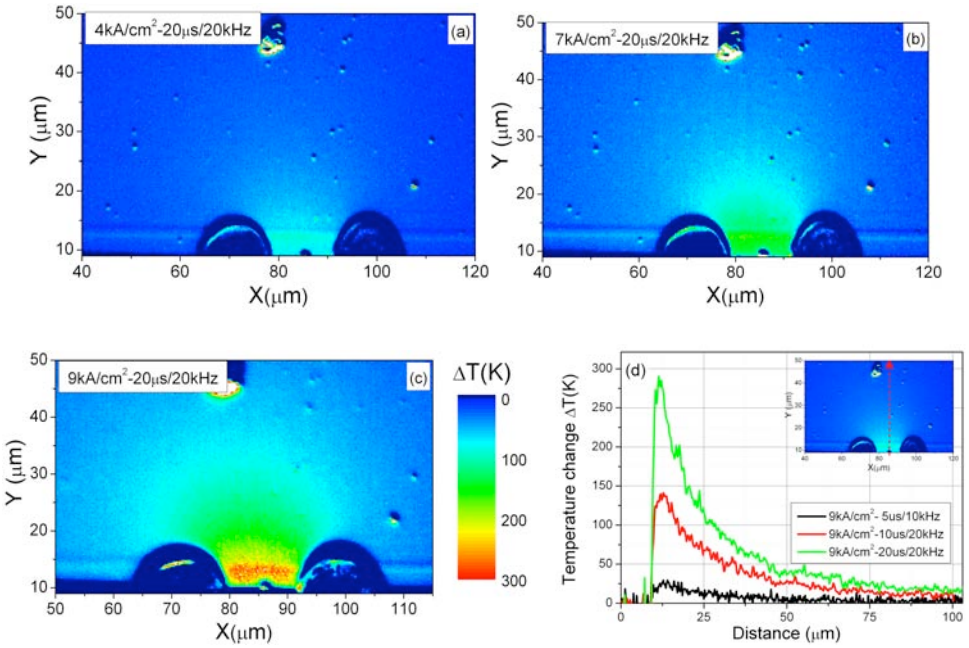

Fig. 1. Temperature distribution maps on the front facet of GaAs/AlGaAs/GaAs QCL, registered for device operated at constant pulse width – 20 μs and frequency 20 kHz for different values of driving current density: (a) 4 kA/cm^2, (b) 7 kA/cm^2 and (c) 9 kA/cm^2. Temperature distribution line scans across the facet, taken at the center of the active area perpendicular to the epitaxial layers, for different driving conditions (d).

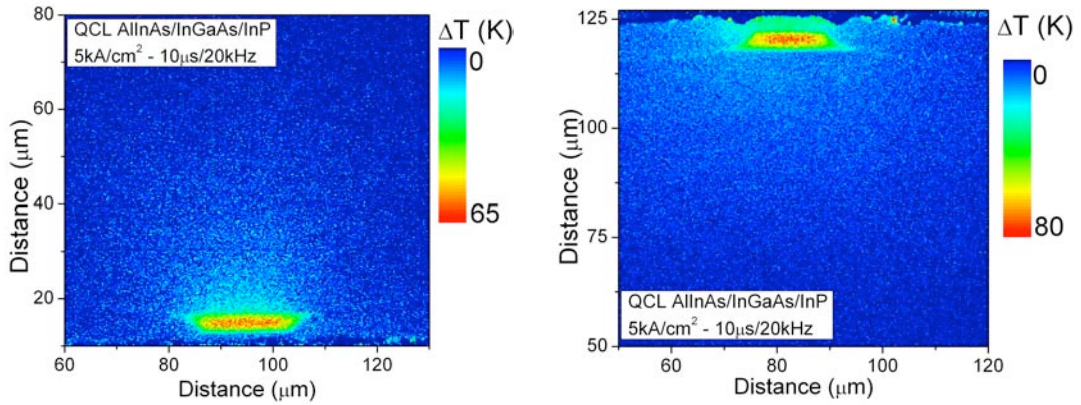

Fig. 2. Temperature distribution maps on the front facet of buried heterostructure AlInAs/InGaAs/InP QCL, registered for device operated at constant pulse width 10 us, frequency 20 kHz and driving currents density 5kA/cm^2. Devices were mounted epi-down (left) and epi-up (right).

*corresponding author: kamil.pierscinski@ite.waw.pl

Mid-infrared laser based gas sensors for atmospheric applications

Dong Chen[1,2], Fengjiao Shen[1], Hongming Yi[1], Tao Wu[3], Gaoxuan Wang[1], Rabih Maamary[1], Dorothée Dewaele[1], Fabrice Cazier[1], Patrick Augustin[1], Marc Fourmentin[1], Cécile Coeur-Tourneur[1], Eric Fertein[1], Weidong Chen[1*]

[1] *LPCA, University of the Littoral Opal Coast, 59140 Dunkirk, France*
[2] *Hefei University of Technology, Anhui 230009, China*
[3] *Nanchang Hangkong University, Nanchang 330063, China*

A "fast-action" climate mitigation strategies is strongly needed to provide more sizeable short-term benefits than CO_2 reductions by reducing emission of short-lived climate pollutants (SLCPs, having atmospheric lifetimes of less than 20 years), which would lead to short-term drops in atmospheric concentrations and hence slow climate change over the next several decades. CH_4, one of the most important SLCPs with an atmospheric lifetime of about 12 years, is considered as the second most powerful climate-forcing agent in the atmosphere after CO_2. On the other hand, chemically reactive atmospheric species (like oxidant radicals, N_2O_5, etc) play a central role in tropospheric processes that dominate regional air quality and global climate change. Reliable and real-time assessment of concentration change of such gases in the atmosphere is thus crucial.

In this talk, we will overview our recent progress in the development and applications of mid-infrared quantum cascade laser (QCL) based gas sensors [1] to field observation or smog chamber study of : (1) CH_4 and N_2O from livestock emission; (2) environmental CH_4 [2]; (3) N_2O_5 in a kinetic process of volatile organic compounds (VOCs) oxidation by NO_3 radical in an atmospheric simulation chamber [3].

Acknowledgments

The authors acknowledge financial support from the French Agence Nationale de la Recherche (ANR) under the CaPPA (ANR-10-LABX-005) contracts. The authors thank the Nord-Pas de Calais Region and the Ministère de l'Enseignement Supérieur et de la Recherche for the support in the framework of the CPER CLIMIBIO program.

References

1. H. Yi, R. Maamary, X. Gao, M. W. Sigrist, E. Fertein, W. Chen. Short-lived species detection of nitrous acid by external-cavity quantum cascade laser based quartz-enhanced photoacoustic absorption spectroscopy, Appl. Phys. Lett. Vol. **106**, 101109, 2015.
2. R. Maamary, X. Cui, E. Fertein, P. Augustin, M. Fourmentin, D. Dewaele, F. Cazier, L. Guinet, W. Chen. Quantum Cascade Laser-based Optical Sensor for Continuous Monitoring of Environmental Methane in Dunkirk (France), Sensors Vol. **16**, 224, 2016.
3. H. Yi, T. Wu, A. Lauraguais, V. Semenov, C. Coeur-Tourneur, E. Fertein, X. Gao, W. Chen. Real time tracing of the kinetic process of NO_3, N_2O_5 and NO_2 with VOCs by long optical pathlength absorption spectroscopy, Geophysical Research Abstracts, Vol. **16**, EGU2014-PREVIEW, 2014.

*corresponding author: chen@univ-littoral.fr

MOEMS external cavity quantum cascade laser for time resolved MIR fingerprint spectroscopy

R. Ostendorf[1*], L. Butschek[1], A. Merten[2], A. Dreyhaupt[2], J. Grahmann[2], M. Rattunde[1], J. Jarvis[1], M Härtelt[1], S. Hugger[1], F. Fuchs[1], J. Wagner*

[1]*Fraunhofer Institute for Applied Solid State Physics, Tullastr. 72, 79108 Freiburg, Germany*
[2]*Fraunhofer Institute for Photonic Microsystems, Maria-Reiche-Str. 2, 01109 Dresden, Germany*

External cavity quantum cascade lasers (EC-QCLs) with broad spectral tuning range in the wavelength regime from 4 µm to 11 µm open the door for new approaches and applications in MIR spectroscopy. The key advantages of EC-QCLs are a very high spectral power density and high spectral resolution as well as the emission of a well-defined output beam which can easily be coupled into subsequent optical systems such as optical fibers or waveguides. Additionally, for many applications like in-line or real-time process analysis in industrial environments, the measurement time of an EC-QCL based sensing system and thus the tuning speed of the laser source is an important factor.

We present recent advances of an EC-QCL employing a custom designed and fabricated Micro-Opto-Electro-Mechanical-Systems (MOEMS) scanning grating as wavelength selective element in the external resonator [1, 2]. This MOEMS based EC-QCL provides a spectral coverage of more than 300 cm^{-1} with a scanning frequency of 1 kHz which corresponds to 2000 full wavelength scans per second. The huge potential of this laser source for real-time spectroscopic MIR sensing is demonstrated by several applications such as transmission measurements performed on polystyrene reference absorber sheets or backscattering infrared spectroscopy for the instantaneously identification of chemical substances like active pharmaceutical ingredients on a distance of one meter (see figure 1). With special focus on applications in the field of on- or even inline process analysis, time resolved IR transmission measurements identifying the chemical composition of liquid samples with temporal resolution of 80 ms are presented

References

[1] J. Wagner, R. Ostendorf, J. Grahmann, A. Merten, S. Hugger, J.-P. Jarvis, F. Fuchs, D. Boskovic, and H. Schenk, “Widely tunable quantum cascade lasers for spectroscopic sensing,” in *SPIE OPTO*, 2015, p. 937012.

[2] R. Ostendorf, L. Butschek, A. Merten, J. Grahmann, J. Jarvis, S. Hugger, F. Fuchs, and J. Wagner, “Real-time spectroscopic sensing using a widely tunable external cavity-QCL with MOEMS diffraction grating,” *Proc. SPIE*, vol. 9755. pp. 975507–975508, 2016.

*corresponding author: ralf.ostendorf@iaf.fraunhofer.de

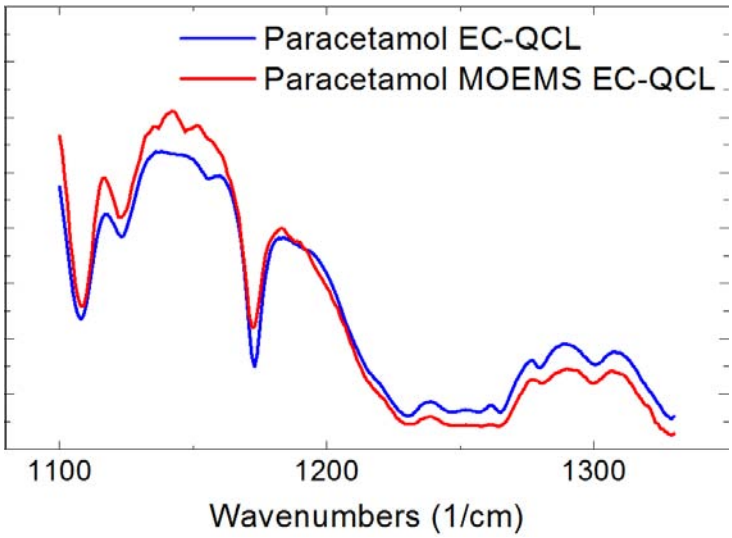

Fig.1. Reflectance spectra of paracetamol. Spectra recorded using a conventional EC-QCL (in blue) are compared with those taken using the MOEMS-based EC-QCL with a scan frequency of 1 kHz (red curves, average of 100 individual spectra resulting in a total measurement time of 100 ms).

InAs and GaInAsSb based Thermophotovoltaic Devices for waste heat recovery applications below 1000 °C

Q. Lu[1]*, M. Kesaria[1], A.R.J. Marshall[1], S.E. Krier[1], S. McDougall[2], W. Meredith[2], J. Inskip[3], A. Scholes[4] and A. Krier[1]

[1] *Physics Department, Lancaster University, Lancaster, LA1 4YB, UK*
[2] *CST Global Ltd., Hamilton International Technology Park, Glasgow, G72 0BN, UK*
[3] *NSG Technical Center, Hall Lane, Lathom, L40 5UF, UK*
[4] *Materials Processing Institute, Grangetown, Middlesbrough, TS6 6US, UK*

In high energy consumption industrial process sites, large amounts of energy are often lost in the form of waste heat. Thermophotovoltaic (TPV) cells can provide a direct and convenient way of converting waste heat energy into electricity [1]. InAs and GaInAsSb are among the most promising TPV materials for lower temperature (<1000 °C) heat sources due to their relatively small band gaps [2]. In this work, we compare the performance of InAs and GaInAsSb based TPV devices and we demonstrate the first large area InAs based TPV panel which can generate an output voltage over 2.0 V.

Individual InAs and GaInAsSb TPV cells were grown by MBE and tested using an 800 °C thermal source. The results are plotted in Fig. 2(a) together with the GaSb and Ge TPV devices. It is clear that InAs and GaInAsSb cells can achieve much higher short circuit current (I_{sc}) than GaSb and Ge cells. The GaInAsSb also exhibited reasonable open circuit voltage (V_{oc}). The performance of the GaInAsSb TPV cell was improved by adding an AlGaSb blocking layer into the device, which resulted in almost double I_{sc} (green curve in Fig. 1).

The InAs based TPV panel was made from 9 arrays each containing 30x40 InAs TPV cells in series and parallel connections, as shown in Fig. 2(a). These arrays were bonded onto a metal plate heat sink which was water cooled during the tests to keep the cells at ambient temperature. The measurements were carried out by placing the whole setup in front of a furnace which could be heated up to a maximum temperature of 650 °C. Fig. 2(b) shows the I-V characteristics of the TPV array panel measured at different source temperatures. The V_{oc} exceeded 2.0 V when the source furnace reached 642 °C, although the I_{sc} was lower than expected (58 mA). The array did not exhibit typical diode behaviour. The low I_{sc} and non-ideal I-V characteristics can be attributed to the effects of parallel and shunt resistances when large numbers of cells are connected, as well as the differences among individual cells and possible non-uniform irradiance of the panel.

References

1. H. Daneshvar, R. Prinja and N. P. Kherani, Thermophotovoltaics: Fundamentals, challenges and prospects, Applied Energy, Vol. 159, pp. 560–575, 2015.
2. M. G. Mauk and V. M. Andreev, GaSb-related materials for TPV cells, Semicond. Sci. Technol., Vol. 18, S191–S201, 2003.

*corresponding author: q.lu3@lancaster.ac.uk

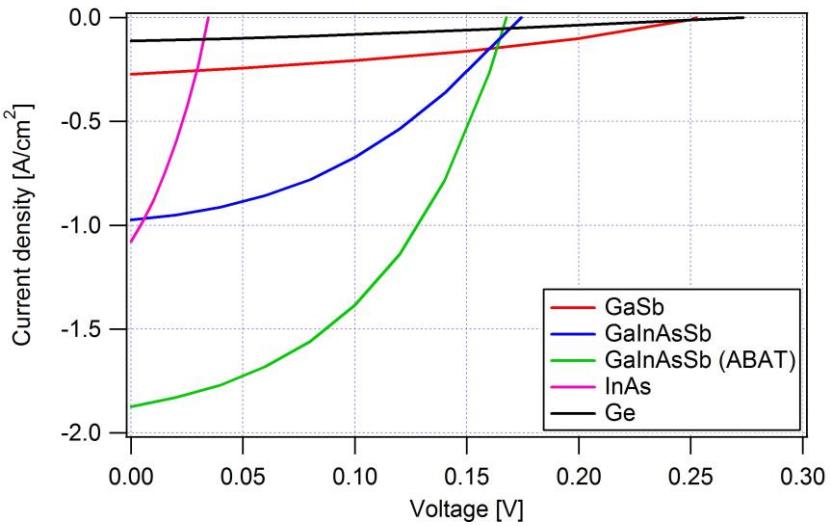

Fig.1. I-V curves of different types of TPV cells tested under 800 °C thermal sources.

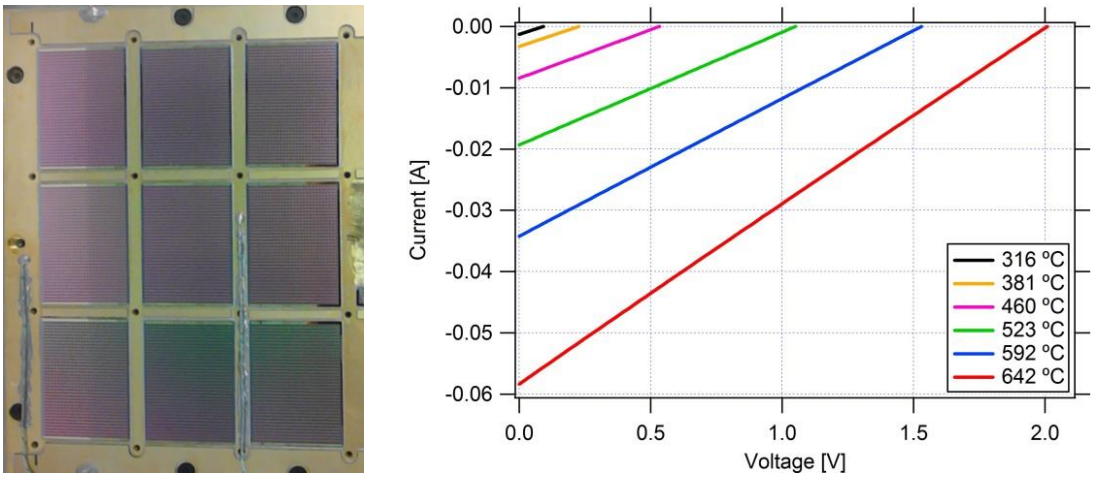

(a) (b)

Fig.2. (a) Plan view photo of the InAs TPV panel. (b) I-V plots from the InAs TPV panel at different source temperatures.

Acknowledgements

Financial support for this work was provided by the UK Technology Strategy Board in collaboration with CST Global, IQE Ltd., Tata Steel and Pilkington Ltd. under grant No: TP11/LCE/6/I/AE096F. We are also grateful for support from EPSRC –TPVs for Waste Heat Recovery in Energy Resilient Manufacturing (EP/M013707/1).

Photoelectrical Hydrogen Sensor Based on Pd-Oxide-InP Structure

Yu.P.Yakovlev[1]*, E.A. Grebenshchikova[1], A. N. Imenkov[1], V.A.Shutaev[1], A.M.Ospennikov[1]

[1] *Ioffe Physical-Technical Institute RAS,194021, St.Petersburg, Russia*

The hydrogen power engineering, together with solar power engineering, may become one of the main fields of electric power production in the near future. Nowadays, in connection with the development of hydrogen power-engineering, metal-insulator-semiconductor (MIS) structures with oxides of metals or SiO_2 as the insulator are finding wide application in gas-sensor structures [1]. A significant disadvantage of such devices is the need to heat the sensitive element to 200-400°C.

For operation at room temperature hydrogen sensors with palladium layer are used [2]. The adsorption of hydrogen molecules on the palladium-layer surface results in a variation in the current through the field-transistor channel or through the Schottky diode. In this work we suggest the new photoelectric hydrogen sensor based on Schottky diodes with a palladium contact to III–V semiconductors.

The proposed photoelectric sensor is composed of the metal–oxide–semiconductor (MOS) structures using a Pd–anodic oxide–InP structure, optically connected through the Pd layer with LED with λ = 0.9 μm. (Fig.1). The current-voltage dependence and the photoresponse spectrum of typical MOS structure are shown in Fig.2 and Fig.3. The kinetics and mechanism of the variation in the photovoltage and photocurrent are considered. It is established that a decrease in photovoltage of the structure and a large increase in photocurrent in the circuit are observed under the pulsed effect of hydrogen on the structure (Fig.4). It is assumed that the photovoltage decreases because of the ionization of hydrogen atoms in the Pd layer, and the photocurrent increases due to the thermionic emission of nonequilibrium electrons from the Pd layer into the semiconductor. Response time of the hydrogen sensor was 2-5 sec (rise to 0.9 level) while the recovery time (down to 0.1) was less than 10 sec. (Fig. 5).

In this paper, we demonstrated application of Pd-Oxide-InP Schottky diodes for manufacturing the compact hydrogen sensors (Fig.6) with sensitivity threshold as small as 0.01% and speed (2-5 sec) at room temperature as well as low power consumption.

References

1. V. M. Arutyunian. Hydrogen sensors, ISJAEE, N.3, pp.33-42, 2007.
2. G..G..Kovalevskaya, A.M.Marinova, S.V. Slobodchikov. Photovoltage in Pd–n–InP Structures with Interfacial Layer in a Hydrogen ore a Water Vapor Medium, Technical Physics, Vol. 59, N.11, pp.155-158, 1989.
3. E.A.Grebenshchikova, V. V.Evstropov , N.D.Il'inskaya, Yu.S.Mel'nikov, O.Yu.Serebrennikova,
4. V. G. Sidorov, V.V.Sherstnev, and Yu. P. Yakovlev. Electrical Properties of Pd–Oxide–InP Structures, Semiconductors, Vol. 49, N. 3, pp. 364–366, 2015.

*corresponding author: yakovlev.iropto@mail.ioffe.ru

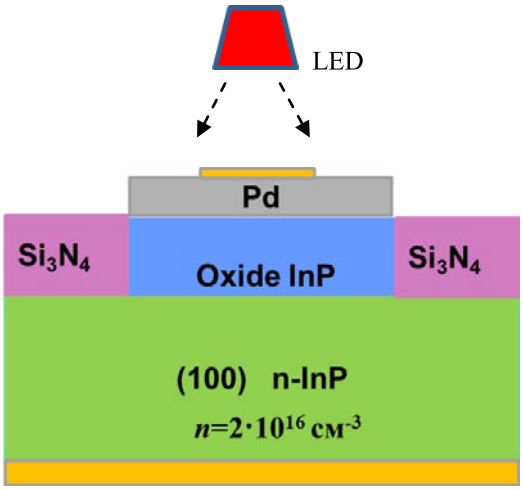

Fig.1.Scheme of the photoelectrical hydrogen sensor

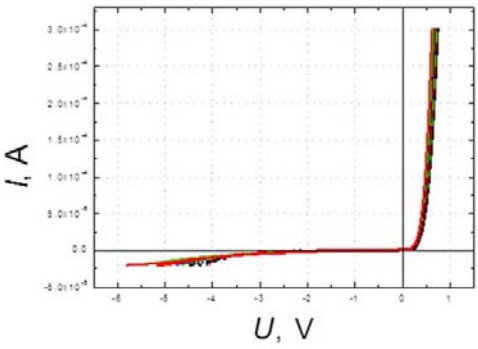

Fig.2.The current-voltage dependence

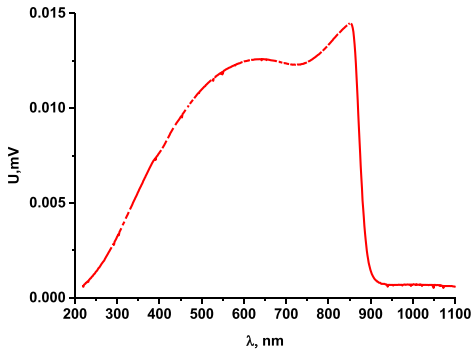

Fig.3. The photoresponse spectrum of MOS structure

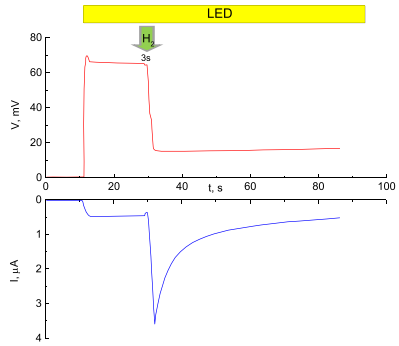

Fig.4. Kinetics of photocurrent and photovoltage changing under the hydrogen exposure

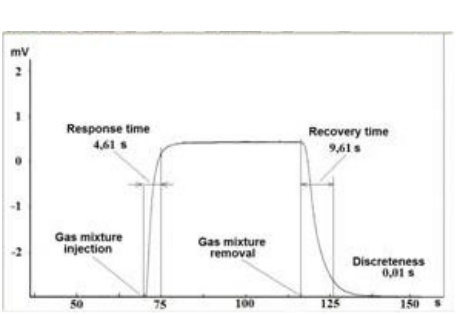

Fig.5.The response and recovery time of hydrogen sensor

Fig.6.The hydrogen sensor

Abstracts

Poster Sessions

Development of nearly lattice matched InGaAsBi photodetector by tailoring In and Bi contents

X. Y. Chen, Y. Gu, Y. G. Zhang*, S. P. Xi, B. Du, Y. J. Ma, W. Y. Ji, Y. H. Shi and A. Z. Li

State Key Laboratory of Functional Materials for Informatics, Shanghai Institute of Microsystem and Information Technology, Chinese Academy of Sciences, Shanghai 200050, China

Dilute bismide III-V semiconductors with wider mid-infrared wavebands have attracted much attention over the past few years since both bandgap and lattice engineerings can be easily achieved by incorporation of bismuth (Bi) [1]. So far, some researches have focused on $In_{0.53}Ga_{0.47}AsBi$ on InP substrate for wavelength extending purpose, but it also introduces lattice mismatches [2, 3], which is detrimental for device performance. In this report, the lattice mismatch was tailored by changing the Bi content in conjunction with the In content simultaneously, and the effect of Bi on the structural properties and device performances was investigated. Compared with the previous work, by decreasing the In content from 0.53 to 0.5 and increasing Bi content in InGaAsBi alloy, the lattice mismatch was pulled back to a device level while extending the wavelength. This near-lattice-match condition is the background for developing high quality devices.

By incorporation of Bi into the crystal lattice, X-ray diffraction analysis revealed that alloy lattice constants have been extended positively as shown in Fig. 1. The photoluminescence peaks at 77 K shift to a lower energy side with increasing Bi content, implying that the band gap of $InGaAs_{1-x}Bi_x$ alloy reduces with increasing Bi content, as shown in Fig. 2. From the excitation dependent photoluminescence measurement, the donor-acceptor pair emissions were inferred for samples containing moderate and high levels of Bi.

By using the quaternary InGaAsBi alloy with Bi content of 3.2% as the absorption layer, a short-wave infrared detector nearly lattice matched to InP substrate was demonstrated. The 50% cut-off wavelength, shown in Fig. 3, red-shifted from about 1.6 to 2.1 μm at room temperature with respect to that of InGaAs without Bi, indicating a bandgap reduction of about 180 meV due to bismuth incorporation. The detector shows an encouraging dark current density of 2.4×10^{-4} A/cm^2 at bias voltage of -10 mV at 300 K. This work shows the promising potential of InP-based lattice-matched InGaAsBi detectors for short-wave infrared detection.

References

1. Alberi, J. Wu, W. Walukiewicz, K. M. Yu, O. D. Dubon, S. P. Watkins, C. X. Wang, X. Liu, Y. -J. Cho, and J. Furdyna, Physical Review B 75(4), 045203 (2007).
2. I. P. Marko, Z. Batool, K. Hild, S. R. Jin, N. Hossain, T. J. C. Hosea, J. P. Petropoulos, Y. Zhong, P. B. Dongmo, J. M. O. Zide and S. J. Sweeney, Applied Physics Letters 101(22), 221108 (2012).
3. S R Jin and S J Sweeney, Journal of Applied Physics 114(21), 213103 (2013).

*corresponding author: ygzhang@mail.sim.ac.cn

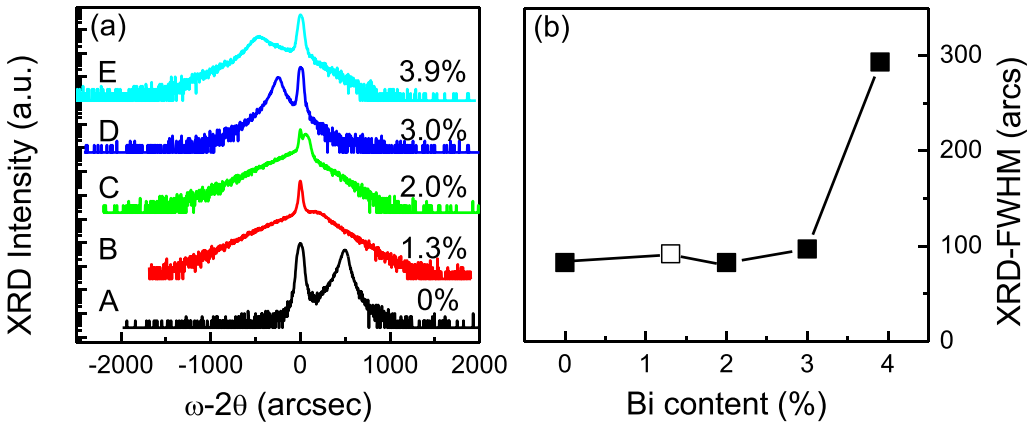

Fig. 1. (a) HRXRD (004) ω-2θ scans for $In_{0.5}Ga_{0.5}As_{1-x}Bi_x$ epilayers on InP with Bi contents of 0, 1.3%, 2.0%, 3.0%, and 3.9% respectively. (b) The FWHMs of InGaAsBi epilayers versus Bi contents. The datum (hollow square) of $In_{0.5}Ga_{0.5}As_{1-x}Bi_x$ with 1.3% Bi has been estimated.

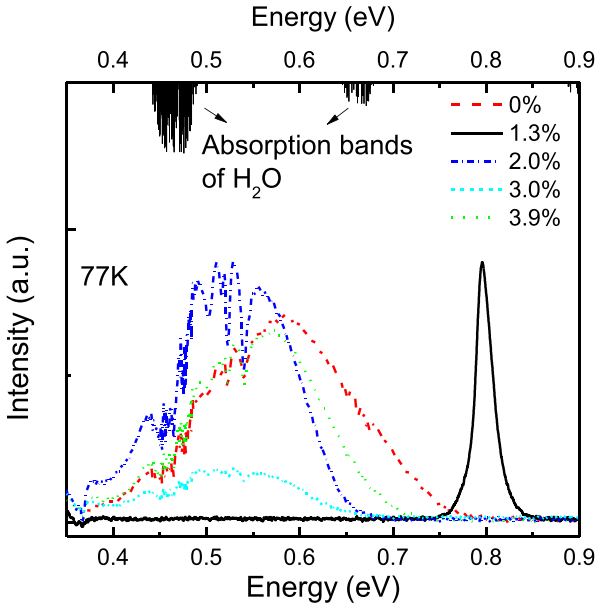

Fig. 2. PL spectra at 77 K for the InGaAsBi epilayers with different Bi contents.

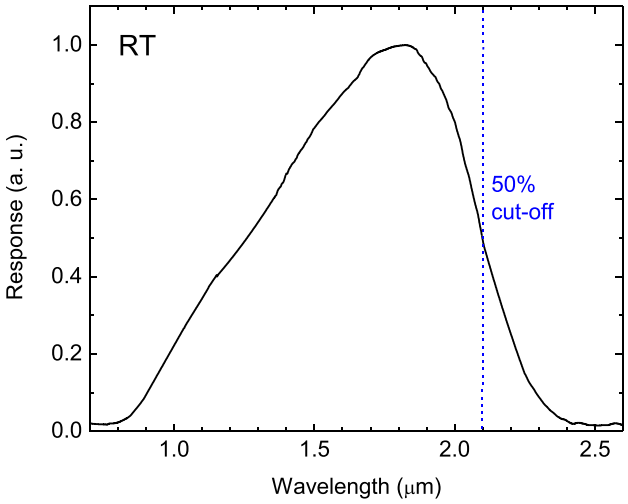

Fig. 3. Optical response spectrum of the InGaAsBi detector at RT.

Raman scattering in InP1-xSbx alloys grown by gas-source MBE

Chieh-Miao Chang1, Cheng-Ying Tsai2, and Hao-Hsiung Lin1,2*

1Graduate Institute of Photonics and Optoelectronics, National Taiwan University, Taipei 10617, China 2Graduate Institute of Electronics Engineering, National Taiwan University, Taipei 10617, China
**hhlin@ntu.edu.tw*

InPSb is an alloy with an energy gap covering the mid-infrared spectral range. In the lattice of the alloy, the InP and InSb bonds are highly mismatched in length [1] and thus suffer from strong stretching and bending. Such distortions result in a high interaction parameter for the alloy, leading to difficult in the growth [2]. However, the distortion also could bring about peculiar properties [3]. Relevant research, so far, still remains lacking. In this work, we grew a series of ternary InP1-xSbx with Sb composition x=0.16, 0.17, 0.33, 0.36 on (001) InAs substrates by gas-source molecular-beam epitaxy and studied their Raman scattering to understand how the bond distortion affects the structural properties. X-ray diffraction was firstly used to study the crystal structure with the result shown in Fig. 1. As can be seen, only the sample with x = 0.36 shows a sharp (004) reflection, while sample with x = 0.33 has a very weak bump close to (004) InSb in addition to a strong epi-peak embedded in the right of the substrate peak. The very low InSb bump is believed only giving negligible effect on the structural properties. For the other two low x samples, besides the tiny InSb bump, there are strong wavy plateau on the right of the substrate peak, indicating strong composition fluctuation in these layers. Results from Raman scattering clearly can be divided into two groups for the two low x samples with strong composition disorder and the two high x samples with limited composition disorder, respectively, as shown in Fig. 2. The strong DALA signals at ~147 cm-1 for the two low x samples, as compared with those for the two low x samples, confirms the strong disorder in the two samples [4, 5]. The broad peak at ~190 cm-1 is assigned to InSb-like modes. A tiny spike at 162 cm-1 for the samples with x = 0.33 and 0.36 samples could be due to Sb A1g mode [6]. All the samples exhibit two peaks in the range from 290 to 350 cm-1, which are assigned to InP-like phonon modes. In order to identify the modes, we performed polar measurements for the sample with x = 0.36 and show the results with the incident laser polarization parallel to the [110] and [100] directions in Fig. 3 and Fig. 4 in respectively. In Fig. 3, all the measured curves are roughly close to the theoretical curves, following a square cosine law parallel to the incident polarization. Note that the projection of bonds on (001) plane in zincblende lattice is along [110] and [-110] direction, the coincidence suggests the polarization after scattering is unchanged when its direction parallels the bond direction. However, in the case in Fig. 4, when the incident polarization is not parallel to the expected direction of the polarized bonds, the four modes show different features. First, the DALA mode still follows the square cosine law, suggesting the involving of structural defects in the mode. The structural defects such as vacancies or dislocations result in very strong angle change for the neighboring bonds. As a result, for any incident polarization direction, parallel scattering is always observed. Second, we observe that InSb-like mode, albeit quite broad, still roughly matches the theoretical curve, indicating the behavior of LO mode. The broadening is believed due to the inherent bond distortion in the alloy. According to our simulation based on valence forced field (VFF) model, the bending angle in the alloy is within 5 º, whose effect on Raman selection rule is not expected as strong as the aforementioned defects. For the two InP-like modes, we can see the higher frequency one is similar to the DALA mode and the lower frequency one shows a nearly angle independent behavior. The different behaviors imply that the two InP-like modes are from different unit cells. From our VFF analysis, as listed in Table 1, we found that In-centered

unit cells with 2 neighboring P atoms and 2 neighboring Sb atoms (2P2Sb in short) undergo least stretching and strongest bending then other unit cells. The 2P2Sb cells could responsible for the higher frequency mode, while the lower frequency mode is due to the rest P-containing unit cells [7]. The polar measurement was also performed for the sample with x=0.17. All the four modes in this sample are similar to the behavior of DALA mode, confirming the strong composition disorder observed from its XRD result. In conclusion, the strong bond distortion in the alloy could limit the propagating of the phonons. The localization of the phonons releases the selection rule, broadens the Raman scattering and makes multi-scattering from different P-containing unit cells. This work is supported by Ministry of Science and Technology, Taiwan, ROC under contract number NSC 102-2221-E-002-191-MY3.

References

[1]C. J. Wu, Z. C. Feng, W. M. Chang, C. C. Yang, and H. H. Lin, Appl. Phys. Lett. vol. 101, p. 091902, 2012.

[2]T. Fukui, J. Appl. Phys. vol. 57, p. 5188, 1985.

[3]G. Tsai, D. L. Wang, C. E. Wu, C. J. Wu, Y. T. Lin, H. H. Lin, J. Crystal Growth. vol. 301–302, p. 134, 2007.

[4]Y. T. Cherng, K. Y. Ma, and G. B. Stringfellow, Appl. Phys. Lett. vol. 53, p. 886, 1988.

[5]R Carlesi, N Saint-Cricq, J B Renucci, and R J Nicholas, J. Phys. C: Solid St. Phys. vol. 13 p. 899, 1980.

[6]K J Cheetham, A Krier, I I Patel, F L Martin, J-S Tzeng, C-J Wu and H-H Lin, J. Phys. D: Appl. Phys. vol. 44, p. 085405, 2011.

[7]O. Pagès, J. Souhabi, A. V. Postnikov, A. Chafi, Phys. Rev. B vol. 80, p. 035204, 2009.

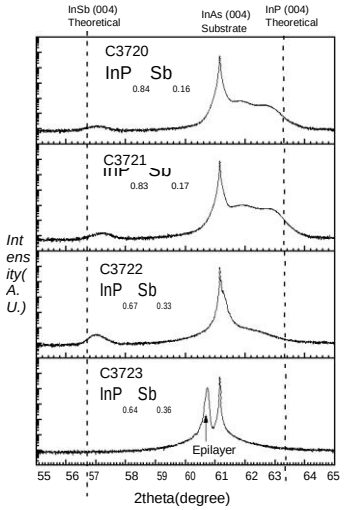

Fig. 1 X-ray Diffraction of $InP_{1-x}Sb_x$ samples. Samples in the top 2 panels show a wavy plateau on the left of the substrate peak, suggesting strong composition disorder. Sample with x=0.33 only has a tiny bump close to (004) InSb. Sample with x=0.36 shows a sharp epi-peak, indicating its good crystallinity.

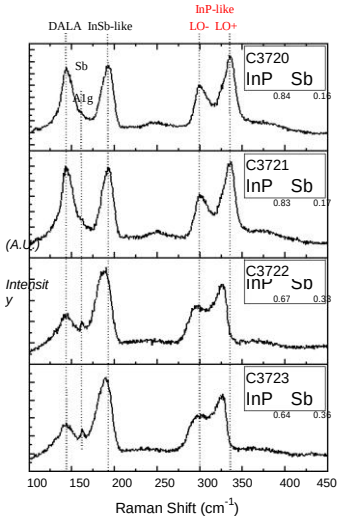

Fig. 2 Raman scattering for $InP_{1-x}Sb_x$ samples. Four major peaks are observed. They are DALA, InSb-like, and two InP-like modes. A tiny peak observed in the samples with x=0.33 and 0.36 could be due to A_{1g} mode from Sb cluster.

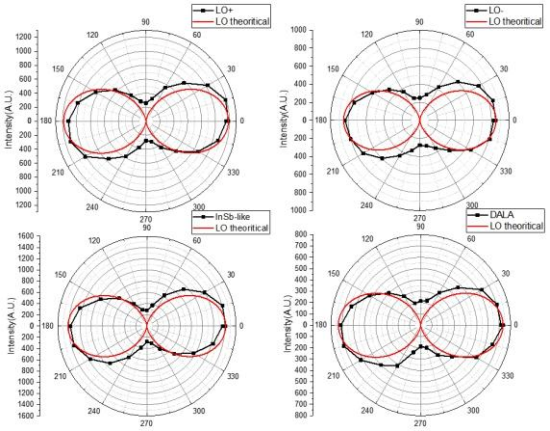

Fig. 3 Polar plots for sample with x=0.36. Polarization of the laser was fixed at [110] direction. Red and black curves represent theoretical curve for zincblende LO mode, square cosine law, and experimental results. Note that in this arrangement, unity symmetry for modes activated by defect also gives the same square cosine law.

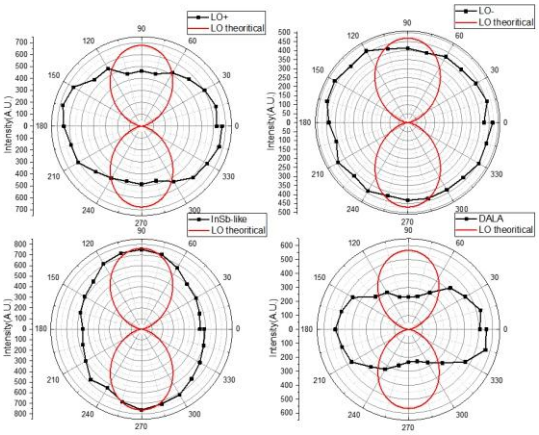

Fig. 4 Polar plots for sample with x=0.36. Polarization of the laser was fixed at [100] direction. Red and black curves represent theoretical curve for zincblende LO mode, square sine law, and experimental results. Note that in this arrangement, unity symmetry for modes activated by defect gives square cosine law.

Table. 1. Results from valence force field model simulation for $InP_{0.64}Sb_{0.36}$. The stretching and bending energy let 2Sb2P cells stand out from the rest, accounting for the higher frequency InP-like phonon mode.

Tetrahedral unit cell	In-P Bond length (Å)	Stretching energy (meV)	Bending energy (meV)	Formation probability
0Sb4P	2.573	4.66	5.09	0.168
1Sb3P	2.559	1.67	10.31	0.377
2Sb2P	2.546	0.36	13.00	0.319
3Sb1P	2.529	0.87	8.35	0.119

Correlation between band structures and quantum Hall effect in GaAs/$Al_xGa_{1-x}As$ nanostructure superlattice for near infrared detection

A. Nafidi*, D. Barkissy, A. Boutramine, A. Khalal, T. El Gouti and M. Massaq

Laboratory of Condensed Matter Physics and Nano Re, University Ibn Zohr, Agadir, Morocco

The realization of type I nanostructures superlattices (SLs), consisting of alternating GaAs and $Al_xGa_{1-x}As$ compounds, was associated with different fundamental studies, since they are promising in different applications fields, like in optoelectronics [1] and in detectors [2,3].

We have investigated the band structures $E(d_1)$, $E(k_z, k_p)$ in Fig 1. (a,b) and the effective mass m^*/m_0 along the growth axis and in the plane of GaAs(d_1=19 nm)/$Al_{0.3}Ga_{0.7}As$(d_2=5 nm) nanostructure superlattice, based on the envelope function formalism.

At 0.4 K, the band gap 1.53 eV situates this sample as near infrared detector. The electronic states are quantized and discrete along k_z direction because of the thick (d_2= 50 Å) barrier thickness, which separates two adjacent wells GaAs, leading to a weakly coupled system. In this case the electronic transport is dominated in the plane of this superlattice, in particular, in the GaAs layer with a large confinement of carriers charge. We have also interpreted in the Fig. 1.(c) the oscillations in the magneto-resistance (Shubnikov-de Haas effect) observed by Smrčka et al [4] and the quantum Hall effect in the GaAs quantum wells. At 0.4 K, the electrons effective mass, the sheet carrier density and the Fermi level of the two dimensional electron gas (2DEG) are, respectively, m^*_{E1}= 0.13m_0, n_{2D}= 4.4 10^{11} $cm^{-2}$and E_F= 1.710 eV. Therefore, this sample exhibits n type conductivity.

References

1. F. Janiak, M. Dyksik, M. Motyka, K. Ryczko, J. Misiewicz, K. Kosiel and M. Bugajski, Opt. Quantum Electron, Vol. 47, 945–652, (2015).
2. P. Martyniuk, M. Kopytko and A. Rogalski, Opto-Electronics Rev, Vol. 22, (2014).
3. D. Barkissy, A. Nafidi, A. Boutramine, H. Charifi, A. Elanique and M. Massaq, J. Low Temp. Phys, Vol.182, 185–191, (2016).
4. L. Smrčka, N. A. Goncharuk, P. Svoboda, P. Vašek, Y. Krupko, and W. Wegscheider, Microelectronics J, Vol. 39, No. 3–4, 411–413, (2008).

*corresponding author: nafidi21@yahoo.fr

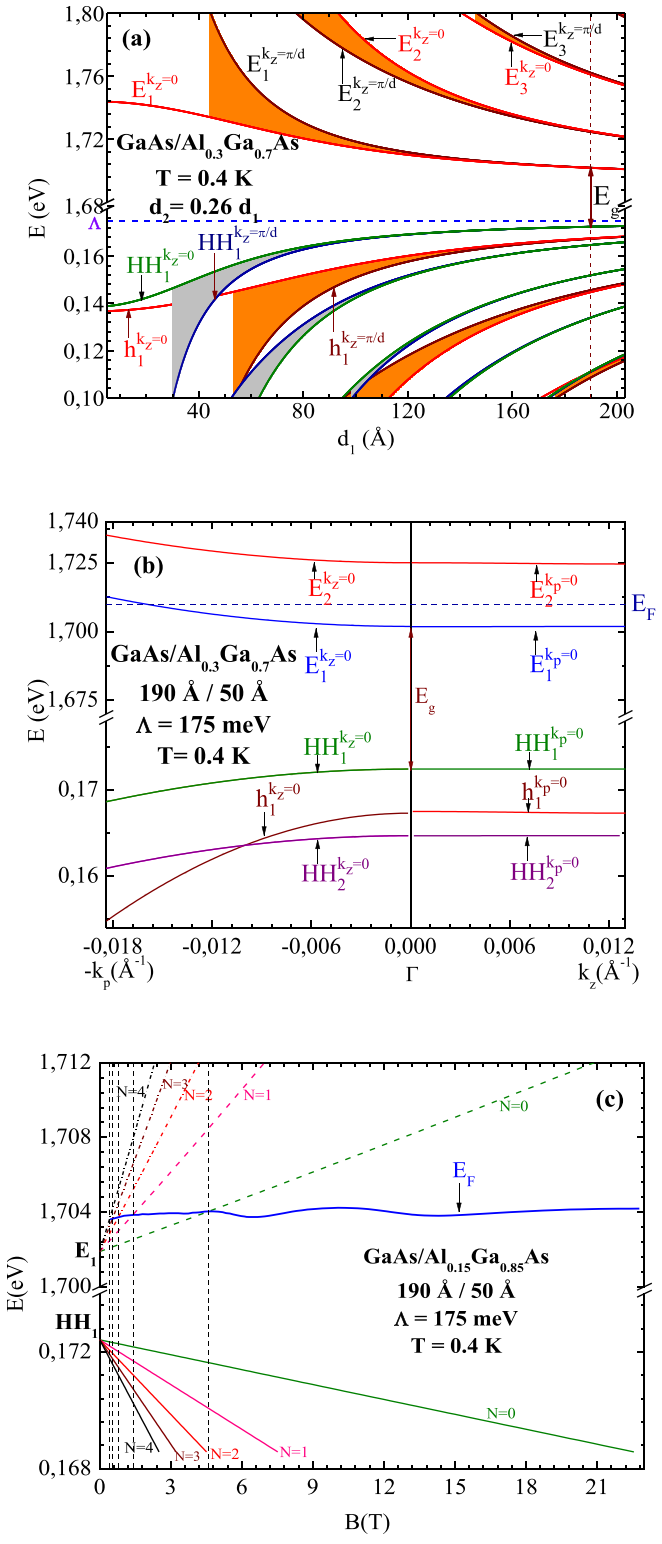

Fig. 1: **(a)** Energy of both conduction (upper part) and valence (lower part) sub-bands as function of well thickness at 0.4 K. The solid areas show the width of sub-bands. **(b)** Dispersion curves in the k_z wave vector direction and in the plane k_p of the superlattice, respectively. **(c)** Energy position of the calculated Landau levels of the first conduction and valence sub-bands as a function of magnetic field. The position of the Fermi level E_F is also shown as a function of the magnetic field.

Thickness dependent InSb photoconductivity under low temperature with weak light illumination

YuHui Zhang[1] , Ting-Ting Kang[2*] , Ping-Ping Chen[2]

[1] *School of Materials Science and Engineering, University of Shanghai for Science and Technology, Shanghai 200093, China*
[2] *National Laboratory for Infrared Physics, Shanghai Institute of Technical Physics, Chinese Academy of Sciences, 200083 Shanghai, People's Republic of China*

We study the photoconductivity (PC) in InSb film grown heteroepitaxially on GaAs (100) substrates by molecular beam epitaxy (MBE). The PC measurements were conducted under 12K—300K temperature by using an LED instead of a laser. We can observe the negative PC for InSb film with varying thickness under. The negative PC is enhanced with reduced temperature(in the 20K<T<195K range) and thickness, which is mainly attributed to electron trapped at the interface [1,2].

However, if the temperature is low enough (T<20K), the negative PC is no longer enhanced by reduced temperature. Hall measurements indicate that, the light–induced electron density reduction is some not so significant under T<20K. And this trend becomes more and more obvious for thinner InSb film. This phenomenon can be explained by the suppressed efficiency of light generated electrons to be captured by the interface, via a thermal activated transport mechanism.

References

1. Y. Beaulieu, J. B. Webb, and J. L. Brebner, J. Appl. Phys. 79,1772(1996);
2. Y. Beaulieu, J. B. Webb, and J. L. Brebner, Solid State Commun. 76, 233 (1990).

*corresponding author: kang@mail.sitp.ac.cn

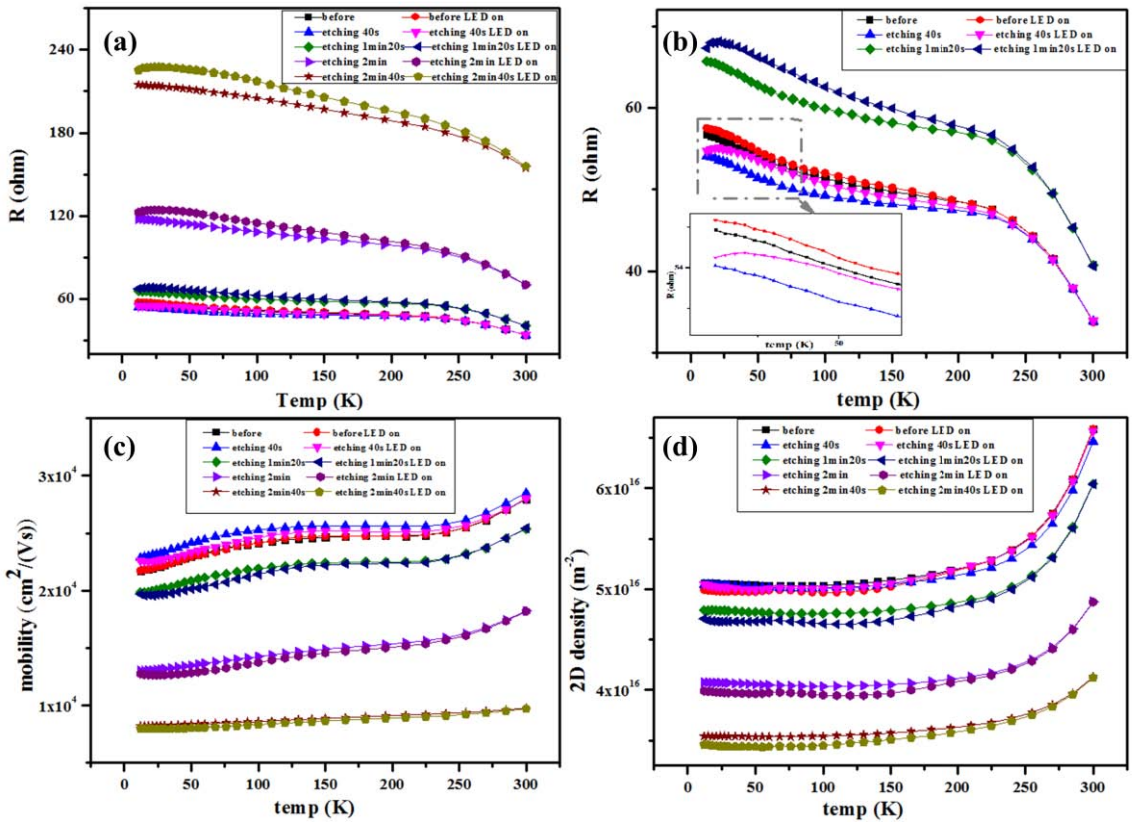

Fig.1. (a) Negative PC of InSb films vary with range from 12K to 300K for before etching ,etching 40s ,etching 1min20s ,etching 2min ,etching 2min40s,respectively.(b) Negative PC of InSb films vary with range from 12K to 300K for before etching and etching 40s. Inset shows negative PC vary with range from 10 to 80K for before etching and etching 40s;(c) Mobility change upon the LED off/on from 12K to 300K for before etching ,etching 40s ,etching 1min20s ,etching 2min ,etching 2min40s,respectively;(d) 2D density change upon the LED off/on from 12K to 300K for before etching ,etching 40s ,etching 1min20s ,etching 2min ,etching 2min40s,respectively;

Interfacial Conductivity of Mn-Co-Ni-O Thin Films and CBP Coating

Fei Zhang[1], Zhiming Huang[1,2,a)] Jing Wu[1,2],Cheng OuYang[1], Wei Zhou[1,2],Yanqing Gao[1,2]

[1] *National Laboratory for Infrared Physics, Shanghai Institute of Technical Physics, Chinese Academy of Sciences, 500 Yu Tian Road, Shanghai 200083, People's Republic of China*

[2] *Key Laboratory of Space Active Opto-Electronics Technology, Shanghai Institute of Technical Physics,Chinese Academy of Sciences, 500 Yu Tian Road, Shanghai 200083, People's Republic of China*

Absract

$Mn_{1.5}Co_1Ni_{0.5}O_4$ (MCNO) thin films were deposited on different materials by Chemical Solution Deposition (CSD) Method, and then CBP was spun-coated on MCNO thin film. The study shows that $Mn_{1.5}Co_1Ni_{0.5}O_4$ thin film deposited on $Mn_{1.5}Co_1Ni_{0.35}Cu_{0.15}O_4$ (MCNCuO) or $Mn_{1.5}Co_1Ni_{0.2}Cu_{0.15}Sc_{0.15}O_4$ (MCNCuScO) thin film facilitates the electrical conductivity of MCNO/CBP multilayer. The energy gap between Fermi level of $Mn_{1.5}Co_1Ni_{0.5}O_4$ thin film and HOMO level of CBP film in MCNCuO/MCNO/CBP multilayer is smaller than the one in MCNCuScO/MCNO/CBP multilayer. The energy gap between the Fermi level of $Mn_{1.5}Co_1Ni_{0.5}O_4$ thin film and the HOMO level of CBP film in $MnCo_2O_4$/MCNO/CBP multilayer is smaller than the one in $NiMn_2O_4$/MCNO/CBP multilayer.

Key words: $Mn_{1.5}Co_1Ni_{0.5}O_4$ thin film; Organic coating; Fermi level; Multilayer; Resistivity

a) Corresponding author: **Zhiming Huang.**
Tel: (+86) 021 25051705, E-mail address: zmhuang@mail.sitp.ac.cn.

Table 1. Resistances of the first multilayer group.

Multilayers	R (Ω)
MCNCuO/CBP	1.56×10^{6}
MCNCuO/MCNO/CBP	9.82×10^{5}
MCNCuScO/CBP	5.56×10^{5}
MCNCuScO/MCNO/CBP	1.15×10^{6}
MCNCuO/MCNO	8.87×10^{5}
MCNCuScO/MCNO	5.60×10^{5}
MCNO/CBP	5.54×10^{6}

Table 2. Resistances of the second multilayer group.

Multilayers	R (Ω)
$MnCo_2O_4$/CBP	2.24×10^{8}
$MnCo_2O_4$/MCNO/CBP	1.05×10^{7}
$NiMn_2O_4$/CBP	2.84×10^{8}
$NiMn_2O_4$/MCNO/CBP	9.38×10^{6}
$MnCo_2O_4$/MCNO	1.37×10^{7}
$NiMn_2O_4$/MCNO	1.48×10^{7}
MCNO/CBP	5.54×10^{6}

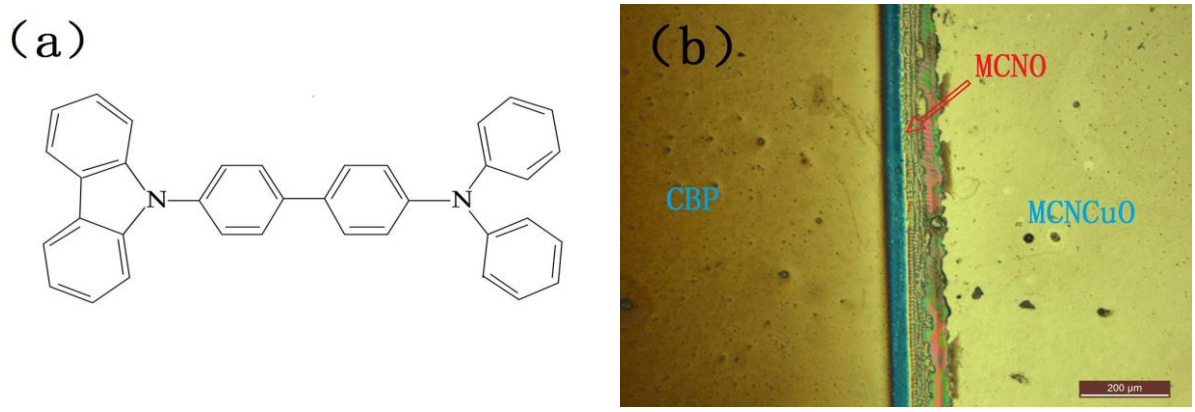

Fig. 1. (a) Molecular formula of CBP; (b) MCNCuO/MCNO/CBP multilayer.

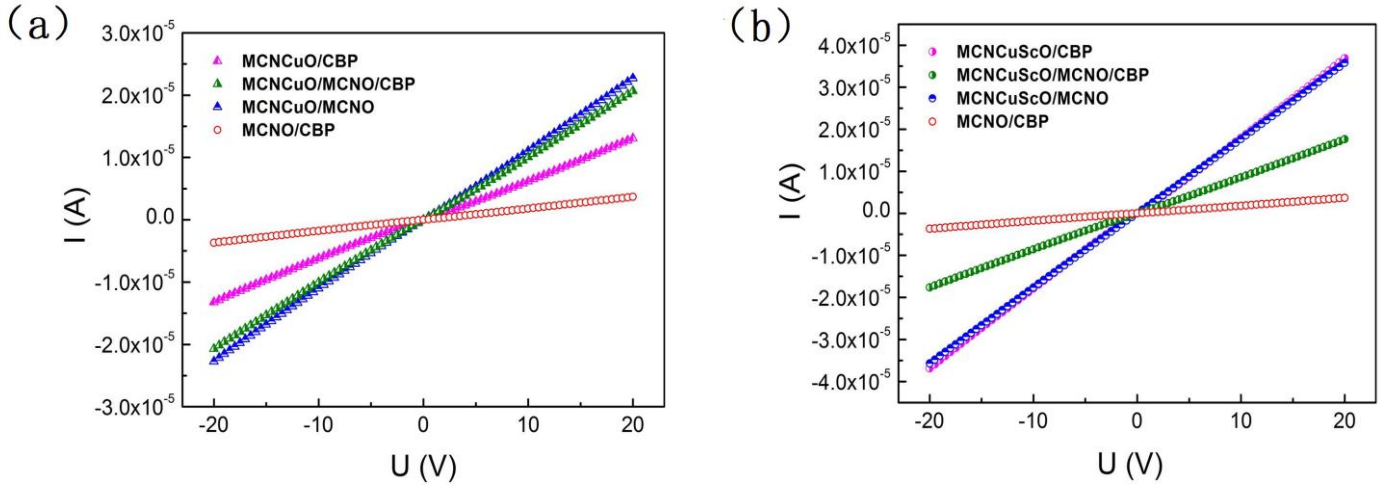

Fig. 2. Graphics of current VS voltage for multilayers (a) $Mn_{1.5}Co_1Ni_{0.35}Cu_{0.15}O_4$ thin film included; (b) $Mn_{1.5}Co_1Ni_{0.2}Cu_{0.15}Sc_{0.15}O_4$ thin film included.

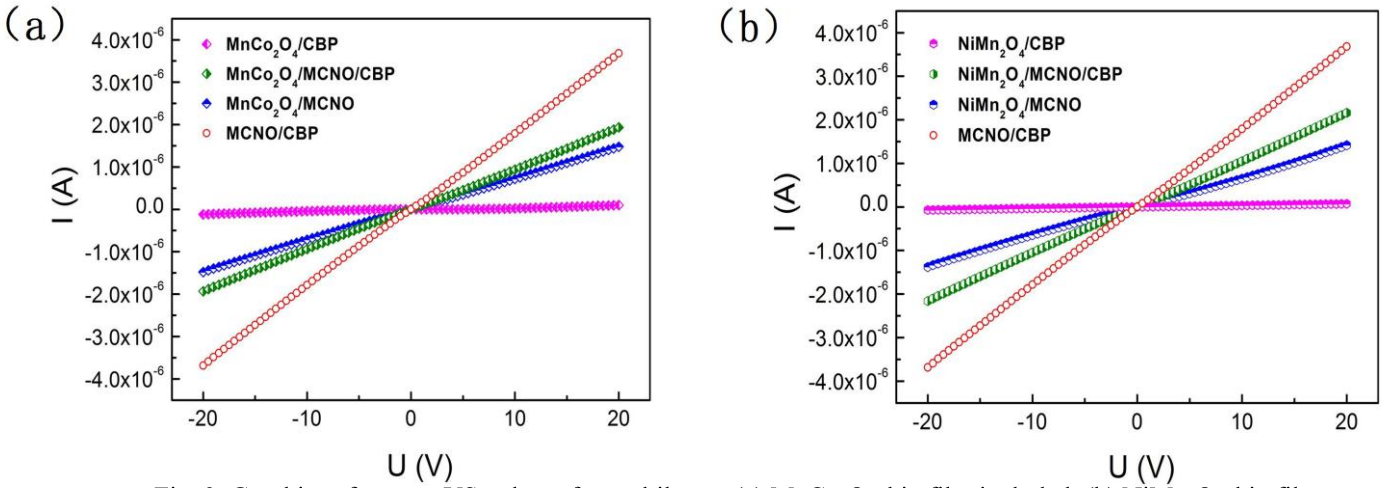

Fig. 3. Graphics of current VS voltage for multilayers (a) $MnCo_2O_4$ thin film included; (b) $NiMn_2O_4$ thin film included.

Incident angle dependence of WSi wire-grid polarizer

I. Yamada[1,2]*

[1] *Dept. of Electronic Systems Engineering, the University of Shiga Prefecture, Shiga, Japan*
[2] *Center for Glass Science and Technology, School of Engineering, the University of Shiga Prefecture, Shiga, Japan*

Infrared wire-grid polarizers, which are generally used for mid-infrared measurements, consist of metal wires of submicron width. However, current wire-grid polarizers are inadequate in terms of mechanical strength and adhesiveness between wires and substrates. Therefore, special care must be taken when using these polarizers.

Silicides generally have excellent chemical and thermal stabilities. In various silicides, tungsten silicide (WSi) is known as electrodes in integrated circuits, since it has high electric conductivity, chemical and thermal durability as well as strong adhesiveness to Si. This study examined the incident angle characteristic of a WSi wire-grid polarizer in the infrared range by measuring transmittances at different incident angles. [1]

We fabricated an infrared wire-grid polarizer consisting of a WSi grating and a Si substrate. Photolithography using two-beam interference was conducted for generating the short-period grating structure. Figure 1 shows the fabrication process. (a) A WSi film was deposited on the Si substrate using the sputtering method. Then, a photoresist was coated onto the substrate and exposed to an interference fringe of He-Cd laser beams (325 nm wavelength). (b) After development and rinsing off the exposed photoresist, (c) WSi was etched off by reactive ion etching (RIE) with SF_6 gas as a mask for the photoresist. The process was completed by removing the residual photoresist. Figure 2 shows a scanning electron microphotograph of the fabricated element. As Fig. 2 shows, the grating depth, period, and filling factor of the wire-grid layer were, respectively, d = 260 nm, Λ = 400 nm, and $f \sim 0.5$. The side wall roughness of the WSi grating is attributable to the RIE condition. Immersion in acetone, immersion in ethanol, and immersion in water with ultrasonic vibration caused little damage to the surface of this element.

Figure 3 depicts (a) the polarization transmission spectra and (b) the extinction ratios of the element measured by changing the incident angle θ from 0° to 40° upon the WSi grating direction. As the incident angle increases, the TM transmission spectrum increases. It was greater than 60% at the incident angle of 40° in the 4–8 μm wavelength range, although the TE transmission spectrum decreases. The extinction ratio achieved 22.2 dB at 2.5 μm wavelength, although the value at normal incidence was 20.8 dB.

Acknowledgement

The author thanks Professor J. Nishii of Hokkaido University for his help in experiment of sample fabrication. The author thanks Professor M. Saito of Ryukoku University for useful discussions.

Reference

1. I. Yamada, J. Nishii, and M. Saito, "Incident angle and temperature dependence of WSi wire-grid polarizer", Infrared Phys. Technol. Vol. 63C, pp. 92–96 (2014).

*corresponding author: yamada.i@e.usp.ac.jp

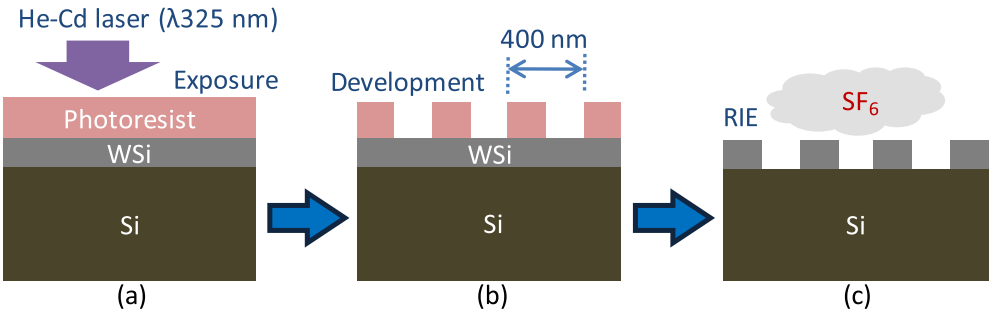

Fig. 1. Schematic illustration of the wire-grid polarizer fabrication process. (a) After a WSi layer is deposited on a Si substrate using sputtering, a photoresist is coated onto the WSi layer, and a stripe beam of the He-Cd laser (325 nm wavelength) is irradiated using the two-beam interference method. (b) A photoresist grating is patterned by the development. (c) The WSi layer is etched the photoresist grating as a mask selectively using the RIE.

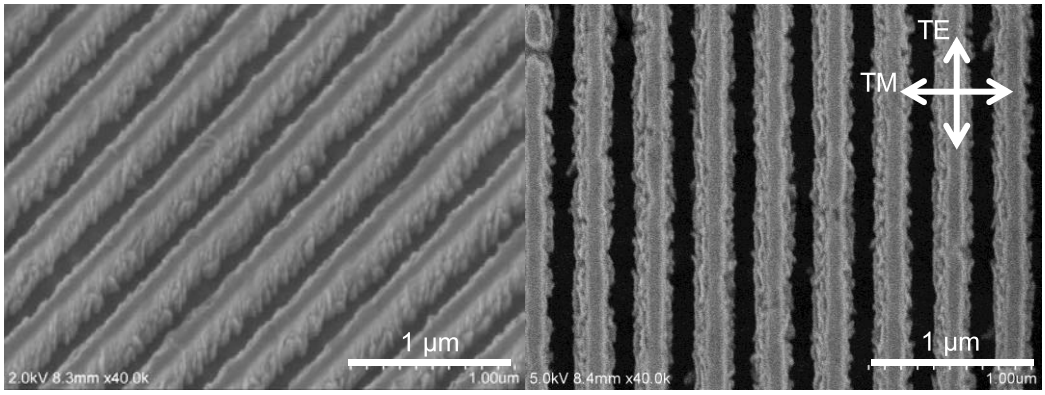

Fig. 2. SEM images of WSi grating on Si substrate: thickness d = 260 nm, period Λ = 400 nm, and fill factor f of approximately 0.5. [1]

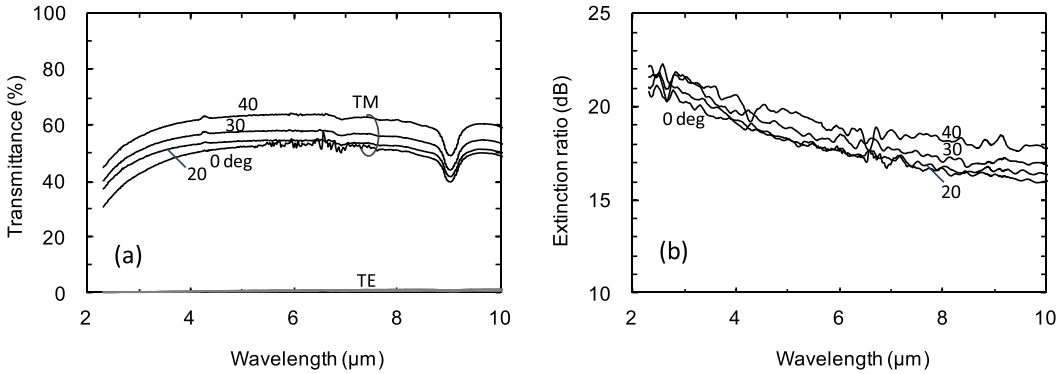

Fig. 3. (a) Polarization transmission spectra and (b) extinction ratio of the element by varying the incident angle θ. TE and TM show the polarization directions. Numerals next to the curves denote the incident angle. [1]

Quantum Dots/Dashes Based Narrow-Gap Heterostructures

V. Romanov, Ya. Parkhomenko, E. Ivanov, P. Dement'ev, V. Nevedomsky, K. Moiseev*

Ioffe Institute, Politekhnicheskaya 26, St. Petersburg, 194021, Russia

Nowadays there is a strong demand of heterosrtuctures based on low-dimensional systems (LDS), such as quantum dots, quantum dashes, nanowires etc, for potential applications in optoelectronic devices for detection of various chemical, explosive and biological agents, which have pronounced absorption bands in the infrared wavelength range (2-5 μm). To penetrate in the long-wavelength region (λ>2 μm) it is necessary to produce nanoobjects inserted in matrices with the energy gap as narrow as 0.7 eV (for example, GaSb and InAs) [1,2]. Multicomponent alloys based on GaSb- and InAs-rich compounds provide a heterostructure design, which satisfies the requirement for the lattice parameter of the whole structure remaining constant to minimize the internal strain in the epitaxial multilayered heterostructures, while the band gap and the spin–orbit splitting energy could be changed, and therefore the energy spectrum of radiative transitions is determined by variation of the alloy composition [3,4]. Furthermore, use of a multicomponent alloy as a subsequent matrix layer allows to control the matrix surface chemistry and to determine the shape of the deposited nano-islands [5,6].

We here report on narrow-gap nanoheterostructures with self-assembled InSb quantum dots/dashes grown by MOVPE. The structures under study were obtained on binary InAs(001) and GaSb (001) matrices as well as on multicomponent InAsSbP and GaInAsSb alloys lattice-matched to the corresponding substrate [7,8]. Transformation of a multifaceted dome like quantum dot with the octagonal base confined by (111) and (021) planes to a truncated pyramid-like one with the rectangular base formed by (021) planes only was occurred in the InAsSbP matrix system. A dramatic evolution of the nanoisland geometry from a quantum dot to a quantum dash with a changing of the matrix surface chemistry of the InAsSbP epitaxial layer was found out. It was also shown that the surface density, shape, and size of nanoislands are strongly dependent on the matrix surface chemistry in the GaInAsSb alloy system. Heterostructures based on the InSb quantum dashes buried into the InAs unipolar matrix exhibited the electroluminescence near 3.62 μm at room temperature whereas the photoluminescence spectrum for the heterostructures with InSb quantum dots on the GaSb-rich matrix has been achieved.

This work was in part supported by the RBRF (14-02-01102).

References

[1] V.V. Romanov, E.V. Ivanov, K.D. Moiseev, Semicond. **48**, 911 (2014).

[2] K. Moiseev, V. Romanov, P. Dement'ev, E. Ivanov, J. Cryst. Growth **414**, 177 (2015).

[3] M. Motyka, M. Dyksik, F. Janiak, K.D. Moiseev, J. Misiewicz, J. Phys. D-Appl. Phys. **47**, 285102 (2014).

[4] V.V. Romanov, M.V. Baidakova, K.D. Moiseev, Semicond. **48**, 733 (2014).

[5] K. Moiseev, V. Romanov, P. Dement'ev, M. Mikhailova, J. Cryst. Growth **318**, 379 (2011).

[6] V.V. Romanov, P.A. Dement'ev, K.D. Moiseev, Semicond. **50**, 910 (2016).

[7] K.D. Moiseev, Ya.A. Parkhomenko, V.N. Nevedomsky, Thin Solid Films **543**, 74 (2013).

[8] Ya.A. Parkhomenko, P.A. Dement'ev, K.D. Moiseev, Semicond., **50**, 976 (2016).

*corresponding author: mkd@iropt2.ioffe.ru

Infrared photo-thermal absorption effect on CdZnTe materials

C. Xu[1, 2, *], S.W.Sun[1, 2], J.R. Yang[1, 2], J.T.Dong[3], J.H.Zhao[3], Z.L.Wu[3]

[1] *Key Laboratory of Infrared Image Materials and Devices, Shanghai Institute of Technical Physics of the Chinese Academy of Sciences, Shanghai, P. R. China, 200083;*
[2] *University of Chinese Academy of Science, Beijing, P. R. China, 100049;*
[3] *ZC Optoelectronic Technologies, Hefei,Anhui Province, P. R. China, 230031;*

Infrared photo-thermal absorption effect was used extensively in detecting the micro-defects in semiconductor materials (silicon wafers) as a nondestructive and noncontact technology. In this work, the effect was adopted to detect the physical and structural characteristic of the CdZnTe crystal. By using a photo-thermal system composed of the pump-probe instrument, some optical images of strives and irregular spots were observed in CdZnTe materials. To investigate the mechanism, different CdZnTe samples were tested under the special designed conditions. Based on series experiments, the optical stripes were confirmed as the result of light interference related with the material's physical characteristic, which can be applied to measuring the thickness of the tested substrates. By analyzing the mechanism of this interference process, a method of inhibiting the formation of these stripes was proposed to eliminate the negative effects on characterizing the micro-defects in CdZnTe materials, such as choosing the proper wavelength and changing the angle of the pump light or probe light to vary the material absorption. On the base of verifying the mechanism of infrared photo-thermal absorption effect on CdZnTe materials, some micro-defects, such as Cd and Te inclusion/deposition, twin boundary and micro-cracks in the substrate materials was detected and characterized. Therefore, the infrared photo-thermal absorption effect offers an effective method to investigate the micro-defects in CdZnTe materials using for infrared detectors.

.

*corresponding author: charlesxu@mail.sitp.ac.cn

Studying extended wavelength In0.83Ga0.17As detectors with different etch gas

Ping Li , Hengjing Tang , Tao Li , Xue Li , Xiumei Shao , Haimei Gong
Shanghai Institute of Technical Physics, Chinese Academy of Sciences , University of Chinese Academy of Sciences, Beijing 100049, P. R. China

Abstract

In order to obtain an optimized method for low etch damage, the different etch gas for extended wavelength In0.83Ga0.17As detector materials by Cl2/N2 ICP etching and Cl2/CH4 ICP etching was studied in this paper. The quality of the sample before and after etching was investigated using photoluminescence (PL) technology. The etch damage of InGaAs sample in our work were characterized by Transmission Line Model (TLM) and current voltage (IV) technology. The results indicate that the sample with etch gas Cl2/CH4 has lower PL intensity than the Cl2/N2 sample. The square resistance of the Cl2/CH4 sample is larger than the Cl2/N2 sample. The dark current of the Cl2/CH4 sample has lower than the Cl2/N2 sample. The research shown that the sample with Cl2/CH4 etch gas has some advantages than the Cl2/N2 etch gas sample. The reason leaded the lower dark current and larger square resistance and lower PL intensity may attribute to the hydrogen decomposed by CH4 which is created the non-radiative recombination centers in inner material and passivated the dangling bond of the surface of material. The non-radiative recombination centers would make the PL intensity lower and the dangling bond passivated by hydrogen would reduce the dark current of the extended wavelength In0.83Ga0.17As detectors.

Keyword:etch,extended wavelength In0.83Ga0.17As,TLM,PL,dark current

Performance of gas source MBE grown InGaAsP and InAlGaAs PIN detectors targeted on 1.06 μm wavelength detection

S. P. Xi, Y. Gu, Y. G. Zhang*, X. Y. Chen, Y. J. Ma, B. Du, Y. H. Shi, W. Y. Ji

State Key Laboratory of Functional Materials for Informatics, Shanghai Institute of Microsystem and Information Technology, Chinese Academy of Sciences, Shanghai, China

In the optoelectronic applications adopting laser sources, for instance the active imaging, ranging or 3D lidar, the performances of the lasers and photodetectors (PDs) are the most important issues of concern. Among a variety of lasers the 1.06 μm solid or fiber lasers, which employs neodymium as active medium and normally pumped using mature 808 nm semiconductor lasers, should be the best one for its high efficiency and power. As for the PD materials, Si should be the most successful one but not so suitable for 1.06 μm detection because of its slightly wider and indirect band-gap. The optical absorption coefficient of Si at 1.06 μm is less than 10 cm^{-1}, which are about three orders lower than those of direct band-gap III-V materials with the same band-gap energy. Therefore, thick absorption layers are needed and the devices are usually operated under high reverse bias to form a wide depletion region. Direct band-gap $In_{0.53}Ga_{0.47}As$ works well at 1.31 μm and 1.55 μm wavelengths and can also be used for 1.06 μm detection, but in this case its narrower band-gap results in higher dark current, also the much response out of the target wavelength is not good for the noise performance of the system. InGaAsP and InAlGaAs quaternary materials could be lattice matched to InP substrates exactly over a range of specific compositions and a wide spectral range. Both InGaAsP [1] and InAlGaAs [2] materials are suitable choices for their above mentioned advantages. However, the comparison of these two different material detectors has not been well studied. In this work, InP-based detectors targeted on 1.06 μm wavelength detection in these two different materials have been grown by gas source molecular beam epitaxy. Through a comprehensive comparison, the effects of InGaAsP (Sample A) and InAlGaAs (Sample B) material on the performance of the detectors targeted on 1.06 μm wavelength detection were investigated.

The absorption layers of sample A and smple B show negative mismatch of -7.2×10^{-4} and -1.2×10^{-3} to InP substrates with FWHM around 39 arcs and 51 arcs. The PL intensity of sample A corresponding to the InGaAsP absorption layer is about 350 times higher than that of sample B, which indicates less non-radiation recombination centers in the absorption layer of sample A. For the detectors with 200 μm mesa diameter, the dark currents of sample A and sample B at reverse bias V_R=10 mV are 2.19 pA (6.97×10^{-9} A/cm^2) and 1.41 pA (4.49×10^{-9} A/cm^2) at room temperature which are in the same order of magnitude. The photocurrent of sample A is about 4 times larger than that of sample B at V_R=10 mV under the same incident light power by using a 1064 nm laser source. Detailed analysis will be contained in the presentation.

References

[1] G. E. Stillman, L. W. Cook, N. Tabatabaie, et al. IEEE T Electron Dev. 30 (1983) 364-381.
[2] L. Zhou, Y. Gu, Y. G. Zhang, et al. J. Cryst. Growth. 378 (2013) 579-582.

*corresponding author: ygzhang@mail. sim. ac.cn

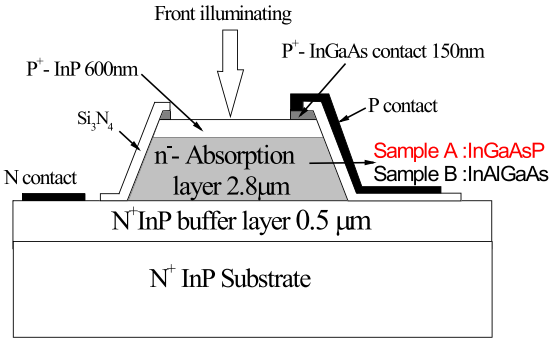

Fig. 1. The schematic of the mesa-type detectors.

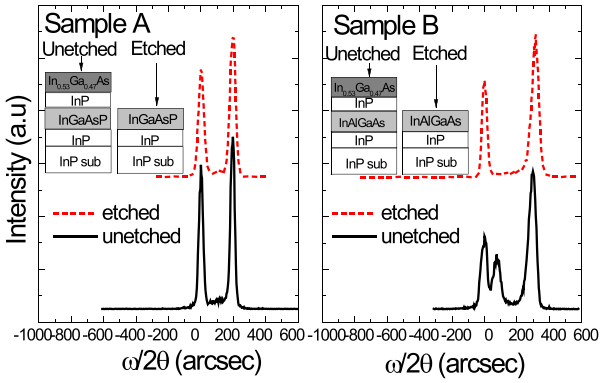

Fig. 2. (004) ω-2θ scan curves of the samples, the solid and dash lines are the unetched and etched samples respectively. The inset shows the schematic structures of the samples.

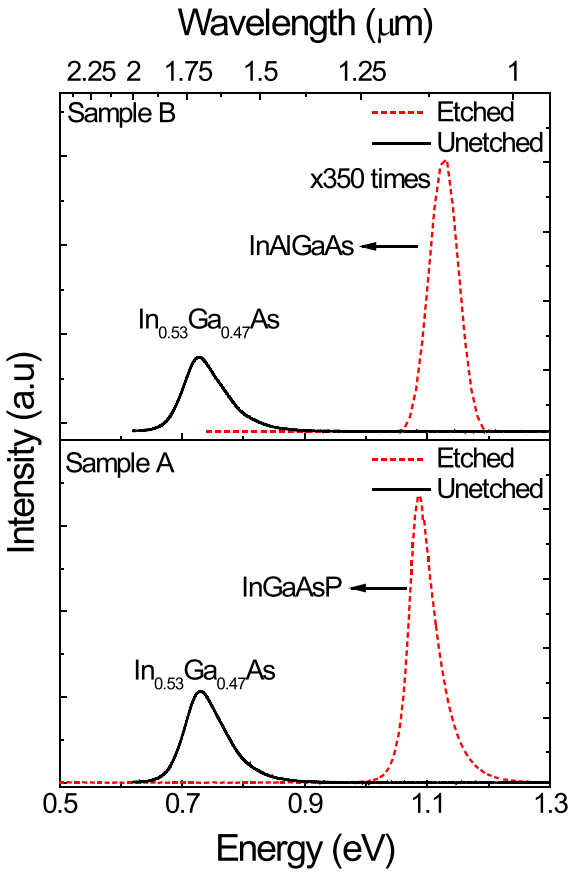

Fig. 3. PL spectrum of sample A and sample B at room temperature, the solid and dash lines are the unetched and etched samples respectively.

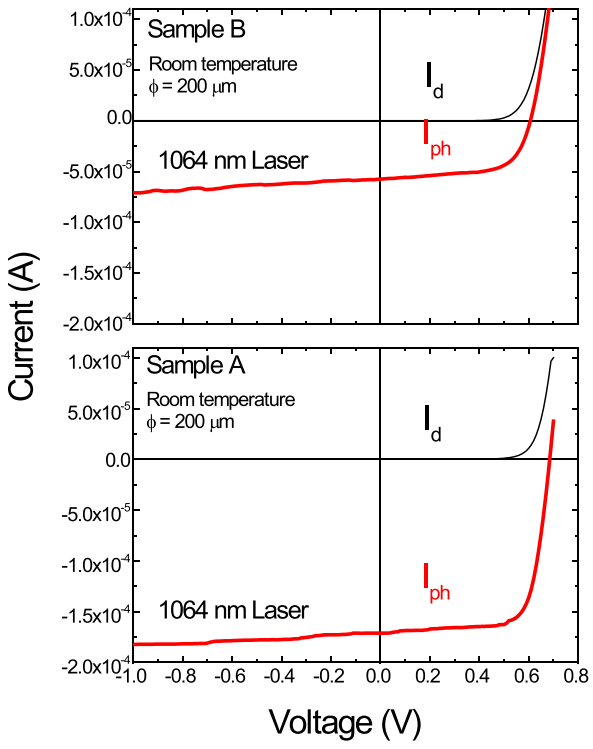

Fig. 4. The forward and reverse I-V characteristics of the samples in dark or light cases

Mid-infrared absolute spectral responsivity scale based on an absolute cryogenic radiometer and an optical parametric oscillator laser

Kun Zhao[1,2], Xueshun Shi[1,2,3*], Haidong Chen[1,2], Yulong Liu[1,2], Changming Liu[1,2], Hongbo Liu[1,2], Kunfeng Chen[1,2]

[1]*The 41st Institute of China Electronics Technology Group Corporation, Qingdao, Shandong, China 266555*

[2]*National Opto-Electronic Primary Metrology Laboratory, Qingdao, Shandong, China 266555*

[3]*Science and Technology on Electronic Test & Measurement Laboratory, Shandong, China 266555*

The mid-infrared spectral region with wavelengths from 3 μm - 5 μm is of great importance as many molecules including CH_4, HCl and NO2 have strong fundamental rotational or vibrational absorption bands in this spectral region. Moreover, the 3 μm - 5 μm spectral region is an important infrared atmospheric window for earth observation and so on. Mid-infrared radiation is of particular interests to applications such as chemical analysis, medical examination, environment protection and homeland security. Consequently the mid-infrared radiometry for accurate and reliable calibration of the spectral responsivity of the mid-infrared detectors has drawn increasing attention. The primary task is to calibrate the absolute spectral responsivity of the mid-infrared detectors, which is usually the ratio of the detector's voltage output to the radiant flux input to the detector[1,2].

We are reporting on a laser-based absolute spectral responsivity scale in the mid-infrared spectral range. This scale is established to meet the increasing demand for mid-infrared detector calibration in the spectral range from 2.5 μm to 4.5 μm. Fig. 1 is a schematic diagram of the mid-infrared absolute spectral responsivity calibration facility. By using a mid-infrared tunable optical parametric oscillator as the laser source, the absolute responsivity scale has been established by calibrating thin-film thermopile detectors against an absolute cryogenic radiometer. The thin-film thermopile detectors can be then used as transfer standard detectors. The extended uncertainty of the absolute spectral responsivity measurement has been analyzed to be 0.58 ~0.68% (k = 2), as shown in table 1 and table 2.

References

1. A. Migdall, G. Eppeldauer. Realization of an infrared spectral radiant power response scale on a cryogenic bolometer, Metrologia, 35, 307-15, 1998.
2. C. A. Schrama, Monochromator-based cryogenic radiometry between 1 μm and 20 μm, Metrologia, 37, 567-70, 2000.

*corresponding author: xshshi@163.com

Source of uncertainty	type	Relative standard uncertainty / %
Window transmittance	B	0.068
Cavity absorbance	B	0.001
Electrical measurement	B	0.002
Sensitivity of radiometer	B	0.001
Measurement repeatability	A	0.006 to 0.077
Combined uncertainty		0.068 to 0.103

Table 1. The components of the combined relative standard uncertainty associated with the measurement of the optical power of the mid-infrared laser using the absolute cryogenic radiometer

Source of uncertainty	type	Relative standard uncertainty / %
Optical power measurement	B	0.068 to 0.103
Amplifier calibration	B	0.007
Detector linearity	B	0.2
Detector spatial nonuniformity	B	0.2
Temperature variation	B	0.02
Measurement repeatability	A	0.020 to 0.177
Combined uncertainty		0.29 to 0.34
Expended uncertainty(k=2)		0.58 to 0.68

Table 2.The contributing components to the uncertainty of the absolute spectral responsivity of TS-76 thermopile detectors in mid-infrared region

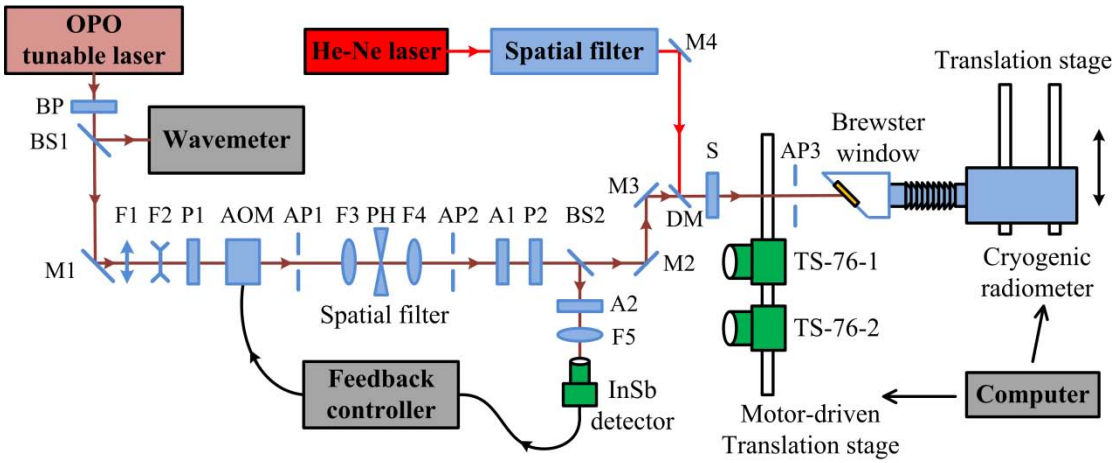

Fig.1. Diagram of the absolute spectral responsivity calibration facility. BP, bandpass filter; BS1, BS2, beamsplitters; M1, M2, M3, M4, steering mirrors; f1, f2, f3, f4, f5, lenses; P1, P2, polarizers; AOM, acousto-optic modulator; AP1, AP2, AP3, apertures; PH, pinhole; A1, A2, attenuating filters; DM, dichroic mirror; S, shutter.

Dark current characteristics of InP-based InGaAs photodetectors with different cut-off wavelengths

Y. H. Shi, Y. G. Zhang*, Y. Gu, Y. J. Ma, X. Y. Chen, S. P. Xi, B. Du, W. Y. Ji, A. Z. Li

State Key Laboratory of Functional Materials for Informatics, Shanghai Institute of Microsystem and Information Technology, Chinese Academy of Sciences, Shanghai, China

Dark current is one of the most crucial parameters for the high-indium $In_xGa_{1-x}As$ (x>0.53) photodetectors (PDs) applied in remote sensing [1]. As the indium content increases, the cut-off wavelength is extended. Owing to the lack of a natural lattice-matched substrate for the high-indium $In_xGa_{1-x}As$ [2], a higher threading dislocation density is generated for longer wavelength devices, and the device performance characteristics suffer from higher dark current levels. On the other hand, the bandgap of the high-indium $In_xGa_{1-x}As$ narrows with the cut-off wavelengths increased, so the dark current is also increased even further due to the enhance background radiation. To investigate the effects of lattice-mismatch and bandgap narrowing, we have analyzed the dark current of InP-based $In_xGa_{1-x}As$ PDs with different cut-off wavelengths.

All samples in this work were grown by using a VG Semicon V80H gas source molecular beam epitaxy system. The major structures of these detectors were the same but the $In_xGa_{1-x}As$ absorption layers. The $In_xGa_{1-x}As$ absorption layers of the samples with different cut-off wavelengths of 1.8, 2.2 and 2.5 μm are nominally $In_{0.585}Ga_{0.415}As$, $In_{0.75}Ga_{0.25}As$, and $In_{0.83}Ga_{0.17}As$ absorption layers, respectively. After growth, the samples were fabricated into circular mesa-type PDs of 500μm diameter.

The normalized response spectrum of the samples were measured at 300 K. The 50% cut-off wavelengths are about 1.79, 2.30 and 2.59 μm, respectively. The temperature dependence of the dark current was measured from 325 to 200 K, and the dark current can be expressed using an effective thermal activation energy. At 300 K, the dark current density of PD-1.8 μm is 3.21×10^{-5} A/cm^2 at the reverse bias voltage of 10 mV. As the temperature decreases, the -10 mV dark current density decreases significantly to 3.31×10^{-8} A/cm^2 at 200 K. For PD-2.2 μm and PD-2.5 μm, the -10 mV dark current density is 2.37×10^{-4} A/cm^2 and 5.78×10^{-4} A/cm^2 at 300 K, respectively. It is found that the dark current density of PD-2.2 μm at 200 K has been reduced by about 1 order of magnitude compared with that of PD-2.5 μm, while those of PD-1.8 μm is the lowest. The shunt resistance R_0 of the samples at zero bias was also measured and the resistance area products R_0A versus reciprocal temperature was shown. As the temperature decreases, the R_0A keeps increasing for all PDs. It is found that the R_0A of PD-1.8 μm and PD-2.2 μm increased quicker than that of PD-2.5 μm in the range of 250-200 K.

References

1. Y. Gu, L. Zhou, Y. G. Zhang, et al., Appl. Phys. Express., 8, 022202 (2015).
2. Y. G. Zhang, Y. Gu, K. Wang, et al., Semicond. Sci. Technol., 23, 125029 (2008).

*corresponding author: ygzhang@mail.sim.ac.cn

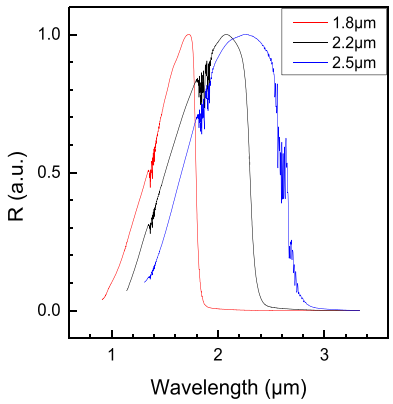

Fig.1. Measured response spectra of the 1.8, 2.2 and 2.5 μm photodetectors at 300K and zero bias.

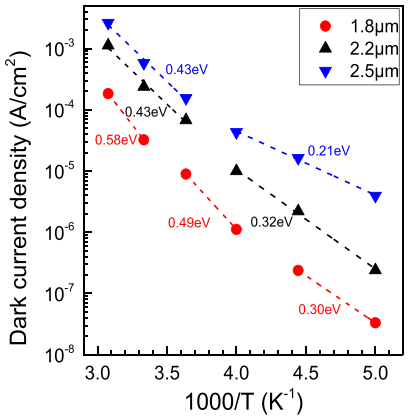

Fig.2. Arrhenius plots of the dark current at -10 mV of the 1.8, 2.2 and 2.5 μm photodetectors. The activation energies in specific temperature regions are also shown in the figure.

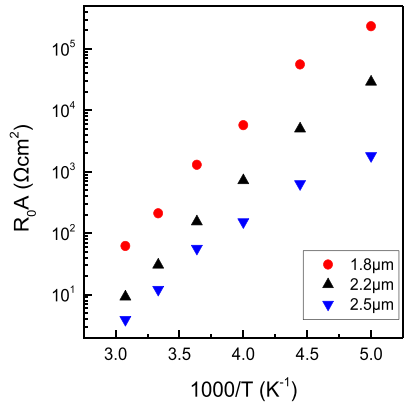

Fig.3. Arrhenius plots of zero bias resistance area products R_0A versus reciprocal temperatures of the 1.8, 2.2 and 2.5 μm photodetectors.

Impact of band structure of Ohmic contact layers on the response feature of p-i-n very long wavelength type II InAs/GaSb superlattice photodetector

J.L. Huang[1*], W.Q. Ma[1], Y.H. Zhang[1], Y.L. Cao[1], K. Liu[1], W.J. Huang[1], C.C. Zhao[1], and S.L. Lu[2]

[1] *Key Laboratory of Semiconductor Materials Science, Institute of semiconductors, Chinese Academy of Sciences, Beijing,10083, China*

[2] *Suzhou Institute of Nano-tech and Nano-Bionics, Chinese Academy of Sciences, Jiangsu, 215123, China*

Type II InAs/GaSb superlattice (SL) materials have attracted considerable interest for infrared photodetection due to the low Auger recombination rate, relatively long carrier lifetime, flexible tuning of the detection wavelength, good material uniformity, and so on. Type II InAs/GaSb SL photodetectors can cover a broad range of the detection wavelength by tuning the constituent layer thickness of the SL material and the thickness ratio of InAs to GaSb. Until now, the infrared detection in the short, mid, long, and very long wavelength (SW, MW, LW, and VLW) infrared ranges has been demonstrated by using type II SLs. However, the dark current is larger for VLW T2SL infrared photodetectors. The so-called barrier engineering scheme has been using to reduce the dark current such as inserting some barrier materials into the certain position. Here we show that the energy band structure of the Ohmic contact layers can have a big impact on the dark current and response feature of VLW detection using p-i-n type II SLs. It is found that, if the p and n Ohmic contact layers are comprised of MW InAs/GaSb SLs (Fig. 1(a)), the photoresponse of the detector is dominated by a short wavelength band with the 50% cutoff wavelength at 2.67 μm, while the designed VLW response is very weak at 0V (Fig. 2(a)). With increasing the bias voltage, the designed VLW response with the 50% cutoff wavelength at 17.8 μm becomes stronger and stronger (Fig. 2(b) and (c)). In contrast, if the p and n Ohmic contact layers are made up of the same SLs (Fig. 1(b)), as those of the VLW absorber region, only a broad VLW response shows up (Fig. 2(d)). The response difference between the two samples is attributed to blocking of the photo generated carriers by the energy barriers at the interfaces between the absorber and the contact layers for the sample using MW SLs as the contact layers.

References

1. Jianliang Huang, Wenquan Ma, Yanhua Zhang, Yulian Cao, Ke Liu, Wenjun Huang and Sulong Lu, “Impact of band structure of Ohmic contact layers on the response feature of p-i-n very long wavelength type II InAs/GaSb superlattice photodetector”, Appl. Phys. Lett., 106, 263502（2015）
2. Jianliang Huang, Wenquan Ma, Yang Wei, Yanhua Zhang, Kai Cui and Jun Shao, “Interface effect on structural and optical properties of type II InAs/GaSb superlattices”, Journal of Crystal Growth, 407, 37-41, (2014).

*corresponding author: jlhuang@semi.ac.cn

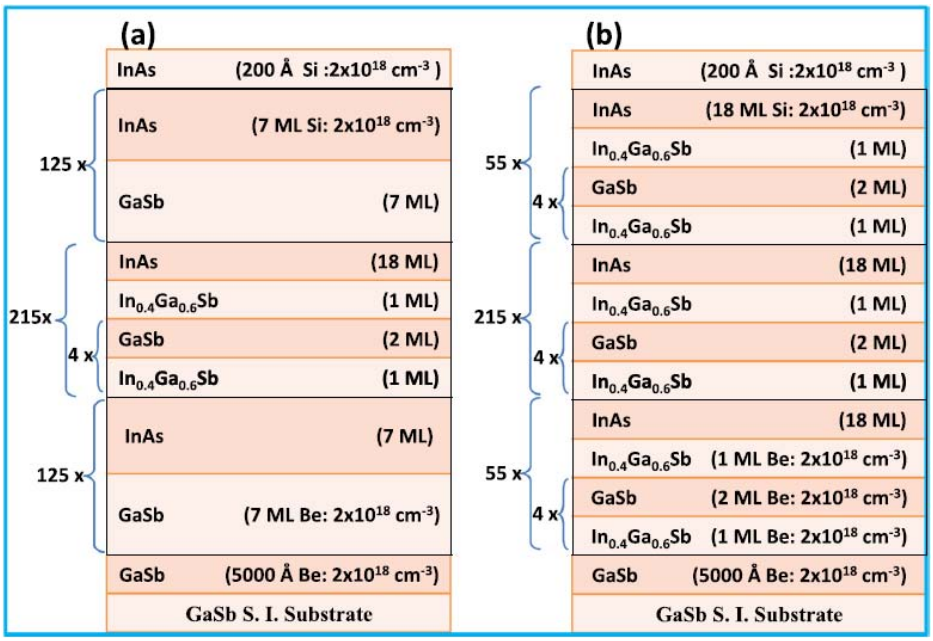

Fig.1. Schematic drawings of the grown structure of samples a and b.

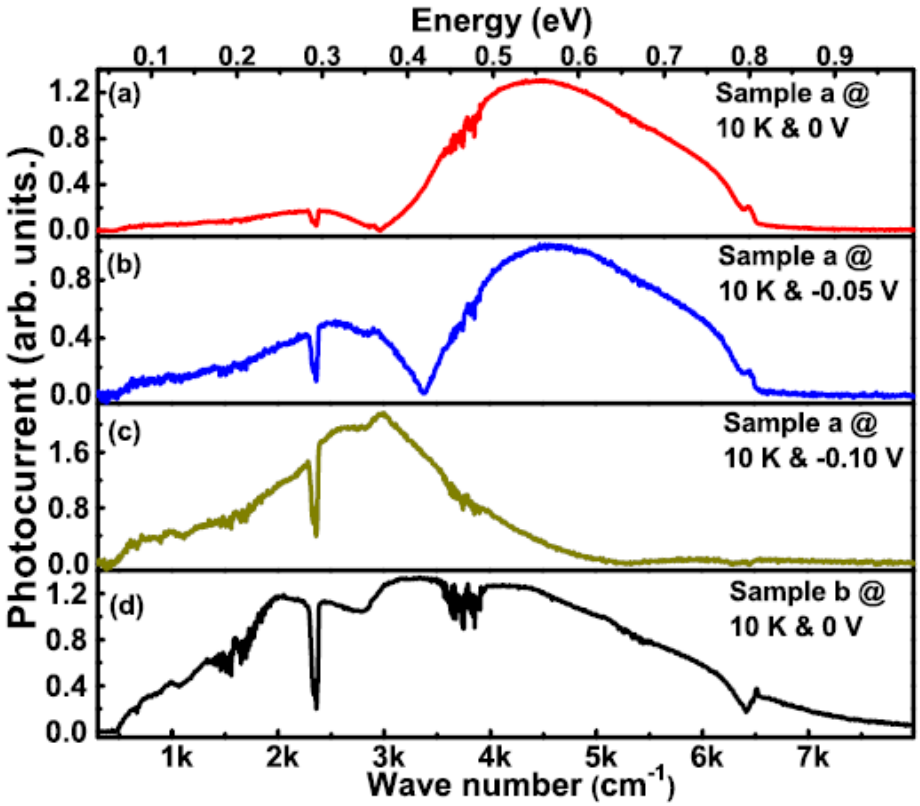

Fig. 3. (a), (b), and (c) are the photocurrent spectra of sample a at 0V, -0.05 V, and -0.1V measured at 10 K, respectively; (d) is the photocurrent spectrum of sample b at 0V at 10 K.

Pushing detection wavelength toward 1um using antimonide-based type-II superlattices

Y. H. Zhang*, W. Q. Ma, J. L. Huang, Y. L. Cao, K. Liu, W. J. Huang, C. C. Zhao, H. M. Ji, T. Yang

The Key Laboratory of Semiconductor Materials Science, Institute of Semiconductors, Chinese Academy of Sciences, Qinghua East Road A 35, Beijing 100083, China

We report on a short wavelength p-i-n detector using antimonide-based type-II superlattices (T2SL) with inserting AlSb layers. Fig. 1(a) is the measured photocurrent spectrum at zero bias at 77 K. It can be seen that the response spectrum is a narrow-band type and reveals an asymmetric feature with a longer tail on the higher energy side. These features are ascribed to the stronger absorption for the higher energy photons from the n region [1, 2]. At 77 K, the $\delta\lambda/\lambda$ is about 7.6% and the wavelength at the response maximum is 1.08 um. It is the shortest wavelength reported until now. When a large positive bias voltage like +3 V is applied to the detector even at room temperature (RT), the photoresponse is still clearly obtained. Fig. 1(b) shows the RT photocurrent spectrum at -3 V. At RT, the response maximum changes to 1.15 um. By inserting AlSb thin layers not only helps reach such a short detection wavelength, but also reduces the dark current significantly. Fig. 2 depicts the dark current curves measured at 77 K and 300 K. For example, at 300 K, the dark current is 3.94×10^{-6} A at -3 V and is only 3.36×10^{-4} A at +3 V. Our work demonstrates that the detection wavelength using T2SL structure can be extended to about 1 um and thus can cover the whole range of the SW infrared window.

References

1. J. L. Huang, W. Q. Ma, Y. H. Zhang, Y. L. Cao, K. Liu, W. J. Huang, and S. L. Lu, “Narrow-band type II superlattice photodetector with detection wavelength shorter Than 2 _m,” IEEE Photo. Tech. L., vol. 27, pp. 2276–2279, 2015.
2. Y. H. Zhang, W. Q. Ma, Y. Wei, Y. L. Cao, J. L. Huang, K. Cui, and X. L. Guo, “Narrow-band long-/very-long wavelength twocolor type-II InAs/GaSb superlattice photodetector by changing the bias polarity,” Appl. Phys. Lett., vol. 100, pp. 173 511–1–173 511–4, 2012.

*corresponding author: zhangyanhua@semi.ac.cn

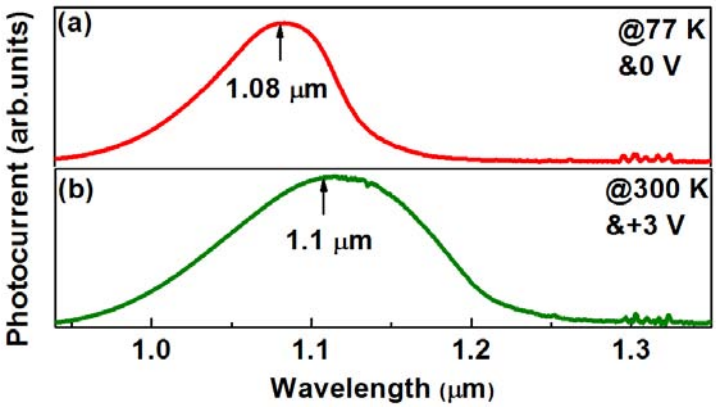

Fig.1. (a), The photocurrent spectrum of the device under zero bias at 77 K. (b), the photocurrent spectra of the device at 300 K when the applied bias voltage is +3 V.

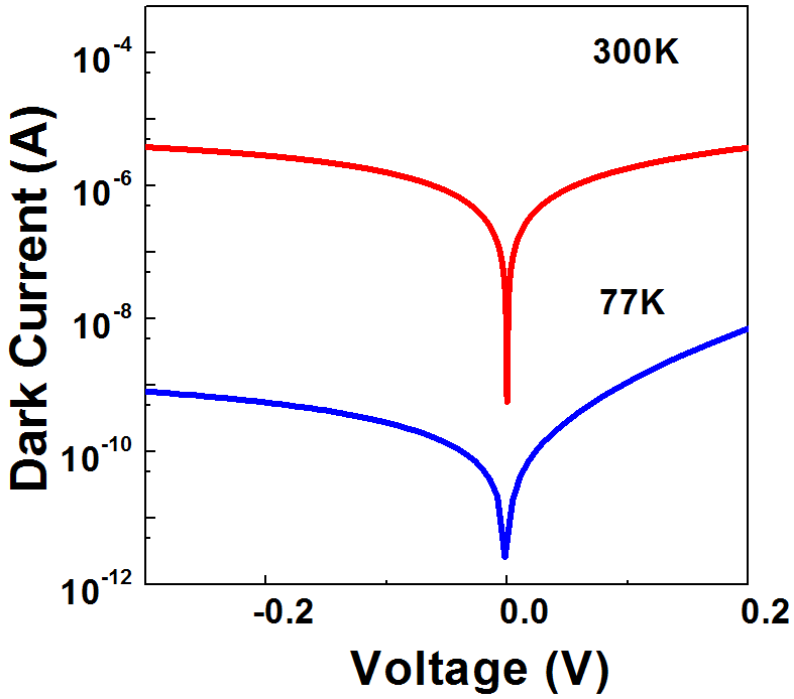

Fig.2. Dark current density curves of the device at 77 and 300 K.

Piezoelectric tuning of perfect plasmonic absorbers

Ao Yang, KeCheng Yang, Fei Yi*

School of Optics and Electronic Information, Huazhong Univeristy of Science and Technology, Wuhan 430074, China

Optical antennas enable the control of light matter interaction on the nanometer scale[1]. Efficient on-chip electrical switching of plasmonic resonances is the crucial step towards the integration of optical antennas into practical optoelectronic circuits[2]. We propose and numerically investigate the on-chip low voltage linear electrical tuning of narrowband optical antenna perfect absorber via a piezoelectric optomechanic cavity. Near unity absorption is realized by an array of gold nanostrip antennas separated from a membrane based deformable back reflector by a small gap. A narrow linewidth of 33 nm at 2.58 μm is realized through the coupling between the plasmonic mode and the photonic mode in the cavity enhanced antenna structure[3,4]. An aluminium nitride piezoelectric layer enabled efficient actuation of the back reflector and therefore change the gap size, allowing for the tuning of the spectral absorption. The peak wavelength can be shifted linearly by 250 nm with 10 V of tuning voltage and the tuning range is not limited by the pull-in effect. The polarization dependence of the nanostrip antenna coupled with the optomechanic cavity allows the use of our device as a voltage tunable polarization control device.

In this presentation I will talk about our recent works on narrowband perfect plasmonic absorbers.

References

1. N. C. Lindquist, P. Nagpal, K. M. McPeak, D. J. Norris, and S. H. oh, “Engineering metallic nanostructures for plasmonics and nanophotonics,” Reports on Progress in Physics, vol. 75, no. 3, pp. 61, Mar. 2012.
2. K. B. Crozier, A. Sundaramurthy, G. S. Kino, and C. F.Quate, “Optical antennas: Resonators for local field enhancement,” Journal of Applied Physics, vol. 94, no. 7, pp. 4632-4642, Oct. 2003.
3. L. Novotny, and N. van Hulst, “Antennas for light,” Nature Photonics, vol. 5, no. 2, pp. 83-90, Feb. 2011.
4. A. Bonakdar, and H. Mohseni, “Impact of optical antennas on active optoelectronic devices,” Nanoscale, vol. 6, no. 19, pp. 10961-10974, 2014.

*corresponding author: feiyi@hust.edu.cn

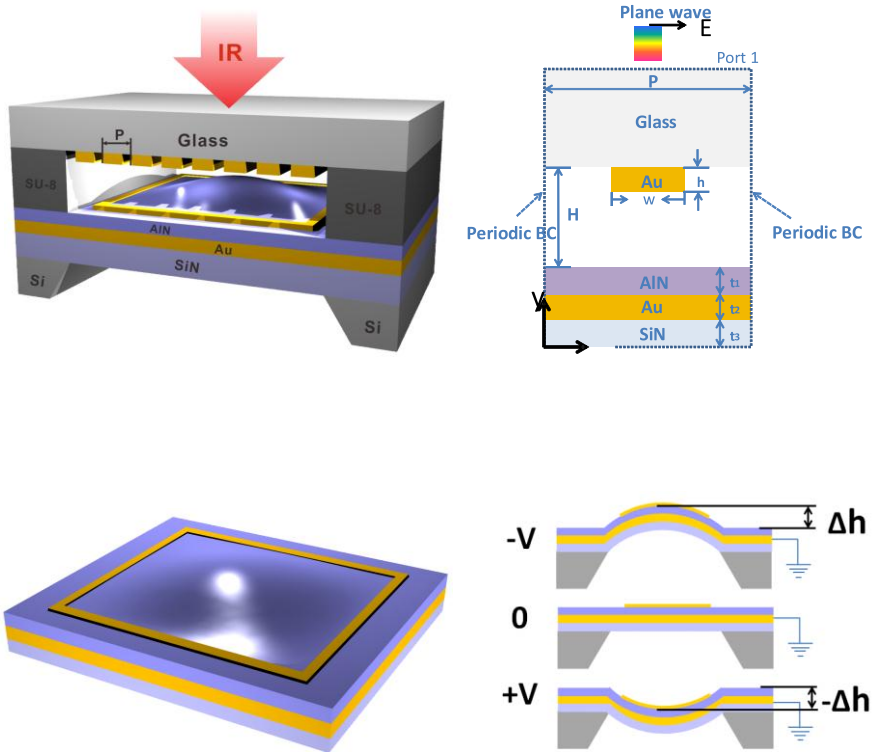

Fig.1. A schematic drawing of the voltage tunable narrow-band perfect plasmonic absorber.

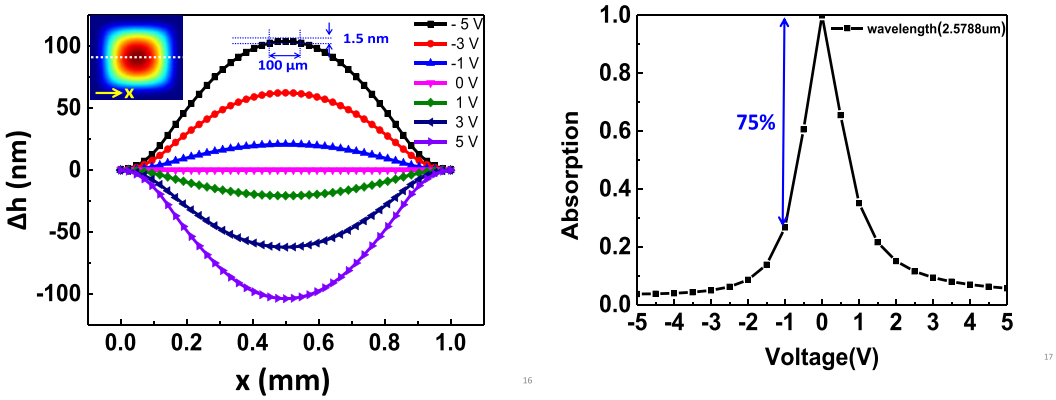

Fig.2. The profile of the membrance deflection as a function of the tuning voltage.

Temperature independent infrared responsivity of a quantum dot quantum cascade photodetector

Feng-Jiao Wang, Ning Zhuo, Shu-Man Liu*, Fei Ren, Feng-Qi Liu, and Zhan-Guo Wang

Key Laboratory of Semiconductor Materials Science, Institute of Semiconductors, Chinese Academy of Sciences and Beijing Key Laboratory of Low Dimensional Semiconductor Materials and Devices, P.O. Box 912, Beijing 100083, People's Republic of China

We demonstrate a quantum dot quantum cascade photodetector (QD-QCD), with a hybrid active region of InAs quantum dots and an InGaAs quantum well, that exhibited a temperature independent response at 4.5 μm. The normal incident responsivity reached 10.3 mA/W at 120 K and maintained a value of 9 mA/W up to 260 K. It exhibited a specific detectivity above 10^{11} cm $Hz^{1/2}$ W^{-1} at 77 K, which remained at 10^{8} cm $Hz^{1/2}$ W^{-1} at 260 K. We ascribe the device's good thermal stability of infrared response to the three-dimensional quantum confinement of the InAs quantum dots incorporated in the active region.

We have modified our former device's [1] design in some aspects, such as reducing the QD deposition thickness, reducing the Al concentration in the barriers and increasing the doping density in the absorption region, to achieve an improved performance. Three new samples were grown: D1, D2, and D3, which had two-dimensional (2D) doping densities of 4.5×10^{11} cm^{-2}, 9×10^{11} cm^{-2}, and 1.35×10^{12} cm^{-2}, respectively, in the QW/QD hybrid region. Figure 1 shows a typical cross-sectional dark-field transmission electron microscopy image of sample D1, which exhibited excellent material quality and showed flat interfaces for all stacks. Figure 2 shows the responsivity values of the three samples. The responsivity of sample D1 remained almost unchanged from 77 K to 300 K. Even the highly doped samples D2 and D3 kept a nearly constant peak responsivity up to a high temperature of at least 260 K, and then dropped about 20% at 300 K. In contrast, the responsivity of the control QW-QCD rapidly decreased with temperature. Thus, we believe that the thermal stability of the QD-QCDs came from the 3D quantum confinement of the InAs QDs.

The QD-QCD's normal incident response, high detectivity, and—in particular—temperature independent infrared response up to nearly room temperature make it an attractive infrared photodetector for high temperature applications. We expect that the performance of these QD-QCDs can be improved more by further optimizing its structure, which will require accurately calculating its energy band diagram including the 3D confinement potential of the InAs QDs, which is a rather complicated process.

Reference

1. X.J. Wang, S.Q. Zhai, N. Zhuo, J.Q. Liu, F[1].Q. Liu, S.M. Liu, and Z.G. Wang, Appl. Phys. Lett. **104**, 171108 (2014).

*corresponding author: liusm@semi.ac.cn

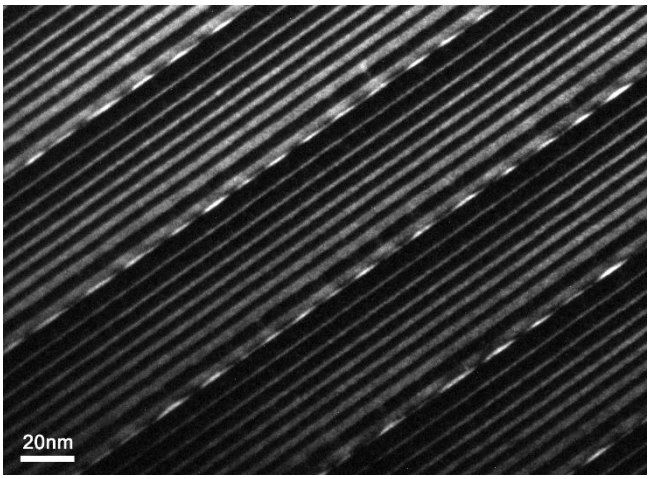

Fig.1. Cross-sectional dark-field transmission electron microscopy image of sample D1.

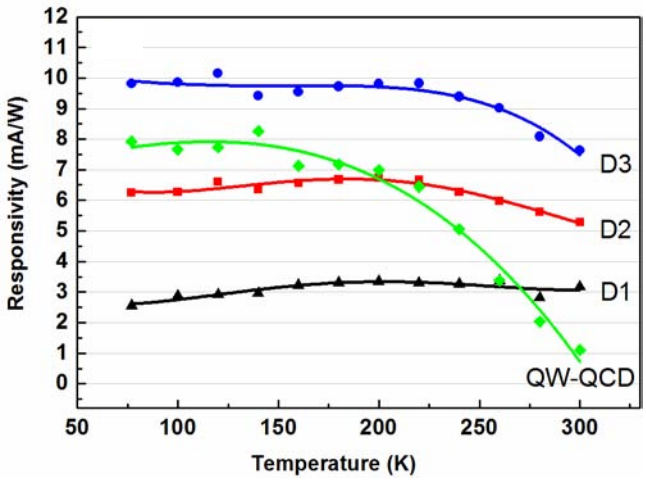

Fig.2. Responsivity of the three QD-QCD samples and the control QW-QCD sample as a function of temperature from 77 K to 300 K.

Life Test of The InGaAs Focal Plane Arrays Detector for Space Applications

ZHU Xian-Liang[1,2], ZHANG Hai-Yan[1,2], LI Xue[1,2], GONG Hai-Mei[1,2*]

[1] *State Key Laboratories of Transducer Technology, Shanghai Institute of Technical Physics, Chinese Acadamy of Sciences, Shanghai 200083, China;*

[2] *Key Laboratory of Infrared Imaging Materials and Detectors, Shanghai Institute of Technical Physics, Chinese Acadamy of Sciences, Shanghai 200083, China*

Compared to tactical applications, IR detectors for space applications require far fewer quantities, and reliability and photoelectric performances must be extraordinarily high. Therefore, the research of its reliability is very difficult because of the little amount and high price. Hybrid Infrared focal plane array (IRFPA) is the core component of the third generation infrared detection systems, which consists of infrared detector chip, readout integrated circuit (ROIC), and flip-chip bonding interconnection by Indium bump. In order to satisfy space application requirements for failure rates or Mean Time to Failure (MTTF), which can only be demonstrated with the large number of detectors manufactured, the single pixel in short-wavelength infrared InGaAs focal plane array is chose as the research object in this paper. As the InGaAs FPAs are usually operated around room temperature, they will not go through thousands times of temperature cycles, so hot temperature is the suitable accelerated stress. Through step-stress accelerated life test, the maximum temperature stress of InGaAs FPAs under the same failure mechanism has been obtained, and it was found that Indium bump is the most possible weakness of the FPAs. According to the results of step-stress accelerated life test, choosing the single pixel in InGaAs FPAs as research object, the constant-stress accelerated life test has been carried out at 70℃， 80℃and100℃. The bad pixels increased gradually during more than 10000 hours at each elevated temperatures. Statistical analysis on the experimental data shows that the activation energy is about 0.46eV, and the average lifetime of a single pixel in InGaAs FPAs will be more than 10^7h at the operating temperature(5℃).

* Corresponding author: hmgong@mail.sitp.ac.cn

InP Based Type-II Quantum Well Photodiodes

Baile Chen[1*], Archie Holmes[2]

[1] School of Information Science and Technology, ShanghaiTech University
[2] University of Virginia

Short wavelength infrared (SWIR) and mid wavelength infrared (MWIR) photodetectors have applications in areas such as chemical sensing, gas monitoring, medical diagnostics, infrared imaging and free-space communications. Mercury Cadmium Telluride (HgCdTe) is the predominant material system used in SWIR, MWIR and long wavelength infrared (LWIR) applications. However, HgCdTe often suffers from poor material uniformity and low yield. Comparable performance can be achieved on GaSb substrates with high quality InAs/GaSb strained-layer superlattices, but significant cooling is required to achieve high detectivity performance.

Indium Phosphide (InP) based InGaAs/GaAsSb type-II quantum wells photodiodes are the promising candidates for the detection in SWIR and MWIR region, especially at room temperature. These photodiodes can take advantage of mature material and device technology of InP material system. Both lattice matched and strain compensated type-II quantum wells photodiodes are designed and studied experimentally. In this talk, I will briefly introduce the state of art of the InP based photodiodes using type-II quantum wells as absorption regions.

*corresponding author: chenbl@shanghaitech.edu.cn

Low crosstalk three color infrared detector using InAs/GaSb superlattices for middle-long and -very long wavelength

Dongwei Jiang[1,2]*, Hongyue Hao[1,2], Xi Han[1,2], Guowei Wang[1,2], Yingqiang Xu[1,2], Zhichuan Niu[1,2]*

[1] *State Key Laboratory for Superlattices and Microstructures, Institute of Semiconductors, Chinese Academy of Sciences, Beijing 100083, China*

[2] *Synergetic Innovation Center of Quantum Information and Quantum Physics, University of Science and Technology of China, Hefei, Anhui 23026, China*

Multi-color infrared detector is highly beneficial for various military and civil applications such as target identification, recognition, tracking, and determination the absolute temperature of targets which is very useful in medical diagnostics and astronomy. It is more accurate and more sensitive in a complicated background with much low false alarm rate.[1-3] The type-II InAs/GaSb binary superlattice (T2SL) has an excellent material performance of adjustable energy band structure(0~0.8 eV) that made T2SL a prime candidate for multi-color sensing.[4] One of the most important issues in the reported multi-color detectors is the cross talk between different channels which limits the applied bias voltage range across the detector. We report a low crosstalk type-II InAs/GaSb superlattice three color infrared detector for mid-wave (MW), long-wave (LW), and very long-wave (VLW) detection using PMP/P-π-M-N structure. The PMP architecture is for MW and LW detection, and hetero-junction P-π-M-N architecture is for VLW detection. The crosstalk have been effectively suppressed. First, it can be decreased by using M barriers in PMP section that would block any photo-generated carriers' migration from one region of the device into another upon proper biasing. Second, it also can be mitigated by doping in the active region that would change the intrinsic carrier type in the SLs and hence controlling the transport direction of the photo-generated minority carriers. At 77 K, the cutoff wavelengths of the three color detection are 5 μm (at 0 mV), 12 μm (at 200 mV) and 18 μm (at -50 mV) with the crosstalk of 0, 0.25, and 0.5, respectively.

References

1. Rehm R, Walther M, Rutz F, et al. Dual-Color InAs/GaSb Superlattice Focal-Plane Array Technology[J]. Journal of Electronic Materials, 40(8):1738-1743, 2011.
2. Plis E A, Krishna S S, Gautam N, et al. Bias Switchable Dual-Band InAs/GaSb Superlattice Detector With pBp Architecture[J]. IEEE Photonics Journal, 3(2):234-240, 2011.
3. Gunapala S D, Bandara S V, Singh A, et al. 640× 486 long-wavelength two-color GaAs/AlGaAs quantum well infrared photodetector (QWIP) focal plane array camera[J]. Electron Devices, IEEE Transactions on, 47(5): 963-971, 2000.
4. Aifer E H, Jackson E M, Boishin G, et al. Very-long wave ternary antimonide superlattice photodiode with 21 μm cutoff[J]. Applied Physics Letters, 82(25): 4411-4413, 2003.

*corresponding author: jdw@semi.ac.cn (D.W.Jiang) zcniu@semi.ac.cn (Z.C.Niu) @+86-10-82304268

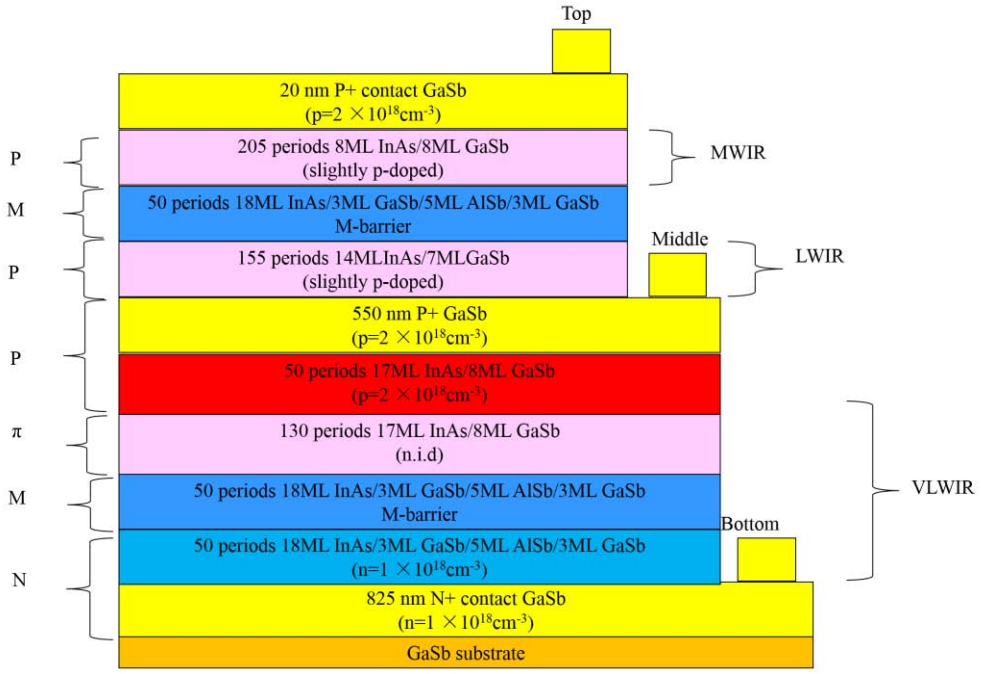

Fig.1. Hetero-structure schematic of the three color PMP/P-π-M-N detector.

InAs/GaSb Type II superlattice Photodetectors with a 12 μm cutoff wavelength

Jiajia Xu[1], Fangfang Wang[1], Chuan Jin[1,2], Yi Zhou[1], ZhichengXu[1], Jianxin Chen[1]*, Ruijun Ding[1], Li He[1]

1 Key Laboratory of Infrared Imaging Material and Detectors, Shanghai Institute of Technical Physics, Chinese Academy of Sciences, 200083 Shanghai, China

2 Graduate School of the University of Chinese Academy of Sciences, 100049 Beijing, China

Long wavelength infrared photo detectors (LWIR) in the 8-12 μm atmospheric absorption window have numerous applications such as earth observation, weather forecast etc. Type-II InAs/GaSb Superlattices were introduced and proposed for infrared detection. This material system offers unique possibilities in bandgap engineering to increase carrier lifetimes, depress Auger recombination, decrease dark current and vary the absorption coefficient. In the past two decades, progress in modeling, growth technique and device processing lifted the performances of superlattice infrared detectors to make them a competitor for high sensitivity and high uniformity imaging device in the LWIR regime.

In this abstract, we reported the growth and fabrication of a type-II InAs/GaSb superlattice infrared focal plane array detector with a 12 μm cutoff wavelength. The superlattice material was grown on GaSb substrate using molecular beam eptiaxy technology. The superlattic structure consisted of 300 periods of 16ML(InAs)/7ML(GaSb) for long wave infrared detection. The focal plane array had a pixel size of 27μm×27 μm. The device fabrication process consisted of mesa etching, side-wall passivation, metallization and flip-chip hybridization with readout CMOS circuits. At 77 K, the average peak detectivity of array pixels was 2.77×10^{10} cmHz$^{1/2}$W^{-1} with NEDT of 29mK .

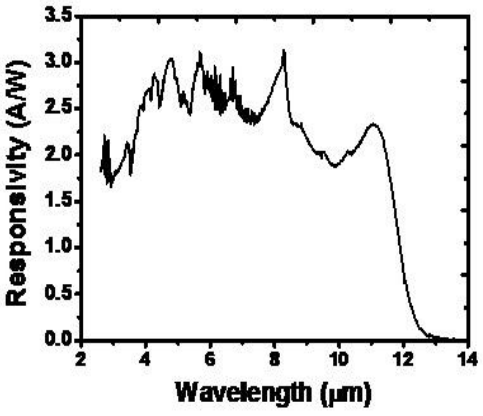

Fig.1 Spectral response of IRFPAs detector at 77 K

*corresponding author: jianxinchen@mail.sitp.ac.cn

Mid-wavelength Interband Cascade Infrared Photodetectors on InAs substrate

Yi Zhou[1], Jianxin Chen[1], Zhicheng Xu[1], Li He[1]

[1] *Key Laboratory of Infrared Imaging Material and Detectors, Shanghai Institute of Technical Physics, Chinese Academy of Sciences, 200083 Shanghai, China*

Infrared (IR) photo-detectors are typically operated at cryogenic temperatures to suppress the noise of the detectors arising from various mechanisms associated with the narrow band gap semiconductors. Cryogenic cooling assemblies are big burdens of the IR detection systems. There are considerable efforts to reduce the noises of the photo-detectors at elevated temperature to achieve the so called high operating temperature (HOT) detectors. Several approaches have been elaborated including Auger suppression, optical immersion, multiple PN junction structures, and barrier enhancement detector structure designs. More recently, interband cascade infrared photodetectors (ICIP) emerged as a new kind of infrared detectors that is very promising to operate at high temperature.

We will report our studies on mid-wavelength infrared interband cascade photodetectors grown on InAs substrates. We studied the transport properties of the photon-generated carriers in the interband cascade structures by comparing two different detectors, a single stage detector and a two-stage cascade detector. The two-stage device showed quantum efficiency around 19.8% at room temperature, clear optical response was measured even at a temperature of 323K. The two detectors showed similar Johnson-noise limited detectivity. The peak detectivity of the one- and two-stage devices was measured to be 2.15×10^{14} cm.Hz$^{1/2}$/W and 2.19×10^{14} cm.Hz$^{1/2}$/W at 80K, 1.21×10^{9}cm.Hz$^{1/2}$/W and 1.23×10^{9} cm.Hz$^{1/2}$/W at 300K, respectively. The 300 K background limited infrared performance (BLIP) operation temperature is estimated to be over 140 K.

We will also report the result of mid-wavelength ICIPs with more stages and optimized absorber thickness, and we will also compare the relationship of device performance and doping level in the absorber region.

References

1. Rui Q. Yang, ZhaobingTian, ZhihuaCai, et al, J. Appl. Phys, 107, 054514 (2010).
2. Zhao-Bing Tian and Sanjay Krishna, IEEE Journal of Quantum Electronics, Vol. 51, No. 4, (2015).
3. Z.-B. Tian, T. Schuler-Sandy, S.Krishna, Infrared Physics & Technology, 70, 44-47, (2015)
4. G. Chen, A. Haddadi, A-M.Hoang, et al, Optics Letters, 40, 1, (2015)

*corresponding author: jianxinchen@mail.sitp.ac.cn

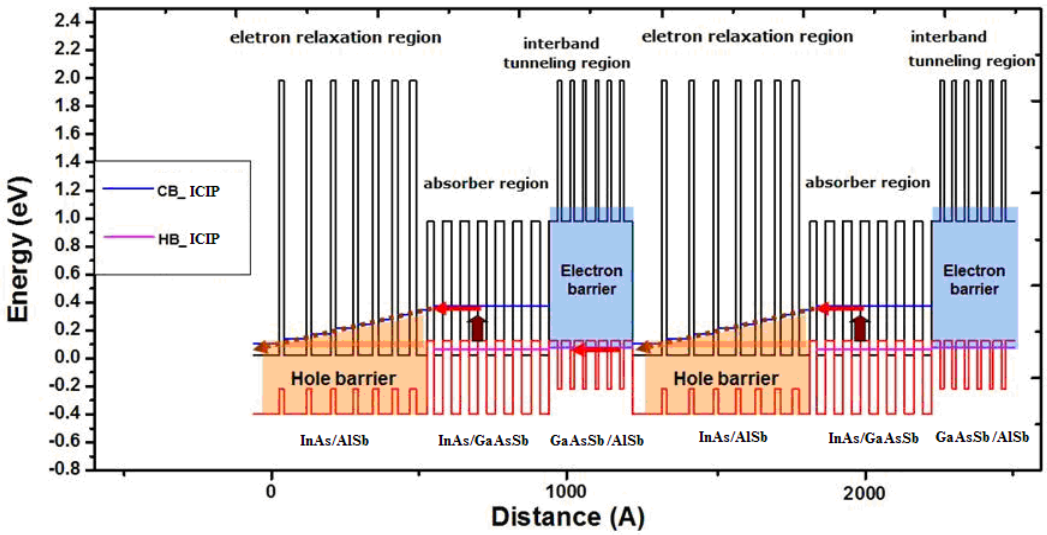

Fig.1. Band structure of designed two stage ICIP based on InAs substrate. (CB stands for conductive band and HB stands for hole band, respectively)

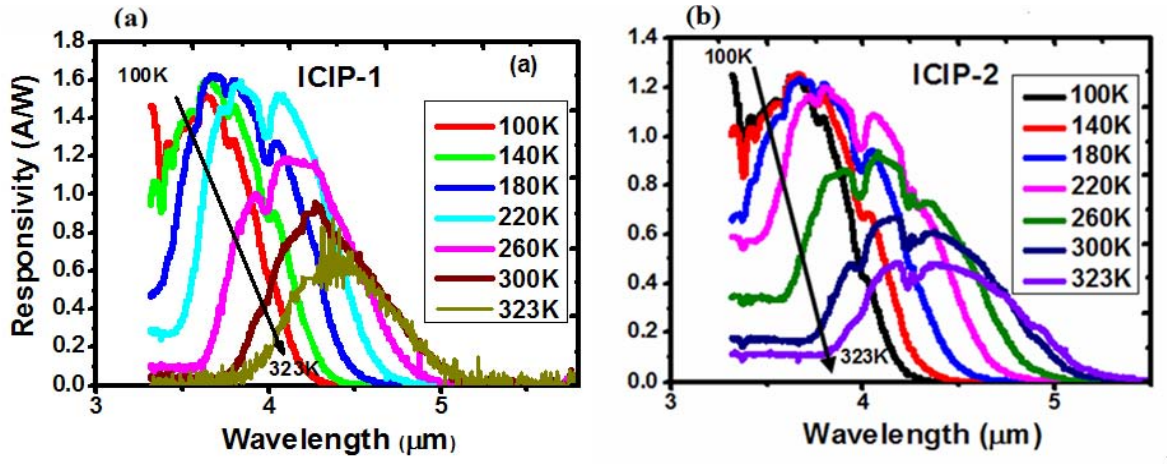

Fig.2. Measured optical responses of the one- (a) and two-stage (b) interband cascade photo detectors at a wide range of temperature.

Study of the characteristics of LPE p^+-on-n heterojunction LWIR photovoltaic detectors in Variable-area Diode Test Structures

Wang Xi[1,2*], Lin Chun[2], Wei Yanfeng[2], Zhu Mingxing[2]

1. University of Chinese Academy of Sciences, Beijing 100039, China

2. Key Laboratory of Infrared Imaging Materials and Detectors，Shanghai Institute of Technical Physics, Chinese Academy of Sciences, Shanghai 20083, China;

Abstract

The LPE in-situ growth p^+-on-n heterojunction LWIR photovoltaic detectors was made in our group. Resistance-voltage (R-V) curves were measured in the 80K. And variable area structure was made in order to access the quality of the material and surface passivation in HgCdTe device technology. Through data analysis and curves fitting of the relationship between zero-bias resistance-area product (R_0A) of a diode and its perimeter-to-area ratio (p/A), the contributions of bulk and surface effects could be distinguished, and the minority carrier diffusion length could be calculated. It is found that the surface current of these device is nearly comparable with the bulk current.

Key words: in-situ growth p^+-on-n heterojunction, surface current, Variable-area

1．Introduction

Long-wavelength infrared (LWIR) focal plane array (FPA) detection is the cutting-edge technique for third-generation infrared remote sensing. However, dark current, which are very sensitive to the growth of small Cd composition HgCdTe, strongly limits the performance of long wavelength HgCdTe photodiode arrays in FPAs.[1,2]

In this paper, variable-area LWIR HgCdTe photodiodes based on liquid phase epitaxy (LPE) in-situ growth of p^+-on-n technology have been fabricated and characterized. The measured zero-bias resistance-area product ($1/R_0A$) with perimeter-to-area (p/A) dependence was analyzed for the surface-related leakage mechanisms.

2．Model

In order to analysis the Variable-area diodes results, we follow the model of Vishnu Gopal. The basic assumptions of the model are broadly the same as stated in same type papers.[3]

The photodiode dynamic resistance at zero bias voltage is denoted by R_0 and is related to the current-voltage characteristic by

$$R_0 = (\frac{dI}{dV})^{-1}_{V=0} \qquad (1)$$

The junction area is A, then the current density J=I/A, so

$$R_0\mathrm{A} = (\frac{dJ}{dV})^{-1}_{V=0} \qquad (2)$$

In a perfectly ideal diode the current contributing to the impedance of the diode consists of thermally generated minority carriers diffusing to the junction. The current density J could be written as

$$\mathrm{J} = \frac{qD_p p_{n0}}{L_p}\left(exp\frac{qV}{kT} - 1\right) \qquad (3)$$

Then, it could be seen that

$$\frac{1}{R_{D0}A_j} = \frac{q\mu_p p_{n0}}{L_p}$$

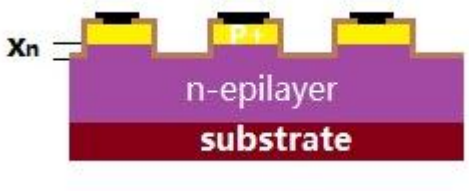

Figure 1.Cross section of an ideal mesa etched variable-area diode array with deep mesa etching, $A_s = \left[d + 2\left(L_p - x_n\right)\right]^2 + 4x_n d - d^2$

For a non-ideal surface/interface an excess current known as the surface leakage current is generated due to the leakage of minority carriers to the surface. This leakage of minority carrier current to the surface can be modelled by physically imagining a shunt resistance R_s, in parallel to the ideal diode impedance R_{D0},

$$\frac{1}{R_0} = \frac{1}{R_{D0}} + \frac{1}{R_s}$$

Then,

$$\frac{1}{R_0 A} = \frac{\left(L_p - x_n\right)^2}{4}\frac{1}{R_s A_s}\left(\frac{p}{A}\right)^2 + \frac{L_n}{R_s A_s}\left(\frac{p}{A}\right) + \frac{1}{R_{D0}A_j}$$

3. Experiment

The LWIR photovoltaic diode was made by deep mesa etching of the LPE in-situ growth p^+-on-n heterojunction. The n-type $Hg_{1-x}Cd_xTe$ ($x \approx 0.2236$) layers doped with In, with the doping density of $N_d = 1.5\times10^{14}cm^{-3}$, were grown on CdZnTe substrates by the liquid phase epitaxial (LPE) method, and then p-type $Hg_{1-x}Cd_xTe$(with larger x) layers doped with As, with the doping density of $N_a = 2.3\times10^{17}cm^3$.After etching the passivation was made by CdTe/ZnS, the thickness of these were 3000Å/3000 Å.

4. Results and Discussions

4.1 R-V curve

Figure 2 shows the resistance-voltage curves for different areas. There are some differences between the diode resistances in the relative large forward voltage, which is the product of the series resistance and contact resistance because of the larger contact resistance between the p-type HgCdTe and metal.

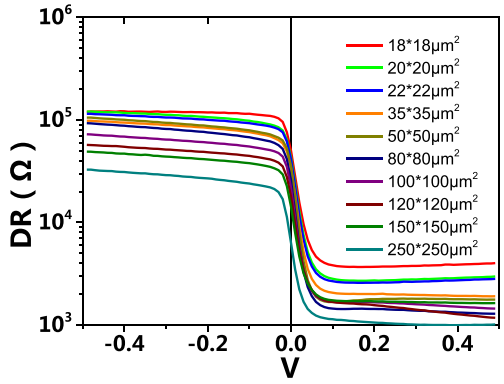

Figure 2. the R-V curves for different area diodes

4.2 Curves fitting

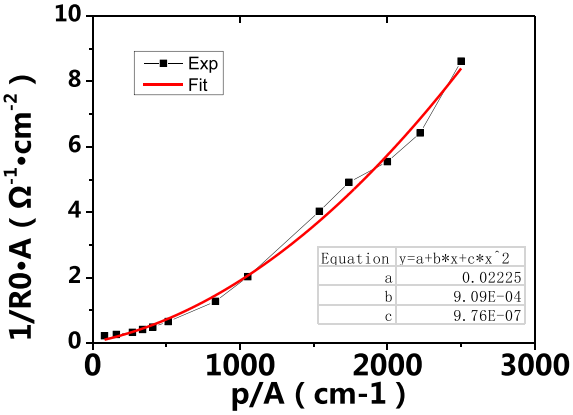

Figure 3. $1/R_0A$ value as a function of perimeter-to-area ratio of respective diodes

Experimental $1/R_0A$ value as a function of perimeter-to-area ratio of respective diodes was shown in Figure 3. In the diodes, we consider the x_n is 1 μm, so we can calculate the values of $R_{D0}A_j$=45Ωcm^2, R_sA_s=5Ωcm^2 and L_n=45μm.

5. Conclusion

This paper has presented the characteristics of LPE in-situ growth of p^+-on-n LWIR HgCdTe diodes in the variable area test structures. So we know the in-situ growth of p^+-on-n LWIR HgCdTe PV detectors have bad surface- epilayer conditions, or the poor passivation quality.

Reference:

[1] T. Nguyen, C. A. Musca, J. M. Dell, J. Antoszewski and L. Faraone, Dark Currents in Long Wavelength Infrared HgCdTe Gated Photodiodes. J. Electron. Mater. 33, 621-629 (2004).

[2] P. Boieriu, C. H. Grein, S. Velicu, J. Garland, C. Fulk, S. Sivananthan, A. Stoltz, L. Bubulac, and J. H. Dinan, Effects of hydrogen on majority carrier transport and minority carrier lifetimes in long wavelength infrared HgCdTe on Si. Appl. Phys. Lett. 88, 062106 (2006).

[3] Vishnu Gopal, Variable-area diode data analysis of surface and bulk effects in HgCdTe photodetector arrays, Semicond. Sci. Technol. 9 (1994) 2267-2271. Printed in the UK

*corresponding author: wangxi88@foxmail.com

InGaAs/GaAsSb superlattice photodiodes with P-type compensation-doped absorption regions

Chuan Jin,[1,2] Qingqing Xu,[1] Chengzhang Yu,[1] Jianxin Chen[1*]

[1] *of Infrared Imaging Materials and Detector, Shanghai Institute of Technical Physics, Chinese Academy of Sciences, Shanghai, 200083, China*

[2] *University of Chinese Academy of Sciences, Beijing 100049, China*

InGaAs/GaAsSb Type II superlattices (SLs) are very attractive in short-wavelength infrared (SWIR) and mid-wavelength infrared (MWIR) photodetectors (PD) and light emitting devices [1]. By changing the layer thickness and tuning the strain, the cutoff or the emission wavelength of the Type II SLs can span from 2μm to 4μm. Comparing with HgCdTe and high Indium composition InGaAs photodiodes, the Type II SLs have the advantages of lattice-matched to substrate, flexible in wavelength tuning, cooling free at room temperate, etc. Therefore Type II SLs are promising material systems for extended wavelength SWIR detection, which has been widely applied in chemical sensing, gas monitoring, infrared imaging and and so on.

While, the quantum efficiency (QE) of Type II SL photodetector at a reverse bias close to zero reported in the literature is only about 10-30% [2]. There are reports shows that the QE can be increased to about 20% and 40% with reverse bias of -0.5V and -0.7V, respectively, however, the dark current densities are also, respectively, increased to 1.66×10^{-3}A/cm^2 and 3.94×10^{-3}A/cm^2 [4]. QE increases with reverse bias also indicate a small diffusion length in the material structures.

In this paper, effects of p-type compensation doping are studied on QE and dark currents of SL Short wavelength infrared photodiodes. Since the diffusion length of electrons is much longer than that of the holes, a p-type absorption layer is desired to achieve high QE. In this paper, Beryllium (Be) doping is adopted in InGaAs/GaAsSb Type II SLs photodiodes to convert the n-type absorption layer to a p-type one. A high QE of 61.4% can be obtained at a doping density of 7.5×10^{15}cm^3 and the dark current density is only 5.4×10^{-4}A/cm^2 at Room temperature with a reverse bias of -0.05V. Furthermore, the quantum efficiency does not change with the increase of reverse bias indicating the diffusion length is longer than the thickness of the absorption region.

References

1. S.Maëro,L.A.D.Vaulchier,Y.Guldner, C.Deutsch, M.Krall, T.Zederbauer, G.Strasser, K.Unterrainer, Applied Physics Letters, 103(2013)051116 - 051116-051114
2. Y. IGUCHI, H. MORI, M. MIGITA, Y. NAGAI, H. INADA, K. FUJII, T. ISHIZUKA and K. AKITA, SEI TECHNICAL REVIEW, 2013, 103-106.
3. G. F. Fulop, Proceedings of Spie, 2015, 9451, 945106-945106-945112.

*corresponding author: jianxinchen@mail.sitp.ac.cn

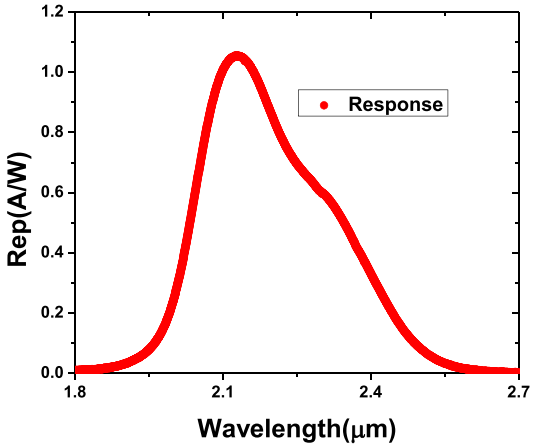

Fig.1 Normal-incidence photoresponse of the device

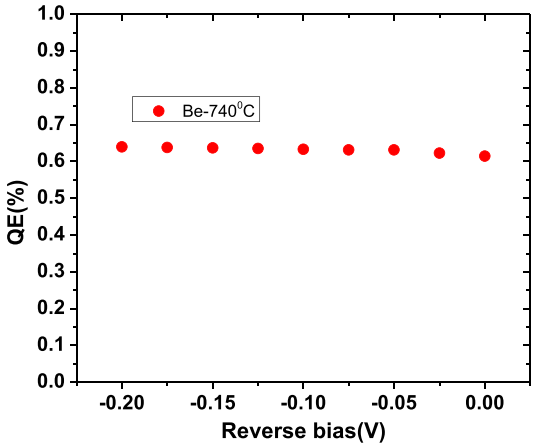

Fig.2 Measured quantum efficiency at different reverse bias

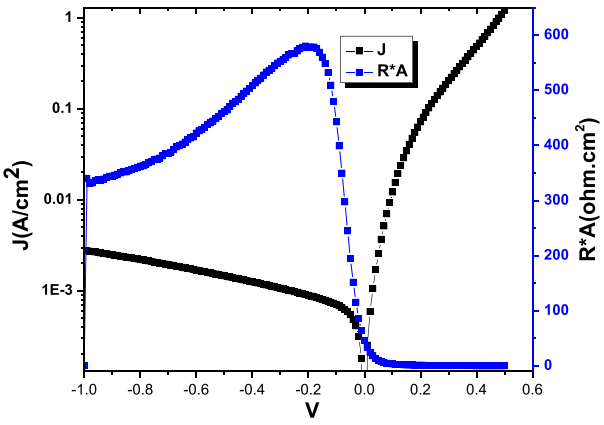

Fig.3 Dark current density and dynamic resistance-area product (R*A) versus voltage measured at room temperature

Molecular Beam Epitaxial (MBE) Growth of 3μm Laser using InGaAsSb/AlInAsSb Quantum Well Structure

Chunte Lu, Ron Kaspi, Tim Newell, Chi Yang, Sun Luong, and Don Gianardi

Air Force Research Laboratory, Directed Energy Directorate
Albuquerque, New Mexico, 87117 USA

We report the experimental results of growth and characterization of InGaAsSb/AlInAsSb quantum well laser structure. The epitaxial structure was grown using molecular beam epitaxy system on GaSb substrate and characterized using a 2μm pump source. We observed 3.1μm laser emission at 200K and 2.98μm laser emission near 100K.

The epitaxial growth of the 3 x QWs laser structures was conducted using MBE. The alloy composition and thickness of the laser structure are shown in Figure 1. The entire structure was grown using the digital alloy growth method [1]. The laser heterostructure was designed to have a 566nm-thick digitally grown quaternary Al0.5In0.5AsSb waveguide inserted in between 1.7 μm thick top and bottom digitally grown Al0.9Ga0.10As0.07Sb0.93 clad layers. The laser structure was completed with three 10nm-thick compressively strained In0.6Ga0.4AsSb quantum wells at the center of the waveguide. Figure 2 shows the (Ω-2θ) plot of laser sample from X-ray diffractometer.

3mm long laser sample was mounted on gold coated copper plate and tested using a 2μm pump laser. We observed strong photoluminescence with spectrum peaked around 3.4μm when operated near room temperature; however the sample did not lase. Lasing was achieved when cooling the sample down to 200K and below. We obtained 2.98μm wavelength laser emission at 100K and 3.1μm wavelength laser emission at 200K. The respective spectra are shown in Figure 3.

In summary, we present the experimental results of growth and characterization of InGaAsSb/AlInAsSb quantum well laser structure. We conducted the laser growth using a MBE system on GaSb substrate and characterized the sample optically via a 2μm laser. The sample emitted 3.1μm wavelength at 200K and 2.98μm wavelength at 100K. We plan to conduct similar experiment with the diode laser structures.

References

1. Kaspi, Ron, and Giovanni P. Donati. "Digital alloy growth in mixed As/Sb heterostructures." Journal of crystal growth 251.1 (2003): 515-520.

*corresponding author: luchunte24@yahoo.com

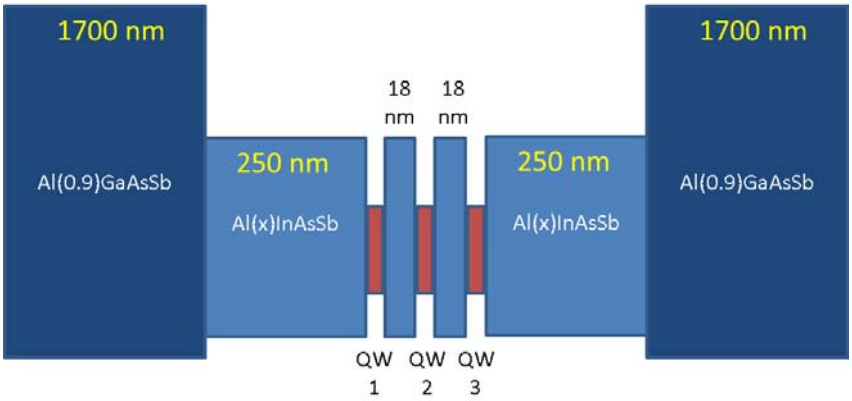

Figure 1. Laser structure using AlInAsSb quaternary barrier.

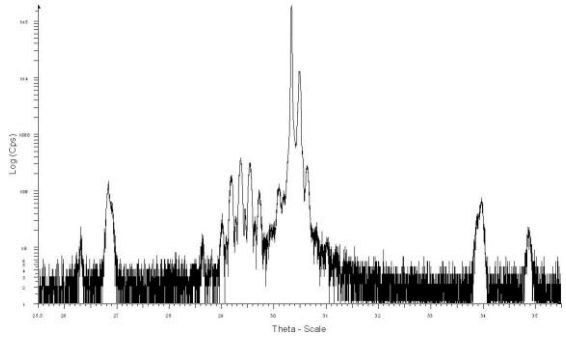

Figure 2. (Ω-2θ) X-ray diffractometer plot of laser structure.

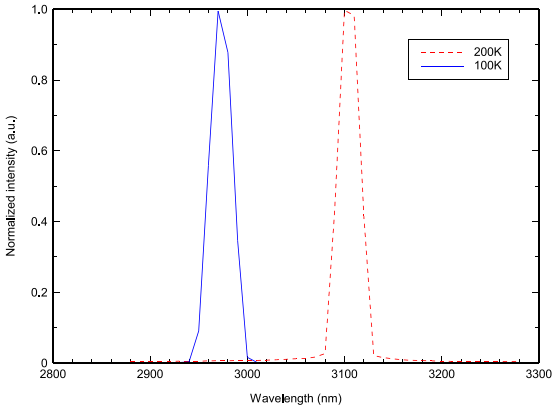

Figure 3.Lasing spectra of the laser sample. Measured lasing wavelength 2.98μm at 100K and 3.1μm at 200K.

Surface morphology study of ZnTe crystals grown from Te solution

Rui Yang[1,2]*, Yasir Zaman[2], Chensheng Wang[1], Zhijie Zhang[1], Wanqi Jie[2]

[1] *Huazhong Institute of Electro-Optics —Wuhan National Laboratory for Optoelectronics, Wuhan 430223, China*

[2] *State Key Laboratory of Solidification Processing, Northwestern Polytechnical University, Xi'an 710072, China*

ZnTe is found to be a promising material used for the generation and detection of terahertz (THz) wave [1]. ZnTe crystals grown from Te solution have much better quality than that in melt growth, since the growth temperature could be significantly low. However, Te inclusions, which may affect the optical qualities greatly, is a main defect that can be easily introduced into ZnTe when grown using Te-solvent method [2]. Since the formation of Te inclusions is generally attributed to the instability of the growth interface, thus, morphological studies of the surface of ZnTe crystals grown from Te solution are conducted by us.

ZnTe crystals with various surface morphology are revealed. Layer by layer growth mechanism was found to be the main growth mechanism when grow ZnTe from Te solution, attributed to the great growth anisotropic feature of ZnTe crystal. The cooling rate plays a very important role in determine the crystal surface morphology, crystals formed under smaller cooling rate have smooth surface. However, larger cooling rate leads to the generation of more layers on the crystal surface, Te inclusions can easily be trapped between these layers. Fast cooling rate even may lead to the formation of skeletal ZnTe crystals. In addition, corner effect [3] (with a concentration difference between the center and edges of a face) may also cause the instability of the crystal surface by produce more layers on the edges and corners of a crystal. And the corner effect is found more obvious on ZnTe crystals with larger size.

References

1. Z. Ollmann, J.A. Fülöp, J. Hebling, and G. Almási, Design of a high-energy terahertz pulse source based on ZnTe contact grating, Opt. Commun., 315(6), 159-163, 2014.
2. R. Yang, W. Jie, H. Liu, Growth of ZnTe single crystals from Te solution by vertical Bridgman method with ACRT, J. Cryst. Growth, 400, 27–33, 2014.
3. I. Sunagawa, Crystals: Growth, Morphology and Perfection. Cambridge: Cambridge University press, 2005: 71.

*corresponding author: yangrui0105@163.com

Grading strategy of the buffers for high indium InGaAs photodetectors

B. Du, Y. Gu, Y. G. Zhang*, X. Y. Chen, S. P. Xi, Y. J. Ma, W. Y. Ji, Y. H. Shi

State Key Laboratory of Functional Materials for Informatics, Shanghai Institute of Microsystem and Information Technology, Chinese Academy of Sciences, Shanghai, China

Wavelength extended InGaAs photodetector with high indium content plays an important role in the short-wave infrared (SWIR) band detection. To restrain the threading dislocation from the mismatch between substrate and high In content InGaAs, various buffer structures are investigated. In our previous research, fixed-composition [1], continuously graded and step-graded buffer [2] have been used and analyzed. Generally speaking, if the mismatch degree between substrate and epitaxial layer is relatively larger, using fixed-composition buffer could realize a higher strain relaxation degree and improve the structural and optical properties than using continuously graded buffer because of the faster lattice relaxation process. On the other hand, when the mismatch degree is relatively smaller, in comparison to the step-graded buffer, adopting continuously graded buffer could get full relaxation, superior optical properties and lower dark current. In the growth of wavelength extended photodetector, we always choose the less mismatched substrate and continuously graded buffer to achieve better device properties. In consideration of using continuously graded buffer is more conducive to lead to the full relaxation [2] while adopting the step-graded buffer can bend the threading dislocation in the inactive region more effectively [3], the combination of step with continuously graded buffer, is likely to possess the advantages of both schemes.

To investigate the effects of so called step-continuously graded buffer, a one-step buffer followed by a composition continuously graded buffer, has been adopted, as shown in Fig. 1. According to the mechanism discussions, in the initial part of the step-continuously graded buffer, a large lattice mismatch exists due to the high initial In content, which could promote the lattice relaxation in the one-step buffer by generating threading dislocations. The step-continuously graded buffer also owns a lower lattice-mismatch grading rate in the later continuously graded buffer, which could reduce the glide of threading dislocations and improve the lattice quality of the top buffer and the InGaAs absorption layer.

Comprehensive comparison to the simplex continuously graded buffer structure was carried out with the same thickness. Two samples were grown on InP at normal growth temperatures. The results shown in Fig. 2 indicate that using step-continuously graded buffer could confine the threading dislocation in inactive region more effectively.

References

1. X. Y. Chen, Y. Gu, Y. G. Zhang, et al. , J. Cryst. Growth, 425, 346(2015).
2. S. P. Xi, Y. Gu, Y. G. Zhang, et al., J .Cryst. Growth. 425, 337 (2015).
3. M. Haeberlen, D. Zhu, C. McAleese, et al., Phys. Status Solidi B. 247, 1753 (2010).

*corresponding author: ygzhang@mail.sim.ac.cn

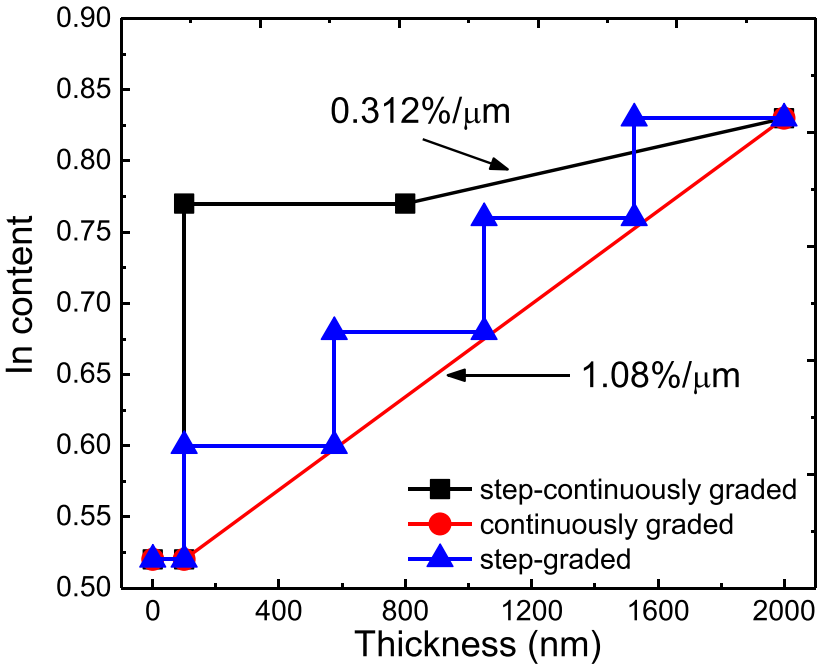

Fig.1. The In content along with the growth thickness.

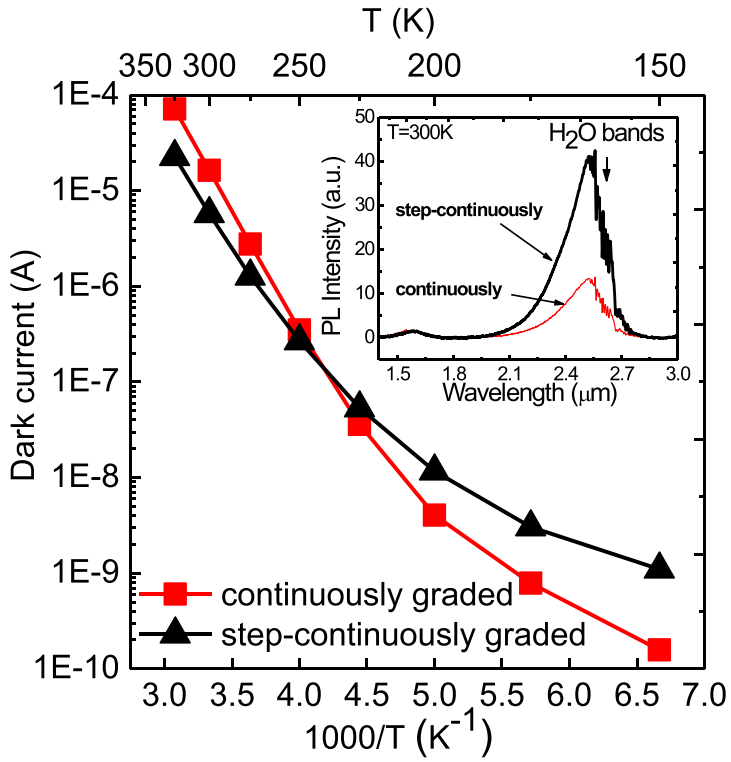

Fig.2. Temperature-dependent dark current at 50 mV reverse voltage of high indium InGaAs detector structures with continuously and step-continuously graded buffers. The insert shows the PL spectra at room temperature.

Influences of Chemical Etching on Nanosized Patterns on the Surface of HgCdTe Epilayers

Changzhi Shi*, Chun Lin, Yanfeng Wei

[1] *Shanghai Institute of Technical Physics, 500 Yutian Road, Shanghai, China 200083*

The surface treatment of HgCdTe epilayers has a rather significant effect on the electrical and optoelectronic characteristics of the material and the device performance. The etching techniques, such as ion beam milling, inductively coupled plasma and bromide solution etching, have been investigated for the surface treatment of HgCdTe [1-3]. Recently, the nano-scale pattern formation on the surface of HgCdTe produced by Ag ion bombardment was characterized by Smirnov, et al[4]. However, the evolution of nanosized patterns on the surface of HgCdTe induced by chemical etching has not been characterized and studied. Here, the HgCdTe epilayers were grown by LPE to investigate the influences of the bromine-based wet etching on their nano-scale surface patterns.

The virgin surface morphology of the LPE HgCdTe epilayer was characterized by AFM as shown in Fig.1. It can be seen from Fig.1 that an array of nanosized islands (diameter~80nm, height~5nm) exists on the material. Then, the surface of HgCdTe samples was etched in the bromine ethanol solution at different flow rates ranging from 0~300 rpm. Figure 2 demonstrates the formation of nanosized grains on the surface. The heights and diameters of these grains increase with improving the flow rate of the bromine etchant, but fall down when the flow rate is raised to 300 rpm, which is likely due to the rapid removal of the reaction product at a relatively high flow rate of etchant.

Although the surface roughness can be improved with increasing the flow rate of the etchant to a certain value, the deviation of the etch rate increases drastically with elevating flow rate (shown in Fig.3). It is notable that the high deviation value could degrade the uniformity and the flatness of HgCdTe epilayers, thereby influencing the device performance.

References

1. X.T. Chen, H. Qiao, X.Y. Liu, et al. Electrical properties of Hg1-xCdxTe by different etching techniques, Infrared Physics & Technology, Vol. 73, pp. 251-254, 2015.
2. A. Causier, I. Gerard, M. Bouttemy, et al. Wet Etching of HgCdTe in Aqueous Bromine Solutions: a Quantitative Chemical Approach, Journal of Electronic Materials, Vol. 40, No. 8, pp. 1823-1829, 2011.
3. R. Kiran, R. Sporken, T. N. Casselman, et al. Effect of atmosphere on n-type Hg(1-x)Cd(x)Te surface after different wet etching treatments: An electrical and structural study, Journal of Electronic Materials, Vol. 37, No. 9, pp. 1471-1479, 2008.
4. A. B. Smirnov, A. I. Gudymenko, V. P. Kladko, et al. Nano-scale pattern formation on the surface of HgCdTe produced by ion bombardment, Phys. Status Solidi C, Vol. 12, No. 8, pp. 1175-1178, 2015.

*corresponding author: shichangzhi@mail.sitp.ac.cn

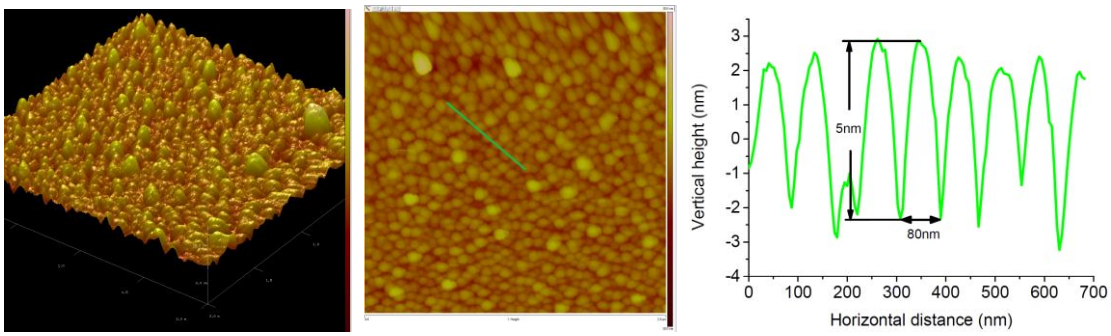

Fig.1. AFM images and surface profile of HgCdTe without chemical etching.

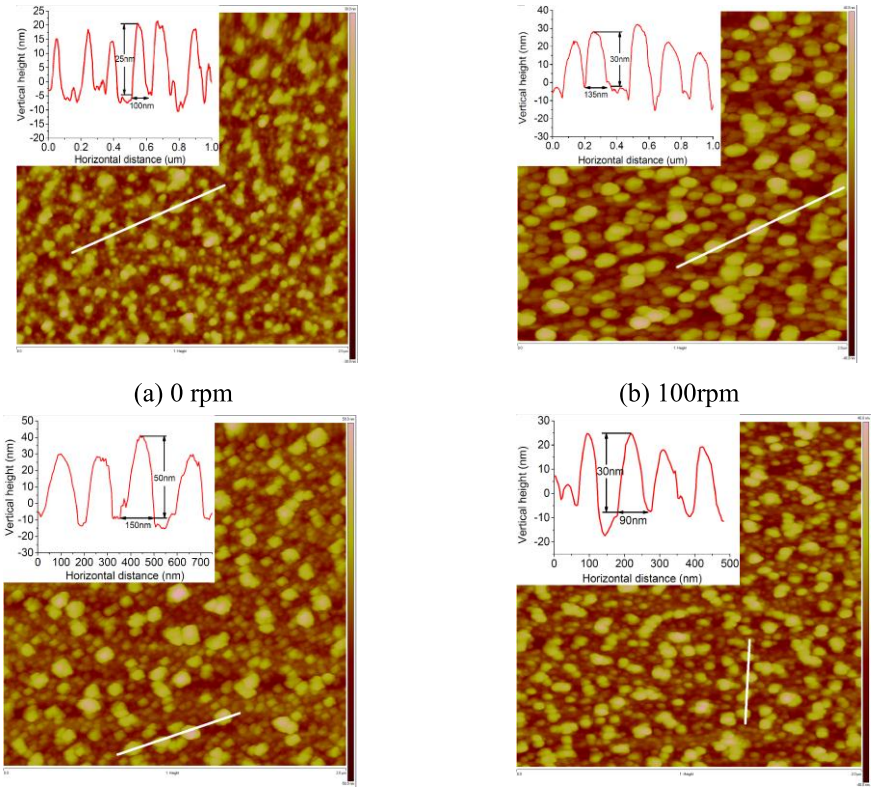

(a) 0 rpm (b) 100rpm

(c) 150rpm (d) 300rpm

Fig.2. AFM images and surface profiles of HgCdTe epilayers etched by bromine ethanol solution at flow rates of (a) 0rpm, (b) 100rpm, (c) 150rpm and (d) 300rpm.

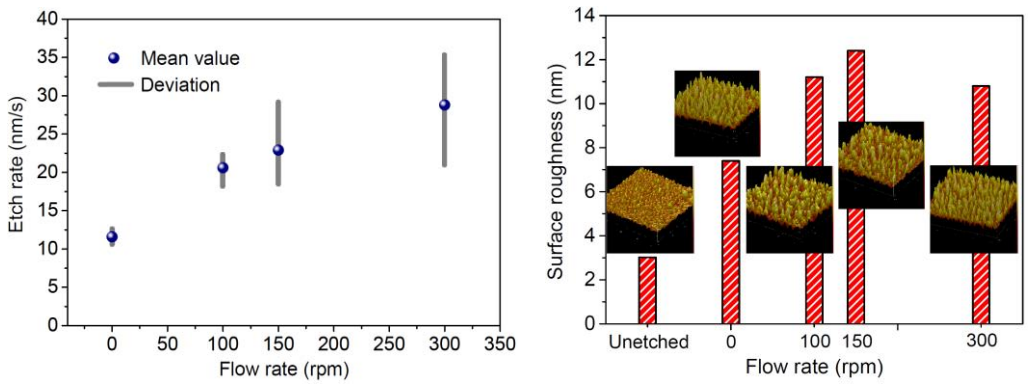

(a) Etch rate (b) Surface roughness

Fig.3. Etch rates and surface roughnesses versus the flow rate of bromine ethanol solution.

The junction profile of LW HgCdTe conversed through ion beam milling

Zhou Songmin[1,*], Weng Bin[2], Lin Chun[3], Li Hao[4], Wang Xi[5], Wei Yanfeng[6], Ye Zhenhua[7], Ding Ruijun[8] and He Li[9].

[1]*Key laboratory of Infrared Imaging Material and Detectors, Shanghai Institute of Technical Physics, Chinese Academy of Sciences, Shanghai 200083, P. R. China;*

(All authors have the same affiliation and mailing address)

Abstract: In this work, type conversion induced by ion beam milling(IBM) in LW HgCdTe is characterized. A serial of junctions were fabricated by IBM. There is a series of N-type pairs that distances are varied from 0μm to 20μm between every two junctions, which obtained by high resolution lithography. Current-voltage and Laser Beam Induced Current (LBIC) measurements are applied to determine the HgCdTe junction edge. The LBIC signal and current-voltage orrectification characteristic indicates the existence of a pn junction. The width of junctions that induced by IBM in intrinsic doped HgCdTe are measured. A significant horizontal expansion N-type region was observed. Moreover, the thickness of n-type that conversed by IBM was measured through differential hall measurement.

Introduction

The maturity of infrared (IR) technologies enables detectors to be used for varying applications such as in the security, science or space sector. At the present time, the most commonly used material for infrared detection is the HgCdTe semiconductor. Because of its wide tuning range of bandgap, high quantum efficiency, and high operating temperature, HgCdTe is the most preferred material to fabricate infrared focal plane array (IRFPA). [1]–[3] For HgCdTe, ion beam milling introduces damages that the Hg atoms diffuse into inner layer to form n type layer.[4][5] The junction profile and the electron concentration in the conversion layer that after IBM is very important in these processing. The appropriate width and distance of PN junction are critical to achieve the highest performance of photodiodes.

In this work, junctions that fabricated through different IBM and pre-annealing processes are investigated. There is 2 micrometer expansion in the junction that form by 2.5 minutes IBM, and without expansion after 2.5minutes annealing under 150-180℃. The thickness of the conversion layer is about 4.1μm. And the same results obtained in 5 minutes IBM with or without annealing, 15μm and 8.5μm are respectively.

Experimental detail

The V_{Hg}-doped, P-type $Hg_{1-x}Cd_xTe$ (x=0.230) layers were grown by liquid phase epitaxy on CdZnTe substrates. In view of the property of HgCdTe, a column of 50μm×50μm N-type pairs whose distances varied from 0μm to 20μm between every two junctions were fabricated by high resolution lithography and IBM as shows in the Fig.1. The IBM process was carried

*corresponding author: zhousm@mail.sitp.ac.cn

out at beam energy of 180-200eV with 40-50sccm argon flow rate at room temperature about 2.5 and 5 minutes. After the milling process, a ZnS film with a thickness of 100nm was evaporated on the device as a passivation layer. The distance increases from 0μm to 20μm between the two N-type regions of every pair. The pair of N-type regions is connective at first, as the distance increasing, they will isolate as N-P-N sandwich structure. Therefore the width resolution of this method could be as high as 0.5μm.The milling regions with gold contacts were fabricated for current-voltage characteristics. Two remote contacts on either side of the n-on-p junctions were also deposited with gold in preparation for LBIC measurements. Both LBIC and current-voltage measurement were carried out at liquid nitrogen temperature.

At the same time, differential hall measurements are used to investigate the thickness and electron concentration of the conversion layer.

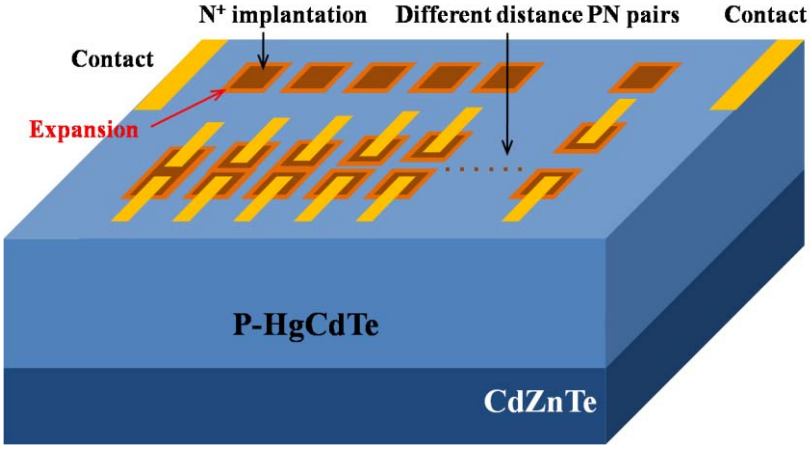

Fig.1. The schematic of the test structure

Results and Discussions

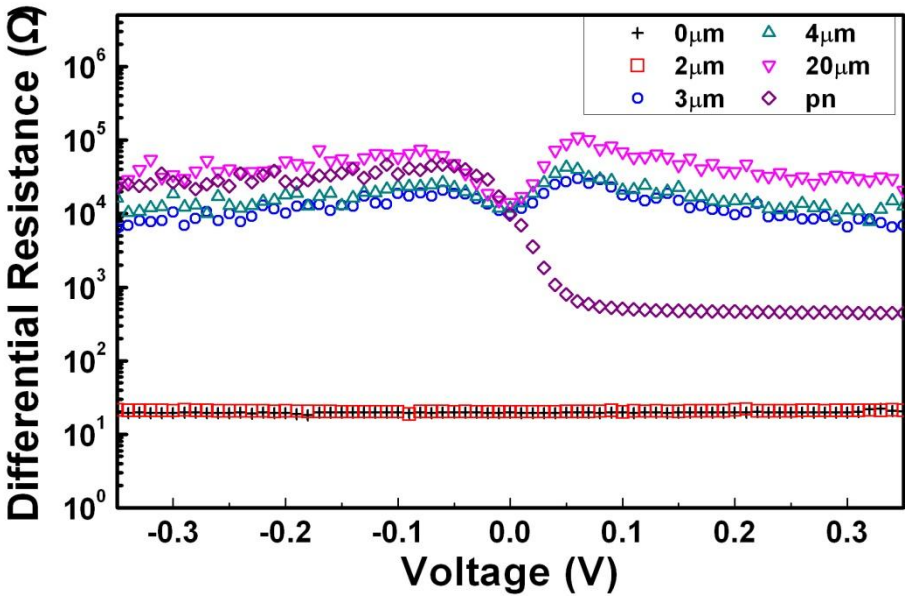

Fig.2. The differential resistance of N-type pairs and PN junctions conversed by IBM, the R-V curves of a PN junctions and N-type pairs of distances with 0μm,2μm,3μm,4μm,20μm.

The current-voltage characteristics of some N-type regions in the structure are measured and

showed in the Fig.2. In Fig.2, a junction current-voltage characteristic is measured, and they show the rectification characteristics. In the junction pairs current-voltage measurement, both results of junction pairs with distance of 0μm and 2μm in the Fig.2 indicate ohmic-contact. It can infer that the N-type pair is connective. While the distances are not less than 3μm, the results obviously indicate that two PN junctions of the pairs are back-to-back, so their N-type regions are isolated. So, it can easily infer that the N-type region is expanded less than 3μm.

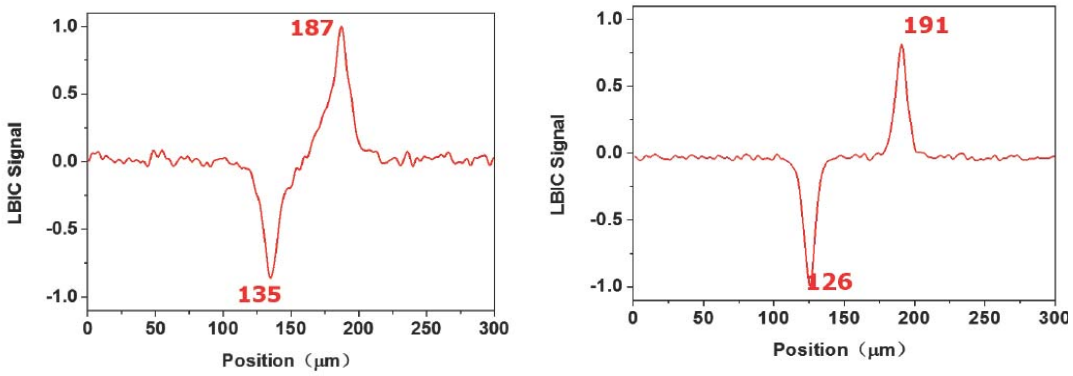

Fig.3. N-type regions are measured by LBIC with different IBM times, (a) 2.5 minutes, (b) 5 minutes.

The LBIC signal of a pixel row whose N-type regions size is designed as 50μm is illustrated in Fig.1. The LBIC signal showed in the Fig.3 is the very strong, a pair of signal peak and valley correspond to the opposite edges of N-type region. The N-type region size can be calculated from signal, it is equal to the peak-to-peak distance on the typical junction LBIC signal. The calculated size of N-type region is showed in Fig.3. Therefore, we can infer that the actual size of 2.5 minutes IBM N-type region is 52μm. And it also can infer that the actual size of 5 minutes IBM N-type region is 65μm.

Table.1 shows the results of junctions with or without annealing during 150-180℃ about 2.5 minutes. It can be found that junctions formed by IBM do not expand when anneal 2.5 minutes. And junction widths are seriously related to IBM times. The width of junctions who IBM 2.5 minutes that expand 2μm, while those expand 15μm with 5 minutes. Moreover, differential hall measurements are used to characterize the thickness of the conversion layers showed in Fig.4. Table.1 shows the thickness of conversion layers with IBM 2.5 minutes and 5minutes are 4.1μm and 8.5μm respectively.

Table.1 junction width and conversion layer thickness of different IBM process.

IBM (min)	Annealing (min)	I-V measurements (μm)	LBIC (μm)	Differential hall measurements (μm)
2.5		52	52	4.1
2.5	2.5	52	52	
5		65	65	8.5
5	2.5	65	65	

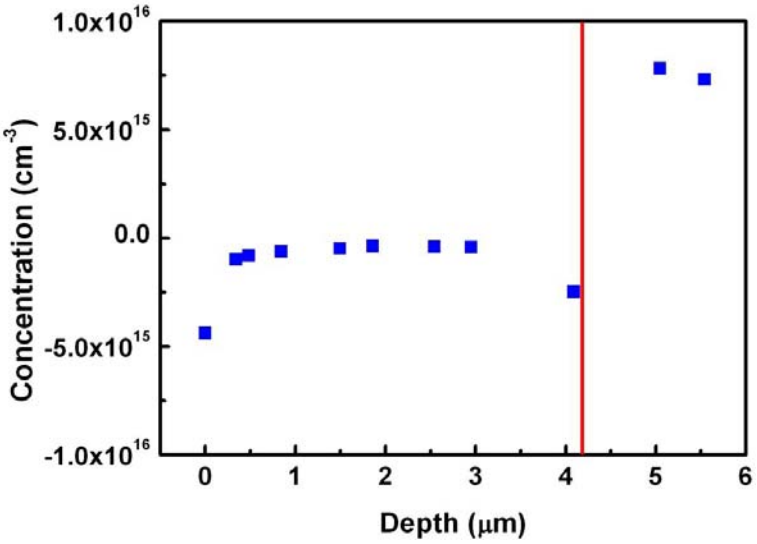

Fig.4. Type conversion of HgCdTe by IBM 2.5 minutes, the thickness of conversion layers is about 4.1μm.

Conclusion

In conclusion, we measured the junctions induced by IBM in LW HgCdTe through special designed structures for current-voltage and LBIC measurements. The results show that the junction IBM with 2.5 minutes and 5 minutes expanded 2μm and 15μm respectively. At the same time, differential hall measurements are used to characterize the thickness of the conversion layers. Table.1 shows the thickness of conversion layers with IBM 2.5 minutes and 5minutes are 4.1μm and 8.5μm respectively. These results are useful to the device design and FPA fabrications.

References

1. A. Rogalski, J. Antoszewski and L. Faraone, Third-generation infrared photodetector arrays, J. Appl. Phys., 105, 091101, 2009.
2. P. Norton, HgCdTe infrared detectors, Opto-Electron. Rev., 10, 159-174, 2002.
3. J. Wang, X. S. Chen, W. D. Hu, L. Wang, W. Lu, F. Q. Xu, J. Zhao,Y. L Shi, and R. B. Ji, “Amorphous HgCdTe infrared photoconductivedetector with high detectivity above 200 K,” Appl. Phys. Lett., 99, 113508-1–113508-3, 2011.
4. P. O. Leisher, J. J. Raftery, A. M. Kasten, et al. Etch damage and deposition repair of vertical-cavity surface-emitting lasers, Journal of Vacuum Science & Technology B Microelectronics & Nanometer Structures, 24(1):104-107, 2006.
5. M. Rahman, L. G. Deng, C. D. W. Wilkinson, et al. Studies of damage in low-power reactive-ion etching of III–V semiconductors, Journal of Applied Physics, 89(4):2096-2108, 2001.

Electroluminescence and photovoltaic effect in n-GaSb/InAs/p-GaSb heterostructure grown by MOVPE with a single quantum well

Igor Andreev;Maya Mikhailova;Leonid Danilov;Edward Ivanov;Gleb Konovalov;Roman Levin;Boris Pushnyi;Natalya Il'inskaya;Georgy Zegrya;Yury Yakovlev

Ioffe Institute Russian Fed yakovlev.iropto@mail.ioffe.ru

Keywords:

Electroluminescence Quantum well Photoeffect

Abstract:

InAs/GaSb quantum well (QW) structures attract a great attention due to their unique type II broken-gap alignment [1]. Such heterojunctions are important for design of QC lasers and MIR-superlattice photodiodes [2]. Previously, energy band structure, magnetotransport, magneto-optical and photoluminescence properties were studied in the GaSb/InAs/GaSb system with a single InAs QW grown by MBE [3]. However, electroluminescence and photovoltaic effect in such structures were not researched. Here we report on study of electroluminescent and photoelectrical properties of the n-GaSb/InAs/p-GaSb nanostructures with a single InAs QW grown by MOVPE. For the first time QW InAs/GaSb structure was grown by MOVPE in AIXTRON-200 system with a horizontal reactor on n-GaSb (100) substrates. The method of MOVPE grown was described in [4]. The growth temperature was T=600°C for the GaSb layers and T=500°C for the InAs active region. The structure under study consisted of n-GaSb:Te substrate (n=5-7·10^17 cm^−3), undoped InAs QW (d=8 nm) and p-GaSb:Si cap layer (d=1 μm, n=3-4·10^17 cm^−3). The samples for measurements were prepared by standard photolithography and wet etching as mesa-diodes with diameter of ~300 μm. The energy band diagram of the structure is shown in Fig. 1. The samples were driven by square shape current pulses with 50% duty cycle and frequency of 512 Hz. The EL spectra at 77 K for the different drive currents are given in Fig. 2. They represented strong asymmetric bands with a sharper high-energy edge and broad longwavelength shoulder. Theoretical calculation of energy band diagram and recombination rate was made in dependence on InAs QW width. The maximum at λ=3.1 μm (0.41 eV) originates from radiative recombination in InAs layer between electrons from ground energy state E1 in QW and heavy holes from continuum. There is a low intensity additional EL band with a maximum at λ=4.6 μm (0.269 eV) that corresponds to optical transition E1-HH2 involving the heavy holes localized near heterointerface in p-GaSb layer at forward bias. Up to 50 mA drive current the FWHM of the main EL band was about 15-20 meV. The I-V curves of the structure under study may be approximated by the exponential law J=J0·exp(eV/nkT). The value of non-ideality coefficient n changes from 9 to 10.4 at room temperature and up to 65.5 at 77 K that corresponds to tunneling mechanism of current flow in the structure. The photocurrent spectra were measured for n-GaSb/InAs/p-GaSb samples at 77 and 300 K. At the liquid nitrogen temperature they lied in the short wavelength region from 1 μm to 2.2 μm (see Fig. 3). We observed two maxima at 1.55 μm and at 1.1 μm. The depletion region in n-GaSb/n-InAs heterojunction is situated in n-GaSb. That is why the wavelength of the edge of the

photocurrent spectra (1.55 μm) corresponds to GaSb energy gap of 0.8 eV. The energy value of the maximum at 1.1 μm is approximately equal to sum of the energy gap values of InAs and GaSb in n-p heterojunction at thermodynamic equilibrium [5]. This work is supported in part by RFBR grants № 15-02-03151-A and № 16-08-01130-A.

High-speed quantum cascade laser at room temperature

Y.H. Zhou[1], S.Q. Zhai[1], J.Q. Liu[1*], F.Q. Liu[1], J.C. Zhang[1], N. Zhuo[1], L.J. Wang[1] and Z.G. Wang[1]

[1] *Key Laboratory of Semiconductor Materials Science, Institute of semiconductors, Chinese Academy of Sciences*

High-speed quantum cascade lasers (QCLs) are critically important elements in the infrared region for applications in free space optical (FSO) communication because of their small size, high bandwidth, high quantum efficiency, eye safety and significant atmospheric transparency advantage [1]. To use the QCLs in free space optical (FSO) communication widely, room-temperature, high-speed and high-power operation is still desired.

We fabricated high-speed QCLs emitting at 4.7 μm. 3-steps chemical etching technology [2] and a thick low-dielectric SiO_2 insulating layer were applied to reduce the parasitic capacitance. The room-temperature operated lasers show a flat frequency response up to 3 GHz and the CW output power is higher than 100 mW.

Fig. 1 shows the light output and bias voltage versus current of a 2 mm long laser. The laser is mounted epilayer side down on AlN heat sink with indium solder and works in CW mode at the temperature of 10 °C and 15 °C. As shown in Fig. 1, a high power of 115 mW can be gotten at 300 mA at 10 °C. The low threshold current densities of 1.35 kA/cm^2 (10°C) and 1.41 kA/cm^2 (15°C) are attractive in applications of low power-consumption. The differential series resistance and the slope efficiency of the laser are 7.5 Ω and 1.33 W/A, respectively.

Fig. 2 shows the measured rectified voltage at 10 °C as function of the modulation frequency [3]. It is clear that the curve remains relatively flat up to roughly 3 GHz, and the -3 dB cutoff frequency is about 1.7 GHz. With ignorable inductance, the capacitance of the laser can be calculated by $\frac{1}{2\pi RC} = f_{3dB}$, in which the measured differential series resistance R is 7.5 Ω, so the computed capacitance $C \cong 12.5$ pF. In the inset of Fig. 2, we present the CW lasing spectra of the QCLs at 10 °C and the injection current is 250 mA. Stable single-mode emission can be observed and the side-mode suppression ratio is better than 30 dB.

References

1. R. Martini, and E.A. Whittaker. 'Quantum Cascade Laser-Based Free Space Optical Communications', *Journal of Optical and Fiber Communications Reports*, **2**, (4), pp. 279-292, 2005.
2. P. Liang, F.Q. Liu, J.C. Zhang, F.L. Yan, Y. Hu, L.J. Wang, J.Q. Liu and Z.G. Wang. Patent No. CN201510329218.6.
3. H.C. Liu, J. Li, M. Buchanan, and Z.R. Wasilewski. 'High-Frequency Quantum-Well Infrared Photodetectors Measured by Microwave-Rectification Technique', *IEEE J. Quantum Electron.,* **32**, (6), pp. 1024-1028, 1996.

*corresponding author: jqliu@semi.ac.cn

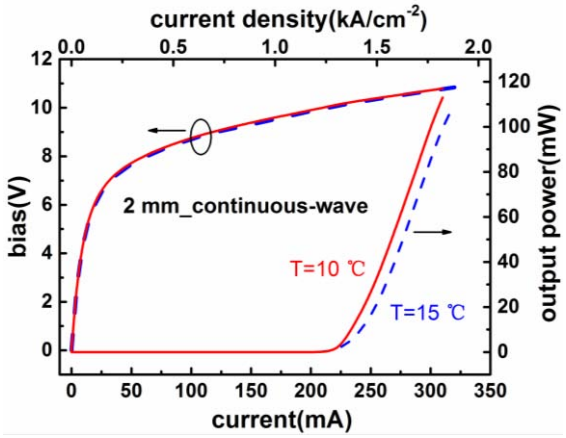

Fig.1. Typical CW bias-to-current and light output-to-current characteristics of a QCL tested at 10°C and 15°C.

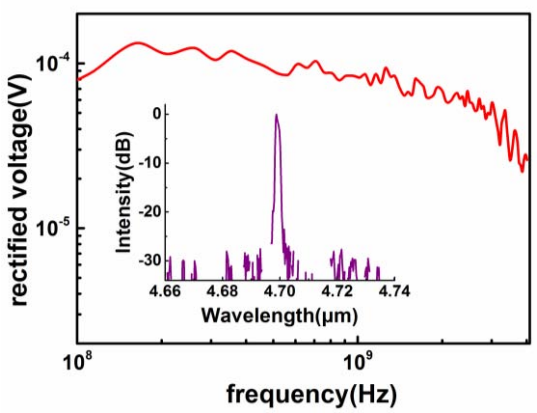

Fig.2. Measured rectified voltage at 10°C for the QCL as function of the modulation frequency. (Inset) CW emission spectra of the QCL at 10°C.

The design of interband cascade laser's active region towards polarization independent mid infrared emission

M. Motyka[1], M. Dyksik[1], K. Ryczko[1], R. Weih[2], M. Dallner[2], M. Kamp[2], G. Sęk[1], J. Misiewicz[1]

[1]*Laboratory for Optical Spectroscopy of Nanostructures, Department of Experimental Physics, Faculty of Fundamental Problems of Technology, Wrocław University of Technology, Wybrzeże Wyspiańskiego 27, 50-370 Wrocław, Poland*

[2]*Technische Physik, University of Würzburg & Wilhelm Conrad Röntgen Research Center for Complex Material Systems, Am Hubland, D−97074 Würzburg, Germany*

Interband cascade lasers (ICLs) have already been proven as a promising mid-infrared (MIR) source desirable for many applications. Their potential originates mostly from unique operational characteristics as, e.g., single mode, continuous-wave and high power operation at elevated temperatures in the range from below 3 to about 6 μm [1,2], broad spectral tunability [3], and low threshold currents and hence small electrical power consumption [4] when compared to the main competitor which are quantum cascade lasers.

The study has been focused on maximizing the optical transition oscillator strength (OS) via tailoring the electronic structure, the related strain and wave function engineering, as OS is the most critical parameter of the type II system, which can allow for compensating the intrinsic losses. We demonstrated that application of GaAsSb layers instead of GaInSb for confinement of holes switches the system to tensely strained with light-hole-like ground state transition allowing for the use of thicker layers in the active region and hence less sensitivity to growth inaccuracies. We have performed optical measurements on a set of type II QW samples utilizing a GaAsSb. The properly chosen widths of the layers, together with strain engineering provided by changing the arsenic content of the GaAsSb wells, allowed involving the light holes states into the fundamental optical transition. On one hand, this approach provided an additional degree of freedom for the emission wavelength transition oscillator strength tuning. Theoretical predictions of multiband kp theory have been experimentally verified by using photoluminescence and polarization dependent photoreflectance measurements. Obtained results open a pathway for practical realization of mid-infrared lasing devices with uncommon polarization properties including, for instance, polarization-independent mid infrared light emitters [5].

Rferences

1. J. Scheuermann et al., Appl. Phys. Lett. 106, 161103 (2015)
2. M. Dallner et al., Appl. Phys. Lett. 107, 181105 (2015)
3. Y. Jiang et al., J. Appl. Phys. 115, 113101 (2014)
4. I. Vurgaftman et al., Nat. Commun. 2, 585 (2011)
5. M. Motyka et al., Appl. Phys. Lett. 108, 101905 (2016)

Frequency tuning mechanisms in Mid-IR coupled-cavity quantum cascade lasers

K. Pierściński[1]*, D. Pierścińska[1], M. Płuska[1], P.Gutowski[1], P. Karbownik[1], A.Czerwiński[1] and M. Bugajski[1],

[1] *Institute of Electron Technology, Warsaw, Al. Lotników 32/46, 02-668, Poland*

We have investigated frequency tuning mechanisms in coupled cavity QCLs (CC-QCL) based on GaAs, as well as InP material systems. In CC devices there are two modes of wavelength tuning: discrete Vernier type tuning and continuous temperature tuning.

Discrete Vernier tuning is observed, when the short section of the CC system is acting as tunable frequency filter. Controllable Vernier-effect-based mode switching was observed, induced by the spectral shift of the short cavity's Fabry-Pérot mode comb due to Joule heating. With the help of this discontinuous tuning mechanism, single-mode operation with high side mode suppression ratio was achieved over a broad spectral range. The total tuning range was 4.65 cm^{-1}, where the tuning range within one mode was 0.9 cm^{-1}. The SMSR over the whole range was above 20 dB.

The continuous temperature tuning is a consequence of the change of effective group refractive indices of both sections. Authors have observed stable tuning of emitted wavelength frequency over a broad range of device operating temperatures. In the range of temperature tuning from 10^0C to 60^0C the wavelength tuned from 1112.3 cm^{-1} to 1108.5 cm^{-1}. Throughout the tuning range the SMSR was above 20 dB.

The devices studied in this work were fabricated by means of focused ion beam (FIB) post-processing. Special care has been taken to optimize the FIB milling process to obtain high quality mirrors. The room temperature, single mode, pulsed emission from InGaAs/AlGaAs/GaAs CC-QCL with SMSR of 43 dB has been achieved. Emission is centered at ~1059.4 cm-1 (9.44 μm). The laser exhibits a peak output power of 15 mW per facet at room temperature. Stable, single mode emission is observed within the useful temperature tuning range (280K to 320K), exhibiting shift at the rate of 0.59 nm/K. We have also investigated InP-based QCLs. In this case, SMSR better than 20 dB were observed.

*corresponding author: kamil.pierscinski@ite.waw.pl

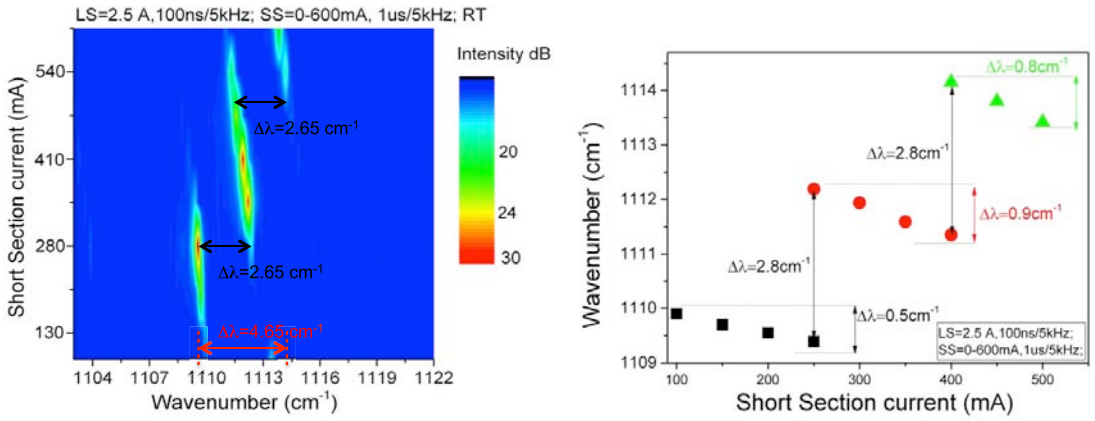

Fig.1. Discrete Vernier like frequency tuning of coupled cavity QCL.

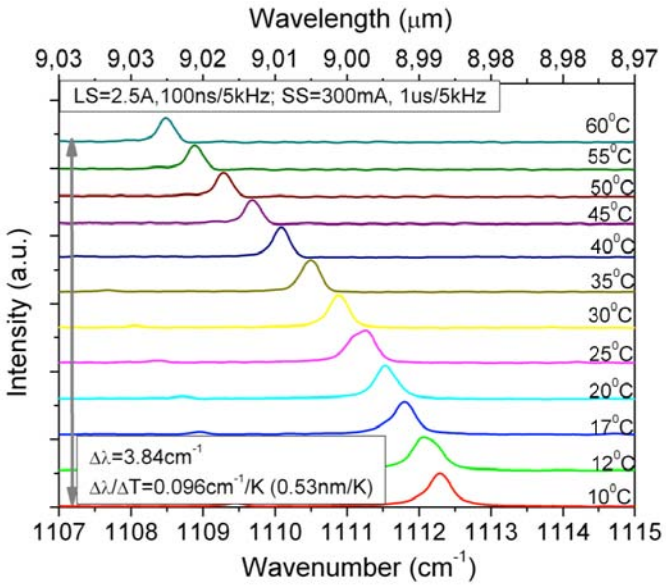

Fig.2. Continuous temperature tuning of coupled-cavity QCL.

Optimization of 2.5 μm InP-based metamorphic InAs quantum well lasers

W. Y. Ji, Y. Gu, Y. G. Zhang*, X. Y. Chen, Y. J. Ma, S. P. Xi, B. Du, Y. H. Shi

State Key Laboratory of Functional Materials for Informatics, Shanghai Institute of Microsystem and Information Technology, Chinese Academy of Sciences. 865 Chang Ning Rd., Shanghai 200050, China

Mid-infrared semiconductor lasers emitting in 2-3 μm wavelength range are very attractive for free space communications and atmospheric pollution monitoring [1]. Antimony-free metamorphic InAs quantum well (QW) lasers on InP substrates are a promising approach to achieve favorable performances from 2.5 μm to around 3 μm. However, appropriate optimization of structure is highly required for the lasers due to the limited material choice. The material quality also plays a crucial role for the strained QW structures on metamorphic buffers [2].

In this work, we investigated the effects of well shapes and waveguides on InP-based metamorphic InAs QW lasers at around 2.5 μm. As shown in Fig. 1, an $In_xAl_{1-x}As$ (x from 0.52 to 0.65) graded buffer and an $In_{0.65}Al_{0.35}As$ layer were grown on InP substrate to form a virtual substrate. After that, the active regions of lasers were grown on the metamorphic structures. Laser structures with $In_{0.65}Ga_{0.35}As$ (sample A) and $In_{0.65}Al_{0.20}Ga_{0.15}As$ (sample B) waveguide layers were grown and compared, where 7-nm InAs/24-nm $In_{0.53}Ga_{0.47}As$ QWs were used as the active regions. A novel trapezoidal QW, which was composed of 3-nm InAs layer sandwiched by two 4-nm $In_yGa_{1-y}As$ (y from 0.53 to 1) grading layer, leading to a QW thickness of 11 nm (sample C), was used to relieve the strain and improve the quality of QW.

The grown samples were processed into ridge waveguide lasers. The continuous-wave (CW) lasing spectra at 100 K are shown in Fig. 2. The maximum operation temperature of sample A, B and C is 100 K, 160 K and 240 K. Figure 3 shows their separate maximum output power in the range of 77-180 K. The temperature dependence of the threshold current density under CW driving condition is shown in Fig. 4. Results indicate that the performances of sample B are superior to sample A, while the performance of sample C is the best. The maximum operation temperature under CW mode has been increased mainly due to the enhanced carrier injection and confinement of $In_{0.65}Al_{0.20}Ga_{0.15}As$ waveguide for sample B and the gradual lattice mismatch at the interfaces between $In_{0.53}Ga_{0.47}As$ barrier and trapezoidal well layers for sample C. The decreased threshold current density and enhanced output power of sample C could be attributed to the reduced non-radiative recombination centers and improved structural quality of trapezoidal QWs.

References

[1] Y. Gu, Y. G. Zhang, X. Y. Chen, et al., J. Crystal Growth 425, 376-380 (2015).

[2] Y. Gu, X. Y. Chen, Y. G. Zhang, et al., J. Phys. D: Appl. Phys 46, 505103 (2013).

*corresponding author: ygzhang@mail.sim.ac.cn

300 nm p-$In_{0.65}Ga_{0.35}As$ contact
1700 nm p-$In_{0.65}Al_{0.35}As$ cladding
150 nm p-$In_{0.65}Ga_{0.35}As$ or $In_{0.65}Al_{0.2}Ga_{0.15}As$ waveguide
InAs rectangular or trapezoidal 4QW
150 nm p-$In_{0.65}Ga_{0.35}As$ or $In_{0.65}Al_{0.2}Ga_{0.15}As$ waveguide
800 nm n-$In_{0.65}Al_{0.35}As$ cladding
1 μm n-$In_xAl_{1-x}As$ graded buffer
100 nm n-$In_{0.52}Al_{0.48}As$ buffer
200 nm n-InP buffer
n-InP substrate

Fig. 1. Schematic structure of the metamorphic InAs quantum well lasers.

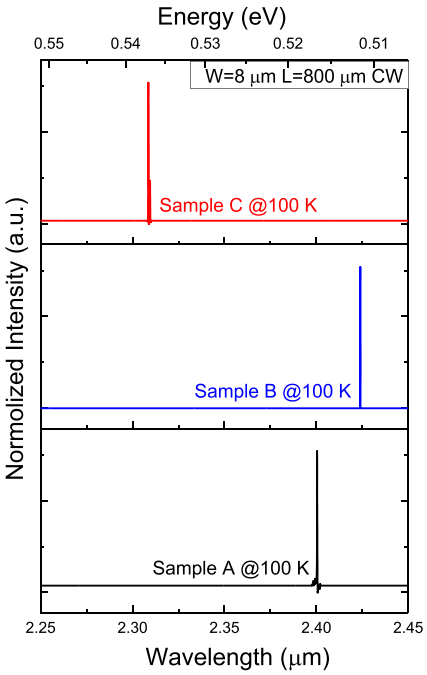

Fig. 2. Lasing spectra of the lasers under CW driving condition at 100K.

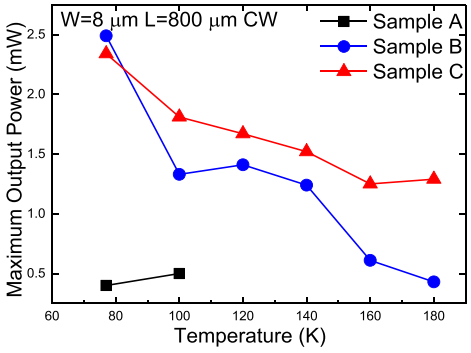

Fig. 3. Temperature dependence of maximum output power of the lasers.

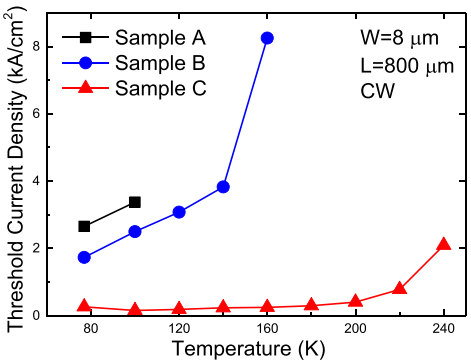

Fig. 4. Threshold current density versus temperature of the lasers.

Barrier structures of InAs/GaSb type-II superlattices LWIR photodetectors

Zhicheng Xu, Jianxin Chen*,and Li He

Shanghai Institute of Technical Physics, Chinese Academy of Sciences, 500 Yutian Road, Shanghai, 200083, China

**Corresponding author: jianxinchen@mail.sitp.ac.cn*

In the paper, barrier structures in InAs/GaSb longwave infrared (LWIR) photodetectors were studied to suppress dark current and improve performances. Two double barrier detector structures $pB_1\pi B_2n$-AL and $pB_1\pi B_2n$-GA were designed and grown by molecular beam epitaxy (MBE), where B_1 and B_2 stand for electron barrier and hole barrier, respectively, and π is the slightly p-doped absorption region1. The two structures have similar epitaxial structures of a 1.5-μm-thick n-type InAsSb layer, a hole barrier layer, 300 periods of p-doped 15 ML InAs/7 ML GaSb SLs π region, 60 periods of p-doped 7 ML InAs/7 ML GaSb SLs electrons barrier layer and a 50-nm-thick p doped GaSb layer. The top P-GaSb and the bottom N-InAsSb were served as electrical contact layers. They differ only in the hole barrier structures. The pB1πB2n-AL has 80 periods of n-doped 16 ML InAs/4 ML AlSb SLs as the hole barrier2, while the pB1πB2n-GA has 100 periods of n-doped 8 ML InAs/3.5 ML GaSb SLs as the hole barrier.

The two detectors showed similar 100% cutoff wavelength of 12.5 μm at 80 K, and a peak current responsivity of around 2.5 A/W, which was independent of the applied reverse bias, showing that two detector structures have no unintended conduction band potential barriers. The dark current density of the $pB_1\pi B_2n$-AL detector at -30 mv bias was 8.0×10^{-4} A/cm^2, which leads to the peak detectivity D* of 1.6×10^{11} cm Hz$^{1/2}$/W. The dark current density of the $pB_1\pi B_2n$-GA detector at -30 mv bias was 1.5×10^{-3} A/cm^2, which leads to the peak detectivity D* of 1.1×10^{11} cm Hz$^{1/2}$/W.

In conclusion, we demonstrated that LWIR InAs/GaSb superlattices detectors with the InAs/GaSb hole barrier can achieve similar performances as that with the InAs/AlSb hole barrier.

[1] Yi Z, Jian-Xin C, Zhi-Cheng X, et al. High Performance Long Wavelength Superlattice Photodetectors Based on Be Doped Absorber Region[J]. Chinese Physics Letters, 2014, 31(10): 108503.

[2] Ting D Z Y, Hill C J, Soibel A, et al. A high-performance long wavelength superlattice complementary barrier infrared detector[J]. Applied Physics Letters, 2009, 95(2).

Reliability of Quantum Cascade Lasers under γ Irradiation

L. Mihai[1], D. Sporea[1]*, D. Neguţ[2]

[1] *National Institute for Laser, Plasma and Radiation Physics, 409 Atomistilor St., Magurele, RO-077125, Romania*

[2] *"Horia Hulubei" National Institute of Physics and Nuclear Engineering, 30 Reactorului St., Magurele, RO-077125, Romania*

An interband cascade semiconductor laser operating at λ = 3.27 μm is embedded into the tunable laser spectrometer (TLS) placed on board of the Mars Science Laboratory (MSL) of NASA's Curiosity rover, looking for methane and carbon dioxide detection during the Mars mission [1,2]. A quantum cascade laser (QCL), having the central wavelength at λ = 7.7 μm, was proposed to be part of a local oscillator in the Laser Heterodyne Radiometer (LHR) for the detection of methane in Mars atmosphere [4]. The Stratospheric Observatory for Infrared Astronomy (SOFIA) includes a QCL heterodyne receiver for rotation spectra detection in high resolution spectroscopy [5]. It is expected the usage of QCLs in other planetary missions such ESA's JUICE - JUpiter ICy moons Explorer to be launched in 2022 [6].

In the context of the proliferation of interplanetary missions, encounters with comets and asteroids, which require small footprint instrumentation for mid-IR and THz spectroscopy, we started two years ago a project funded by the Romanian Space Agency (contract 67/2013) for the evaluation of active and passive mid-IR components as they are subjected to different irradiation conditions. The present paper reports for the first time, according to our knowledge, some results on mid-IR QCLs reliability under gamma irradiation. The tested QCL is tunable from 7.542 - 7.553 μm. Irradiations were performed at a dose rate of 4.7 kGy/h, and total doses of 0.5, 2.5, 10 and 20 kGy. The setup for the measurement of voltage-current curve, temperature and current dependence of beam quality, emitted power, central wavelength and emitted spectrum are illustrated in Fig. 1. Figure 2 provides information on radiation induced changes on some of these parameters.

References

1. S. K. Atreyaa, P. R. Mahaffyb, Ah-San Wonga, Methane and related trace species on Mars: Origin, loss, implications for life, and habitability, Planetary and Space Science, Vol. 55, Issue 3, pp. 358-369, 2006, doi:10.1016/j.pss.2006.02.005.
2. http://microdevices.jpl.nasa.gov/capabilities/semiconductor-lasers/tunable-laser-spectrometers.php,.
3. R. L. Passmore et al, Using IR laser heterodyne radiometry to search for methane on Mars, University of Oxford report (2010).
4. H.-W. Hübers et al., Liquid-cryogen free front-end for a 2.5-THz heterodyne receiver, Proc. of 22nd Intl Symposium on Space Terahertz Technology, Tucson, pp. 12 (2011).
5. http://sci.esa.int/juice/, accessed on July 31, 2016.
6. D. Weidmann, R. Rose and M. Jenkins, A fully integrated, miniaturized quantum cascade laser heterodyne radiometer for EO, presented at NCEO/CEOI Conference, Nottingham (2012).

*corresponding author: dan.sporea@inflpr.ro

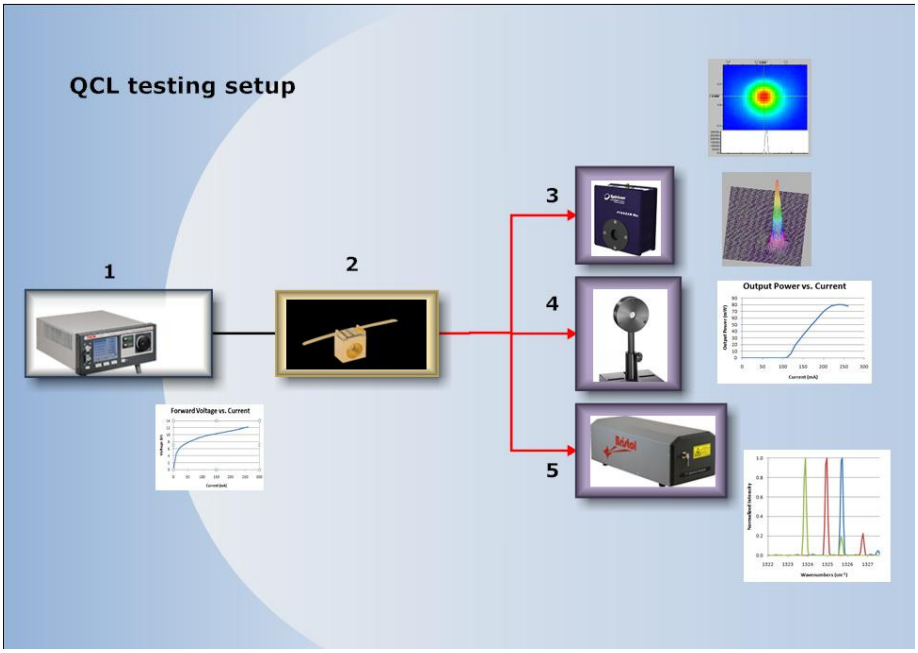

Fig.1. Setup for the evaluation of the irradiated QCL parameters: 1 – QCL driver; 2 – QCL; 3 – IR Pyrocam; 4 – optical power meter; 5 – wavelength meter/ optical spectrum analyzer. .

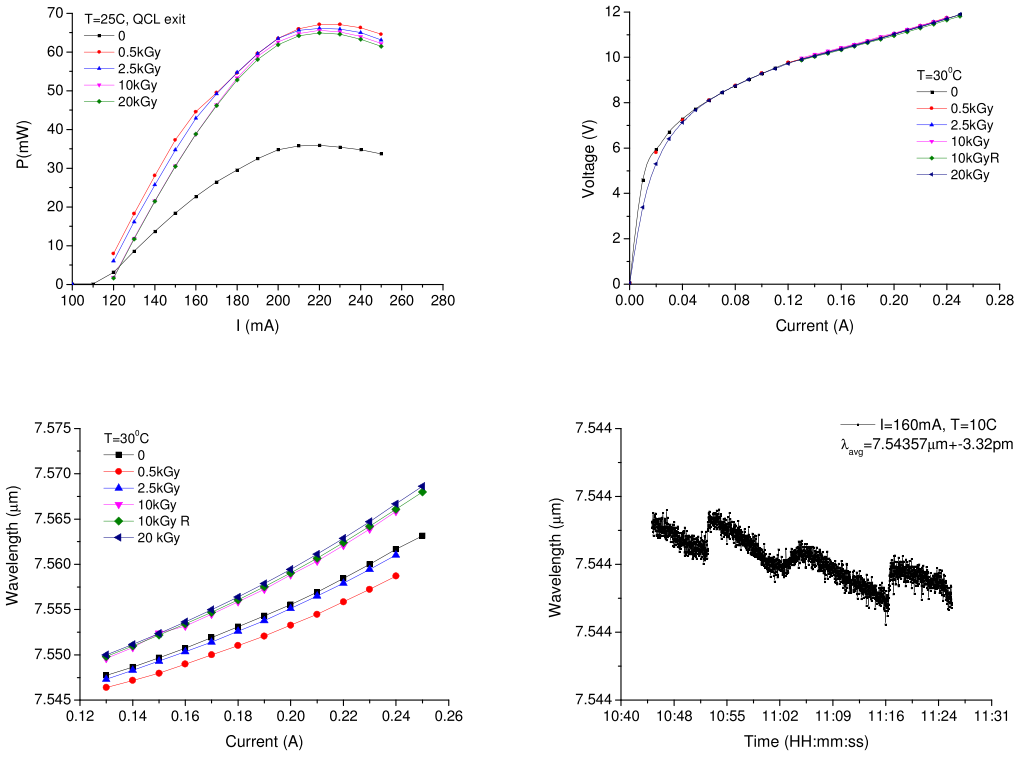

Fig. 2. The gamma irradiation induced changes in: a – the optical power-driving current; b – the current-voltage curve; c – the central wavelength shift; d – the wavelength stability.

Investigation in band structure, gap engineering and transport in semimetallic two-dimensional InAs/GaSb far-infrared detector

A. Boutramine, A. Nafidi*, D. Barkissy, N. Benchtaber, A. Khalal, T. El Gouti

Laboratory of Condensed Matter Physics and Nano Re, University Ibn Zohr, Agadir, Morocco

Over the last decade, photodetector based on InAs/GaSb type-II superlattice (T2SL) material has become of great interest as an attractive system for both military and civilian applications [1,2]. We investigated theoretically the bands structure $E(d_2)$, $E(k_z)$ and $E(k_p)$, respectively, in the direction of growth and in plane of the InAs (d_1=160 Å)/GaSb (d_2=105 Å) type II superlattice in the envelop function formalism [3] with the valence band offset Λ=510 meV [4].

The design parameters, d_2 and Λ, dependence of the SL's band gap, shows that the transition semiconductor-semimetal goes to high d and Λ when the temperature decreases. E (k_z, k_p) shows that, $E_g(\Gamma)$ shifts from -48.2 meV to -98.3 meV in the range of 4.2 -300 K. The photoresponse cut-off wavelength lies in the range of 12.6-25.7 μm. The obtained band gaps energies are in agrement with those measured experimentally. The position of the determined Fermi level E_F=500.2 meV indicates a p-type semimetallic conductivity at 141 K. On the basis of the classical expression for the Hall coefficient of two-band model, derived from the Boltzmann equation, we have found: $1.8.10^{13}cm^{-2}$, $3.9.10^{13}cm^{-2}$, $3345\,cm^{-2}/V.s$, $975\ cm^{-2}/V.s$, and $2117\ cm^{-2}/V.s$ for n_e, n_h, μ_e, μ_h, and μ_H respectively in agreement with the experimental data of D. M. Symons et al [5]. This study indicates that the present SL can be used as a Far-infrared detector.

References

[1] L. Esaki, in Narrow Gap Semiconductors - Physics and Applications, 133 of Lecture Notes in Physics (Edited by W. Zawadzki). Springer, Berlin, 302 , 1980.

[2] M. Razeghi and Binh-Minh Nguyen. "Advances in mid-infrared detection and imaging: a key issues review," Rep. Prog. Phys, Vol. 77, 082401(17pp), 2014.

[3] G. Bastard. "Superlattice band structure in the envelope-function approximation", Physical Review B 24: 5693-5697, 1981.

[4] A. Boutramine, A. Nafidi, D. Barkissy, et al, "Electronic bands structure and Shubnikov-de Haas effect in two-dimensional semimetallic InAs/GaSb nanostructure superlattice", Appl. Phys. A 122:70, DOI 10.1007/s00339-015-9561-x, 2016.

[5] D. M. Symons, M. Lakrimi, M. van der Burgt, T. A. Vaughan, R. J. Nicholas, N. J. Mason, and P. J. Walker, "Temperature dependence of the band overlap in InAs/GaSb structures, Phys. Rev. B 51: 1729, 1995.

*corresponding author: nafidi21@yahoo.fr

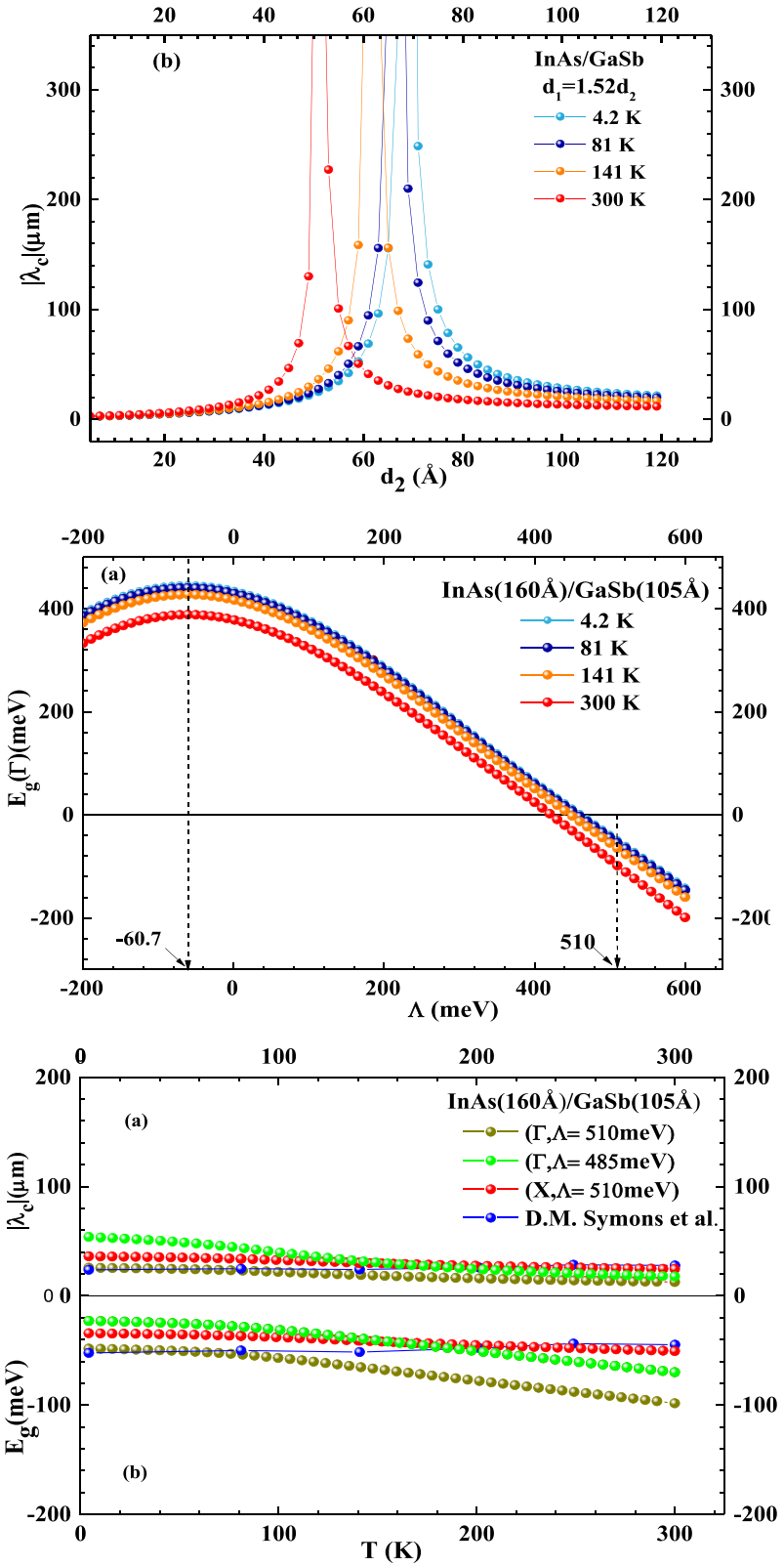

Fig. : In the investigated InAs/GaSb SL, (a) Evolution of the cutoff wavelength $|\lambda_c|$ versus the GaSb layer thickness. (b)The band gap, $E_g(\Gamma)$, as a function of the valence band offset and temperature. **(c)** Temperature dependence of the band gap E_g. and the cut-off wavelength λ_c. The experimental data were extracted from [4].

Nitrous acid monitoring by external-cavity quantum cascade laser based quartz-enhanced photoacoustic spectroscopy

Hongming Yi[1,2], Rabih Maamary[1], Xiaoming Gao[2], Markus W. Sigrist[3], Eric Fertein[1], Weidong Chen[1*]

[1] *LPCA, University of the Littoral Opal Coast, 59140 Dunkerque, France*
[2] *Anhui Institute of Optics and Fine Mechanics, CAS, Hefei, Anhui 230031, China*
[3] *ETH Zurich, Institute for Quantum Electronics, CH-8093 Zürich, Switzerland*

Spectroscopic detection of short-lived gaseous nitrous acid (HONO) at 1254.85 cm^{-1} was realized by off-beam coupled quartz-enhanced photoacoustic spectroscopy (QEPAS) in conjunction with an external cavity quantum cascade lasers (EC-QCL) [1]. High sensitivity monitoring of HONO was performed within a very small gas-sample volume (of ~ 40 mm^3) allowing a significant reduction (of about 4 orders of magnitude) of air sampling residence time which is highly desired for accurate quantification of chemically reactive short-lived species. Calibration of the developed QEPAS-based HONO sensor was carried out by means of lab-generated HONO samples whose concentrations were determined by simultaneous measurements of direct HONO absorption spectra in a 109.5 m multipass cell using a distributed feedback (DBF) QCL. A minimum detection limit (MDL) of 66 ppbv (1) HONO was achieved at 70 mbar using a laser output power of 50 mW and 1 s integration time, which corresponded to a normalized noise equivalent absorption coefficient of 3.6×10^{-8} $cm^{-1}.W/Hz^{1/2}$. This MDL was down to 7 ppbv at the optimal integration time of 150 s. The corresponding 1 minimum detected absorption coefficient is ~ 1.1×10^{-7} cm^{-1} (MDL : ~ 3 ppbv) in 1 s and ~ 1.1×10^{-8} cm^{-1} (MDL : ~ 330 pptv) in 150 s, respectively, with 1 W laser power.

Acknowledgements The authors acknowledge financial supports from the CaPPA project (ANR-10-LABX-005) and the CPER CLIMIBIO program.

References

1. H. Yi, R. Maamary, X. Gao, M. W. Sigrist, E. Fertein, W. Chen. Short-lived species detection of nitrous acid by external-cavity quantum cascade laser based quartz-enhanced photoacoustic absorption spectroscopy, Appl. Phys. Lett. **106**, 101109, 2015

*corresponding author: chen@univ-littoral.fr

Numerical calculation of the plume infrared radiation of a long-endurance UAV

HUANG Zhang-bin[1,a] , LI Xiao-xia[1,2,b] ,FENG Yun-song[2,c]

（1State Key Laboratory of Pulsed Power Laser Technology, Electronic Engineering Institute, Hefei 230037, China）

（2Key Laboratory of Infrared and Low Temperature Plasma of Anhui Province, Hefei 230037, China）

[a]408867079@qq.com,[b]lxxhong@163.com,[c]fyseei@163.com

Key words: long-endurance UAV; plume; temperature field; C-G theory; infrared rediation

Abstract:Plume is the main infrared source of a long-endurance UAV, and its infrared radiation numerical calculation is very important for calculating the infrared characteristcs of the whole UAV. This paper built the geometrical model of the flow field structure of UAV plume by analyzing the characteristcs of the flow structure. And, The temperaturre field distribution of the UAV plume was calculated based on the eddy current propagation theory. And then, spectral infrared radiation characteristics of the UAV plume at 2-5μm were obtained by the single band C-G approximation method. The results show that the temperature in the core area of the UAV plume is higher , and the infared radiation characteristics are stable and obvious. The infrared radiation energy of the plume mainly ditributed at the infrared wavelength of 2.7μm and 4.5μm,which is in accordance with the actual situation. The results maybe contribute to the further study of the infrared radiation characteristics of the long-endurance UAV.

Dual band radiometric temperature measurements using InAs and InAsSb based photodiodes

B.A.Matveev[1, 2], S.E.Aleksandrov[1], G.A.Gavrilov[1], A.A.Kapralov[1], M.A.Remennyi[1, 2] and G.Yu.Sotnikova[1*]

[1] *Ioffe Institute, Polytekhnicheskaya 26, 194021, St.Petersburg, Russia*
[2] *IoffeLED, Ltd. , Polytekhnicheskaya 26, 194021, St.Petersburg, Russia*

There is curtain amount of processes, like micro-structuration of thin metal film deposited onto plastic substrate, which needs fast and reliable radiometric temperature measurements of substances in the "low" range of temperatures, that is, in the 0-300°C interval. Analysis showed that photodiodes (PDs) with narrow-band responsivity in the 3-5 um spectral range, e.g. immersion lens back-side illuminate (BSI) PDs based on A^3B^5 semiconductors, are optimal for the above job.

Our report describes performance and some of the applications of two dual band (or "two color") pyrometers with sensor head composed of two narrow gap A^3B^5 photodiodes (PDs) placed along single optical axis. In fact two "back-to-back" BSI InAsSbP/InAs (λ_c=3.4 μm) [1] and InAsSbP/InAsSb (λ_c=4.2 μm) [2] double heterostructure PDs have been joined together by a transparent chalcogenide glue and mounted onto a hyperhemispherical Si immersion lens (D_{lens}=3.5 mm). Both sensor head and amplifier were placed into a sealed case onto a TEC plate (t=20±0.1°C). For long-distant measurements (2 meters) of a small area objects spherical (D_1= 60 mm) and plane (D_2 = 25 mm) mirrors have been added for providing sighting index of about 100 (measuring spot dimensions was of about 2 cm). Second pyrometer was equipped with fiber allowing "near field" temperature measurements. Owing to narrow spectral response of the BSI PDs used in the sensor the transmission function of the sensor was directly derived from the Planck's law adjusted to PD spectral response [3].

Simulated sensor noise values constituted to $4.5\cdot10^{-3}$ $nA\sqrt{Hz}$ and $5.4\cdot10^{-2}$ $nA\sqrt{Hz}$ for amplified output of InAs and InAsSb PD respectively, the above numbers matched measured dispersion values of ±1 nA and ±10 nA at the 30 kHz detection band (the corresponding response time τ~30 μs). High signal-to-noise ratio (SNR) value allows measurement of significantly lower temperature with higher accuracy and/or extremely smaller response time (e.g. around 0°C with accuracy of 2-5 degrees at a response time of τ~30 μs) compared to other uncooled mid-infrared sensors.

References

1. P.N. Brunkov et al, Infrared Physics and Technology (2016), pp. 542-545
2. N. D. Il'inskaya et al, Semiconductors, (2012), Vol. 46, No. 5, pp. 690–695.
3. G.Yu. Sotnikova, S.E. Aleksandrov, G.A. Gavrilov, Proc. SPIE, vol. 8073, 80731A (2011).

*corresponding author: G.Sotnikova@mail.ioffe.ru

Figures

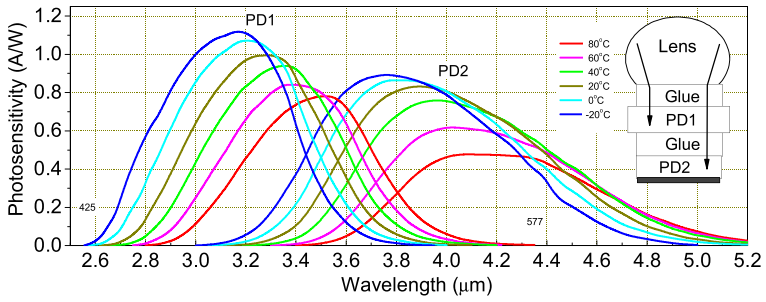

Fig. 1. Photoresponse spectra of the dual band photodiode with InAs (PD1) and InAsSb (PD2) active layers at several photodiode temperatures. In the insert – schematic of the dual band sensor head.

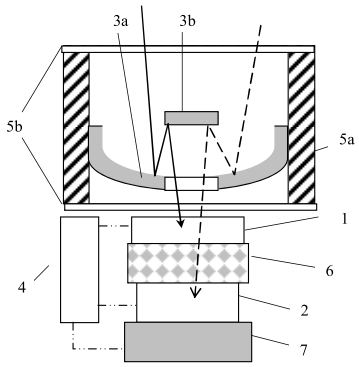

Fig.2 Schematic of the dual band pyrometer, 1- InAs based PD, 2- InAsSb based PD, 3a – spherical mirror, 3b – plane mirror, 4 – read-out and TEC control circuits, amplifiers, A/D converters, microprocessor and display, 5a – hermetically sealed case, 5b – windows, 6- chalcogenide glue, 7- TEC. (Immersion lens is not shown).

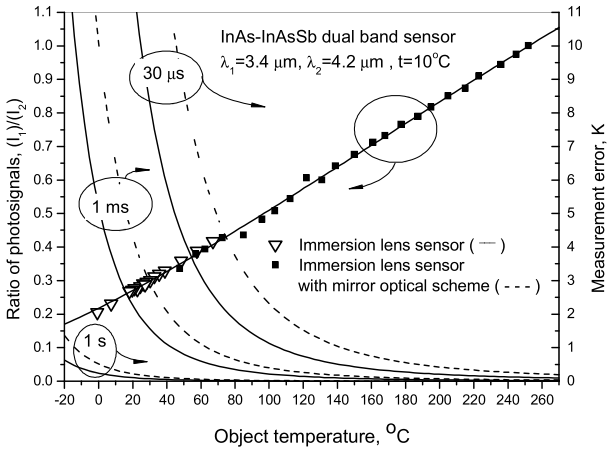

Fig.3 Ratio of photosignals and measuring error in two-color pyrometer vs object temperature for single immersion lens sensor (open triangles) and sensor equipped with immersion lens and mirror optics (filled squares). Error magnitude is presented for three integration times of 30 μs, 1 ms and 1 s.

Study of surface passivation on InAs/GaSb superlatice photodetectors with side-wall gate controlled structure

Yurong Cui[1,2], Jianxin Chen[1*] ,ZhichengXu[1], Jiajia Xu[1], Yi Zhou[1], Li He[1]

1: Key Laboratory of Infrared Imaging Materials and Detectors, Shanghai Institute of Technical Physics, Chinese Academy of Sciences, Shanghai 200083, China.

2: University of Chinese Academy of Sciences, Beijing100039, China

E-mail: jianxinchen@mail.sitp.ac.cn

The side-wall passivation and chemical properties studies of InAs/GaSb type-II superlattice are very important to realize the high performance photodetectors.[1] The gated structure as widely utilized to determine the quality of passivation and the mechanisms of surface dark currents.[2] On the other hand, the thermal stability of the passivation layer is indispensable to ensure the constant chemical and electrical passivation.

In our experiments, a p-i-n structure with InAs/GaSb superlattice was grown by molecular beam epitaxy (MBE). The superlattice has an 8 ML InAs and 6 ML GaSb in each period, corresponding to a cut-off wavelength of 5.4μm. The mesas were wet-etched by a mixture of citric acid, phosphoric acid and hydrogen peroxide. The passivation of Si_3N_4 and SiO_2 were deposited by ICP CVD. Electrodes were made on dielectric films to apply gate bias. All the measurements were performed at 80K.

The resistance-area product at zero bias (R_0A) of the as-passivated device by Si3N4 is 2.8×10^5 Ω • cm^2 without gate bias. While the max R_0A reached $4.5\times10^5\Omega cm^2$ under a gate bias of VG=-3V. However, after a process of rapid thermal annealing (RTA) at 250℃ for 60s, the R_0A decreases to $12\Omega cm^2$. When the optimal gate bias was applied (VG=-35V), the R_0A recovered back to $3.3\times10^5\Omega cm^2$. According to the change of flat band voltage and capacitance of the dielectric film, we could calculate surface charge $Qs=6.15\times10^{12}cm^{-2}$. On the other hand, the SiO_2 passivated devices did not show considerable difference with a changing gate bias. The max $R_0A=5.4\times10^5\ \Omega\ cm^2$ of the device was achieved without any gate bias before RTA. After RTA, the R0A decreased slightly to $1.6\times10^5\ \Omega\ cm^2$.

[1] Plis E A, Kutty M N, Krishna S. Passivation techniques for InAs/GaSb strained layer superlattice detectors[J]. Laser & Photonics Reviews, 2013, 7(1): 45-59.

[2] Chen G, Nguyen B M, Hoang A M, et al. Elimination of surface leakage in gate controlled type-II InAs/GaSb mid-infrared photodetectors[J]. Applied Physics Letters, 2011, 99(18): 183503.

On-line non-destructive vacuum detection by high resolution infrared laser spectroscopy

Dong Chen[1]*, Pengfei Fang[1], Zhaoli Jia[1], Yanwei Gao[2], Yujun Zhang[2]

[1] *School of Instrument Science and Opto-electronic Engineering, Hefei University of Technology, Hefei 230009, China*

[2] *Anhui Institute of Optics and Fine Mechanics, The Chinese Academy of Science, Hefei 230031, China*

Vacuum sealed packaging is a common means of preventing the deterioration of long-term storage products. Leak detection for vacuum-sealed packaging of manufactured products is a national mandatory requirements and necessary step for related products in the food, medicine and other industries. On-line, non-destructive vacuum measurement and leak detection for vacuum sealed package in the industrial area is of great significance and has broad application requirements.

The traditional vacuum measurement instruments need air passage communicating，would destroy vacuum sealed packaging , and have slow detection speed, therefore, can not be used for on-line measurement and leak detection of the degree of vacuum for vacuum sealed packaging.

In this work, a laser-based on-line non-destructive vacuum detection method is studied. It is based on the broadening characteristics of the high resolution absorption spectrum of water vapor in the headspace of vacuum sealed container, the pressure broadening parameter is separated from total line broadening, and precise measurement of vacuum pressure is achieved through simultaneous water vapor concentration detection.

Acknowledgments

The authors acknowledge financial support from National Key Scientific Instrument and Equipment Development Project of China(2012YQ220119) and Natural Science Foundation of Anhui Province(1408085MKL84)

*corresponding author: dchen@hfut.edu.cn

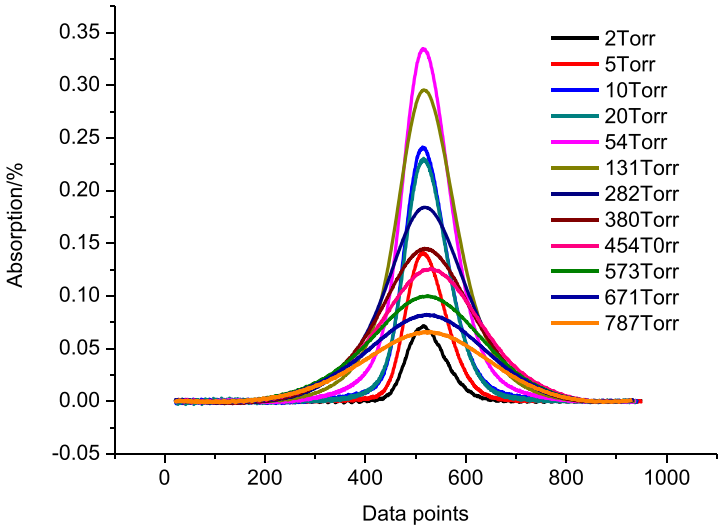

Fig.1. High resolution laser spectrum of H_2O at different pressures

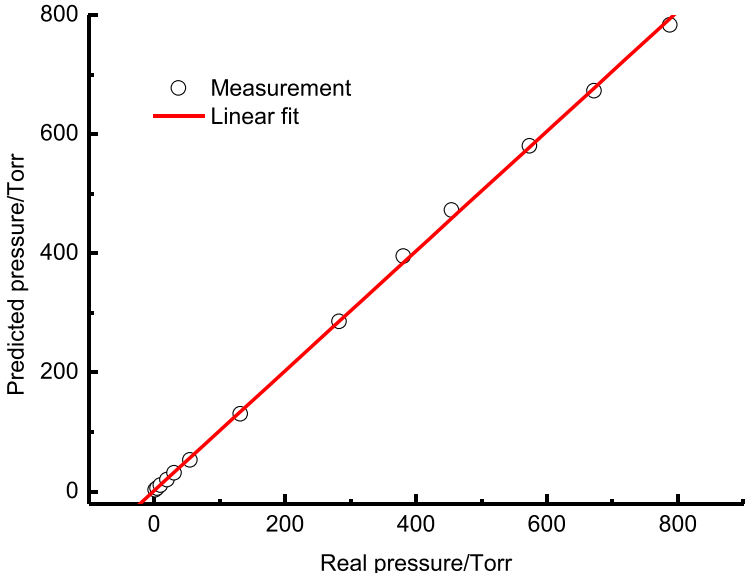

Fig.2. Relationship between predicted and real vacuum pressures

Author Index

RIBER

昆明沃特尔机电设备有限公司
KUNMING AUTO MACH.&ELE. CO. LTD
13708457334

SHMQ FOR SEMI-CONDUCTOR

SSIMC

HGH Infrared Systems

SÜSS MicroTec

LOGITECH Materials Technologists & Engineers

北京友谊宾馆示意图

Plan of Beijing Friendship Hotel

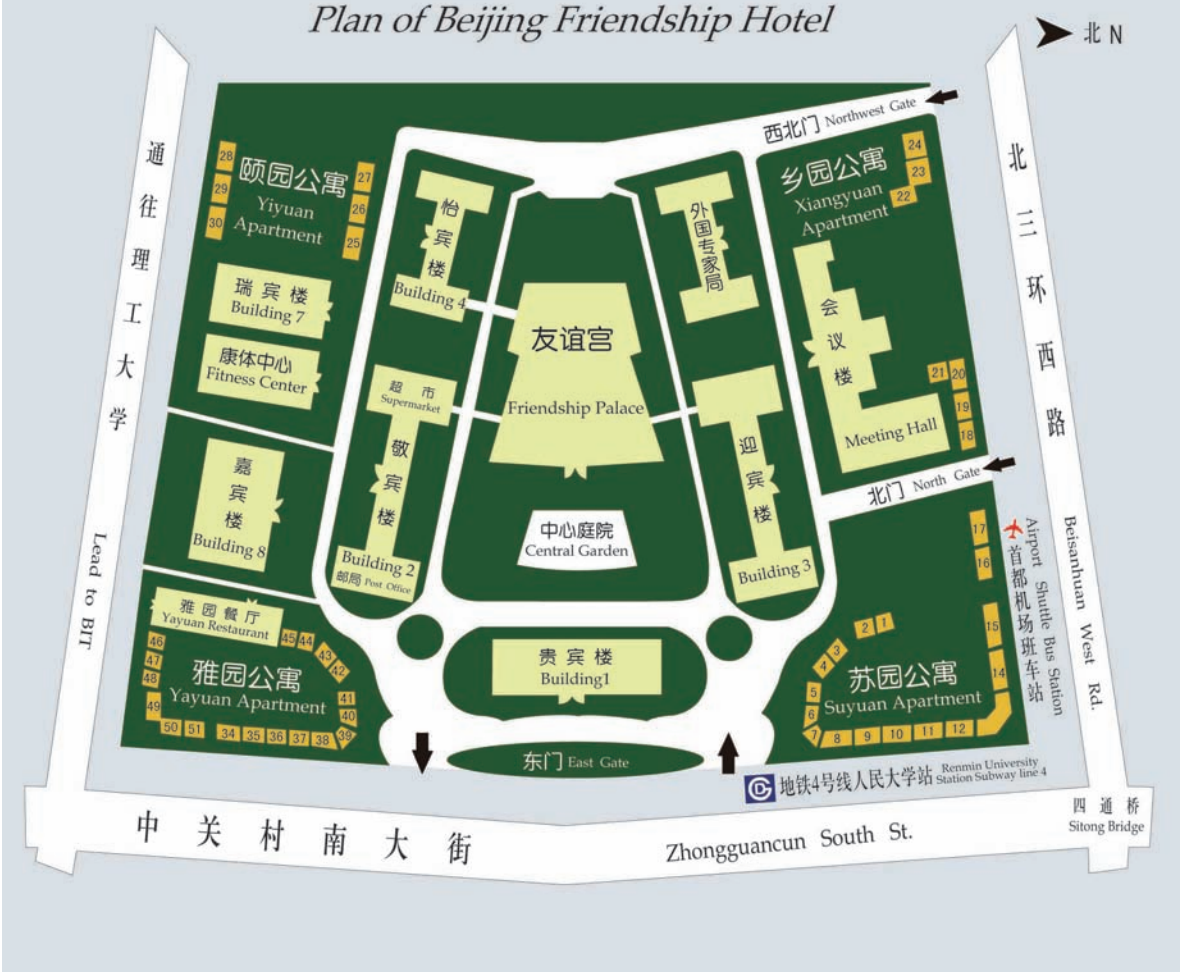

The Shanghai Institute of Technical Physics (SITP) was cofounded by the Chinese Academy of Sciences (CAS) and Fudan University in October 1958 and became an independent CAS institute in 1962. The institute is a comprehensive research-oriented state-owned institute with tremendous strength that engages in basic and applied research and the industrialization of new and high technology. It was selected as one of the first institutes to participate in CAS's Knowledge Innovation Program in 1998.

SITP's primary research area is the application of infrared physics and optoelectronics technology with particular attention to new infrared photoelectric materials, devices and methods, etc. SITP focuses on developing advanced airborne and space-borne payloads, infrared staring imaging and signal processing, infrared focal plane arrays and infrared photoelectric devices, optical coatings, miniature coolers, medical image processing and remote sensing information processing, etc. The institute comprises 13 research departments, including the State Key Laboratory for Infrared Physics, the State Key Laboratory of Transducer Technology Sensors (the photo-sensor branch), the CAS Key Laboratory for Infrared Imaging Materials and Devices and the CAS Key Laboratory for Infrared Detection and Imaging Technology, among others.

Since its establishment, the institute has produced more than 800 important scientific achievements including 54 national-level achievements and 380 provincial-level achievements. It has also been granted more than 480 Chinese patents.